LEABHARLANN CHOLÁISTE NA TRÍONÓIDE, BAILE ÁTHA CLIATH | TRINITY COLLEGE LIBRARY DUBLIN
Ollscoil Átha Cliath | The University of Dublin

Terms and Conditions of Use of Digitised Theses from Trinity College Library Dublin

Copyright statement

All material supplied by Trinity College Library is protected by copyright (under the Copyright and Related Rights Act, 2000 as amended) and other relevant Intellectual Property Rights. By accessing and using a Digitised Thesis from Trinity College Library you acknowledge that all Intellectual Property Rights in any Works supplied are the sole and exclusive property of the copyright and/or other IPR holder. Specific copyright holders may not be explicitly identified. Use of materials from other sources within a thesis should not be construed as a claim over them.

A non-exclusive, non-transferable licence is hereby granted to those using or reproducing, in whole or in part, the material for valid purposes, providing the copyright owners are acknowledged using the normal conventions. Where specific permission to use material is required, this is identified and such permission must be sought from the copyright holder or agency cited.

Liability statement

By using a Digitised Thesis, I accept that Trinity College Dublin bears no legal responsibility for the accuracy, legality or comprehensiveness of materials contained within the thesis, and that Trinity College Dublin accepts no liability for indirect, consequential, or incidental, damages or losses arising from use of the thesis for whatever reason. Information located in a thesis may be subject to specific use constraints, details of which may not be explicitly described. It is the responsibility of potential and actual users to be aware of such constraints and to abide by them. By making use of material from a digitised thesis, you accept these copyright and disclaimer provisions. Where it is brought to the attention of Trinity College Library that there may be a breach of copyright or other restraint, it is the policy to withdraw or take down access to a thesis while the issue is being resolved.

Access Agreement

By using a Digitised Thesis from Trinity College Library you are bound by the following Terms & Conditions. Please read them carefully.

I have read and I understand the following statement: All material supplied via a Digitised Thesis from Trinity College Library is protected by copyright and other intellectual property rights, and duplication or sale of all or part of any of a thesis is not permitted, except that material may be duplicated by you for your research use or for educational purposes in electronic or print form providing the copyright owners are acknowledged using the normal conventions. You must obtain permission for any other use. Electronic or print copies may not be offered, whether for sale or otherwise to anyone. This copy has been supplied on the understanding that it is copyright material and that no quotation from the thesis may be published without proper acknowledgement.

ACRITARCH AND PRASINOPHYTE COLOURS AS THERMAL MATURITY INDICATORS

By

CATHERINE DUGGAN

A thesis submitted in accordance with the requirements for the degree of Doctor of Philosophy

Department of Geology, University of Dublin, Trinity College.

June 2006

TRINITY COLLEGE
0 5 AUG 2008
LIBRARY DUBLIN
THESIS
8566

DECLARATION

This thesis has not been submitted as an exercise for a degree at any other university. Except where stated, the work described therein was carried out by me alone.

I give permission for the Library to lend or copy this thesis upon request.

Signed: Catherine Duggan

DECLARATION

I hereby declare that the work in this thesis is entirely my own, unless otherwise stated, and has not previously been submitted as an exercise for a degree at this or any other university. Reproduction in whole or part of this work is authorised, provided that the source is acknowledged, at the discretion of the depository library of the University of Dublin. This thesis may be lent in accordance with library regulations.

_____

Catherine Duggan

SUMMARY

Measurement of changes in the reflectivity of vitrinite (fossil woody material) in incident light is the standard technique for assessing the organic maturity of sedimentary rocks. However, vitrinite grains are rare or absent in pre Late Silurian sediments so thermal histories of these units cannot be investigated by this method. Also, marine hydrocarbon source rocks of Late Silurian and younger age often contain little or no vitrinite.

Acritarchs are enigmatic microfossils commonly found in Lower Palaeozoic sedimentary units and marine source rocks. Like miospores, the colour of acritarchs becomes darker with increasing thermal maturity. The colour of the long-ranging acritarch genus *Veryhachium* was calibrated as a thermal maturity indicator during this study. Rock samples were collected that contained vitrinite grains and *Veryhachium* specimens. The vitrinite reflectance of the sample was determined using standard techniques. Image analysis rather than traditional visual estimation was used to determine the colour of *Veryhachium*. Colour was described in terms of red, green and blue intensities (RGB). The RGB system is partially device dependent but 'standards' developed to correct for variations within and between systems were of only limited success. Mean blue and green *Veryhachium* intensities were found to be more sensitive to changes in thermal maturity than red intensity.

Prasinophytes are generally considered a class of green algae. An attempt was made to calibrate the colour of the prasinophyte *Tasmanites* with vitrinite reflectance. *Tasmanites* colour was found to be less useful than *Veryhachium* colour due to the more varied morphology of the former compared with the latter.

Two cases studies were completed. Mean *Veryhachium* RGB intensities were used to assess the thermal maturity of samples from well RH-3 in the Risha Gas Field, Jordan. Estimates of maturity using this technique were consistent with a previous thermal maturity study of the area using other methods. RGB determinations of *Veryhachium* from a Bolivian sample were used to successfully identify reworking.

ACKNOWLEDGEMENTS

Thank you to Dr. John Graham who permitted the use of departmental facilities.

Thanks to Prof. Geoff Clayton for his support, encouragement, advice and sense of humour. I couldn't have wished for a better supervisor.

The Petroleum Affairs Division of the Irish Government, Marathon Oil Corporation, Occidental Petroleum Corporation, and Phillips Oil funded part of this project.

Petrel Resources plc. also funded part of this project and provided valuable sample material. Special thanks to Dr. Dave Naylor for his assistance.

The Trinity Trust provided several travel grants.

Thank you to the staff of the Geology Department for their continuous support and encouragement. George, Ian and John in particular were a constant source of useful advice and comments as well as good company at coffee time.

Frank Hendron taught me all I needed to know about palynological processing and how not to get dead using Hf. Thank you for all your help and friendship.
Thank you to the other technical staff - Neil, Declan for all your assistance and Maura for always having a smile on your face.

Robbie Goodhue provided invaluable technical expertise, showed immense patience with me and always had time to listen. Thank you.

Thanks to Mags for always being free for a chat when I needed it, and all her practical assistance. Also thanks to Joann Layng.

Thanks to all the acritarch workers who provided valuable advice, samples and encouragement. Special thanks to Thomas Servais for his assistance in Belgium and on numerous other occasions. I am very grateful to Reed Wicander for his technical guidance, his amusing emails and friendship.
Thank you to James Killen for all his assistance with the statistics.

To the Geology Department as a whole, thank you for all the opportunities and experiences you gave me – from the numerous fieldtrips I had the privilege to attend, to the chance to improve my upholstery skills, to the involvement with mass painting of rocks: I was so lucky and I loved every minute of it.

Thanks to the class of 2002, who gave me the confidence to pursue the things that would make me happy. Special thanks to Ann Marie and Jane who are the best friends anyone could ask for. I am so grateful to you for everything.

To the class of 2005 who let me hang out with them for three years – I had so much fun with you, thanks for all the laughs.....priceless.

To Heather, Meriel, Claire and Karen in Rathfarnham Girl Guides for giving me six months off to write up – much appreciated.

To the postgrads both past and present who I got to know over the years. Thanks to Becky for blazing the trail and showing us how it was done. Also special thanks to Becky and Jacqui for helping me collect my Belgian samples – stars.
To Stuart for his amazing curries and all the advice. To Gerry for writing an amazing thesis which became something of a bible to me. To F.X. for educating me on the geography of Belgium…always useful. Thanks to all the other postgrads for the craic.

To Aileen for her company and friendship over the past four years, for being on the same wavelength and for all the tea breaks. Thanks.

Thank you to Chew for being a drinking partner, a rugby supporter, a sounding board, and a friend.

To my brother Colm, for his helpful advice and encouragement like 'when are you going to stop nerding around and get a real job?'.

Finally, to my parents; you have always supported me in everything I've done and I simply could not have done this without you. Thank you from the bottom of my heart.

CONTENTS

SUMMARY

ACKNOWLEDGEMENTS

CHAPTER 1: INTRODUCTION 1

1.1. THE NEED FOR A NEW THERMAL MATURITY INDICATOR 1
1.1.1. INTRODUCTION 1
1.1.2. MAIN ORGANIC THERMAL MATURITY INDICATORS 1
1.2. ACRITARCHS, PRASINOPHYTES, AND THERMAL MATURITY 3
1.2.1. ACRITARCHS AND PRASINOPHYTES 3
1.2.2. CORRELATION OF PALYNOMORPH COLOUR AND THERMAL MATURITY 4
1.3. ASSESMENT OF PALYNOMORPH COLOUR 6
1.3.1. VISUAL ESTIMATION 6
1.3.2. IMAGE ANALYSIS 6
1.4. CASE STUDIES 7

CHAPTER 2: SAMPLES 8

2.1. SAMPLE REQUIREMENTS 8
2.1.1. GEOLOGICAL SETTING 8
2.1.2. VITRINITE PROXIES 9
2.2. SAMPLING 9
2.2.1. UNSUCCESSFUL SAMPLES 9
2.2.2. SUCCESSFUL SAMPLES 9
2.3. MOOSE RIVER BASIN, CANADA 10
2.3.1. GEOLOGICAL HISTORY 10
2.3.2. SAMPLE DETAILS 11
2.4. APPALACHIAN BASIN, AMERICA 11
2.4.1. GEOLOGICAL HISTORY 11
2.4.2. CLAY CITY QUARRY 16
2.4.3. SUNBURY 16
2.4.4. THREE LOCKS ROAD SECTION 16
2.4.5. WILLIAMS COUNTY CORE 16
2.5. DINANT BASIN, BELGIUM 24
2.5.1. GEOLOGICAL HISTORY 24
2.5.2. VILLERS SUR LESSE SECTION 25
2.6. CANTABRIAN ZONE, SPAIN 25
2.6.1. GEOLOGICAL HISTORY 25
2.6.2. GERAS DE CESARES SECTION 30
2.7. ANGLO WELSH BASIN, WALES 30
2.7.1. GEOLOGICAL HISTORY 30

2.7.2. Cwrt-yr-ala Borehole *34*
2.8. SIERRA DE PERIJÁ, VENEZUELA 34
2.8.1. Geological History *34*
2.8.2. Sierra de Perijá Outcrop *36*
2.9. JORDANIAN WELL SAMPLES 36
2.9.1. Geological History *36*
2.9.2. Well RH-3 ..... *41*
2.9.3. Well RH-19 ..... *41*
2.9.4. Well WS-6 ..... *41*

CHAPTER 3: VITRINITE REFLECTANCE: THEORY AND METHOD 46

3.1. THEORY 46
3.1.1. Vitrinite *46*
3.1.2. Vitrinite Reflectance *47*
3.1.3. Thermal Maturity *49*
3.1.4. Benefits of Vitrinite Reflectance *49*
3.1.5. Limitations of Vitrinite Reflectance *50*
3.2. PREPARATION 51
3.2.1 Maceral Seperation *51*
3.2.2. Mounting *52*
3.2.3. Polishing *54*
3.3. VITRINITE REFLECTANCE MEASUREMENTS 55
3.3.1. System Setup *55*
3.3.2. System Calibration *55*
3.3.3. Reflectance Measurements *57*
3.3.4. Chitinozoa Reflectance *60*

CHAPTER 4: COLOUR DETERMINATIONS: THEORY AND METHOD 62

4.1. COLOUR AS A MATURITY INDICATOR 62
4.1.1. Introduction *62*
4.1.2. Image Analysis *63*
4.2. ACRITARCHS 65
4.2.1. Introduction *65*
4.2.2. Veryhachium *66*
4.3. PRASINOPHYTE PHYCOMATA 68
4.3.1. Introduction *68*
4.3.2. Tasmanites *68*
4.4. ACRITARCH ALTERATION INDEX 71
4.4.1. Previous Work *71*
4.5. COLOUR DETERMINATIONS 73
4.5.1. Sample Preparation *73*
4.5.2. Image Analysis System Introduction *73*
4.5.3. Microscope Set up *74*
4.5.4. Camera Setup *76*
4.5.5. Standards *76*

4.5.6. Image Analysis System *79*
4.5.7. Veryhachium Measurements *79*
4.5.8. Tasmanites Measurements *82*
4.5.9. Correction of Results *82*
4.5.10. Qualitative Fluorescence *82*

CHAPTER 5: RGB DETERMINATIONS: CALIBRATION AND ERRORS 87

5.1. RGB COLOUR STANDARDS 87
5.1.1. Introduction *87*
5.1.2. Standards *87*
5.2. ERRORS ASSOCIATED WITH THE RGB SYSTEM 96
5.2.1. Introduction *96*
5.2.2. Gradual variations with time *96*
5.2.3. Variations between operators *107*
5.2.4. Variations between Qwin and Photoshop determinations *112*
5.2.5. Variations between different setups *117*
5.2.6. Conclusions *118*

CHAPTER 6: RESULTS AND DISCUSSION 126

6.1. REFLECTANCE DETERMINATION RESULTS 126
6.1.1. Factors affecting accuracy of results *126*
6.2. RGB DETERMINATIONS RESULTS 128
6.2.1. Correction of RGB Determinations *128*
6.2.2. Veryhachium Colour Determinations *130*
6.2.3. Tasmanites Colour Determinations *132*
6.3. RGB determinations and Maturity 138
6.3.1. Calibration of Corrected RGB determinations against vitrinite reflectance *138*
6.3.2. RGB Intensities as maturity indicators *145*
6.3.3. Comparison of Veryhachium and spore colour *150*
6.3.4. Comparison of Veryhachium and spore fluorescence *150*
6.3.5. Comparison with published acritarch alteration indexes *152*

CHAPTER 7: APPLICATION OF THE METHOD: TWO CASE STUDIES... 154

7.1. RISHA GAS FIELD, NORTH EAST JORDAN - previous work 154
7.1.1. Introduction *154*
7.1.2. Geological History *154*
7.1.3. Source Rock *155*
7.1.4. Thermal Maturity *159*
7.1.5. Timing of Hydrocarbon Generation *159*
7.1.6. Kerogen Type and Organic Content *160*
7.1.7. Traps *161*

7.1.8. Geothermal Gradients *162*
7.1.9. Reservoirs and Seals *162*
7.2 RISHA GAS FIELD, NORTH EAST JORDAN – Samples investigated (this study) 163
7.2.1. Introduction *163*
7.2.2. Sample P12 ..... *163*
7.2.3. Sample P13 ..... *164*
7.2.4. Sample P11 ..... *165*
7.2.5. Sample Pet 3 ..... *166*
7.2.6. Sample Pet 6 ..... *167*
7.2.7. Sample Pet 9 ..... *167*
7.2.8. Conclusions *168*
7.3. REWORKING IN THE ITACUA FORMATION, BOLIVIA 177
7.3.1. Introduction *177*

CHAPTER 8: CONLUSIONS and FURTHER WORK 183

8.1. Image Analysis 183
8.2. Thermal Maturity and *Veryhachium/Tasmanites* Colour 183
8.3. Maturity Case Study 184
8.3. Reworking Case Study 184
8.4. Further Work 185

REFERENCES 186

Appendix I Sample Details

Appendix II Vitrinite and Chitinozoa Reflectance Histograms

Appendix III RGB Determinations of Cokin Photographic Filters ('Standards')

Appendix IV Calibration and Errors Data

Appendix V *Veryhachium* RGB Determinations

Appendix VI *Tasmanites* RGB Determinations

Appendix VII Correlation of *Veryhachium* RGB Data and Vitrinite Reflectance Data

Appendix VIII Confidence Interval Calculations

Appendix IX Digital Data (CD)

LIST OF FIGURES

Figure 1.1:	Stratigraphic range chart of the major organic thermal maturity indicators together with the reported ranges of *Veryhachium* and *Tasmanites*	5
Figure 2.1:	Geographical location of the Ontario Department of Mines Campbell Lake Drill hole	12
Figure 2.2:	Map showing the location of the Moose River Basin (redrawn from Sanford *et al.* (1975).	12
Figure 2.3:	Map showing the location of the Ontario Department of Mines Campbell Lake Drill hole. (Sandford *et al.* 1975)	13
Figure 2.4:	Diagramatic log of the Ontario Department of Mine Campbell Lake Drill hole showing the location of sample Can. 9.	13
Figure 2.5:	Geological outline of the Eastern Interior of the United States (Quinlan *et al.* 1984).	15
Figure 2.6:	Correlation of Devonian strata in the states of Ohio and Kentucky.	15
Figure 2.7:	Geographical location of Clay City Quarry, Powell County, Kentucky	17
Figure 2.8:	Photograph of Clay City Quarry, Powell County, Kentucky	17
Figure 2.9:	Desaturated photograph highlighting the units exposed at Clay City Quarry	17
Figure 2.10:	Location map and geology of the Clay City Quarry Area (after Noger 1988)	18
Figure 2.11:	Diagramattic log of Clay City Quarry exposure showing the location of sample CC3.	18
Figure 2.12:	Geographical location of Bedford Shale and Berea Sandstone outcrop, Sunbury, Delaware County, Ohio	19
Figure 2.13:	Photograph of load casts in the Berea Sandstone exposed at Sunbury, Ohio.	19
Figure 2.14:	Location map and geology of the Sunbury Area (after Slucher, 1997)	20
Figure 2.15:	Log of section exposed at Big Walnut Creek, Sunbury, Ohio, with location of samples marked (after Molyneux *et al.* 1984).	20
Figure 2.16:	Geographical location of Bedford Shale and Berea Sandstone outcrop, Three Locks Quarry, Ross County, Ohio.	21
Figure 2.17:	Photograph of Three Locks Quarry, Ross County, Ohio,	21
Figure 2.18:	Desaturated photograph highlighting the units exposed at Three Locks Quarry, Ross County, Ohio,	21
Figure 2.19:	Location map and geology of the Three Lock Quarry Area (after Schumacher, 1995)	22
Figure 2.20:	Log of section exposed at Three Lock Quarry with location of samples marked (Coogan *et al.* 1981).	22
Figure 2.21:	Composite photograph of Williams County Core showing where samples were taken.	23
Figure 2.22:	Location map of the Williams County Core, Superior Township, Williams County, Ohio.	23

Figure 2.23:	Geological setting of the Dinant Basin (after Helson 1995)	27
Figure 2.24:	Location map and geology of Villers Sur Lesse area (after Forir, 1900)	27
Figure 2.25:	Sketch of section exposed along the abandoned railway line at Villers Sur Lesse (Sartenaer (1956) in Martin (1981)).	28
Figure 2.26:	Sample V4	28
Figure 2.27:	Sample V5	28
Figure 2.28:	Sample V7	28
Figure 2.29:	Sample V8	28
Figure 2.30:	Exposures of pre-Permian rocks within the six zones of the Iberian Massif (Dallmeyer *et al.* 1990).	29
Figure 2.31:	Geographical location of Geras de Casares, Cantabrian Mountains.	29
Figure 2.32:	Location map and geology of the area around Geras de Casares (after Alonso *et al.* 1990).	31
Figure 2.33:	Generalised stratigraphy of the south western part of the Cantabrian Cordillera drawn to approximate scale (Wallace 1972).	31
Figure 2.34:	Geographical location of the Cwrt-yr-ala borehole, Wales.	33
Figure 2.35:	Dinantian palaeogeography of the area surrounding the Cwrt-yr-ala borehole (after Woodcock *et al.* 2000).	33
Figure 2.36:	Location map and geology of the area around the Cwrt-yr-ala borehole (after Davies *et al.* 1991)	35
Figure 2.37:	Log of the Cwrt-yr-ala borehole showing the location of Sample Wales 1 (McNestry 1989)	35
Figure 2.38:	Geographical location of the Sierra de Perijá, Venezuela	37
Figure 2.39:	Geological setting of the Sierra de Perijá, Venezuela (after Forero Suarez 1990)	37
Figure 2.40:	Devonian outcrop exposed in the Sierra de Perijá, Venezuela (after Harvey 2001)	38
Figure 2.41:	Location of samples used in this project (after Harvey 2001)	38
Figure 2.42:	Sedimentary log for the Upper Member of the Campo Chico formation, *Archaeopteris* locality (Harvey 2001).	39
Figure 2.43:	Sedimentary log for the Upper Member of the Campo Chico formation, Caño Colorado del Sur (Harvey 2001).	39
Figure 2.44:	Simplified lithostratigraphic correlation of the uppermost Silurian and Ordovician of Jordan and neighbouring areas (Lüning *et al.* 2005).	40
Figure 2.45:	Geological setting of the wells used in this project (After Lüning *et al.* 2005)	42
Figure 2.46:	Diagramatic log of well RH-3 showing location of samples taken.	43
Figure 2.47:	Diagramatic log of well WS-6 showing location of samples taken.	43

Figure 3.1:	Diagram showing the stages of vitrinite evolution in relation to the timing of hydrocarbon generation and coal rank (McCaughan 2002, Teichmüller 1987).	48
Figure 3.2a:	Schematic representation of procedure used to make cold resin blocks	53
Figure 3.2b:	Schematic representation of procedure used to make palynological resin sections	53
Figure 3.3:	Schematic diagram of image analysis system used to measure vitrinite reflectance in this study (Modified from McCaughan 2002)	56
Figure 3.4:	Vitrinite grain in transmitted light with characteristic brown stripes. View of vitrinite grain under reflected light.	59
Figure 3.5:	Flow chart of the process for choosing vitrinite grains suitable for reflectance determinations.	58
Figure 3.6:	Chitinozoa in transmitted light and reflected light.	59
Figure 3.7:	Chitinozoa (R_r%) reflectance vs. Vitrinite Reflectance (R_r%) from Tricker *et al.* (1992).	62
Figure 4.1:	Correlation of various thermal maturity indicators after Legall *et al.* (1981) and Williams *et al.* (1998)	72
Figure 4.2:	Sample labels were placed on the right of each strewn slide	73
Figure 4.3a:	Green intensity vs. red intensity of four *Veryhachium* specimens under different lighting conditions.	75
Figure 4.3b:	Four *Veryhachium* specimens used to asses the suitability of a range of lighting conditions.	75
Figure 4.4:	Diagram showing the microscope and camera settings used in this study (After McCaughan 2002).	77
Figure 4.5:	Schematic diagram of Leitz Wetzlar Dialux 20 Microscope showing position of colour 'standard', a Cokin photographic filter.	78
Figure 4.6a:	Image Setup	80
Figure 4.6b:	Colour Detect	80
Figure 4.6c:	Binary Edit	81
Figure 4.6d:	Measure Feature	81
Figure 4.7:	Guidelines of how the RGB determinations of *Veryhachium* specimens with variable surface features were determined. Also diagram showing a *Tasmanites* specimen with its thinnest fold in focus and its wall in focus.	83
Figure 4.8:	Flow chart showing each step used in calibrating RGB data of acritarchs collected during one session.	84
Figure 4.9:	Photomicrograph showing *Tasmanites* specimen surrounded by amorphous organic material (AOM).	86
Figure 4.10:	*Veryhachium* specimen.	87
Figure 4.11:	*Tasmanites* specimen.	86
Figure 4.12:	*Veryhachium* specimen in transmitted light and fluorescing in ultra violet light.	86

Figure 5.1:	Plot showing the spread of RGB data for the Cokin photographic filters, with the name of each 'standard' attached.	89
Figure 5.2:	Schematic diagram of Leitz Wetzlar Dialux 20 Microscope showing position of colour 'standard', a Cokin photographic filter.	89
Figure 5.3:	Mean red intensities and standard deviations of 'standards' used in this project.	91
Figure 5.4:	Mean green intensities and standard deviations of 'standards' used in this project.	92
Figure 5.5:	Mean blue intensities and standard deviations of 'standards' used in this project.	93
Figure 5.6:	Diagram showing the 11 'standards' used in this study.	94
Figure 5.7:	Red intensity of two different sets of Cokin filters, measured on the same setup at the same time.	95
Figure 5.8:	Green intensity of two different sets of Cokin filters, measured on the same setup at the same time.	95
Figure 5.9:	Blue intensity of two different sets of Cokin filters, measured on the same setup at the same time.	95
Figure 5.10:	*Veryhachium* specimens (1-6) from sample TL3 used to test variations in RGB determinations	97
Figure 5.11:	*Veryhachium* specimens (7-12) from sample TL3 used to test variations in RGB determinations	98
Figure 5.12:	*Veryhachium* specimens (13-17) from sample TL3 used to test variations in RGB determinations	99
Figure 5.13:	Daily 'standard' red intensities, grouped in six month intervals, plotted against the red intensities of the Cokin filters measured at the beginning of the study.	100
Figure 5.14:	Daily 'standard' green intensities, grouped in six month intervals, plotted against the green intensities of the Cokin filters measured at the beginning of the study.	101
Figure 5.15:	Daily 'standard' blue intensities, grouped in six month intervals, plotted against the blue intensities of the Cokin filters measured at the beginning of the study.	102
Figure 5.16:	Red Intensity data gathered on the 18th October 2004 vs. red intensity data gathered on the same specimens on the 15th November.	104
Figure 5.17:	Green Intensity data gathered on the 18th October 2004 vs. green intensity data gathered on the same specimens on the 15th November.	105
Figure 5.18:	Blue Intensity data gathered on the 18th October 2004 vs. blue intensity data gathered on the same specimens on the 15th November.	106
Figure 5.19:	Red intensity determinations of seventeen *Veryhachium* specimens made by the author vs. red intensity determinations of the same seventeen *Veryhachium* made by different novice operators.	109
Figure 5.20:	Green intensity determinations of seventeen *Veryhachium* specimens made by the author vs. green intensity determinations of the same seventeen *Veryhachium* made by different novice operators.	110
Figure 5.21:	Blue intensity determinations of seventeen *Veryhachium* specimens made by the author vs. blue intensity determinations of the same seventeen *Veryhachium* made by different novice operators.	111

Figure 5.22:	Screen shot of Adobe Photoshop CS window showing use of the circular marquee to select a suitable area on the *Veryhachium* specimen on which to make a colour determination.	113
Figure 5.23:	Red Intensity determinations made on 15 *Veryhachium* specimens using Adobe Photoshop CS vs. red intensity determinations made on the same images of the *Veryhachium* specimens using the Qwin image analysis system.	114
Figure 5.24:	Green Intensity determinations made on 15 *Veryhachium* specimens using Adobe Photoshop CS vs. green intensity determinations made on the same images of the *Veryhachium* specimens using the Qwin image analysis system.	115
Figure 5.25:	Blue Intensity determinations made on 15 *Veryhachium* specimens using Adobe Photoshop CS vs. blue intensity determinations made on the same images of the *Veryhachium* specimens using the Qwin image analysis system.	116
Figure 5.26:	Red Intensity determinations made on the original set of Cokin photographic filters using the Leica/Qwin system vs. red intensity determinations made using the Nikon/Lucia system.	120
Figure 5.27:	Green Intensity determinations made on the original set of Cokin photographic filters using the Leica/Qwin system vs. green intensity determinations made using the Nikon/Lucia system.	121
Figure 5.28:	Blue Intensity determinations made on the original set of Cokin photographic filters using the Leica/Qwin system vs. blue intensity determinations made using the Nikon/Lucia system.	122
Figure 5.29:	Red Intensity determinations made on 13 *Veryhachium* specimens using the Nikon/Lucia system vs. red intensity determinations made on the same specimens using the Leica/Qwin system.	123
Figure 5.30:	Green Intensity determinations made on 13 *Veryhachium* specimens using the Nikon/Lucia system vs. green intensity determinations made on the same specimens using the Leica/Qwin system.	124
Figure 5.31:	Blue Intensity determinations made on 13 *Veryhachium* specimens using the Nikon/Lucia system vs. blue intensity determinations made on the same specimens using the Leica/Qwin system.	125
Figure 6.1:	Idealised histogram of an indigenous vitrinite/chitinozoa population plotting reflectance against frequency.	127
Figure 6.2:	Idealised histogram of data set that contains an indigenous and caved population.	127
Figure 6.3:	Idealised histogram of data set that contains an indigenous and reworked population.	127
Figure 6.4:	Example of reworked vitrinite that was selected and removed from sample TL1 on the basis of a bimodal histogram.	128
Figure 6.5:	Examples of anomalous calibrated RGB intensities and photomicrographs of the specimens in question.	129
Figure 6.6:	Idealised histogram of the red, green and blue intensities of an indigenous population.	131
Figure 6.7:	Idealised histogram of the red, green and blue intensities of an indigenous and caved population.	131
Figure 6.8:	Idealised histogram of the red, green and blue intensities of an indigenous and reworked population.	131

Figure 6.9:	Examples of *Tasmanites* taken from three samples, showing the variation in colour and size that can be found in a single sample.	133
Figure 6.10:	Previously published plot of wall thickness against maximum diameter of *Tasmanites* specimens.	134
Figure 6.11:	Plot of red body intensity against diameter for individual *Tasmanites* specimens.	135
Figure 6.12:	Plot of red fold intensity against diameter for individual *Tasmanites* specimens.	135
Figure 6.13:	Plot of green body intensity against diameter for individual *Tasmanites* specimens.	136
Figure 6.14:	Plot of green fold intensity against diameter for individual *Tasmanites* specimens.	136
Figure 6.15:	Plot of blue body intensity against diameter for individual *Tasmanites* specimens.	137
Figure 6.16:	Plot of blue fold intensity against diameter for individual *Tasmanites* specimens.	137
Figure 6.17:	Average red intensity of *Veryhachium* specimens within a sample vs. average vitrinite reflectance of the same sample.	139
Figure 6.18:	Average red intensity of *Veryhachium* specimens within a sample vs. average vitrinite reflectance of the same sample.	139
Figure 6.19:	Average green intensity of *Veryhachium* specimens within a sample vs. average vitrinite reflectance of the same sample.	140
Figure 6.20:	Average green intensity of *Veryhachium* specimens within a sample vs. average vitrinite reflectance of the same sample.	140
Figure 6.21:	Average blue intensity of *Veryhachium* specimens within a sample vs. average vitrinite reflectance of the same sample.	141
Figure 6.22:	Average blue intensity of *Veryhachium* specimens within a sample vs. average vitrinite reflectance of the same sample.	141
Figure 6.23:	Average RGB intensity of a sample against the standard deviation of each intensity for that sample.	144
Figure 6.24:	Plot used to determine the relative reliability of vitrinite reflectance equivalent values calculated from RGB intensities.	144
Figure 6.25:	Average *Veryhachium* green intensity against average *Veryhachium* red intensity of all samples studied in this project.	146
Figure 6.26:	Average blue *Veryhachium* intensity against average green *Veryhachium* intensity of all samples studied in this project.	147
Figure 6.27:	Average blue *Veryhachium* intensity against average red *Veryhachium* intensity of all samples studied in this project.	148
Figure 6.28:	Average blue *Veryhachium* intensity against average green *Veryhachium* intensity.	149
Figure 6.29:	Average blue *Veryhachium* intensity against average green *Veryhachium* intensity.	149
Figure 6.30:	Approximate correlation of a range of thermal maturity indicators based mainly on a correlation by Schwab (1995) (published in Batten 1996).	151
Figure 6.31:	Photomicrographs of degraded *Veryhachium* specimens unsuitable for RGB colour determinations.	153

Figure 6.32:	Photomicrograph of *Veryhachium* and *Unellium* from sample TL3 demonstrating the range in colour between different acritarchs in the same sample.	153
Figure 7.1:	Simplified map of Jordan showing the main features of the area and the location of the Risha Gas Field (Beydoun *et al.* 1994)	156
Figure 7.2:	Simplified cross section of the north east Jordan, where the Risha Gas Field is located (Beydoun *et al.* 1994)	156
Figure 7.3:	Lithostratigraphic column of the Risha area, north east Jordan (Beydoun *et al.* 1994).	157
Figure 7.4:	Average green *Veryhachium* intensity versus average red *Veryhachium* intensity for all sample investigated from well RH-3, Jordan.	169
Figure 7.5:	Average blue *Veryhachium* intensity versus average red *Veryhachium* intensity for all sample investigated from well RH-3, Jordan.	170
Figure 7.6:	Average blue *Veryhachium* intensity versus average green *Veryhachium* intensity for all sample investigated from well RH-3, Jordan.	171
Figure 7.7:	*Veryhachium* specimens from Pet 6 and Pet 9	172
Figure 7.8:	Summary of maturity data collected for well RH-3 during this project, including average RGB intensity of the *Veryhachium* of each sample plotted versus depth.	173
Figure 7.9:	Summary of maturity data collected for well RH-3 during this project, detailing the change in average red intensity with depth.	174
Figure 7.10:	Summary of maturity data collected for well RH-3 during this project, detailing the change in average green intensity with depth.	175
Figure 7.11:	Summary of maturity data collected for well RH-3 during this project, detailing the change in average blue intensity with depth.	176
Figure 7.12:	Distribution of the red intensity values of *Veryhachium* in Bolivia 3.	179
Figure 7.13:	Distribution of the green intensity values of *Veryhachium* in Bolivia 3.	179
Figure 7.14:	Distribution of the blue intensity values of *Veryhachium* in Bolivia 3.	179
Figure 7.15:	Average green intensity of *Veryhachium* specimens in Bolivia 3 versus average red intensity.	180
Figure 7.16:	Average blue intensity of *Veryhachium* specimens in Bolivia 3 versus average red intensity.	181
Figure 7.17	Average blue intensity of *Veryhachium* specimens in Bolivia 3 versus average green intensity.	182

LIST OF TABLES

Table 2.1:	Details of outcrop samples used in this project.	44
Table 2.2:	Details of well samples used in this project.	45
Table 3.1:	Standards used for reflectance microscope calibration.	57
Table 4.1:	Relative use of colour of different microfossil groups to assess thermal maturity (Marshall 1990).	63
Table 4.2:	Notable events in *Tasmanites* research (After Muir *et al.* 1971).	69
Table 5.1:	List of 30 RGB determinations, made on three of the nine Cokin 'standards'.	90
Table 5.2:	Raw data collected by the same operator, on the same specimens, the same Leica/Qwin system on two different days.	107
Table 5.3:	Corrected data collected by the same operator, on the same specimens, the same Leica/Qwin system on two different days.	107
Table 5.4:	Raw data collected by different operators, on the same specimens, on the same day and using the same Leica/Qwin system.	108
Table 5.5:	Raw data collected by the same operator, on the same specimens, from the same images using the Qwin image analysis program and Adobe Photoshop® CS.	112
Table 5.6:	Raw data collected by the same operator, on the same specimens using the Leica/Qwin system and the Nikon/Lucia System.	118
Table 5.7:	Corrected data collected by the same operator, on the same specimens using the Leica/Qwin system and the Nikon/Lucia System.	118
Table 6.1:	R^2 value of the linear trend lines extrapolated for each intensity plotted against vitrinite reflectance.	142
Table 6.2:	Data table of samples with degraded *Veryhachium* (N = number of readings).	145
Table 7.1:	Details of Sample P12 provided by Petrel Resources plc.	163
Table 7.2:	Details of average red, green and blue intensities of *Veryhachium* in sample P12.	163
Table 7.3:	Details of Sample P13 provided by Petrel Resources plc.	164
Table 7.4:	Details of average red, green and blue intensities of *Veryhachium* in sample P13.	164
Table 7.5:	Details of Sample P11 provided by Petrel Resources plc.	165
Table 7.6:	Details of average red, green and blue intensities of *Veryhachium* in sample P11.	165
Table 7.7:	Details of Sample Pet3 provided by Petrel Resources plc.	166
Table 7.8:	Details of average red, green and blue intensities of *Veryhachium* in sample Pet3.	166
Table 7.9:	Details of Sample Pet6 provided by Petrel Resources plc.	167
Table 7.10:	Details of Sample Pet9 provided by Petrel Resources plc.	167

CHAPTER 1
INTRODUCTION

1.1. THE NEED FOR A NEW THERMAL MATURITY INDICATOR

1.1.1. INTRODUCTION

Microscopic organic matter is altered with increasing burial (Staplin 1969, Hart 1986, Marshall 1990). As temperature increases, oxygen and hydrogen in the material are lost relative to carbon (Staplin 1969, Marshall 1990, Taylor *et al.* 1998). This process affects the physical properties of organic matter like colour, reflectivity, and fluorescence as well as the chemical properties of the substance (Cooper 1978, Hart 1986, Marshall 1990). These changes in resistant insoluble organic matter, or kerogen, can be used as indicators of thermal maturity (Staplin 1969, Cooper 1978).

1.1.2. MAIN ORGANIC THERMAL MATURITY INDICATORS

Vitrinite reflectance is the industry standard for assessing thermal maturity (Morrow *et al.* 1993, Wilkins *et al.* 1995, Taylor *et al.* 1998). It is based on the increase in reflectance of the surface of polished vitrinite particles (fossil woody material) with maturity (Stach *et al.* 1982, Ward 1984, Marshall 1990, Taylor *et al.* 1998). This parameter is reported as the percentage of incident light reflected from a polished surface of vitrinite (Stach *et al.* 1982, Ward 1984, Taylor *et al.* 1998) denoted by the symbol $\%R_r$ (see section 3.1.2.). Its widespread application is due to a number of factors, including the relatively objective analytical nature of the method compared to visual estimation of palynomorph colour (Cooper 1978). Determination of vitrinite reflectance is generally swift and inexpensive. Vitrinite grains are found, in varying proportions, in a range of sedimentary rocks from coals to shales to mudstones (Staplin 1969, Marshall 1990, Taylor *et al.* 1998).

Like all techniques, there are limitations associated with the determination of vitrinite reflectance. User experience is fundamental to correctly identifying vitrinite grains in polished blocks with misidentification resulting in anomalously high or low readings (Dow 1982). Determinations must be screened for caved or reworked populations so that only

the reflectance of the indigenous vitrinite grain population is reported (Heroux *et al.* 1979, Dow 1982). Application of the technique is restricted to sediments that contain vitrinite grains. Vitrinite originates from woody tissues of roots, stems, barks and leaves composed of cellulose and lignin (International Commission on Coal Petrology (I.C.C.P.), 1994). It is absent from most Lower Palaeozoic successions, only appearing from the Late Silurian onwards (Tricker *et al.* 1992). Since vitrinite is derived from terrestrial sources, it can be rare or absent from post Silurian marine successions.

Spore and pollen colour is perhaps the second most important thermal maturity indicator after vitrinite reflectance (Marshall 1990). Many numerical scales have been produced to describe spore colour including Staplin's 'Thermal alteration index' (1969), Robertson Research's 'Spore colour index' (1980), Pearson's 'Pollen/spore colour 'standard'' (1984) and Batten's 'Thermal alteration scale' (1981, 1996). While the use of spore colour as a thermal maturity indicator is economical and fast, it relies on visual estimation of colour, which is known to vary between users (Batten 1981). The issue of microscope illumination is also important. Images depicting Batten's 'Thermal Alteration Scale' (1996) clearly show a range of different background illuminations, which must affect the perceived colour of the organic matter.

The fluorescence of spores and pollen is also used in maturity studies. Under ultra violet light, spores and pollen fluoresce until the floor of the oil window is reached (1.2 – 1.35%R_r) (van Gijzel 1982). Spores are found in Silurian to recent sediments (Marshall 1990) and in rare Ordovician occurrences. Like vitrinite, they are terrestrial in origin, and so their abundance generally diminishes with increasing distance from the palaeo-shoreline.

Conodont colour is also a commonly used thermal maturity indicator. The 'Conodont Alteration Index' (Epstein *et al.* 1977) covers a larger temperature range than most organic indicators (<50°C to >600°C) (Rejebian *et al.* 1987). These microfossils are composed of phosphate which generally restricts their recovery to carbonate rocks and low rank shales (Marshall 1990). They are found in Cambrian to Triassic marine sediments although their abundance varies considerably (Epstein *et al.* 1977, Rejebian *et al.* 1987).

Chitinozoa reflectance uses the same preparation procedure and measuring apparatus as vitrinite reflectance. It is a measure of the reflectance of the polished surface of the flask

or bottle shaped enigmatic organic walled marine microfossil (Tricker *et al.* 1992). Unlike the difficulties associated with correct identification of vitrinite particles, the distinctive shape of the chitinozoa test is easily recognised (Tricker *et al.* 1992). These microfossils range from the middle Cambrian to the end of the Carboniferous (Traverse 1988). However, their effective stratigraphic range is Lower Ordovician to Upper Devonian (Tricker *et al.* 1992). Chitinozoa are found in a wide range of marine sediments in variable numbers (Tricker *et al.* 1992).

The absence of vitrinite from many Lower Palaeozoic sediments, as well as from some marine source rocks, leads to difficulties in assessing their level of thermal maturity. Spore colour and fluorescence are useful maturity indicators. However, spores can be absent from marine source rocks, and rare in Lower Palaeozoic units. Chitinozoa reflectance can be used in both of these lithologies, but only where chitinozoa are present, and not in any post Devonian sediments. Conodont colour is applicable over a large stratigraphic range and in many marine facies (Epstein *et al.* 1977). However, these microfossils are mainly recovered from carbonates and generally not recoverable from air-drilled cuttings (Epstein *et al.* 1977, Tricker *et al.* 1992). While all the maturity indicators discussed above can be applied to a wide range of geological settings and facies, there are certain units where these indicators are not applicable. It is hoped that the development of acritarch colour determination as thermal maturity indicator will help address this shortcoming.

1.2. ACRITARCHS, PRASINOPHYTES, AND THERMAL MATURITY

1.2.1. ACRITARCHS AND PRASINOPHYTES

Acritarchs are fossilised organic walled cysts of unicellular protists that cannot be assigned to any known group of organisms (Strother 1996). Generally thought to make their first appearance in the Precambrian, around 1400Ma, their maximum abundance and diversification occurs between the early Cambrian and late Devonian (Martin 1993). Like spores and pollen, acritarchs darken in colour with increasing levels of maturity (Legall *et al.* 1981, Williams *et al.* 1998). Acritarchs are mostly found in marine sediments, although non marine examples have been reported from Recent strata (Brasier 1979).

Attempts have been made to use acritarchs as thermal maturity indicators in the past (Legall *et al.* 1981, Bertrand *et al.* 1989, Williams *et al.* 1998) with varying degrees of success (see section 4.2.4.). The published scales used both the colour of a single genus (Legall *et al.* 1981) and whole assemblages (Williams *et al.* 1998) as maturity indicators. For this project, the colour of the genus *Veryhachium* was chosen as a potential maturity indicator. This genus ranges from the Cambrian to the Tertiary (Sarjeant *et al.* 1994) and is found in both proximal and distal marine settings (Strother 1996).

The prasinophyte *Tasmanites* (Martin 1993) was also chosen as a suitable palynomorph to test as a thermal maturity indicator. Often where tasmanitids are preserved, they are found in high concentrations, with few other palynomorphs present (Muir *et al.* 1971). They are known to range from the Cambrian and abundant specimens are preserved in the Permian tasmanite deposits of Tasmania and Jurassic of Alaska (Revill *et al.* 1994). They are associated with shallow marine and brackish environments (Taugourdeau-Lantz 1979). A stratigraphic range chart of the major organic thermal maturity indicators is shown in Figure 1.1, including with the reported ranges of *Veryhachium* and *Tasmanites.*

1.2.2. CORRELATION OF PALYNOMORPH COLOUR AND THERMAL MATURITY

As previously noted, the industry standard for assessing thermal maturity is vitrinite reflectance. In order to correlate *Veryhachium* and *Tasmanites* colour with specific levels of thermal maturity, sediments were collected that contained ample amounts of the selected palynomorphs as well as indigenous vitrinite grains. By determining the colour of the microfossils, as well as measuring the reflectivity of the coexisting polished vitrinite grains, the colour of the palynomorphs could be calibrated against a known thermal maturity scale.

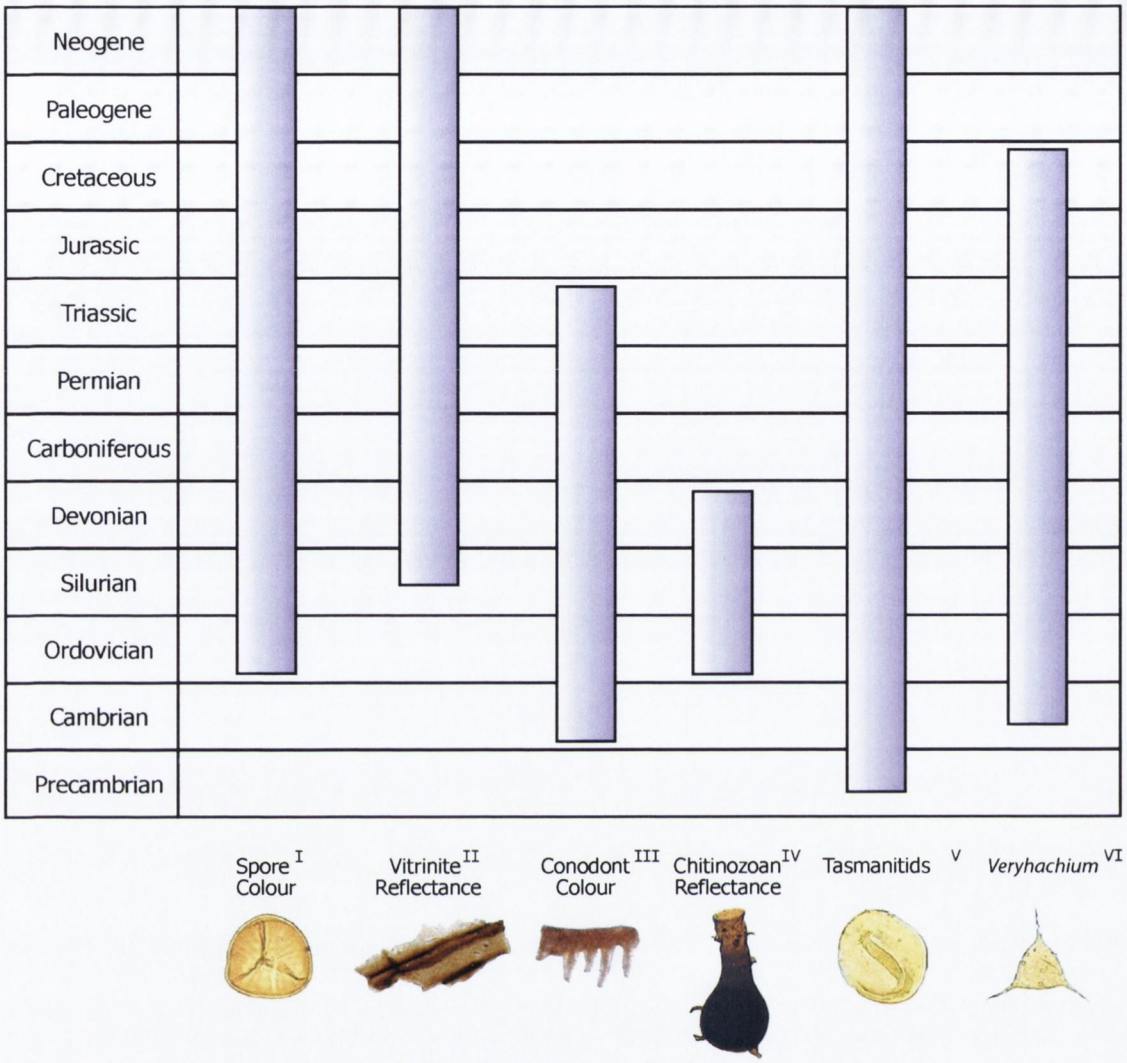

Figure 1.1: Stratigraphic range chart of the major organic thermal maturity indicators together with the overall ranges of *Veryhachium* and *Tasmanites*.

I. Playford *et al.* (1996)
II. Traverse *et al.* (1988)
III. Epstein *et al.* (1977)
IV. Miller (1996)
V. Guy-Ohlson (1996)
VI. Sarjeant *et al.* (1994)

Conodont element image from Epstein *et al.* (1977).

1.3. ASSESMENT OF PALYNOMORPH COLOUR

1.3.1. VISUAL ESTIMATION

Traditionally, assessment of palynomorph colour has been based on visual estimation (Batten 1981, Staplin 1982). A number of indices, charts, and standard sets have been produced to attempt to standardise colour determination; these include publications by Pearson (1984) and Batten (1996). In spite of these charts and the recommendations of how colour should be estimated (Staplin 1982), the technique is still highly subjective and results vary from operator to operator (Yule *et al.* 1998). Nevertheless, Batten (1981) estimated that operator error accounted for no more than half a point variation on his seven point scale. In addition, all colour scale divisions have arbitrary boundaries imposed on a continuum of colour (Marshall 1991). Although numeric values are attached to classes within these scales, they can not be plotted on graphs, or statistically analysed as the intervals have been arbitrarily selected. For example, for any given index, the relationship between colour 2 and colour 3 is not necessarily the same as the relationship between colour 3 and colour 4. Because of the subjectivity related to visual estimation, one of the aims of this project was to use image analysis techniques to determine *Veryhachium* and *Tasmanites* colour.

1.3.2. IMAGE ANALYSIS

The colour of palynomorphs studied during this project was determined using an image analysis system. Images of *Veryhachium* and *Tasmanites* specimens were captured using a colour video camera and analysed using a computer program (see section 4.3.2.). The colour was reported in terms of red, green and blue intensity (RGB). The value of each intensity ranges from 0 to 255, and the system can define 16.7 million different colours (Yule *et al.* 1998). The system used is similar to that applied to spores by Yule *et al.* (1998) but this is thought to be the first application of the technique to acritarchs and prasinophytes.

The clear advantage of using an image analysis system to describe colour, rather than visual estimation, is the marked reduction in the subjectivity of results. While there is still

a degree of variation amongst users, over which area of a palynomorph is sampled, it is a significant improvement on traditional methods. Also, the description of colour in terms of three numerical variables allows for the statistical analysis of results as well as the possibility of plotting different intensities against each other.

The main disadvantage of the RGB image analysis technique is that the system is device dependent (pers. comm Fairchild 2005, Munsell Colour Science Laboratory). RGB determinations made on the same palynomorph will vary from set-up to set-up, depending on the different cameras, light sources, and image analysis programs used. To compensate for this discrepancy, an attempt was made to find a suitable material that could be used as a 'standard' to calibrate different systems.

1.4. CASE STUDIES

Once the colour of *Veryhachium* and *Tasmanites* had been established as a thermal maturity indicator, it was applied to two different geological problems. Samples provided by Petrel Resources plc from the Risha Gas Field, Jordan, were investigated to test if the technique could correctly identify the maturity of a selected succession. Originally it was intended that a maturity case study would be carried out on samples provided by the Petroleum Affairs Division of the Irish Government from the Irish offshore succession. However, these samples, proved unsuitable, lacking any *Veryhachium* or *Tasmanites* specimens. A sample that was known to contain reworked *Veryhachium* from the Itacua Formation, Bolivia, was also examined to determine if RGB colour determinations could correctly identify a reworked population.

CHAPTER 2
SAMPLES

2.1. SAMPLE REQUIREMENTS

2.1.1. GEOLOGICAL SETTING

The fundamental requirement for samples used in this project was that they must contain sufficient amounts of acritarchs to allow their colour to be determined, and sufficient amounts of vitrinite to determine reflectance. Acritarchs were much more abundant in the Lower Palaeozoic than the Upper Palaeozoic, with the Devonian / Carboniferous boundary marking a major decline in their numbers (Martin 1993). Significant quantities of vitrinite (fossil woody material) are only found in post Silurian sediments (Tricker *et al.* 1992). The geological record of vitrinite and acritarchs restricts the range of suitable samples to the mid to late Devonian Period, before acritarch numbers decline at the Devonian/ Carboniferous boundary and after the first appearance of vitrinite particles in the record.

Suitable rock units are not only temporally restricted, they also are spatially limited. They must have been fed by two sources of sediment. Vitrinite grains originate from land plants and so suitable sediments must have some terrestrial input. *Veryhachium* and *Tasmanites*, the two microfossils whose colour was measured in this project, are both marine in origin and so there must also be a marine source of sediment in addition to the terrestrial detritus. The most likely environment for this type of sediment to be deposited is a near-shore setting.

It is impossible to determine the productivity of a sample without simply processing it. In general, palynomorphs tend to be sparse or absent in well sorted sandstones and clays. Deltaic siltstones and shales are often productive (Traverse 1988) and were sampled for this project. Both outcrop and core samples were used.

Sediments that were heated due to burial rather than proximity to igneous bodies were preferred. It was decided that samples should reflect 'source kitchen' conditions as the technique, if shown to work, would most likely be applied to sediments found in this type of geological setting.

2.1.2. Vitrinite Proxies

In some samples, no vitrinite grains were present but chitinozoa were observed. While the preference was to compare actual vitrinite reflectance results with colour determinations this was not always possible. Where chitinozoa were present, their reflectance was be used as a proxy for vitrinite reflectance using an equation derived by Tricker *et al.* (1992).

2.2. SAMPLING

2.2.1. Unsuccessful Samples

Several areas were sampled unsuccessfully during this project. Kimmeridgian sections from the Irish offshore were sampled from cores and cuttings held in the Petroleum Affairs Division Core Store. Most samples were dominated by amorphous organic material and no vitrinite or acritarchs were recorded. Samples were investigated from two boreholes in the Bowen Basin, Australia that were sampled by Geoff Playford and John McKellar. While these samples were extremely productive, neither *Veryhachium* nor *Tasmanites* were observed.

Upper Devonian samples from cores from the Holy Cross Mountains, Poland, were supplied by Monica Masiak but did not contain suitable material. Samples from borehole Carlow DH1, Ireland also provided no useful palynomorphs. Organic residue from the Upper Devonian Yiginli Formation, Turkey, was provided by Ken Higgs but this contained no vitrinite.

2.2.2. Successful Samples

The following section details the productive samples used in this project. A brief geological history of the setting of each sample is provided to demonstrate its burial history, in as much as was possible. Unless stated otherwise, localities are described in terms of latitude and longitude. Tables 2.1 and 2.2 at the end of this chapter summarise all samples used.

2.3. MOOSE RIVER BASIN, CANADA

2.3.1. GEOLOGICAL HISTORY

The Moose River Basin is one of two intracratonic Phanerozoic basins found on the Hudson Platform (Sanford *et al.* 1973, 1975). The Cape Henrietta Maria Arch, a northeast-trending Precambrian basement high, separates the Moose River Basin and the Hudson Bay Basin (Sanford *et al.* 1973, 1975) (Figure 2.2). Both basins are thought to be the remnants of once extensive cratonic cover that connected them with the Appalachian, Michigan and Williston basins to the south.

The Moose River Basin fill consists of gently dipping Ordovician, Silurian, Devonian, Late Jurassic and Lower Cretaceous rocks, up to a maximum thickness of 2,500ft (McGregor *et al.* 1976). It contains early to late Devonian sediments deposited in mainly shallow marine to supratidal conditions (Playford 1977) which are found mainly in northern Ontario (Sanford *et al.* 1975).

A sample from the Kwataboahegan Formation was used in this study. The formation is dominated by massive and thick bedded coral limestones with abundant body fossils recorded. Its age appears to be early Middle Devonian, ranging from late Emsian at its base to Eifelian (McGregor *et. al* 1976). Its contact with the underlying Stooping River Formation ranges from sharp, possibly disconformable (Sanford *et al.* 1975) to apparently conformable towards the centre of the basin (Playford 1977, McGregor *et al.* 1976). These authors suggested there may be relatively little break between the deposition of the two formations.

Deposition in the basin continued throughout the Devonian, but with the withdrawal of the Catskill Sea during the late Devonian, the basin was subjected to renewed uplift at periodic intervals (Bezys *et al.* 1990). During the Upper Jurassic/ Lower Cretaceous, ultramafic dykes and sills were intruded into Devonian sediments on the southern edge of the Moose River Basin (Sanford *et al.* 1975). Two major periods of uplift and erosion have been identified during the Mesozoic and attributed to the activity of the Great Meteor and Island hotspots (Hanne *et. al* 2004). Jurassic sediments are found locally overlying Devonian strata. Terrestrial Cretaceous sediments rest mainly unconformably, on the Upper

Famennian Long Rapids Formation (Sanford *et al.* 1990). The area is capped by Neogene sediments, and is still subject to glacial rebound following melting of the Laurentide ice sheet (Hanne *et al.* 2004).

2.3.2. Sample Details

A sample of the Kwataboahegan Formation was taken from the Ontario Department of Mines Campbell Lake drill hole, also know as the Sanborn Tp drill hole 1 (Figures 2.1, 2.3 and 2.4) [50°14'30"N, 80°09'30"W]. The core is stored by the Ontario Geological Survey in the Timmins Drill Core Library and was kindly sampled by Ann Wilson of the Ontario Geological Survey. A detailed core log description can be found in Sanford *et al.* (1975).

2.4. APPALACHIAN BASIN, AMERICA

2.4.1. Geological History

The Central Appalachian Foreland Basin was formed in response to overthrusts of the Taconic, Acadian and Alleghanian orogenies that resulted in subsidence (Quinlan *et al.* 1984). The basin was bounded on its eastern edge by the Appalachian Highlands and on its western edge by the Cincinnati Arch, a structural high interpreted as a forebulge (Root *et al.* 1999). This arch separates the Appalachian Basin from the Illinois and Michigan cratonic basins (Figure 2.5).

The Bedford Shale and Berea Sandstone represent the relict part of a major delta system that was active in the Appalachian Basin from Devonian times. Pepper *et al.* (1954) provide a detailed account of both of these lithologies; this is the source of the following brief account.

In Upper Devonian/ Lower Mississippian times, most sediment was deposited into the basin by the Ontario River that carried sediments from the highlands that lay to the north and north-east of the Appalachian Basin. However, an estimated 20% of sediment was supplied from eastern sources.

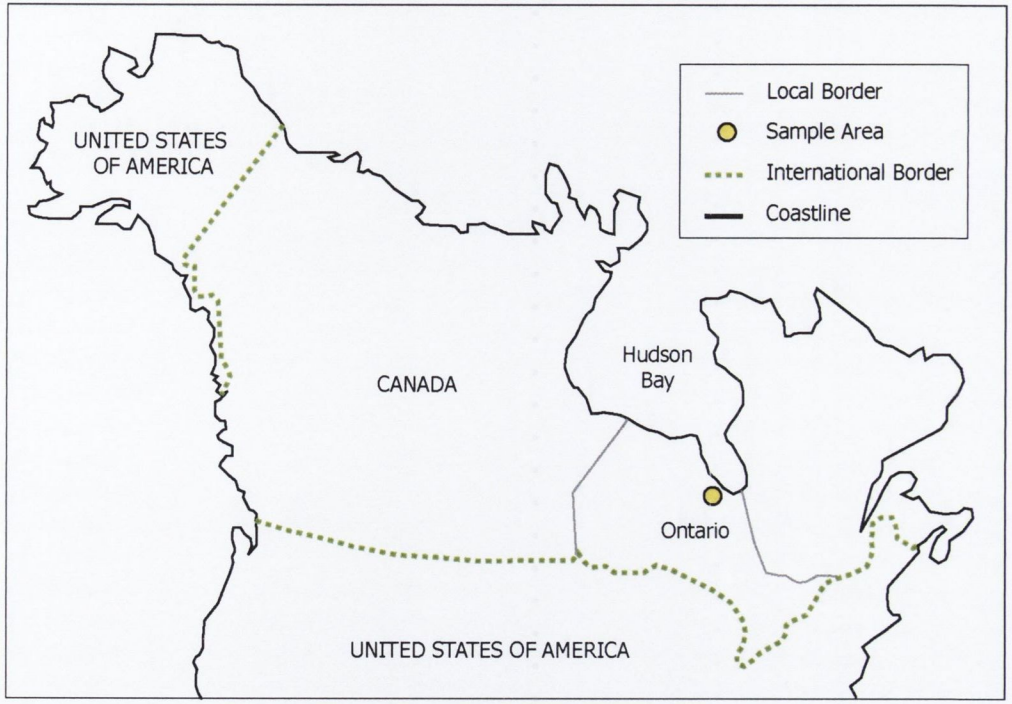

Figure 2.1: (above) Geographical location of the Ontario Department of Mines Campbell Lake Drill hole.

Figure 2.2: (right) Map showing the location of the Moose River Basin (redrawn from Sanford *et al.* (1975).

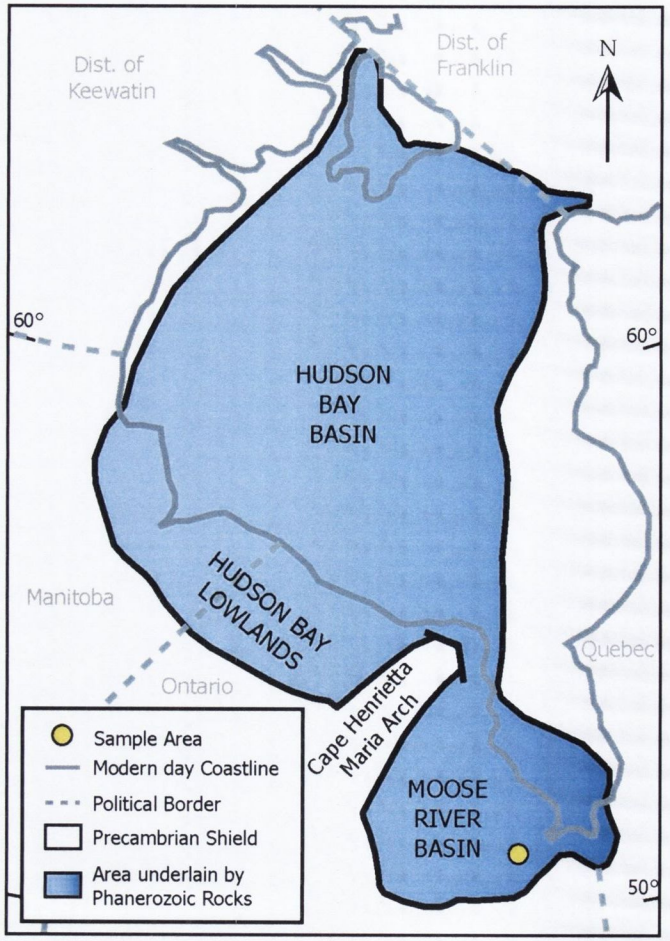

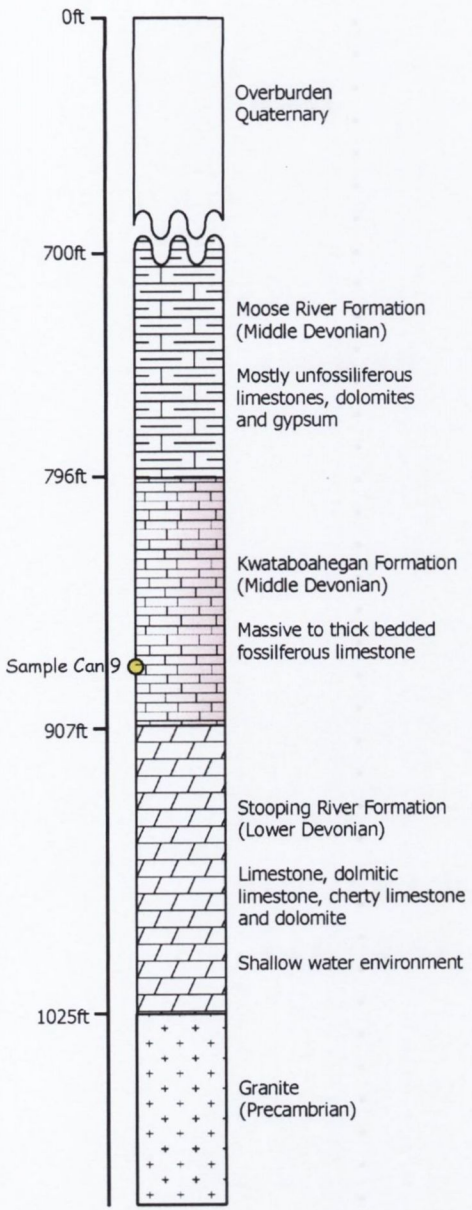

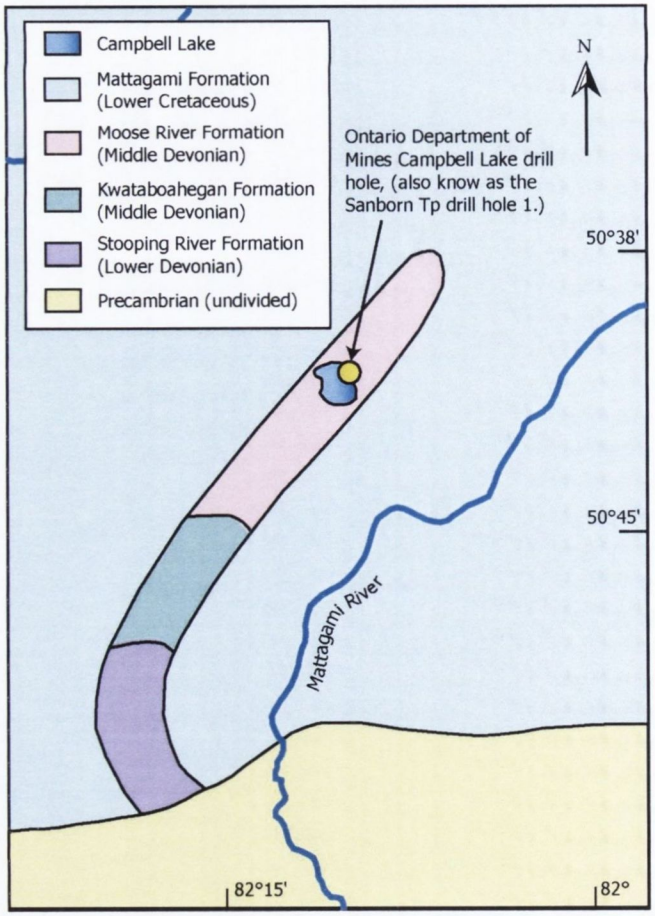

Figure 2.3: (above) Map showing the location of the Ontario Department of Mines Campbell Lake Drill hole (Sandford *et al.* 1975).

Figure 2.4: (left) Diagramatic log of the Ontario Department of Mine Campbell Lake Drill hole showing the location of sample Can. 9. Depths and contacts taken from Sandford *et al.* (1975). Additional comments from Playford (1977)

Sediment was supplied to the area mainly from the elongate Bedford Red Delta that originated on the northern shore of the basin and prograded southward into the Catskill Sea. The Bedford Shale is interpreted as the first manifestation of this delta in the record and appears conformable with the underlying Ohio Shale (Roberts *et al.* 1981). The contact between the Bedford shale and the overlying Berea Sandstone is erosional in northern Ohio with channels cut in older lithologies and filled with cross bedded sands identified in several localities (Winslow, 1962). The nature of the contact changes further south in Ohio where it becomes gradational and conformable (Molyneux *et al.* 1984). In parts of Kentucky, the Chattanooga Shale is the lateral equivalent of the Bedford Shale and Berea Sandstone (Chesnut, 1996) (Figure 2.6).

The age of the Bedford Shale has been reported as both Upper Devonian and Mississippian in the literature. A good review of previous work on the age of this lithology is found in Pashin *et al.* (1992). These authors suggest that at least the base of the Bedford shale, and possibly the entire unit is late Devonian and that the Devonian–Mississippian boundary lies either near the top of the Bedford Shale or within the Berea Sandstone.

After the deposition of the Bedford / Berea sequence, a marine transgression took place that saw the Bedford Red Delta flooded and deposition of black marls that became the Sunbury Shale. This marked the return of fully marine conditions similar to those in which the Ohio Shale had been deposited (Coleman 1991, Pepper et al. 1954). Further deposition of sands and marls continued into the Mississippian. The initial collision of the Laurentian and North African continents during the Alleghanian Orogeny occurred towards the end of the Palaeozoic. This event resulted in diachronous regional uplift, marked by an erosional unconformity on which the Lower Pennsylvanian Pottsville Sandstone rests (Root *et al.* 1999). Pennsylvanian and Permian strata deposited above the unconformity continued to be deformed by the convergence of the two continents (Root *et al.* 1999). Only limited outcrop of Permian sediments remain. However, at some stage the Permian sediments must have been thick enough to raise the rank of the underlying Pennsylvanian sediments to a high volatile bituminous level (Quinlan *et al.* 1984). Post-Pennsylvanian erosion of the Appalachian overthrusts caused flexural upwarping and uplift of the area and the subsequent erosion of much of the Permian sediments (Quinlan *et al.* 1984).

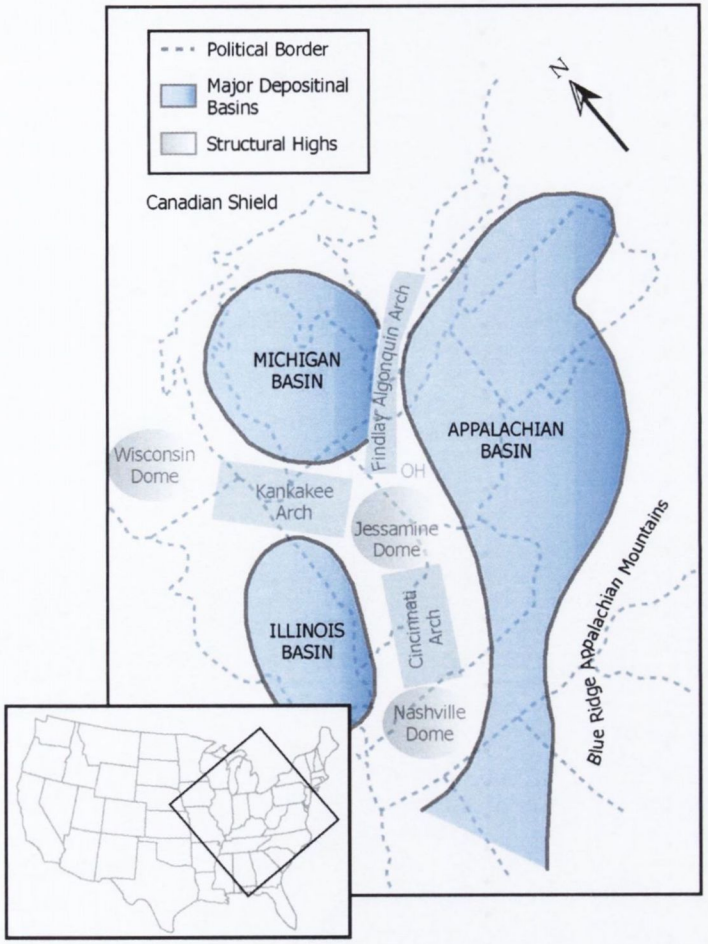

Figure 2.5: Geological outline of the Eastern Interior of the United States (Quinlan *et al.* 1984).

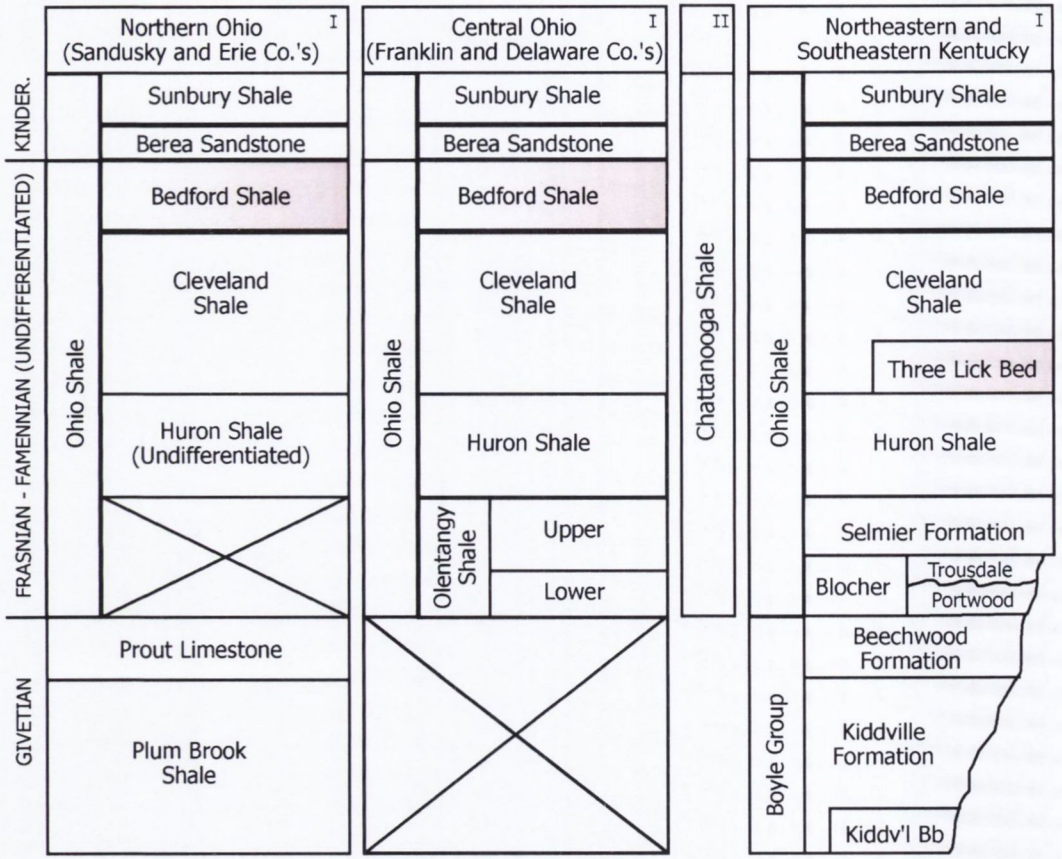

Figure 2.6: Correlation of Devonian strata in the states of Ohio and Kentucky. Samples from highlighted beds were used in this project. (I: After Conkin *et al.* 1981 II: After Chesnut 1996 (refers to parts of Kentucky).

2.4.2. Clay City Quarry

Sample CC3 was taken from the Three Licks Member of the Chattanooga Shale (Figure 2.7, 2.8 and 2.9). The section is located in Clay City, Powell County, Kentucky, [37°52'09"N, 83°56'48"W] (Figure 2.10). Full directions to this locality are given in the GSA Cincinnati 1981 Fieldtrip Guidebook, Part II, p.284. The sample was taken from the middle mudstone in the Three Lick Bed (Figure 2.11).

2.4.3. Sunbury

Samples Sun 3 and Sun 7 were taken from the Bedford Shale section that outcrops along Big Walnut Creek (Figures 2.12 and 2.13). The section is exposed on the west side of the river immediately downstream from Hartford Road Bridge (formerly Croton Road Bridge) at Sunbury, Delaware County, Ohio [40°14'46"N, 82°50'60"W] (Figures 2.14 and 2.15).

2.4.4. Three Locks Road Section

Samples TL1, TL2, TL3 and TL7 were taken from the Bedford Shale section that outcrops in an abandoned quarry near Chillicothe, Ross County, Ohio (Figures 2.16, 2.17 and 2.18). The section is exposed at the back of a property that is now a used trailer dealership (Eslea Housing), south of the intersection of State Highway 104 and United States Route 23 [39°17'26"N, 82°56'36"W] (Figures 2.19 and 2.20).

2.4.5. Williams County Core

Samples WC11, WC15 and WC17 were taken from the Bedford Shale horizon of the Williams County Core (Figure 2.21). The core was drilled by the Ohio Department of National Resources, Division of Geological Survey in the Superior Township of Williams County, Ohio (Figures 2.22 and 2.23). The location is given in the state coordinates of Ohio (North Zone) as (1,409,950/ 696,700). The core is stored by the survey in the Horace R. Collins Laboratory, Delaware, Ohio, and was sampled with the assistance of Ron Rea.

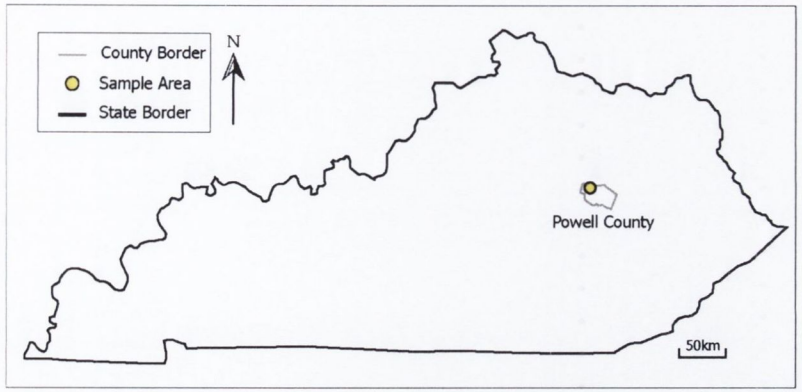

Figure 2.7: Geographical location of Clay City Quarry, Powell County, Kentucky.

Figure 2.8: Photograph of Clay City Quarry, Powell County, Kentucky, [37°52′09″N, 83°56′48″W].

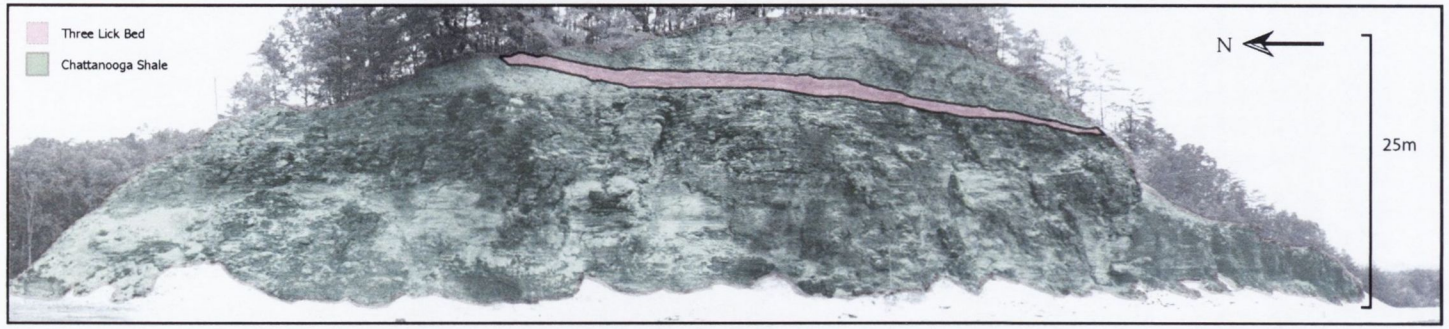

Figure 2.9: Desaturated photograph highlighting the units exposed at Clay City Quarry [37°52′09″N, 83°56′48″W].

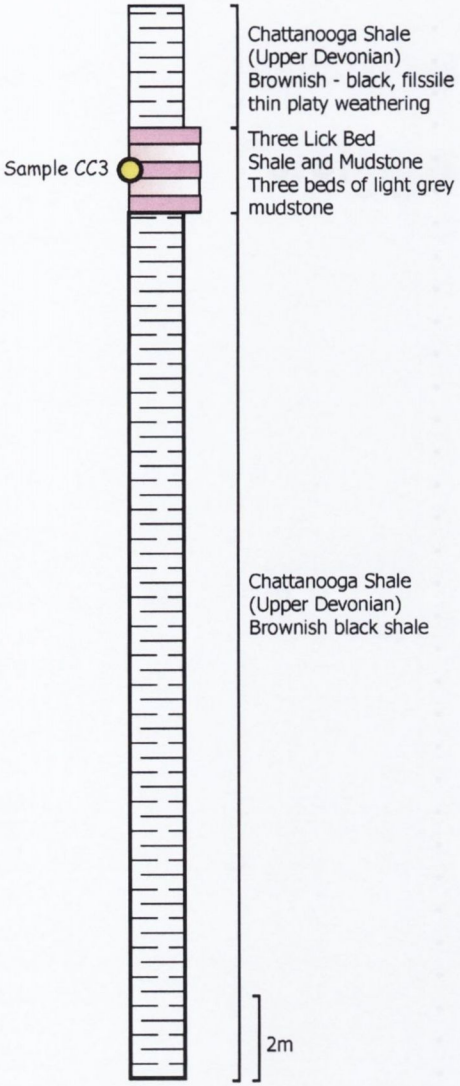

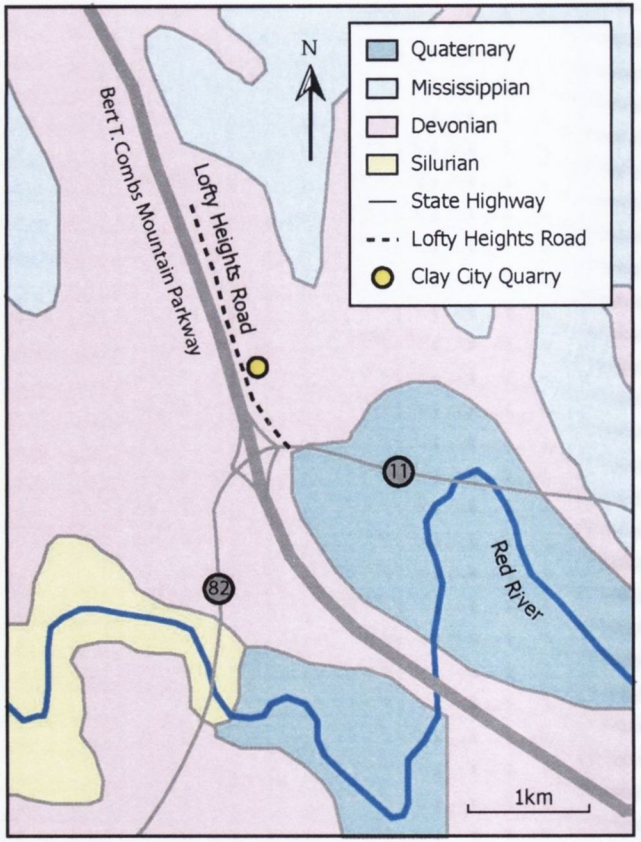

Figure 2.10: (above) Location map and geology of the Clay City Quarry Area (after Noger 1988).

Figure 2.11: (right) Diagramatic log of Clay City Quarry exposure, showing the location of sample CC3. The sample was taken from the middle 'lick' of the Three Lick Bed in the Chattanooga Shale. Additional comments from Kepferle *et al.* (1981).

Figure 2.12: Geographical location of Bedford Shale and Berea Sandstone outcrop, Sunbury, Delaware County, Ohio.

Figure 2.13: Photograph of load casts in the Berea Sandstone exposed at Sunbury, Ohio. (hammer for scale).

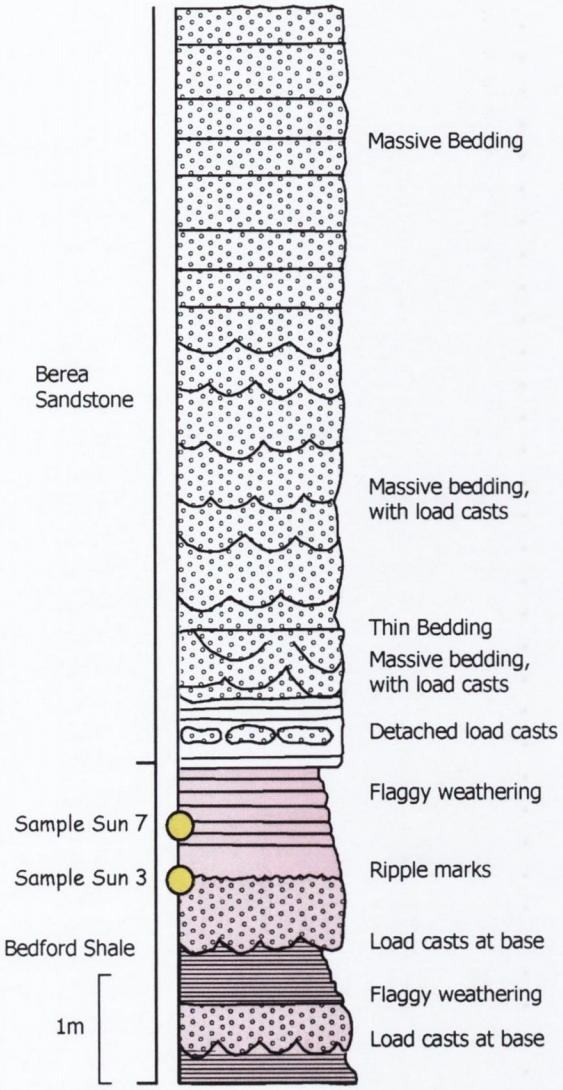

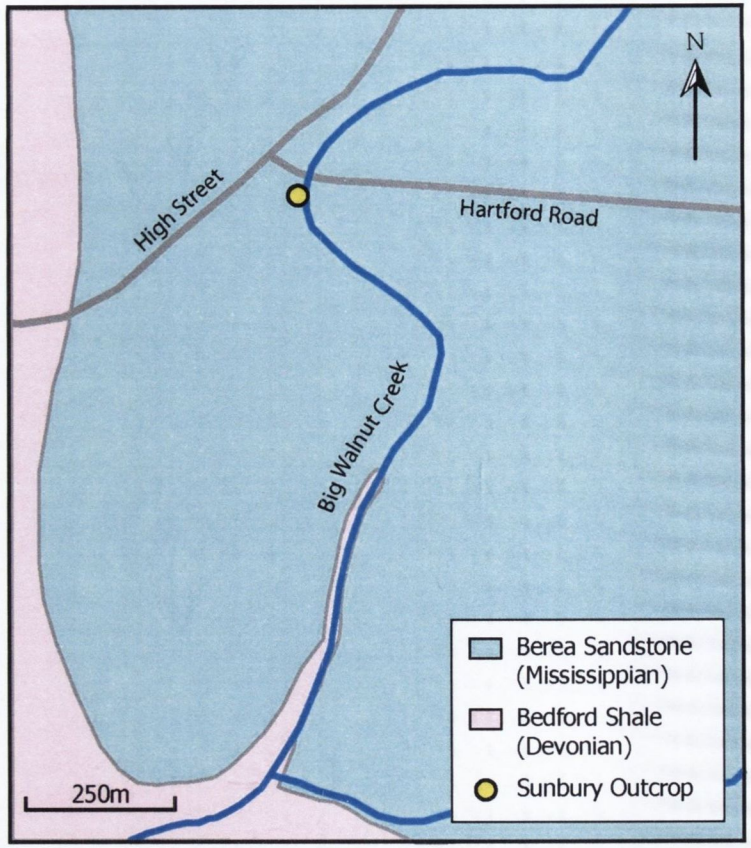

Figure 2.14: (above) Location map and geology of the Sunbury Area (after Slucher 1997).

Figure 2.15: (right) Log of section exposed at Big Walnut Creek, Sunbury, Ohio, with location of samples marked (after Molyneux *et al.* 1984).

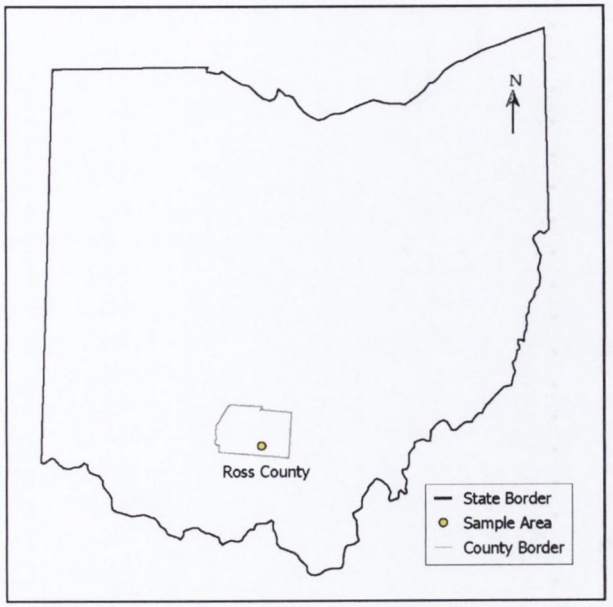

Figure 2.16: Geographical location of Bedford Shale and Berea Sandstone outcrop, Three Locks Quarry, Ross County, Ohio.

Figure 2.17: Photograph of Three Locks Quarry, Ross County, Ohio, [39°17′26″N, 82°56′36″W].

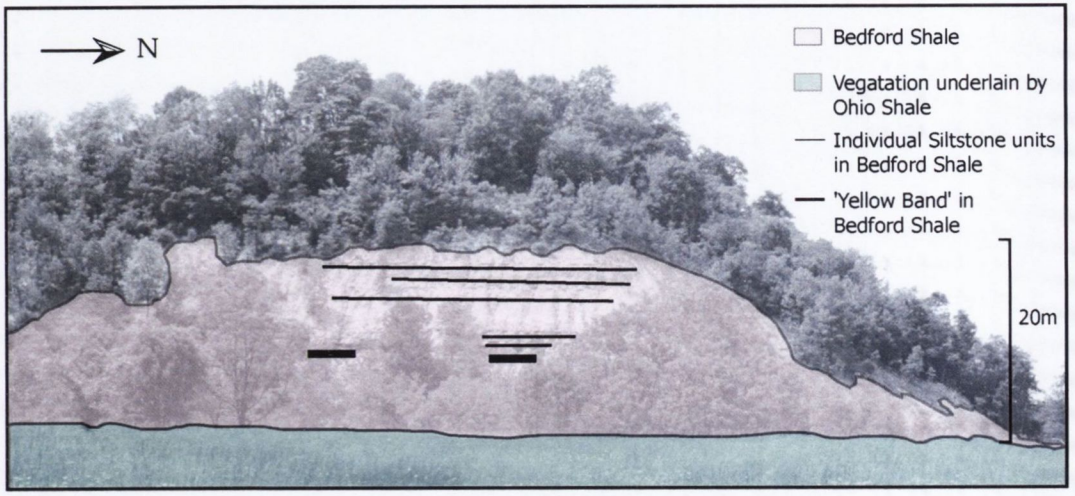

Figure 2.18: Desaturated photograph highlighting the units exposed at Three Locks Quarry, Ross County, Ohio, [39°17′26″N, 82°56′36″W].

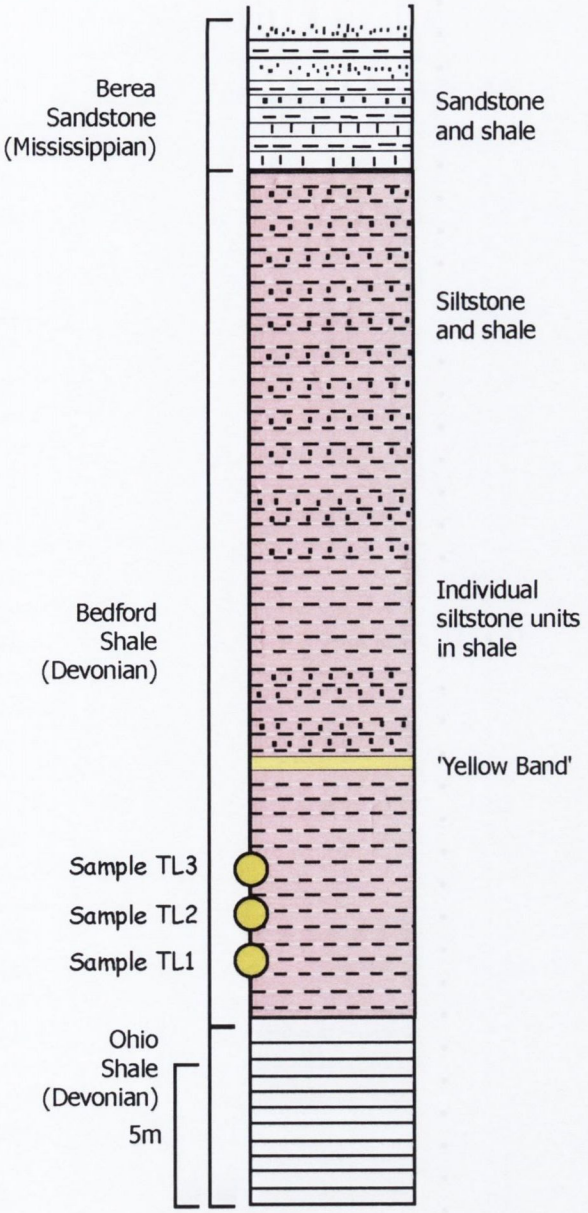

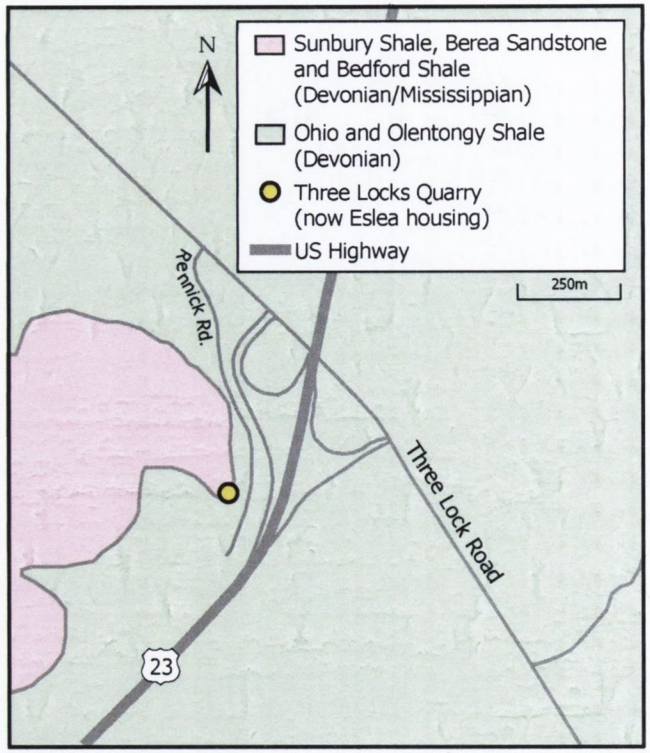

Figure 2.19: (above) Location map and geology of the Three Lock Quarry Area (after Schumacher 1995).

Figure 2.20: (right) Log of section exposed at Three Lock Quarry with location of samples marked (Coogan *et al.* 1981).

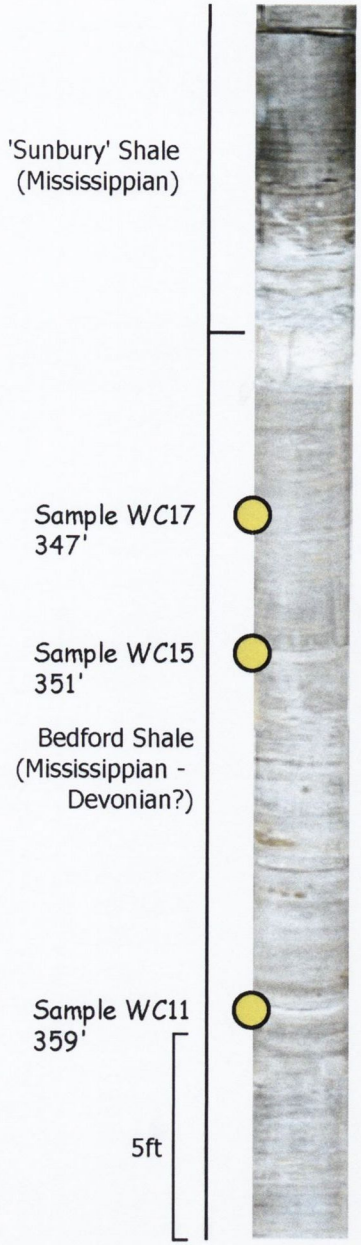

Figure 2.21: (left) Composite photograph of Williams County Core showing where samples were taken. Depths and additional comments taken from Larsen (1992).

Figure 2.22: (right) Location map of the Williams County Core, Superior Township, Williams County, Ohio. state coordinates of Ohio (North Zone) (1,409,950/ 696,700).

2.5. DINANT BASIN, BELGIUM

2.5.1. GEOLOGICAL HISTORY

The following brief summary of the geological history of the Dinant Basin is based mainly on the account in Ager (1980). Part of the Rhenohercynian Zone, Belgium is situated on the Ardenne allochthon of the European Variscides (Fielitz *et al.* 1999, Kenis *et al.* 2005). The area can be divided into two basins, the Namur Basin to the north and the Dinant Basin to the south (Figure 2.23). These basins are preserved in synclines separated by two narrow anticlines trending approximately NE-SW. The start of the Devonian Period in the area was marked by a marine transgression from the south which was stopped by the Silurian ridge of Condroz to the north. As the transgression continued in the Middle Devonian, the land surrounding the Condroz high was flooded creating the Namur Basin to the north and the Dinant Basin to the south.

During middle and late Devonian times, a series of reefs formed in the basins. By the end of the Frasnian the reefs became surrounded by mud as the result of a regression. This was followed by the deposition of shoreline and tidal flat deposits in the Famennian. With the Dinant Basin continuing to subside to the south, it was during the transition between the Frasnian and Famennian that the sediments of the upper part of Formation de la Famenne and lower part of Formation d'Esneux were deposited (Delcambre *et al.* 1993).

During the Carboniferous, cycles of sands, coals and shales were deposited. These cycles were more prominent in the northern Namur Basin than in the southern Dinant Basin. The Carboniferous was also marked by substantial Variscan tectonic movement. The northerly migrating tectonic front caused folding and faulting in the Dinant and Namur basins. The Grande Faille du Midi is the fault along which parts of the Dinant Basin were thrust onto the Namur Basin.

Thermal alteration of the Upper Devonian sediments sampled is believed to be due to burial and is syn-orogenic (Fielitz *et al.* 1999). It is likely that during the Variscan Orogeny, the geothermal gradient was close to between 40°C -70°C/km. CAI values of 4-5 have been reported for the central Dinant Basin (Helsen 1995).

After the period of uplift, the area of the former Namur and Dinant basins became part of the larger continent to the north. This remained the case until post Cretaceous tilting of NE Belgium, caused the northern part of the Ardennes to be uplifted and the southern boundary to subside (Bless 1991). This movement was reversed in the Oilgocene when the south of the country became emergent and the north was submerged (Vandenberghe, *et al.* 1997, Dehandschutter *et al.* 2005).

2.5.2. Villers Sur Lesse Section

This section is exposed along an abandoned railway line that now forms part of the *Ravel* cycle path system (Figure 2.24). Four productive samples were taken from this locality and their locations are shown in Figures 2.25 – 2.29. The only geological map of the area dates from 1900 and names the unit sampled as the Assise de Mariembourg. However, the area is in the process of being remapped and a map published adjacent to this area of Hastière– Dinant, has renamed Upper Devonian units. The new formation names were published in a booklet accompanying the new geological map (Delcambre *et al.* 1993). The text suggests that the unit sampled during this project should now be assigned to the Schistes de la Famenne.

2.6. CANTABRIAN ZONE, SPAIN

2.6.1. Geological History

The following summary of the geological history of the San Pedro Formation is based mainly on Dallmeyer *et al.* (1990) to which reader is referred for more a more detailed account. The pre-Permian geology of the Iberian Peninsula has been divided into three areas; The Iberian Massif, the internal Betic Cordillera and the outcrops of the Alpine ranges. Of these areas, the Iberian Massif represents the western most exposure of the European Hercynides. It has been subdivided into six zones on the basis of stratigraphic, structural and/or metamorphic characteristics (Figure 2.30). Of these six zones, a sample from the Cantabrian Zone was used in this project. This zone consists of the foreland thrust and fold belt of the Hercynian Mountain Belt in the northwest of the Iberian

Peninsula and is located in the inner part of the Asturian Arc. The zone consists of a wide range of different thrust systems that are arranged like the leaves of a photographic camera iris. This thin skinned deformation took place under shallow crustal conditions with only locally developed cleavage.

Stratigraphically, the zone is characterised by an incomplete Cambrian–Ordovician sedimentary sequence, a Siluro–Devonian succession which varies from complete to absent, and a well developed Carboniferous sequence. Tertiary continental deposits are preserved locally within a few fault bounded basins. Using stratigraphy, the zone has been divided into two domains: The Asturian Leonese Domain and the Palentine Domain. The Somedo Correcilla Tectonic Unit which forms part of the Asturian Leonese Domain was sampled.

A sequence of pre-orogenic Palaeozoic rocks rest unconformably on Precambrian basement in the zone. Stratigraphic breaks in the succession, notably within the Lower Ordovician, record variations in the extent of the basin over time. From late Ordovician to late Devonian times, the Asturian uplift to the north east of the zone formed a limit to the sedimentary basin and acted as a source area for sediment. Towards the end of the Devonian, a levelling event occurred that caused a slight eastwards tilting of the basin and removed the Asturian borderlands.

Pre-orogenic Cambrian to Devonian sediments in the zone were deposited in essentially in a shallow marine environments and vary between siliciclastic and calcareous in composition. During the Devonian, the basin experienced generally regressive conditions with some terrigenous sequences deposited, but with fossiliferous limestones, shales, reefs, and dolostones dominating. It was at this time that the San Pedro Formation was laid down. The lower part of this formation is dominated by iron rich clasts. In the upper part of the formation, clean quartz sands are more common and are thought to have been deposited in a high energy shallow water environment (Wallace 1972).

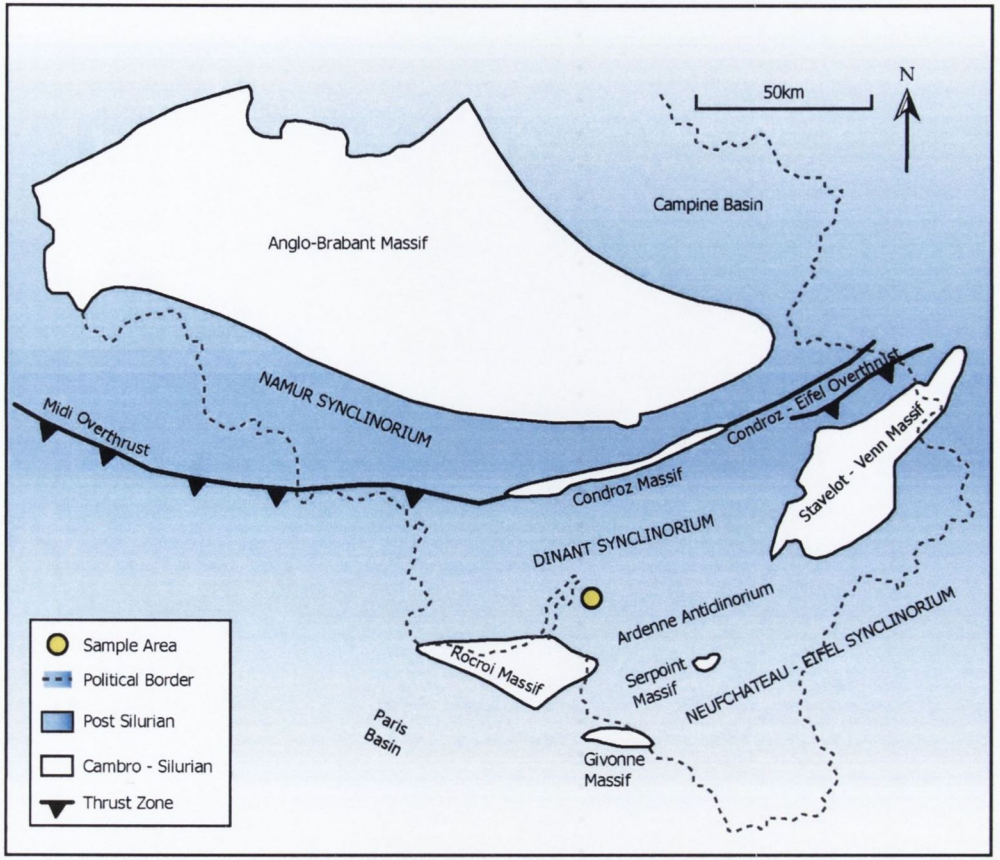

Figure 2.23: Geological setting of the Dinant Basin (after Helson 1995).

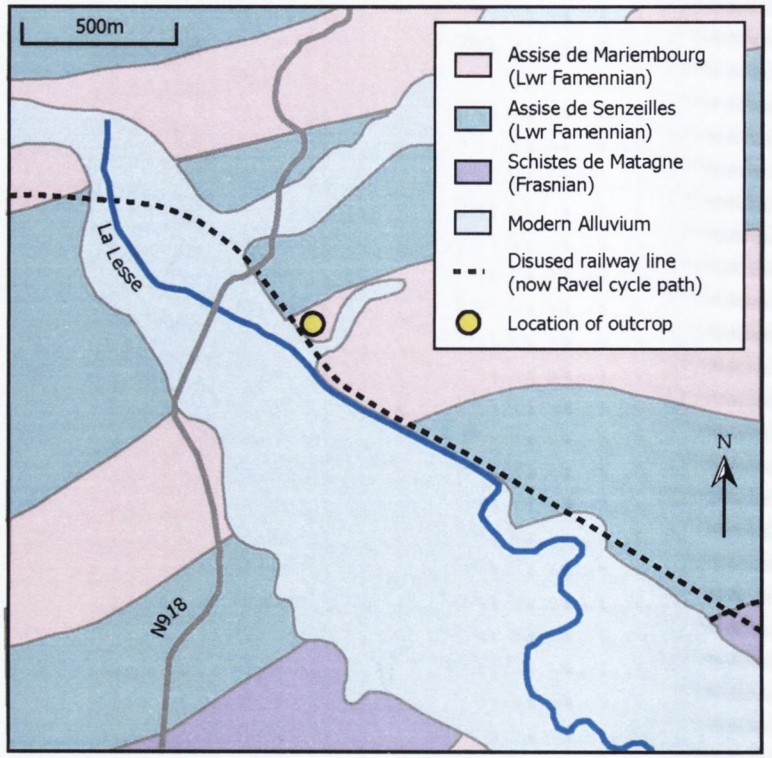

Figure 2.24: Location map and geology of Villers Sur Lesse area (after Forir 1900).

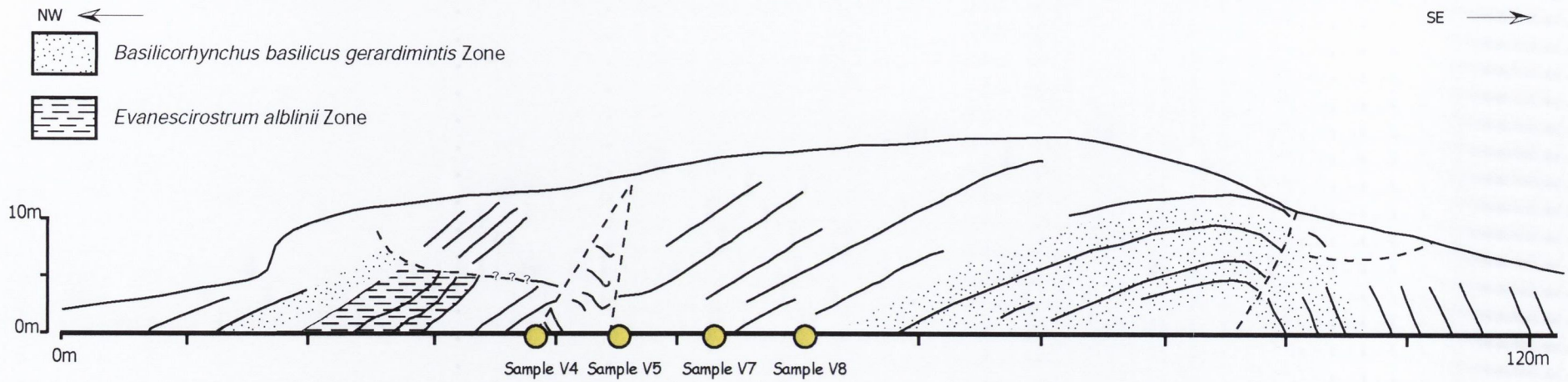

Figure 2.25: Sketch of section exposed along the abandoned railway line at Villers Sur Lesse (Sartenaer (1956) in Martin (1981)). The locations of the four productive samples taken from this section are marked.

Figure 2.26: Sample V4.

Figure 2.27: Sample V5.

Figure 2.28: Sample V7.

Figure 2.29: Sample V8.

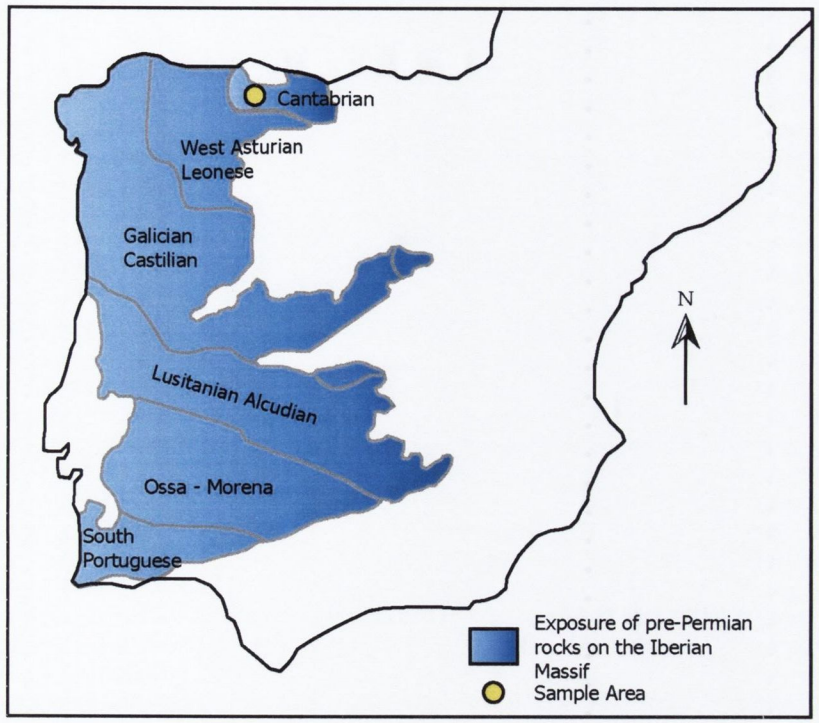

Figure 2.30: Exposures of pre-Permian rocks within the six zones of the Iberian Massif (Dallmeyer *et al.* 1990).

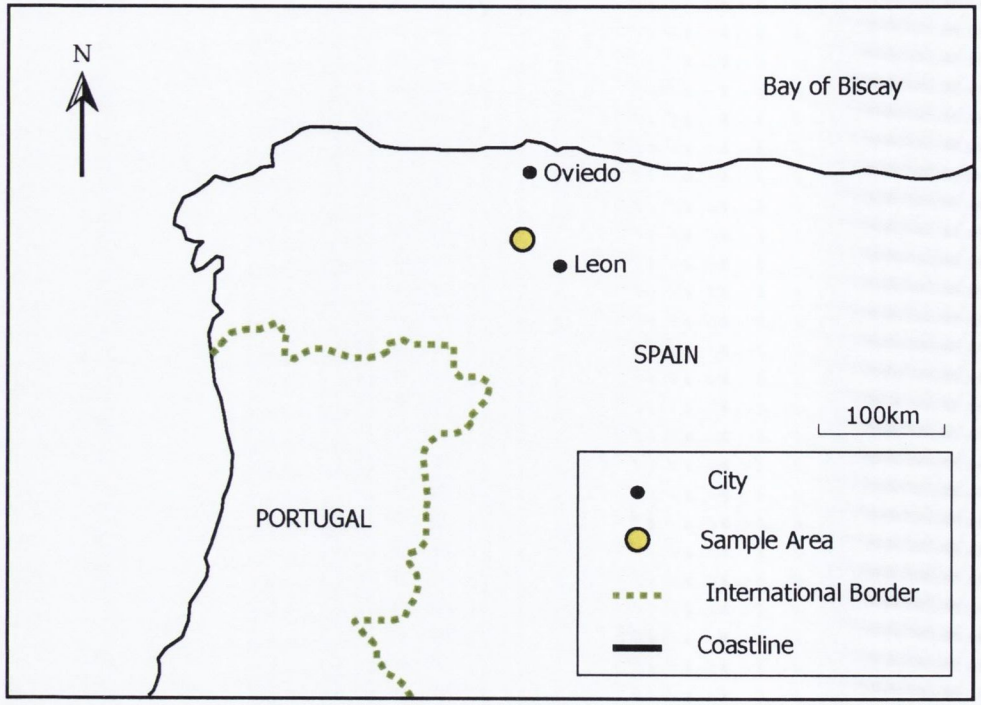

Figure 2.31: Geographical location of Gears de Casares, Cantabrian Mountains.

Towards the end of the Devonian, following levelling of the platform, there was a transgressive period which resulted in a thin sedimentary marine wedge being deposited disconformably over most of the Asturian – Leonese Domain.

Syn-orogenic Carboniferous units that are found in all parts of the Cantabrian Zone were deposited in a wide range of environments from continental to open marine conditions. After the Hercynian Orogeny, a shallow marine basin formed in central and eastern parts of the Iberian Massif. Following the retreat of the sea in the late Carboniferous, deposition in the western part of the zone was continental (Wallace 1972). Some fresh water deposition is recorded in the Jurassic and Cretaceous. During the Alpine Orogeny in the Oligocene – Miocene, a reverse fault on the southern margin of the Cantabrides raised the main part of the chain resulting in rapid erosion. Finally the area was glaciated during Quaternary times (Wallace 1972).

2.6.2. Geras de Cesares Section

Sample JM5 was collected by Paul Tricker and John Marshall and kindly donated for this project. The section is found to the west of Geras de Gordon in the Cantabrian Zone (Figure 2.31). The outcrop locality is stop 1-7, Casares River, west of Geras de Gordon, in the 1978 CIMP field guide [42°53'51"N, 5°47'8.5"E] (Figure 2.32). The sample used came from the Lower Devonian San Pedro Formation (Figure 2.33).

2.7. ANGLO WELSH BASIN, WALES

2.7.1. Geological History

The following brief geological history of the Midland Platform and Anglo Welsh Basin, Wales, is taken from Woodcock *et al.* (2000). The Midland Platform was a relatively stable segment of continental crust in the area southeast of the Welsh Borderland Fault System. During the Cambrian some shallow marine sediments were laid down unconformably on Neoproterozoic basement rocks, while other sections of the platform remained subaerial. In the Ordovician, the platform experienced a number of tectonically

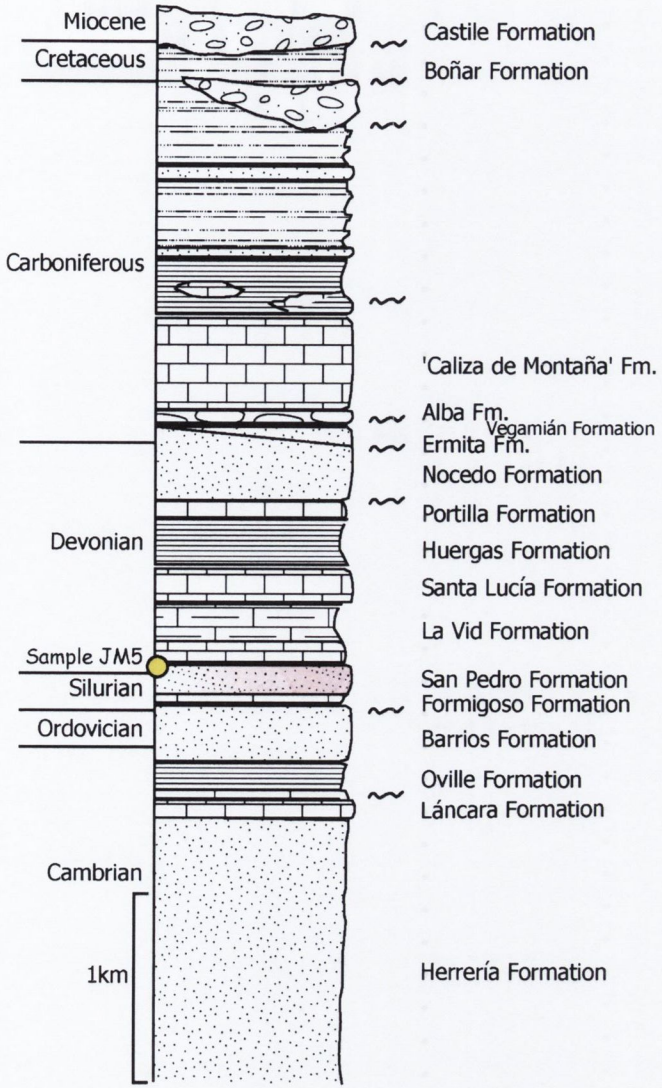

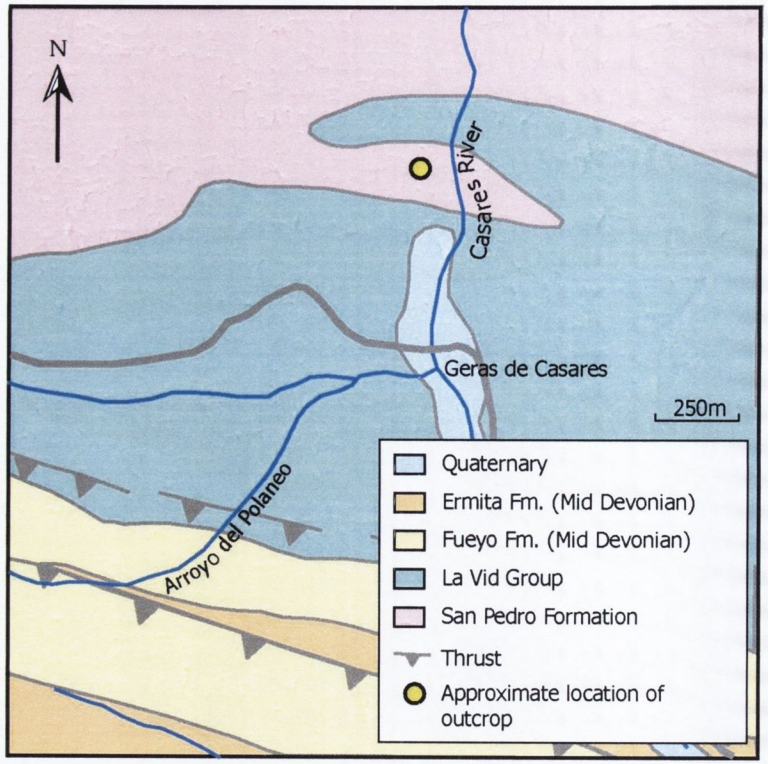

Figure 2.32: (above) Location map and geology of the area around Geras de Casares (after Alonso *et al.* 1990).

Figure 2.33: (right) Generalised stratigraphy of the south western part of the Cantabrian Cordillera drawn to approximate scale (Wallace 1972).

induced regressions and transgressions. A mid Ordovician unconformity across the platform marks the period when the platform emerged as a result of lower sea levels during glaciation. Following the end of the glaciation, the Silurian succession consists of a sequence of calcareous mudstones and occasion reefs.

During the Caledonian Orogeny, when the Eastern Avalonian microcontinent collided with Laurentia, there was crustal shortening and uplift of the area to the north of the Midland Platform. The platform itself was only weakly affected by the event being a relatively cold and strong cratonic area. It reacted to the tectonic stresses only by local reactivation of pre-existing faults. However, regional uplift did bring a reorganisation of depositional centres, with the Anglo Welsh basin now located on what had been the stable Midland Platform (Figure 2.35). During the lower Devonian Period, alluvial plains and channel deposits dominated the area in an upward coarsening sequence. With the continuing southward advance of the Caledonian mountain front during the mid Devonian, the Anglo Welsh Basin was uplifted and deposition only continued in the Cornubian basins to the south. Not until the late Devonian did deposition of alluvial and shallow marine sediments begin again across most of the Anglo Welsh Basin.

In the Carboniferous, global sea levels rose and flooded much of the alluvial plain deposits to produce conformable marine facies. The area then becomes known as the Southern Province and is marked by shelf deposits of muds and limestones. During the early Carboniferous the shallow marine Tongwynlais Formation was deposited (Davies *et al.* 1991). This formation consists of ooidal, peloidal and skeletal limestones, as well as silty and grey mudstones, calcretes and ironstones. The depositional environment of this unit is interpreted as an embayment or open lagoon setting (Davies *et al.* 1991). The formation is a member of the Lower Limestone Shale Group and it was from this formation that sample Wales 1 was taken.

Due to Variscan uplift, the area became shallower with deposition of deltaic and fluvial deposits, followed later by peats and organic rich muds. During the Permian and Triassic the area remained subareal until a major pulsed regression occurred in the Triassic/early Jurassic. This change from non marine to marine conditions resulted in the widespread deposition of muds, followed by intermittent regional regressions. For most of the Cretaceous the area formed part of the subareal Welsh Massif, until it was flooded in

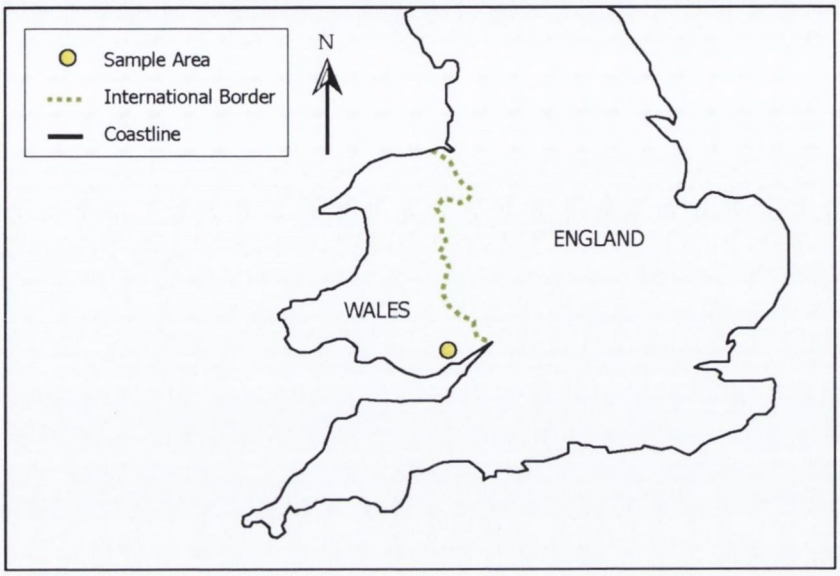

Figure 2.34: Geographical location of the Cwrt-yr-ala borehole, Wales.

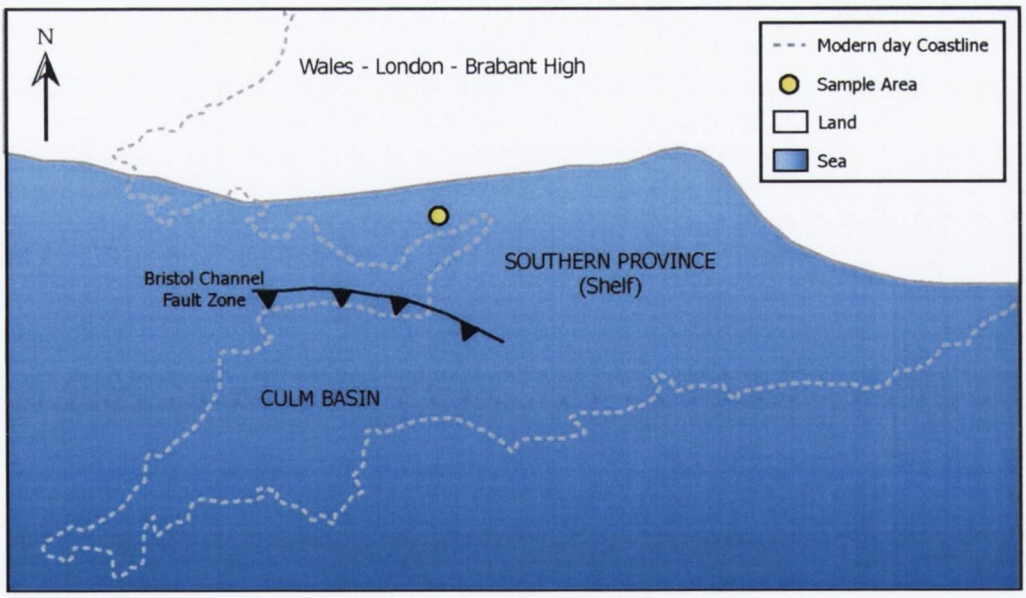

Figure 2.35: Dinantian palaeogeography of the area surrounding the Cwrt-yr-ala borehole (after Woodcock *et al.* 2000).

the late Cretaceous following global sea level rise. The Tertiary Period was marked by regional uplift in southern Britain, including south Wales, caused by thermal uplift and gentle Alpine thrusting. This was the last major tectonic event that affected the area.

2.7.2. Cwrt-yr-ala Borehole

The Cwrt-yr-ala borehole (Figure 2.36) was drilled by the British Geological Survey in 1977 at grid reference [ST 1408 7339] and sampled by Aideen McNestry as part of her Ph.D. project (1989). One sample from the borehole was used in this study and was taken from the Mississippian Tongwynlais Formation (Figure 2.37).

2.8. SIERRA DE PERIJÁ, VENEZUELA

2.8.1. Geological History

Within the northern part of South America, several geological terranes have been recognised distinct from the Guiana Shield (Forero 1990, Restrepo *et al.* 1988). These terranes have been grouped into three main geological provinces: The Western Province, the Central Andean Province and the Eastern South American Province. The Sierra de Perijá is one of two mountain chains that together form the Eastern Cordillera of the Andes and is located within the Central Andean Province (Harvey 2001) (Figures 2.38 and 2.39).

The Central Andean Province is bordered to the east by the Borde Llanero Fault System and to the west by the Romeral Fault (Forero 1990). The basement in this area consists of metamorphic Precambrian to early Palaeozoic rocks. Palaeozoic to late Tertiary magmatites are present, as well as early Devonian to Tertiary sediments. The end of the Silurian Period in this area was marked by the Caledonian Orogeny, characterized by folding, metamorphism and uplift. The last metamorphic event that affected the area was post Ludlowvian – pre Emsian in age (Forero 1970). After a post Caledonian period of erosion, a shallow sea transgressed over a relatively flat topography. Devonian deposits generally consist of fine grained sands and silts, with limestones present but not common (Forero 1990).

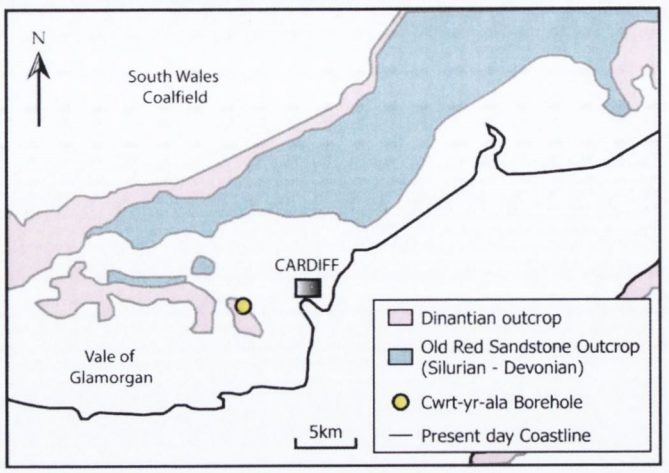

Figure 2.36: (above) Location map and geology of the area around the Cwrt-yr-ala borehole (after Davies *et al.* 1991).

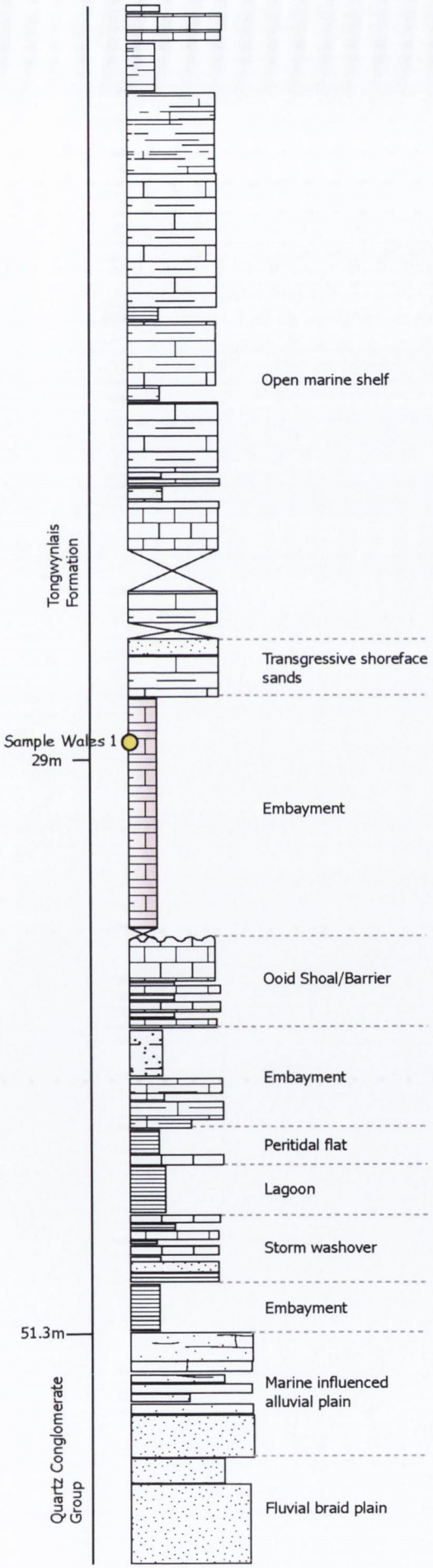

Figure 2.37: (right) Log of the Cwrt-yr-ala borehole showing the location of sample Wales 1 (McNestry 1989).

The Campo Chico Formation was deposited in this shallow water marine environment, with some intratidal and deltaic sections also recorded (Harvey 2001). It is known for its diverse and well preserved floras of the mid and late Devonian age (Berry *et al.* 2000). A sample from the upper part of this formation was used in this project.

A deformation event occurred during the Permian–Triassic, followed by marine sedimentation during the Lower Cretaceous (Restrepo *et al.* 1988). With the accretion of the Western Andean Terrane in the mid Cretaceous, the area experienced more uplift and folding. During the late Cretaceous, tonalitic batholiths were intruded into the suture zone between the Central and Western Andean terranes. The only record of sedimentation after the Lower Cretaceous is a series of terrestrial deposits during the Oligocene-Miocene period (Restrepo *et al.* 1988).

2.8.2. Sierra de Perijá Outcrop

Three samples of the upper part of the Frasnian Campo Chico Formation were used in this project. The samples were collected by Craig Harvey as part of his Ph.D. (2001) and kindly donated for this project. The samples were collected from two localities near the Caño Colorado (Figures 2.40 and 2.41). Sample VA47 was taken from a riverside exposure at Caño Colorado del Sur while samples VA115 and VA118 were taken from the *Archaeopteris* locality (Figures 2.42 and 2.43).

2.9. JORDANIAN WELL SAMPLES

2.9.1. Geological History

The area sampled lies on the stable shelf to the west of the Arabian – Nubian Shield, close to the Jordanian/Iraqi border. Palaeozoic sedimentation on this stable shelf is known collectively as the Arabian Sedimentary Platform. During the early Palaeozoic, the area was situated on the northern margin of Gondwana, forming a tectonically quiet passive continental margin (Lüning *et al.* 2005). A major glaciation occurred in the late Cordovan,

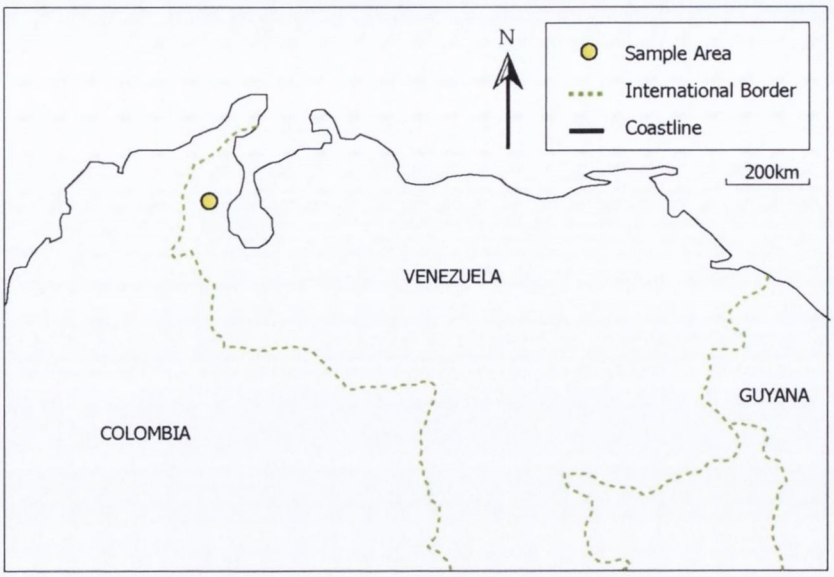

Figure 2.38: Geographical location of the Sierra de Perijá, Venezuela.

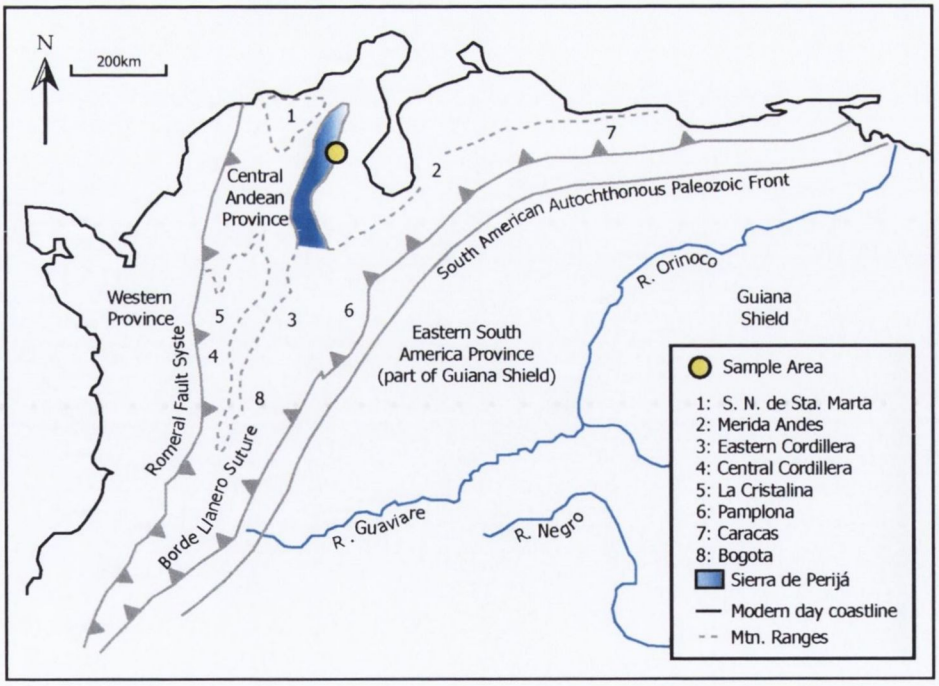

Figure 2.39: Geological setting of the Sierra de Perijá, Venezuela (after Forero Suarez 1990).

Figure 2.40: Devonian outcrop exposed in the Sierra de Perijá, Venezuela (after Harvey 2001).

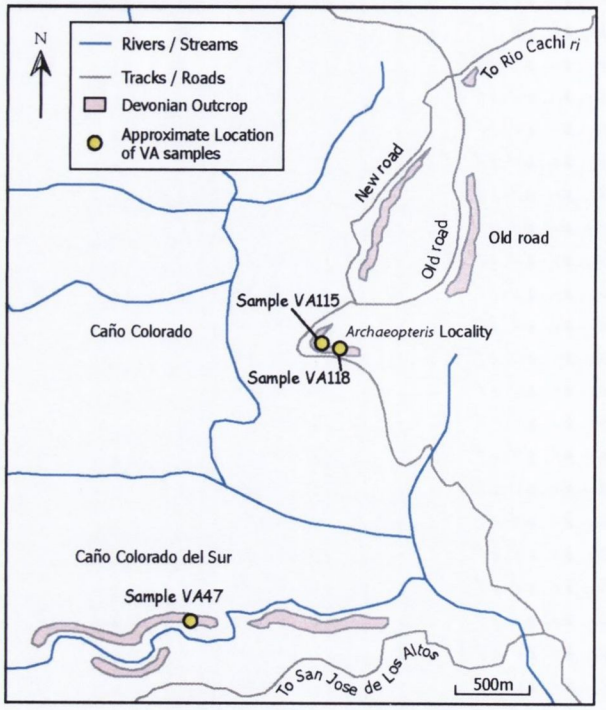

Figure 2.41: Location of samples used in this project (after Harvey 2001).

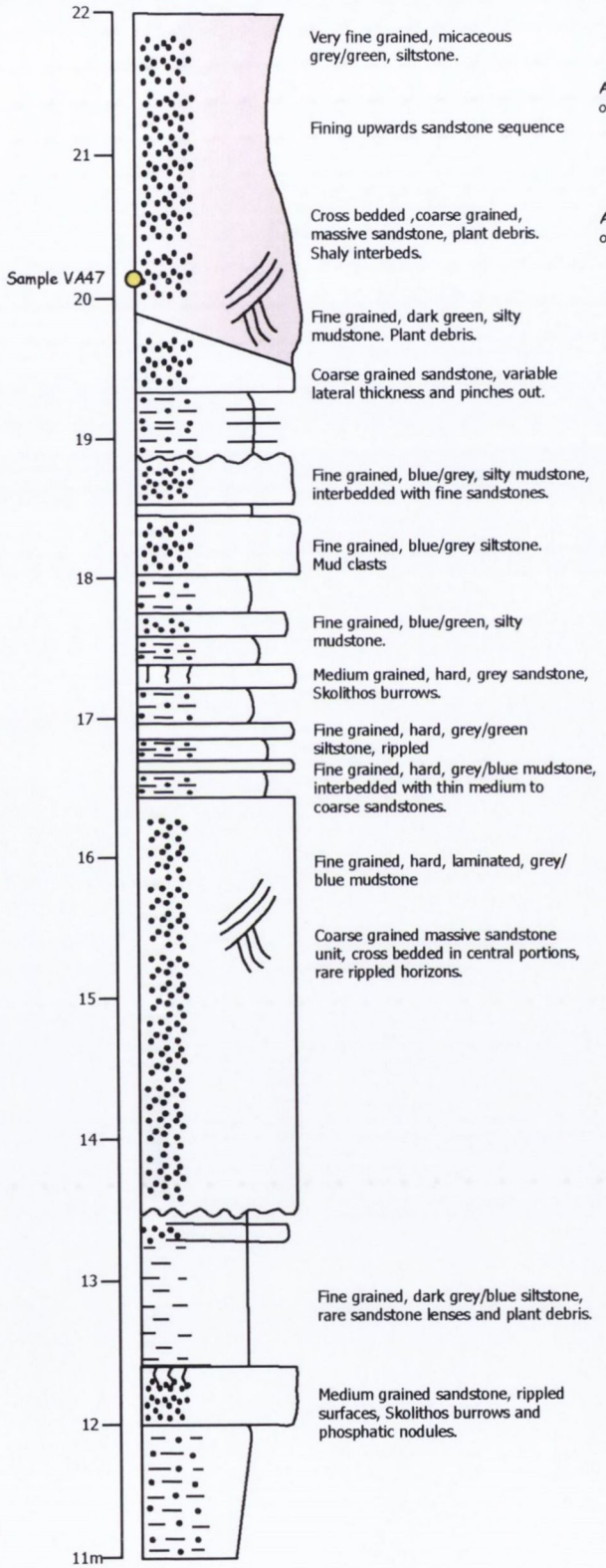

Figure 2.42: Sedimentary log for the Upper Member of the Campo Chico formation, *Archaeopteris* locality (Harvey 2001).

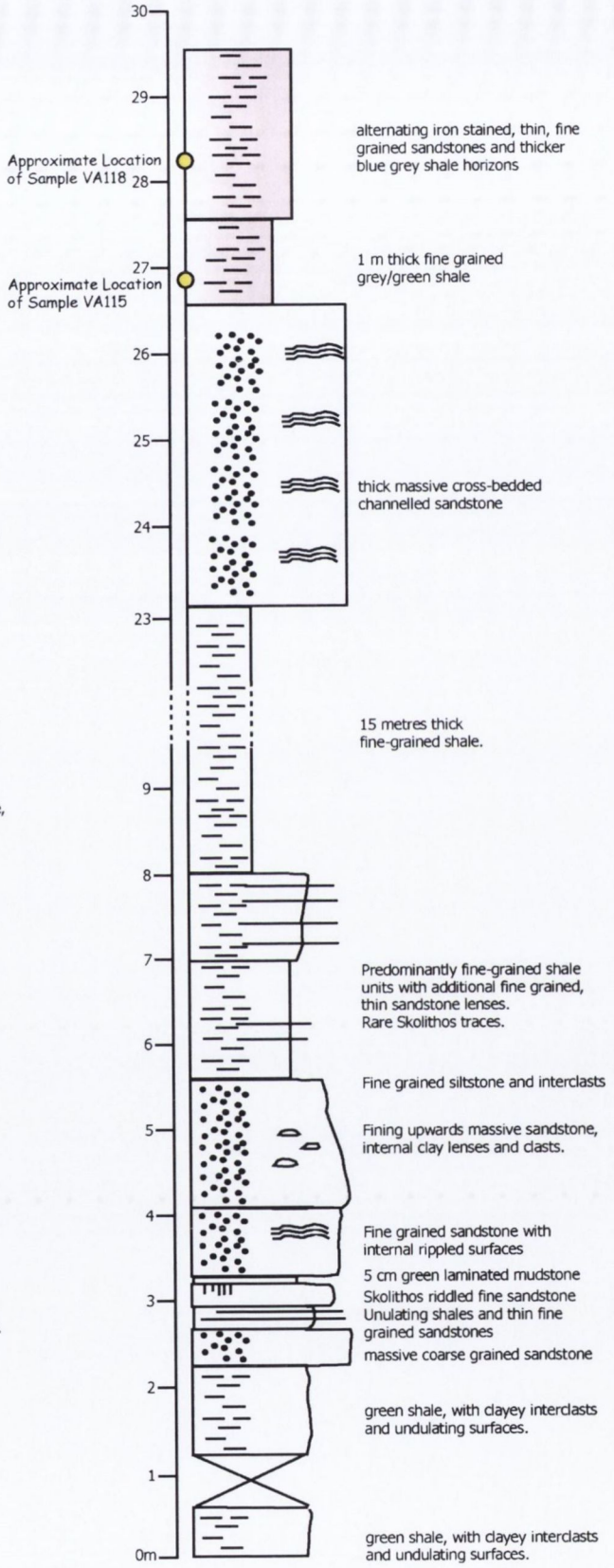

Figure 2.43: Sedimentary log for the Upper Member of the Campo Chico formation, Caño Colorado del Sur (Harvey 2001).

and the melting of a major ice cap situated in central Africa caused a major transgression during the early Silurian. This eustatic rise in sea level led to the flooding of large areas and resulted in the deposition of black muds that became petroleum sources in many places (Lüning *et al.* 2005). This Silurian shale unit is informally named as the Mudawwara Formation in Jordan and was sampled for this project. The Khishsha Formation consists of siltstones and sandstones formed from a prograding deltaic complex and overlies the Mudawwara Formation (Lüning *et al.* 2005). Samples from this unit were also used in this project. Currently, there is no generally accepted formal stratigraphic nomenclature in the region. The system used in this project is based on the Jordanian subsurface log nomenclature. A simplified lithostratigraphic correlation of the uppermost Ordovician and Silurian of Jordan and neighbouring areas is given in Figure 2.44 (Lüning *et al.* 2005). This area is discussed in detail in Chapter 7.

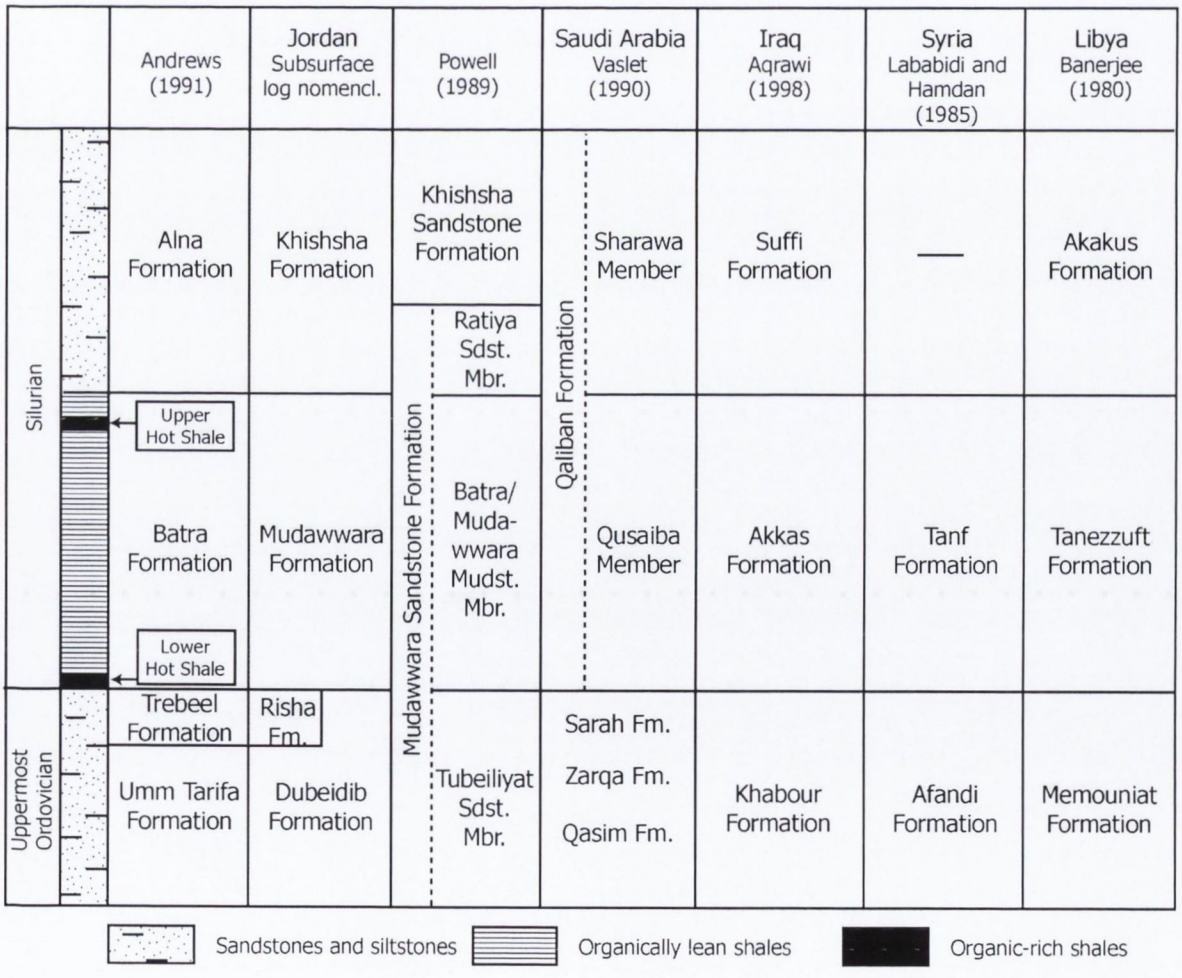

Figure 2.44: Simplified lithostratigraphic correlation of the uppermost Ordovician and Silurian of Jordan and neighbouring areas (Lüning *et al.* 2005).

2.9.2. WELL RH-3

Well RH-3 was drilled on behalf of the Natural Resources Authority of Jordan in February 1987. The well is situated in the Risha Gas Field, Jordan, at 530.061E, 228.688N (Palestine Grid) close to the Jordan/ Iraq Border (Figure 2.45). The samples used in this project were collected and supplied by Petrel Resources Plc (Figure 2.46).

2.9.3. WELL RH-19

This well is situated in the Risha Gas Field, Jordan, at approximately 460E, 151N (Palestine Grid) close to the Jordan/ Saudi Arabia Border. The samples used in this project were collected and supplied by Petrel Resources Plc.

2.9.4. WELL WS-6

Well WS-6 was drilled on behalf of the Natural Resources Authority of Jordan in March 1986. The well is situated in the Wadi Sirhan area, Jordan, at 396.549.414E, 8.299.095N (Palestine Grid) (Figure 2.45). The samples used from this well were collected and supplied by Petrel Resources Plc (Figure 2.47).

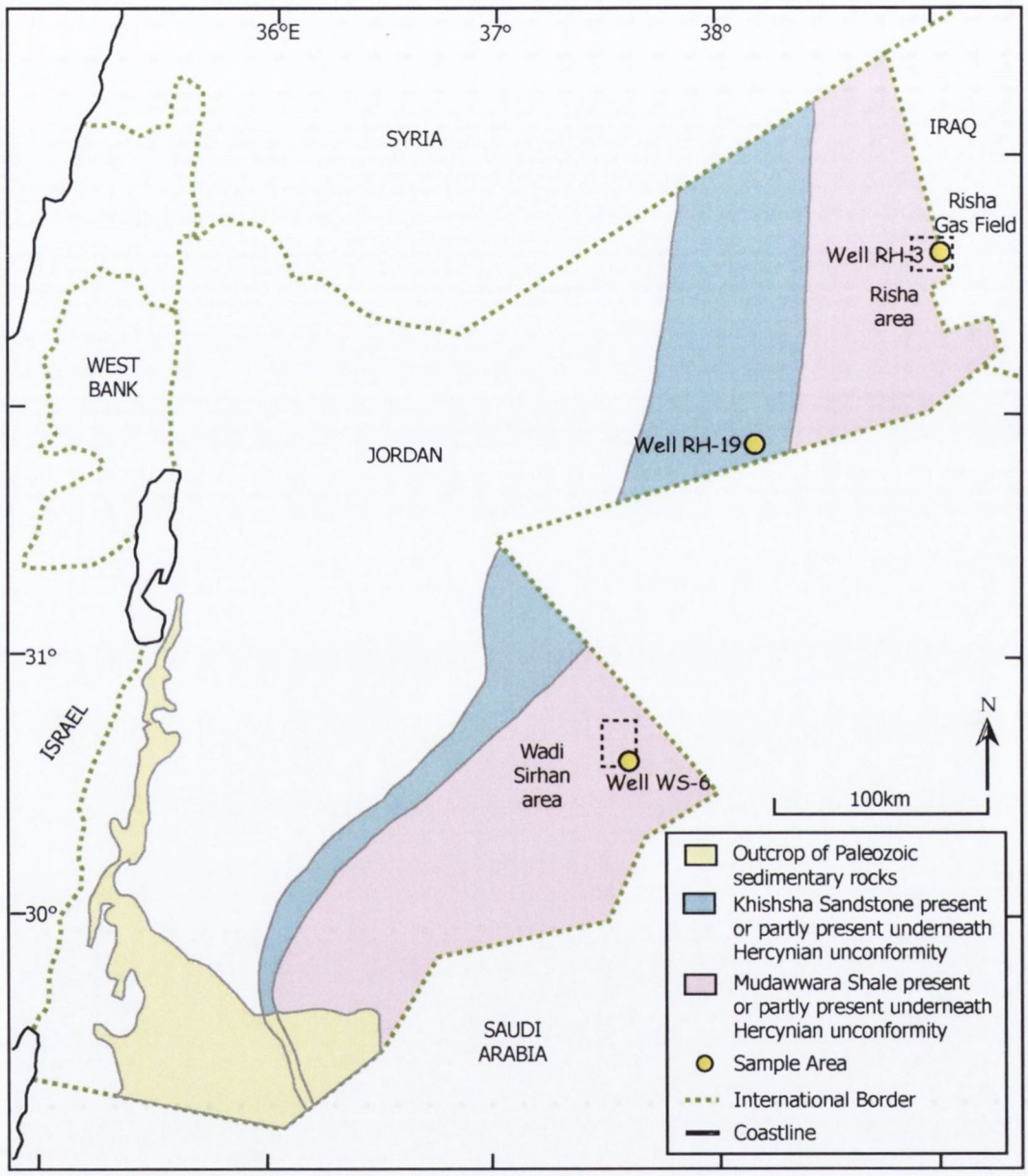

Figure 2.45: Geological setting of the wells used in this project (After Lüning *et al.* 2005).

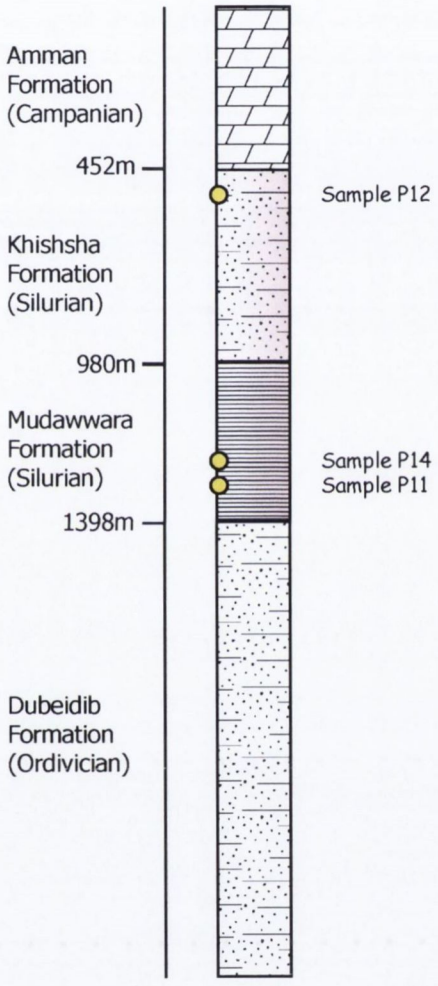

Figure 2.46: Diagramatic log of well RH-3 showing location of samples taken. Formation top depths taken from Hamad (1987).

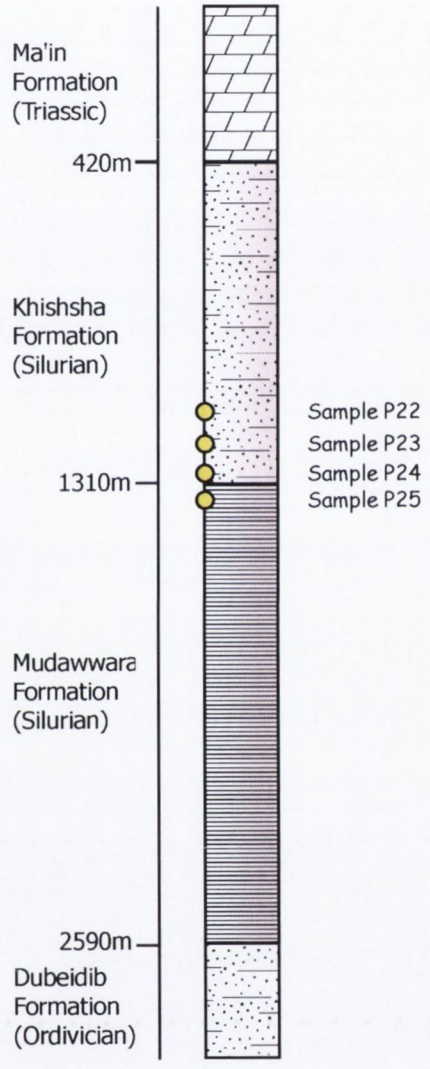

Figure 2.47: Diagramatic log of well WS-6 showing location of samples taken. Formation top depths taken from Qteishat (1989).

Sample Name	Location	Grid Reference	Formation	Age	Sampled by
CC3	Clay City Quarry, Powell County, Kentucky, USA.	37°52′09″N, 83°56′48″W	Three Lick Bed, Chattanooga Shale	Upper Devonian	Catherine Duggan
JM5	Geras de Cesares, Cantabrian Mtns, Spain	42°53′51″N, 5°47′8.5″E	San Pedro Formation	Lower Devonian	John Marshall
SUN3	Walnut Creek, Sunbury, Delaware Co. Ohio, USA	40°14′46″N, 82°50′60″W	Bedford Shale	Upper Devonian	Catherine Duggan
SUN7	Walnut Creek, Sunbury, Delaware Co. Ohio, USA	40°14′46″N, 82°50′60″W	Bedford Shale	Upper Devonian	Catherine Duggan
TL1	Three Lock Quarry, Ross Co., Ohio, USA	39°17′26″N, 82°56′36″W	Bedford Shale	Upper Devonian	Catherine Duggan
TL2	Three Lock Quarry, Ross Co., Ohio, USA	39°17′26″N, 82°56′36″W	Bedford Shale	Upper Devonian	Catherine Duggan
TL3	Three Lock Quarry, Ross Co., Ohio, USA	39°17′26″N, 82°56′36″W	Bedford Shale	Upper Devonian	Catherine Duggan
TL7	Three Lock Quarry, Ross Co., Ohio, USA	39°17′26″N, 82°56′36″W	Bedford Shale	Upper Devonian	Catherine Duggan
V4	Villers Sur Lesse, Belgium	50°09′40″N, 05°06′58″W	Assise de Mariembourg	Upper Devonian	Catherine Duggan
V5	Villers Sur Lesse, Belgium	50°09′40″N, 05°06′58″W	Assise de Mariembourg	Upper Devonian	Catherine Duggan
V7	Villers Sur Lesse, Belgium	50°09′40″N, 05°06′58″W	Assise de Mariembourg	Upper Devonian	Catherine Duggan
V8	Villers Sur Lesse, Belgium	50°09′40″N, 05°06′58″W	Assise de Mariembourg	Upper Devonian	Catherine Duggan
VA115	Caño Colorado, Sierra de Perijá, Venuzuela		Campo Chico Formation	Upper Devonian	Craig Harvey
VA118	Caño Colorado, Sierra de Perijá, Venuzuela		Campo Chico Formation	Upper Devonian	Craig Harvey
VA47	Caño Colorado, Sierra de Perijá, Venuzuela		Campo Chico Formation	Upper Devonian	Craig Harvey

Table 2.1: Details of outcrop samples used in this project

Sample Name	Borehole	Grid Reference	Formation	Age	Depth	Sampled by
CAN 9	Ontario Department of Mines Campbell Lake drill hole	50°14'30"N, 80°09'30"W	Kwataboahegan Formation	Middle Devonian	880 - 881ft	Ann Wilson
P11#	RH-3 Well, Risha Area, Jordan	530.061E, 228.688N*	Mudawwara Formation	Silurian	1320 - 1333m	Petrel Resources Plc
P12#	RH-3 Well, Risha Area, Jordan	530.061E, 228.688N*	Khishsha Formation	Silurian	520m	Petrel Resources Plc
P14#	RH-3 Well, Risha Area, Jordan	530.061E, 228.688N*	Khishsha Formation	Silurian	1260m	Petrel Resources Plc
P22#	WS-6 Well, Wadi Sirhan, Jordan	396.549.414E, 8.299.095N*	Mudawwara Formation	Silurian	1118m	Petrel Resources Plc
P23#	WS-6 Well, Wadi Sirhan, Jordan	396.549.414E, 8.299.095N*	Mudawwara Formation	Silurian	1208m	Petrel Resources Plc
P24#	WS-6 Well, Wadi Sirhan, Jordan	396.549.414E, 8.299.095N*	Mudawwara Formation	Silurian	1288m	Petrel Resources Plc
P25#	WS-6 Well, Wadi Sirhan, Jordan	396.549.414E, 8.299.095N*	Mudawwara Formation	Silurian	1357m	Petrel Resources Plc
RH19 P-12#	RH19, Risha Area, Jordan		Mudawwara Formation	Silurian	1390 - 1400m	Petrel Resources Plc
WALES 1	Cwrt-yr-ala borehole, South Wales, UK	ST 1408 7339**	Tongwynlais Formation	Mississippian	28.50 - 29.44m	Aideen McNestry
WC11	Williams Co. Core Borehole, Superior Township, Ohio, USA	1,409,950/ 696,700***	Bedford Shale	Upper Devonian	359ft	Catherine Duggan
WC15	Williams Co. Core Borehole, Superior Township, Ohio, USA	1,409,950/ 696,700***	Bedford Shale	Upper Devonian	351ft	Catherine Duggan
WC17	Williams Co. Core Borehole, Superior Township, Ohio, USA	1,409,950/ 696,700***	Bedford Shale	Upper Devonian	347ft	Catherine Duggan

Table 2.2: Details of well samples used in this project. # indicates cuttings sample, all other samples were cores.
* indicates Palestinian Grid Coordinates
**indicates British National Grid Coordinates
*** indicates Ohio State Coordinates, North Zone

CHAPTER 3
VITRINITE REFLECTANCE: THEORY AND METHOD

3.1. THEORY

3.1.1. VITRINITE

Vitrinite is one of three groups of macerals traditionally studied by coal petrologists the other two being liptinite and inertinite. The term 'maceral' was first coined by Stopes in 1935 to describe constituents of coal liberated by maceration, from the Latin verb '*macerare*' meaning 'to soften' (Taylor *et al.* 1998). These microscopic particles originate from the remains of plants which may or may not be identifiable depending on the amount of alteration that has taken place. Vitrinite forms from woody tissues of roots, stems, bark and leaves composed of cellulose and lignin (International Commission on Coal Petrology (I.C.C.P.), 1994). Each maceral group is defined in terms of attributes that can be determined by light microscopical examination. These attributes include reflectance, colour, shape and hardness and are defined by the I.C.C.P. The primary difference between the three maceral groups is their level of reflectance. In reflected light, the liptinite group has the lowest reflectance, the vitrinite group has intermediate reflectance and the inertinite group has the highest reflectance.

Due to the generally well preserved nature of organic remains in coal samples, coal petrologists have further subdivided these maceral groups into macerals and submacerals based on more detailed observations of the particles. In many cases these submacerals can only be distinguished at low rank. However, when studying dispersed organic material derived from sedimentary rocks, these divisions commonly prove impossible to apply due the poor preservation and small size of the grains. This was the case in all samples studied for this project and no grains observed were identified beyond maceral group level.

3.1.2. VITRINITE REFLECTANCE

The reflectance of a maceral is the proportion of directly incident light, usually expressed as a percentage, that is reflected from a plane polished surface under specified conditions of illumination (Ward 1984). Vitrinite reflectance is one of the most widespread techniques used to evaluate the maturity of post Silurian sediments (Morrow *et al.* 1993, Wilkins *et al.* 1995, Taylor *et al.* 1998). Reflectance is dependant on the refractive and absorption indices of vitrinite (Taylor *et al.* 1998) and increases with temperature due to an increase in the aromaticity of the organic compounds within vitrinite grains (Ward 1984). As the sediment is heated, volatiles are driven out of the vitrinite structure and isolated aromatic rings are formed. With further increases in temperature these isolated rings form polycyclic aromatic rings and then orientated sheets increasing the reflectance of the surface of the grain (Carr *et al.* 1989). The process by which the vitrinite aromaticity increases is irreversible and is a major advantage of the technique. The degree to which other factors, such as time and pressure, affect the reflectance of vitrinite has long been debated but it is generally accepted that temperature is the main driving force behind the change (Dow *et al.* 1982, Marshall 1990, Huang 1996).

As the level of maturity increases, so does the degree of reflectance anisotropy of vitrinite (Ward 1984). The vitrinite particles develop bireflectance, calculated as the difference between maximum and minimum reflectance of a grain (Stach *et al.* 1982). In most cases where coalification has resulted from burial, rather than tectonic stresses, true minimum reflectance can be determined on surfaces polished perpendicular to banding (Taylor *et al.* 1998). When this section is illuminated by polarized light, with the polarizer set at 45°, maximum (R_{max}) and minimum (R_{min}) reflectance of vitrinite can be observed by rotating the stage stepwise through 360° (Stach *et al.* 1982). This phenomenon is due to 'pressure induced anisotropy' which orientates the humic complexes found in vitrinite (Stach *et al.* 1982). Maximum reflectance can be determined from all coal samples, regardless of tectonic pressures (Taylor *et al.* 1998).

Minimum reflectance can only be determined on orientated coal samples as described above; it is not possible to measure this property from dispersed vitrinite particles. Due to grain size it is not practical, when investigating dispersed organic matter, to measure maximum reflectance of vitrinite (Dow *et al.* 1982). As a result, mean random reflectance (R_r) was used to describe the vitrinite reflectance of samples in this project. This

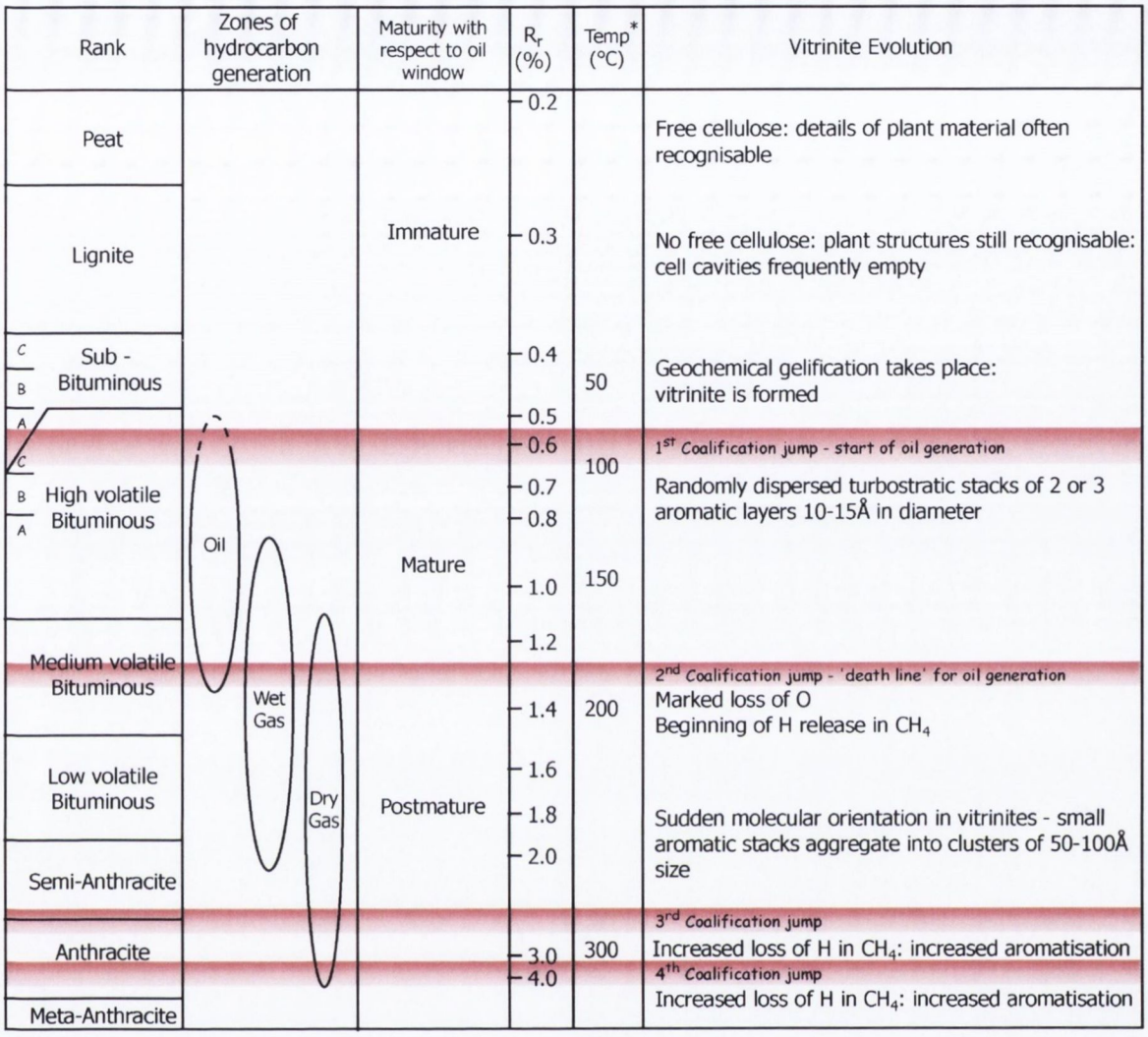

Figure 3.1: Diagram showing the stages of vitrinite evolution (McCaughan 2002, Teichmüller 1987). * = Temperature estimates taken from Barker *et al.* 1986.

parameter depends on the angle at which the reflectance indicating surface of the vitrinite grain has been cut (Taylor *et al.* 1998). It is based on one determination of the reflectance of each vitrinite grain in a random orientation. Koch *et al.* (1995) provide a good summary of the published equations relating R_r to R_{max}.

3.1.3. Thermal Maturity

The term 'maturation' is used to describe the diagenetic development of organic matter that leads to the formation of petroleum and natural gas from oil shales, oil source rocks and related sedimentary rocks (Taylor *et al.* 1998). The level of thermal maturity of a sample is dependent on the heating of the sediments, normally due to burial, and the maximum temperature attained. There are various terms used to describe the level of maturity of a sediment depending on the hydrocarbon produced (see Figure 3.1).

During the maturation process, organic matter undergoes two types of change. First, mobile products like gas and liquids are given off, and second, the condensation of the solid residual products takes place due to their aromatisation (Taylor *et al.* 1998). Oxygen is released in the form of CO_2 and H_2O, and hydrogen as CH_4. This results in a relative increase in carbon content of the structure. While this process is generally gradual it is punctuated by four chemical and optical 'coalification jumps' that have been identified in vitrinites of bituminous coals (Stach *et al.* 1982). The location of these 'jumps' relative to hydrocarbon generation is shown in Figure 3.1.

3.1.4. Benefits of Vitrinite Reflectance

The success and widespread use of vitrinite reflectance as a thermal maturity indicator is due to a number of factors. The reflectance of vitrinite increases more uniformly with temperature than of any other maceral group and vitrinite is found in both coals and many sedimentary source rocks (Stach *et al.* 1982). Unlike visual estimation of microfossil colour which is highly subjective, the determination of reflectance can be accurately determined using calibrated analytical equipment. Results can be obtained relatively quickly and with little expense. Much work has been carried out to quantify the relationship between vitrinite reflectance values and maximum temperatures reached by

sediments for example Barker *et al.* (1994), Barker *et al.* (1990), and Burnham *et al.* (1989). This has proved useful in providing parameters which can improve basin models.

3.1.5. Limitations of Vitrinite Reflectance

With all techniques there are limitations. True vitrinite is only found in post Silurian sediments, and only then in sediments with sufficient terrestrial clastic input. If vitrinite is present in a sample, an important source of error in determining its reflectance is the correct identification of vitrinite grains (Taylor *et al.* 1998, Lin 1995, Wilkins *et al.* 1995). Maceral groups can often be difficult to distinguish, and this becomes harder with increasing rank. In samples of dispersed organic matter, grains are often less than 25μm in diameter which can hamper accurate identification of macerals. However, this can be minimized by viewing the grain in both transmitted and reflected light. Natural variation in reflectance between macerals belonging to the vitrinite group add to the spread of data recorded from dispersed organic matter samples when grains are only identified to group level (Carr 2000). Poor polishing of a sample can reduce the quality of the reflectance determinations and increase the standard deviation of the data (Taylor *et al.* 1998).

Even if vitrinite grains within a sample are correctly identified, the population may have several different sources. Along with the indigenous population of vitrinite, a sample may also include reworked grains, as well as caved particles if cuttings are being examined (Dow *et al.* 1982, Wilkins *et al.* 1995). For this reason, it is important to analyse histograms of each sample to try to limit the error associated with foreign populations. It is desirable to measure about 100 grains per sample (Taylor *et al.* 1998), but this may not be possible when investigating dispersed organic matter.

There is also evidence that the response of vitrinite to increasing temperature may be affected by both environmental and geological factors. Examples of both suppression and retardation of vitrinite reflectance have been reported in the literature. Suppression is defined as the reduction in vitrinite reflectance relative to non suppressed vitrinite and occurs immediately after a sediment has been deposited (Carr 2000). Shales produced from muds deposited in reducing environments, along with those with high alginite content, are often associated with suppressed vitrinite reflectance values. Several samples

studied for this project were deposited under these conditions, and so the risk of suppression could not be avoided.

Retardation of vitrinite reflectance occurs when thermochemical modification of the rate of reactions responsible for increased vitrinite reflectance during burial takes place (Carr 2000). High pore pressure or overpressure appears to restrict the release of volatiles from the system and slow the maturation process. Several studies investigating the role of pressure on the evolution of vitrinite have been published including Fang (1992), Huang (1996), Dalla Torre *et. al* (1997) and Carr (2000).

3.2. PREPARATION

3.2.1 MACERAL SEPERATION

Samples for this project were acquired from a variety of sources including outcrops, cuttings and cores. All samples were processed using standard palynological techniques. In the case of outcrop samples, the rock was cleaned to remove traces of weathering and vegetation. All samples were crushed into gravel size pieces and enough material was placed in 500ml polythene bottles so that the bottom was covered (approx 30 – 40g). Each bottle was then filled with water, and decanted to remove any fine dust. This process was repeated until the water ran clear.

Approximately 150ml of 32% hydrochloric acid (HCl) was then added to the sample to determine if there was any carbonate present. If no carbonate was detected in the sample, the acid was decanted. If a sample reacted to the acid by effervescing, the acid was diluted by adding water to the bottle until it was half full. The sample was then left overnight in the acid to remove the carbonate component, and decanted the next day. The lid of each bottle had a hole pierced in it to allow for the venting of any gas released from the sample. Once carbonate was removed from the sample, 48% hydrofluoric acid (HF) was then added to dissolve the silicates. Each sample was stirred once a day while the rock was breaking down.

The time taken for each sample to dissolve varied from less than a week to 5 weeks. Once dissolved, the sample was decanted six times over a period of three days to neutralise the

hydrofluoric acid. The organic residue extracted from the sample was then sieved using 20μm nylon mesh sieve cloth to separate the fraction greater than 20μm. This residue was collected and then brought to the boil in a glass beaker with 50 – 100ml of hydrochloric acid to remove any neoformed fluorides and to clean the sample. After this procedure, the residue was decanted a further six times before it was sieved again.

3.2.2. MOUNTING

Both vitrinite and chitinozoa reflectance determinations were made during this project. Traditionally, organic residue is mounted in resin blocks approximately 8mm thick and reflectance measurements are made on the polished surface of these blocks (Figure 3.2a). However, due to the thickness of resin blocks, the residue cannot be viewed under transmitted light. Polished palynological sections offer an alternative to resin blocks where residue can be viewed in both transmitted and reflected light (Figure 3.2b). This is especially useful when locating true vitrinite grains. Polished resin slides were used in this study based on a technique adapted from that described in Hillier *et al.* (1988).

In order to make a polished palynological section, 22mm x 22mm cover slips were sprayed with PTFE Lubricant (Figure 3.2b). It was found that two separate light applications of this spray were more effective than one single heavy application (pers. comm. Goodhue 2004). The cover slips were sprayed once and then left to dry for at least 20 minutes. A second application was then applied to the cover slips and they were again left to dry. Once the cover slips were fully dried, sieved organic residue was pippetted onto the lubricant coated side. The residue was left to dry fully which could take up to two days.

Polyester or glass fibre resin was used to mount the organic residue. These resins only set after the addition of a hardener. Both resin and hardener are available from marine supply stores and large DIY stores. Two different brands of resin were used during this project and proved equally suitable. The ratio of hardener to resin varies from brand to brand from 1:19 to 3:7. For convenience, resin was usually prepared in 20ml batches. Once the hardener was added to the resin and thoroughly mixed, the liquid had a working time of approximately 15 minutes before the resin started to set. Similar to how palynological cover slips are mounted on slides using *Elvacite* mounting medium, the cover slips were mounted on slides using the prepared resin.

1) A plastic cap is used for the block mould.

3) The mould is then filled with *Epo-Thin* resin.

2) Dried organic residue is evenly spread on the bottom of the mould.

4) Once the resin has hardened, the mould is removed and the base polished.

Figure 3.2a: Schematic representation of procedure used to make cold resin blocks.

1) A size one cover slip was sprayed with PTFE dry lubricating agent.

2) Once the release agent had dried, a solution of water and organic residue was pipetted onto the cover slip and left to dry.

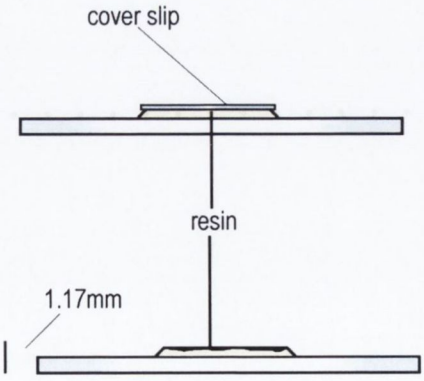

3) Once dry, the cover slip was then mounted onto a slide with polyester resin.

4) When the resin had dried, the cover slip was removed leaving a thin layer of resin with organic residue on its surface. The slide could then be polished.

Figure 3.2b: Schematic representation of procedure used to make palynological resin sections.

It was important to use only the minimum amount of resin required, as any excess would spread from under the cover slip and around its edges, making it difficult to release the cover slip later. To aid polishing, the cover slips were mounted in the centre of the glass slide. The resin was then left to harden overnight.

When the resin had hardened, the cover slip could be removed leaving the organic residue mounted on top of the resin sliver. A razor blade was used to flip the cover slip off the resin beneath. It should be noted that about one third of slides fail to release the cover slip from the resin, and it is always prudent to make more slides than necessary to allow for this. Once the cover slip had been removed the slide was then ready for polishing.

3.2.3. POLISHING

Three stages were involved in polishing the resin mount. Polishing was carried out by holding the section with a slide holder, and moving the slide in a figure of eight motion to prevent over polishing on a particular side. The surface of the resin was generally covered with a layer of PTFE lubricant left over from the cover slip. This was removed by polishing the slide for ten seconds on 1200 grade water-wet silicon carbide paper. The slide was then placed in an ultrasonic bath for 10 seconds to remove any of the polishing 'frit' before moving on to the next polishing stage. The slide was then polished on a lap using F-grade paste (1.0μm) for between 1-2 minutes and placed in the ultrasonic bath for 10 seconds. Using FF-grade paste (0.05μm) the section was polished for 2-3 minutes and then placed in the ultrasonic bath for the final time. Care should be taken not to place resin slides in the ultrasonic bath for any longer than necessary as the vibrations can cause the resin sliver to separate from the glass slide. The polishing procedure described here was usually sufficient to produce a satisfactory surface for reflectance determinations. It was occasionally necessary to repolish some sections to improve the surface finish. This was only apparent after viewing the slide under reflected light.

3.3. VITRINITE REFLECTANCE MEASUREMENTS

3.3.1. SYSTEM SETUP

The system used in this study to determine vitrinite reflectance employs image analysis software and was based on routines originally designed by McCaughan (2002) which were subsequently modified by Goodhue (pers. comm. 2003). A Leitz Ortholux 11 microscope, fitted with a strain-free 50x objective lens and a pair of viewing eyepieces of 10x magnification, was used to view the polished resin slides. In reflected light, the slide was illuminated using a 12V / 100W halogen light source connected to a stabilised power supply. The current was set at 6 .6A and the light was filtered through two neutral density filters. The slide could also be viewed in transmitted light.

A SONY XC-75/75CE CCD black and white video camera was mounted on the microscope's phototube and captured images of vitrinite to be processed (Figure 3.3). Each analogue image was then digitised, processed and analysed using a Leica Q500IW imaging workstation (McCaughan 2002). QWin, Leica's image analysis toolkit was the application that ran the vitrinite reflectance routine or program (RGReflectance. Q5R) created using an interactive macro programming facility know as QUIPS.

3.3.2. SYSTEM CALIBRATION

At the beginning of each session, the system was allowed to warm up for half an hour to allow the light source to stabilise. Following this period, the system was calibrated using four standards (Table 3.1). Room temperature ranged from 19 – 21°C and stray light was prevented from entering the microscope by making the measurements in darkness with the aid of a blackout curtain.

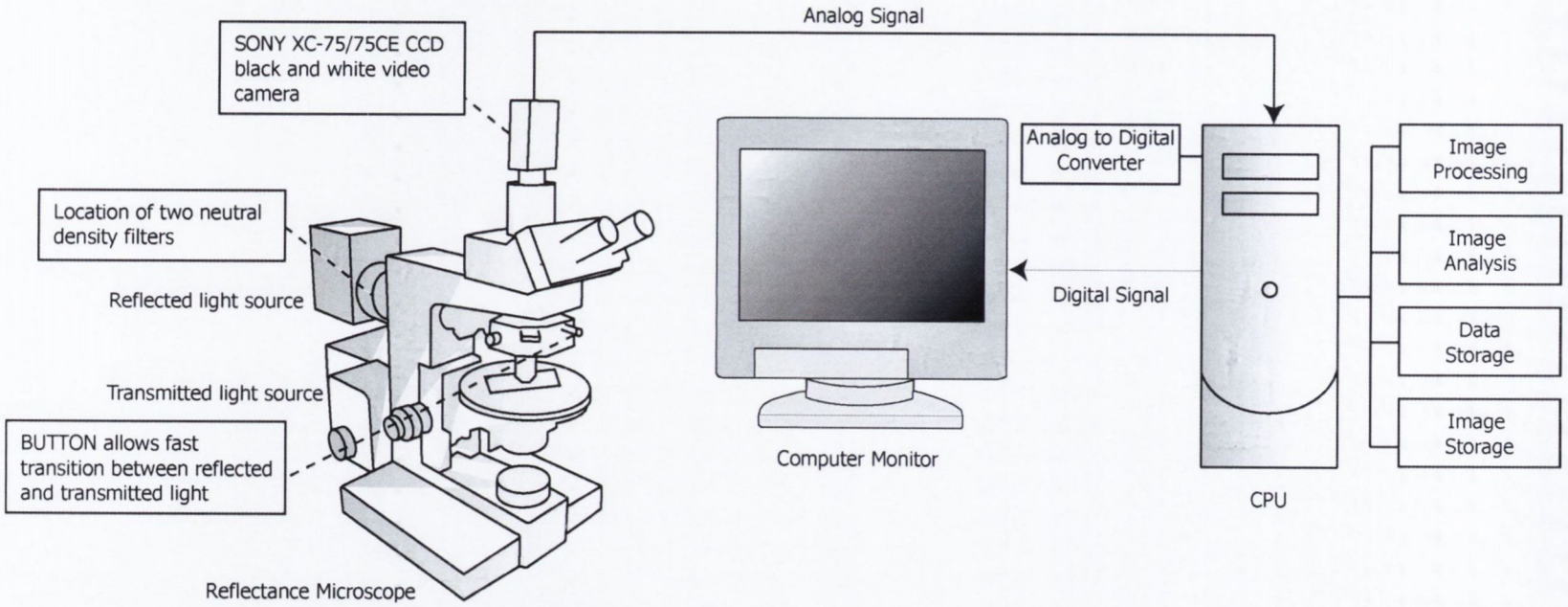

Figure 3.3: Schematic diagram of image analysis system used to measure vitrinite reflectance in this study (Modified from McCaughan 2002).

Standard	$\%R_o$	$\%R_a$
Spinel (McCrone No. 307)	0.42	7.17
Glass (Leitz No. 998)	1.23	9.60
Cubic zirconia (McCrone No. 319)	3.28	13.90
Silicon carbide (McCrone No. 339)	7.56	20.70

Table 3.1: Standards used for reflectance microscope calibration. $\%R_o$ indicates reflectance under oil, $\%R_a$ reflectance in air.

Each standard was placed on the microscope stage and a small drop of *Leica* immersion oil placed on the surface. A focused image of the standard was captured using the attached video camera and sent to the image analysis program. An area was then selected by the user and its mean grey level determined. This procedure was repeated for each standard. Once the four grey levels of the standards had been measured, the image analysis program equated these to the known level of reflectance of each substance and calibrated the system accordingly. This procedure was carried out every time the system is used. All standards were embedded in a matt black medium, cleaned regularly with alcohol and stored in a dessicator.

3.3.3. Reflectance Measurements

Polished samples were placed on the microscope stage and the resin covered with a small drop of *Leica* immersion oil (Figure 3.4). Much of the difficulty associated with making vitrinite reflectance measurements centres around the correct identification of grains. The use of polished resin sections which allows the examination of organic matter in both transmitted and reflected light eliminates much of this uncertainly. The procedure used in choosing suitable grains and determining the reflectance of a sample is summarised in Figure 3.5. All samples studied for this project had experienced some degree of thermal alteration but there was always sufficient detail to avoid confusion between vitrinite grains and any other macerals.

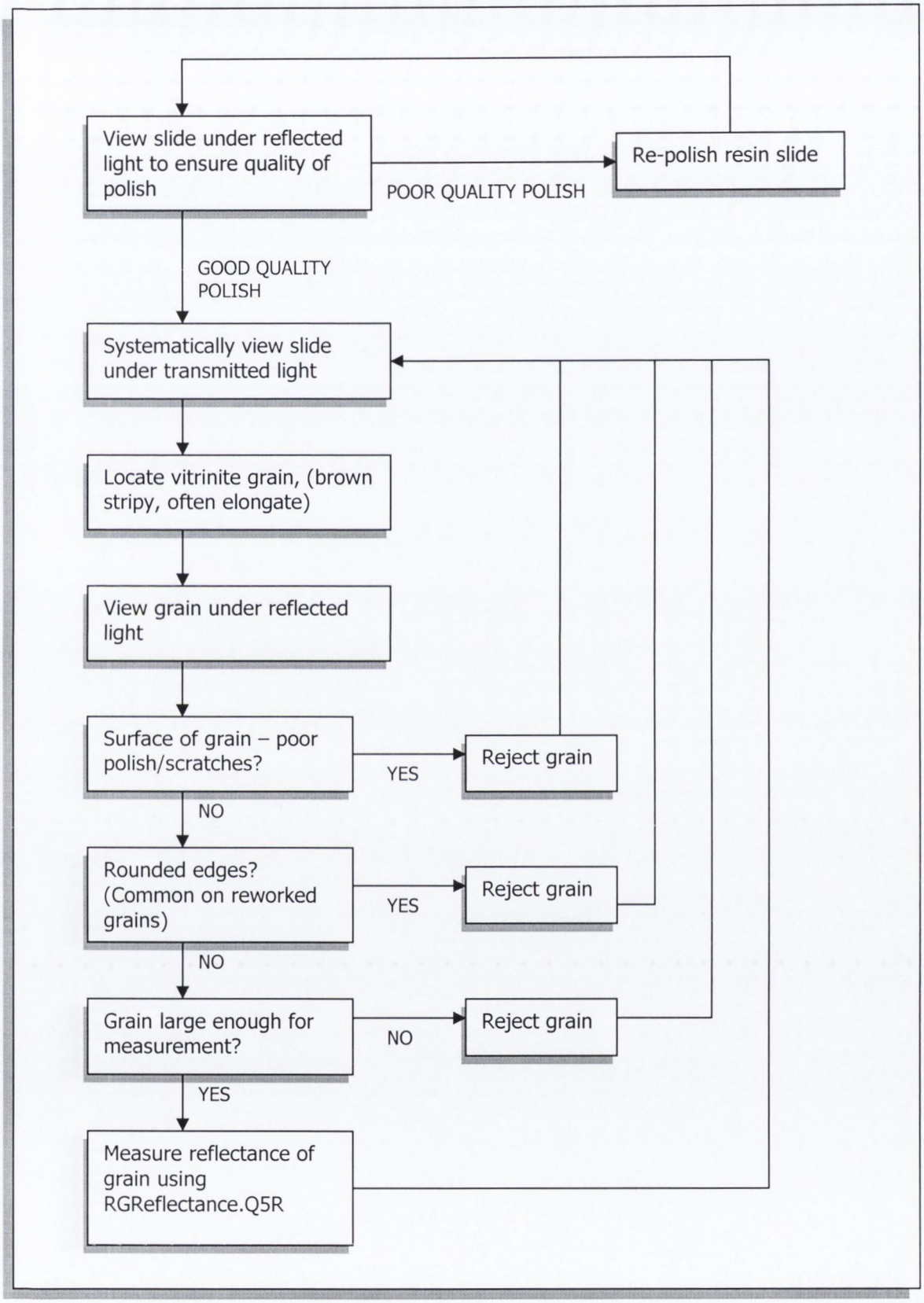

Figure 3.5: Flow chart of the process for choosing vitrinite grains suitable for reflectance determinations.

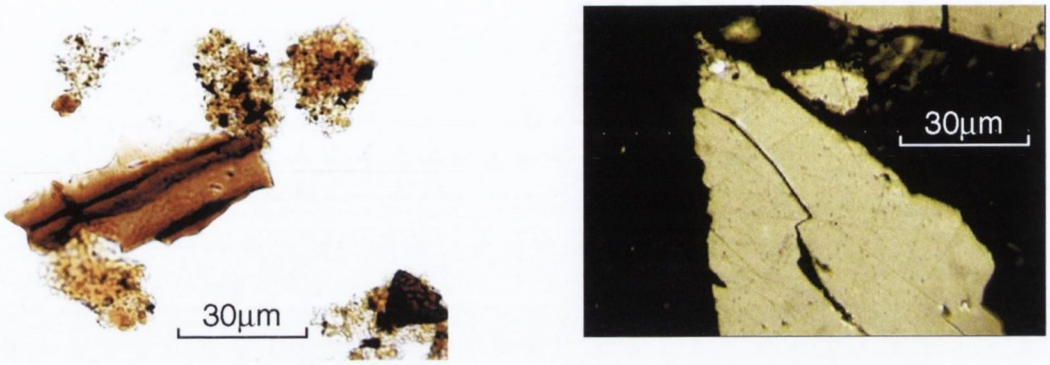

Figure 3.4: Vitrinite grain in transmitted light (left) with characteristic brown stripes. View of vitrinite grain under reflected light (right).

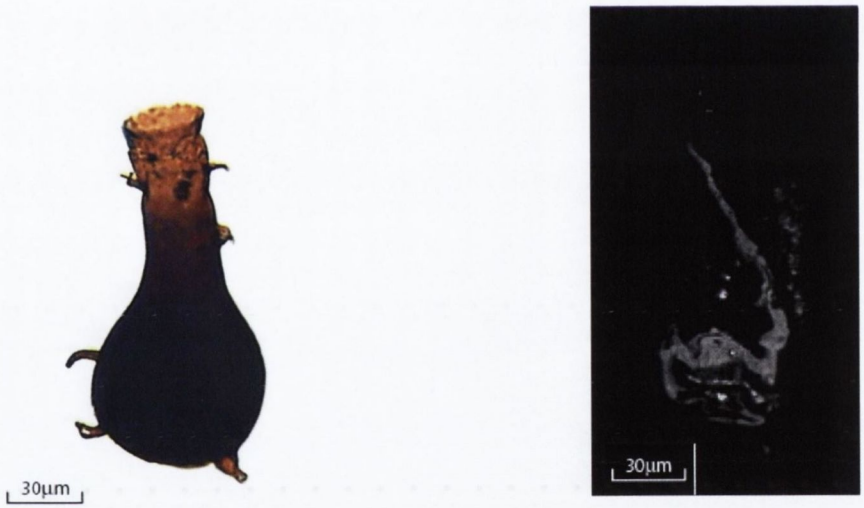

Figure 3.6: Chitinozoa in transmitted light (left) and reflected light (right).

3.3.4. CHITINOZOA REFLECTANCE

In several samples studied for this project, there were very few or no vitrinite grains present on which to make reflectance determinations. However, many of these samples contained chitinozoa which were used as vitrinite reflectance proxies. Chitinozoa are enigmatic organic walled microfossils with distinctive flask or bottle shaped tests (Brasier 1980, Tricker *et al.* 1992, Miller 1996). They have a useful stratigraphic range from the early Ordovician to the latest Devonian (Tricker *et al.* 1992). Their test size varies from 50 – 2000μm (Figure 3.6) (Tricker *et al.* 1992). Most specimens used for reflectance determinations in this project were 100 – 250μm in diameter and were found in the Jordanian samples.

The measurement of chitinozoa reflectance uses the same technique as that employed for vitrinite reflectance with a polished resin section viewed under reflected light. Some work has been carried out calibrating chitinozoa reflectance with other thermal maturity indicators (Bertrand *et al.* 1987, Bertrand *et al.* 1990, Tricker *et al.* 1992, Obermajer *et al.* 1996) with promising results. The work of Tricker *et al.* (1992) appears to be the most robust study undertaken to calibrate vitrinite and chitinozoa reflectance and it is the equation published in their paper that is used in this study: $R_{ch} = 1.152R_v + 0.08$ (Figure 3.7)

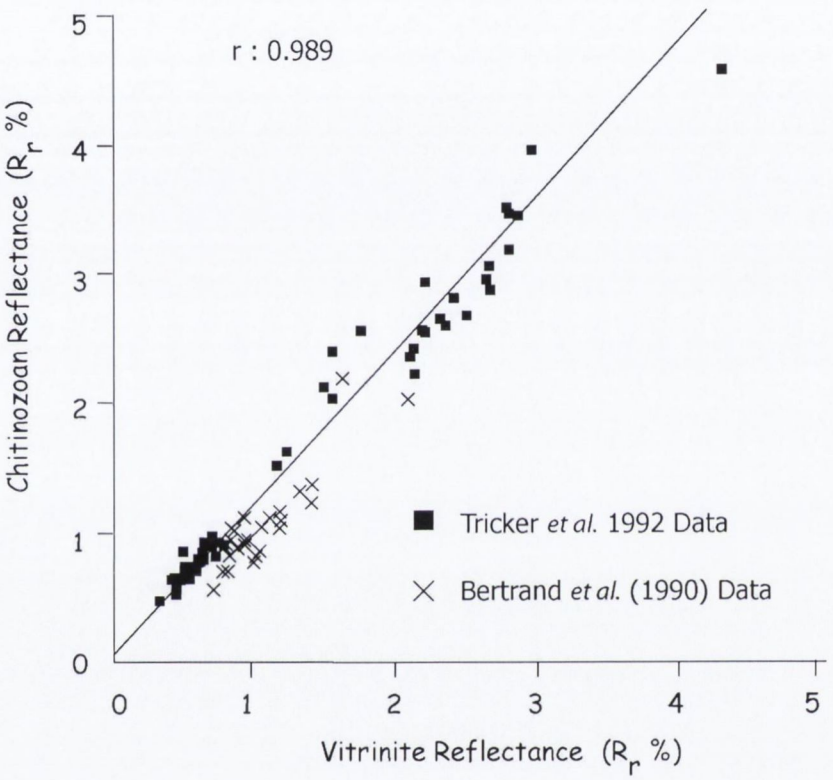

Figure 3.7: Chitinozoa (R_r%) reflectance vs. Vitrinite Reflectance (R_r%) from Tricker *et al.* (1992). The regression line shown is calculated on the data of Tricker *et al.* (1992). Bertrand *et al.* (1990) data are shown for comparison.

CHAPTER 4

COLOUR DETERMINATIONS: THEORY AND METHOD

4.1. COLOUR AS A MATURITY INDICATOR

4.1.1. INTRODUCTION

The assessment of microfossil colour is perhaps the most common tool used to assess thermal maturity of sediments after determination of vitrinite reflectance. Thermal alteration of microscopic organic material within sediments affects both their chemical and physical properties. The most obvious of these changes observed in microfossils is the altering of their colour. Conodonts, spores and pollen are the most frequently used microfossils for assessing thermal maturity based on colour. Epstein *et al.* (1977) produced the 5 point Conodont Alteration Index (CAI) which linked conodont colour with specific temperature ranges. Colour determination was based on visual estimation of colour and comparison with a series of photographs. This technique is widely used and successful because of the range of temperatures that can be estimated and the long fossil record of conodonts found in rocks from the Cambrian to the Triassic (Marshall 1990). However, it is rarely applicable to lithologies other than limestones.

Spore and pollen colour have also been calibrated against other maturity indicators like vitrinite reflectance to provide another method for assessing thermal maturity. Several colour scales have been published with Staplin's 'Thermal Alteration Index' (TAI) (1969, 1977) perhaps the most widely used. It is based on a 5 point scheme. Other examples include The 'Spore Colouration Index' (SCI), a 10 point scale produced by Robertson Research International (Barnard *et al.* 1976) and Batten's (1976, 1996) 7 point spore colour scale. The main advantages of using spore colour as a maturity indicator are the cost and speed at which determinations can be made. However, consistency of colour determinations between laboratories is difficult to establish as visual estimation inherently varies from user to user. Visual references like the Pollen/Spore Colour 'Standard' (Pearson 1984) produced by the Phillips Petroleum Company can help to limit variation. The need for standardized preparation techniques, light sources and types of spores to be measured are all important considerations in reducing variation amongst laboratories (Staplin 1982). As with vitrinite reflectance, it is also important to ensure only the

indigenous population is taken into account, ignoring reworked or caved samples. A summary of microfossil groups whose colours are used as maturity indicators is shown in Table 4.1, together with their relative importance and stratigraphical range.

Microfossil Group	**Use of Colour**	**Geological Range**
Miospores	***	Ordovician - Recent
Conodonts	***	Cambrian – Triassic
Dinoflagellate cysts	*	Triassic – Recent
Acritarchs	*	Precambrian – 'sub-Recent'

Table 4.1: Relative use of colour of different microfossil groups to assess thermal maturity (Marshall 1990). * = minor application *** = significant use

4.1.2. Image Analysis

As discussed above, one of the problems with using colour as a maturity indicator is that determination of colour is based on visual estimation and is subject to human error. To remedy this situation, several workers have concentrated on developing techniques which can describe palynomorph colour quantitatively. Essentially, two different methods have been explored. The first deals with spectral analysis of light transmitted through palynomorphs and the second utilises image analysis.

Gutjahr (1966) and Grayson (1975) showed a systematic decrease in spore transmittance with increasing depth of burial, but their techniques never became widely used (Marshall, 1991). Smith (1983) used spectral data to correlate 'standard' palynomorph material from Staplin's TAI scale, Robertson Research International's SCI scale and Batten's 7 point scale. Lo (1988) measured the transmittance of spores at a wavelength of 546nm and compared it to visually estimated TAI and vitrinite reflectance data. Marshall (1991) also used spectral data to investigate spore colour change and was the first to use the Commission Internationale de l'Eclairage colour system. This system is based on the premise of a standard observer and colour is defined in terms of three variables; the chromaticity co-ordinates(X and Y), and luminance (L), the total amount of light as defined by the transmittance or absorbance of a substance. This standardized system has created stability of both colour measurement and definition and is used widely in the

chemical, food and textile industries (Marshall 1991). Marshall (1991) provides a good summary of the theory behind this system and the reader is referred to this publication for a more detailed description. The advantage of his technique is that, particularly through the use of a standardized colour system (CIE), inter- laboratory variation could be reduced significantly. However the equipment required to make these determinations, micro-spectrophotometers, are expensive and not readily available in most laboratories. Also, use of the CIELAB system which is inherently complicated has limited Marshall's technique (Yule *et al.* 1998).

An alternative approach to the problem of quantifying palynomorph colour utilises colour image analysis (CIA). These systems involve digitising images of palynomorphs which are usually displayed on a VDU and consist of a series of pixels (Ujiié 2001). Each of these pixels has specific RGB (Red, Green, and Blue) values and using an image analysis program various functions can be performed on the digitised image. Yule *et al.* (1998) used an image analysis system to quantify the colour of spores from a series of boreholes and artificially matured samples. Using the RGB system, colours are described in terms of three variables, red, green and blue. The intensity of each colour can vary from 0 – 255 and 16.7 million colours can be described using this scheme. Yule *et al.* (1998) found that average green intensity of spores within a sample was the most effective indicator of maturity. He observed that the widest range of colours within single samples occurred in samples with R_r values between 0.6 and 1.04%, samples that were mature with respect to the oil window. Average green values of spores within these samples ranged from 60 to 160 and he concluded that green intensity was directly related to the chemical phases of the spore wall.

Van de Laar *et al.* (1998) studied spores from a core of Carboniferous Coal Measures and found red intensity was the most sensitive channel to changes in thermal maturity. Ujiié (2001) used image analysis to measure the grey level or 'brightness' of spores and showed a reduction in brightness with increasing maturity. McCaughan (2002) made RGB colour determinations on amorphous organic material obtained from samples taken at variable distances from a number of dykes (Figure 4.9). Both the green and red parameters were sensitive to changes in organic maturity correlating well with vitrinite reflectance data. Blue intensity data were the least useful indicator, with a higher degree of scatter within individual samples than the red or green data sets.

The equipment necessary to make RGB colour determinations is readily available in most facilities and requires only a transmitted light microscope, a colour video or digital camera, and an image analysis system. Although the RGB system of describing colour is not intuitive, it is more accessible than the CIE colour system. However, unlike the CIE colour system, determinations of RGB intensities are device dependent. Combinations of different light sources, cameras and image analysis programs will yield different values of RGB. There also still remains a degree of subjectivity involved in selecting the area of the palynomorph to be measured. Also, in both methods of describing colour, differences in wall thickness among spores will affect the data collected.

4.2. ACRITARCHS

4.2.1. INTRODUCTION

The Group Acritarcha was proposed by Evitt (1963) as an informal group of organic-walled microfossils to accommodate those taxa that had previously been assigned to the hystrichospheres (Wetzel 1933) and could not be referred to the dinoflagellates on the basis of morphological criteria. Thus, by definition the biological affinity of acritarchs is unknown (Servais *et al.* 1996). Once the biological relationship is established for an acritarch, it is reassigned to its proper biological category (Martin 1993, Colbath *et al.* 1995).

Acritarchs are considered to be the resting cysts of single-celled or apparently single-celled eukaryotic, predominantly marine organic walled microfossils (Martin 1993, Wicander 2002). They are widely thought to be polyphyletic in origin, based in part on their diverse morphology (Evitt 1963, Martin 1993, Strother 1996). Most are thought to be some type of resting cyst, due to the fact that many specimens exhibit an excystment structure (Downie 1973, Al-Ameri 1986, Martin 1993). Acritarchs vary in size from <10μm to more than 1mm, but the majority of species range from approximately 15 to 80 μm (Wicander 2002). Generally thought to have made their first appearance in the Mesoproterozoic, their maximum abundance and diversification occurred between the early Cambrian and late Devonian (Martin 1993, Wicander 2002, Playford 2003).

Unlike the systematics of most groups that are based on phylogeny, in which classifications rely on evolutionary relationships, acritarchs are treated as form taxa under the International Code of Botanical Nomenclature and are thus grouped on a phenetic basis that does not necessarily reflect genetic relationships (Servais *et al.* 1996, Strother 1996, Wicander 2002, Playford 2003). Downie *et al.* (1963) produced a phenetic classification that divided the acritarchs into 13 subgroups. The essential structure of this scheme has been retained but modified by other workers including Evitt (1969), Diver *et al.* (1979) and Tappan (1980). However, many acritarch researchers prefer to list taxa alphabetically by genera and species, so as not to suggest a biological relationship between members within a subgroup (pers. comm. Wicander 2006).

With increasing work being carried out on the biogeochemistry and wall ultrastructure of acritarchs (e.g., Jux 1975, Al-Ameri 1986, Arouri *et al.* 2000, Talyzina *et al.* 2000), it is likely that these attributes will illuminate the relationship of acritarchs to other organic-walled microfossils and similarities between acritarch taxa.

4.2.2. *VERYHACHIUM*

A detailed taxonomic review of *Veryhachium* is given by Sarjeant *et al.* (1994) and the following account is based on that publication. Part of the polygonomorph complex of acritarchs, *Veryhachium* is an example of an acritarch whose vesicle shape is modified or controlled by the number and position of the spines (Sarjeant *et al.* 1994)(Figure 4.10). Its fossil record ranges from late Cambrian to Tertiary (Sarjeant *et al.* 1994). *Veryhachium* was originally erected by Deunff (1954, p.306) who classified it as a 'hystrichosphere,' a member of the Family Hystrichosphaeridae O. Wetzel 1933, a group of micro-organisms of uncertain systematic position. The diagnosis of *Veryhachium* has since been emended numerous times (Downie 1960, Wall *et al.* 1963, Downie *et al.* 1963, Loeblich Jr. *et al.* 1969). A notable emendation by Wall and Downie (1963) restricted the genus by only including those hystrichospheres with three to eight spines, where the shape of the test is more or less determined by the number of spines. *Veryhachium,* as used in this study is restricted to those specimens with a psilate vesicle wall when viewed by optical microscopy and with three spines arising from the same plane and extending outwards from the vesicle at its corners.

Following Evitt's evaluation of the hystrichospheres in 1963, *Veryhachium* was transferred along with other enigmatic genera to the Group Acritarcha. Downie *et al.* (1963) divided the acritarchs into thirteen phenetic subgroups and *Veryhachium* was placed in the Polygonomorphitae subgroup (Strother 1996).

VERYHACHIUM Deunff 1954 emend. Sarjeant and Stancliffe 1994

Type species: *Veryhachium trisulcum* Deunff 1954

Synonymy:

Hystrichotriangulatum Andreyeva 1966, p. 132-133 [see Loeblich Jr. and Tappan 1969, p. 55-56]

Impluviculus Loeblich Jr. and Tappan 1969, p. 48; emend. Martin 1975, p.15 [see Eisenack, Cramer and Diez 1979a, p. 265]

Simsangia Baksi 1962, p. 18 [see Sarjeant 1970, p. 293]

Wilsonastrum Jansonius 1962, p. 88-89 [see Schaarschmidt 1963, p. 62-63]

Original Diagnosis: (Deunff 1954a, p. 306). Planktonic fossil micro-organism of organic material, more often yellow or brown in colour, sometimes black, shell with surface smooth or granular. General form depending on the number of processes (1-8), not globular except when only one horn. Processes almost always pointed, generally long or very long, often curved. Diameter of shell body 10μm to 40μm, rarely more or less. Total dimensions often 100μm or more (translation by Norris and Sarjeant 1965, p. 62).

Emended Diagnosis: (Sarjeant and Stancliffe 1994, p. 33). Vesicle cushion shaped, triangular to quadrangular in outline, with sides convex to concave, eilyma thin, single-layered or apparently so. Spines arise from the angles and proximally merge so smoothly with the vesicle wall that no exact limit can be set to their basis. They are arranged in a single plane, though a single accessory spine of markedly smaller size may be developed on one surface of the vesicle. Spines hollow, cuneiform to acuminate in shape and uniform in size or nearly so; distally they are closed, simple and pointed. The spine cavity communicates freely with the interior of the vesicle. Surface of vesicle and spines laevigate to granulate, but without verrucae, striae or secondary spinelets. Escape structure, where developed, typically an epityche but, in quadrangular forms may be a linear slit.

A list of valid species is given in Sarjeant and Stancliffe (1994).

4.3. PRASINOPHYTE PHYCOMATA

4.3.1. INTRODUCTION

The prasinophytes are generally considered a class of green algae (Colbath *et al.* 1995, Guy-Ohlson 1996). Prasinophycean algae are characterised by having two distinct phases in their life history; a motile phase, and a cyst-like non-motile phase that develops from the motile phase (Guy-Ohlson 1996). The cyst-like phycoma is formed when the motile cell sheds its flagella and rounds up (Colbath *et al.* 1995). Following asexual division within the phycoma, four or more daughter cells are produced (Colbath *et al.* 1995). The phycoma includes a very resistant, easily fossilized, external wall which opens upon maturity of the daughter cells (Martin 1993).

Prasinophytes are found in both marine and fresh water environments (Martin 1993, Colbath *et al.* 1995, Guy-Ohlson 1996). Algal blooms of prasinophycean algae have been recorded in the geological record from Jurassic sediments of Alaska, and the tasmanite deposit of Tasmania (Revill *et al.* 1994, Guy-Ohlson 1996).

4.3.2. *TASMANITES*

The tasmanitids, exemplified by *Tasmanites* Newton 1875 are spore-like in general form and were reported for many years as '*Sporangites*' (Winslow 1962)(Figure 4.11). They range in size from less than 100µm up to 600µm with vesicle wall thicknesses as much as 70µm (Winslow 1962, Al-Ameri 1986). Punctation and radial wall pores are common (Winslow 1962, Wall 1962, Guy-Ohlson 1996).

The history of the study of *Tasmanites* has been plagued by confusion and uncertainty concerning its origin and taxonomic placement. A timeline of the major events in tasmanitid research is shown in Table 4.2. When Evitt (1963) reviewed the hystrichosphere group he placed the tasmanitids in his new Group Acritarcha. Shortly thereafter, he abandoned this assignment and instead proposed that the Family Tasmanaceae be regarded as Chlorophyceae (Downie *et al.* 1963). Wall (1962) compared *Tasmanites* to modern day algae, *Pachysphaera* and *Halosphaera*. Based on the similarity

1852	Hooker	Reported sphaeroidal bodies from Silurian of England.
1863	Dawson	Described *Tasmanites* as *Sporangites* from localities in Northern United States and Canada.
1865	Ralph	Identified spherical bodies found in high concentrations at Latrobe, Mersey River, Tasmania as algae.
1875	Newton	Named spherical bodies found in Tasmanite as *Tasmanites punctatus* and also described them as algae.
1883	Orton	Minor record
1886	Wethered	Minor record
1888	Dawson	Considered his name of '*Sporangites*' to have priority over Newton's '*Tasmanites punctatus*'.
1931	Eisenack	Described them from Baltic region, first as new species of the existing genus *Bion. He* later chose *Bion solidum* as the type species for the new genus - *Leiosphaera*
1941	Krausel	Reviewed the component species of Dawson's *Sporangites,* removing the species *huronensis* from this genus and transferred it to *Leiosphaera*
1944	Schopf *et al.*	Reconsidered the taxonomy of *Sporangites* and *Tasmanites* unaware of Krausel's work. They rejected the name *Sporangites* and transferred its algal species to genus *Tasmanites.*
1956	Sommer	Created many new species of *Tasmanites,* on the basis of rich Brazilian assemblages, and erected a new family, the Tasmanaceae, classifying it Algae *incertae sedis*
1958	Eisenack	Recognised the synonymy of *Leiosphaera solida* with *Sporangites huronensis.* The name *Leiosphaera solida* was rejected and the reallocation of *huronensis* to *Tasmanites* accepted. The remaining thin-walled forms of *Leiosphaera* was placed into a new genus *Leiosphaeridia*
1960	Sommer	Erected Order Tasmanales to include his Family Tasmanaceae
1963	Madler	Unaware of Sommer's work, also proposed the erection of a Family Tasmanaceae placed into the Order Tasmanales
1963	Evitt	Major revision of hystrichospheres, a grouping of problematical microfossils into which the leiospheres and the tasmanitids had been placed by some. He transferred both leiospheres and tasmanitids into the Acritarcha (genera of unknown affinity)
1962	Wall	Demonstrated the extremely close morphological similarity between *Tasmanites* and two living genera of unicellular algae, *Pachysphaera* and *Halosphaera*
1962	Christensen	His work led to the establishment of a new algal class, the Prasinophyceae, which now includes the living genera *Halosphaera* and *Pachysphaera*
1963	Downie *et al.*	Produced a 13 group classification of the acritarchs, but excluded *Tasmanites.* Proposed the Family Tasmanaceae be regarded as Chlorophyceae
1964	Deflandre *et al.*	Despite Evitt abandoning the transfer of tasmanitids into the Acritarcha some authors still treated them as such
1965	Norris *et al.*	Endorsed the decision by Downie et al. (1963) to exclude *Tasmanites*
1965	Staplin *et al.*	Proposed genus should constitute an acritarch subgroup Tasmanititae
1966	Timofeyev	Includes tasmanitids in his acritarch classification in the Group Sphaeromorphida, Subgroup Monosphaeritae
1967	Downie	Placed tasmanitids in Prasinophyceae class without commenting on their familial assignation
1968	Jux	Electron microscope studies on the walls of fossil tasmanitids and genera of Prasinophyceae show they share thick walls containing radial structures - canals, laminations, of closely comparable nature
1988	Guy – Ohlson	Carried out scanning electron microscope (SEM) examinations on well-preserved specimens of Mesozoic *Tasmanites.* She revealed a series of developmental stages in the life cycle of the palynomorph and striking similarities with the life cycles of extant algae *Pachysphaera*, *Halosphaera* and *Pterosperma*

Table 4.2: Notable events in *Tasmanites* research (After Muir *et al.* 1971).

of their wall structure and characteristic wall pores, Wall considered *Pachysphaera* to be the extant representative of the fossil *Tasmanites*. Work by Christensen (1962) resulted in the establishment of a new algal class, the Prasinophyceae, which now includes the living genera *Pachysphaera* and *Halosphaera* (Muir *et al.* 1971).

Scanning electron microscope (SEM) studies carried out by Guy-Ohlson (1988) on well preserved specimens of Mesozoic *Tasmanites* revealed a series of developmental stages in the life cycle of the palynomorph and striking similarities with the life cycles of the living algae *Pachysphaera*, *Halosphaera,* and *Pterosperma*. Although occasionally still referred to as an acritarch, *Tasmanites* is accepted by most palynologists as a prasinophyte (Martin 1993, Colbath *et al.* 1995, Guy-Ohlson 1996).

TASMANITES Newton 1875

Type species: *Tasmanites punctatus* Newton 1875

Tasmanites was originally described by Newton (1875) but Eisenack (1958) was the first to publish a diagnosis. Newton's original discussion is reproduced in Eisenack's publication and is not commented on further here.

Diagnosis (Eisenack 1958, p. 231): Hollow spherical, generally comparatively thick-walled and of a very resistant, yellowish to dark red-brown hyaline organic substance consisting of organic remains which often are preserved in a disc-shaped compressed state or also irregularly folded. Wall with more or less numerous pores which rarely penetrate the entire wall, but often either end blindly in the thick wall from the outside or from the inside. Pylome present, however usually uncommon. The wall pores are not always visible in each specimen of a species: it is essential that they should occur in the majority of the species. Young examples are indeed always thin-walled and then lack the pylome. They are then not distinct from *Leiosphaeridia*.

A list of valid species is given in Fensome *et al.* (1991).

4.4. ACRITARCH ALTERATION INDEX

4.4.1. PREVIOUS WORK

While much work has been carried out on spore colour and its use as a thermal maturity indicator, acritarchs have, for the most part, been neglected. Legall *et al.* (1981) first published an 'Acritarch Alteration Index' (AAI). In their study of thermal maturation of Southern Ontario, they calibrated a single acritarch genus against the existing 'Conodont Alteration Index', (CAI). *Leiosphaeridia* Eisenack 1958 emend. Downie and Sarjeant 1963 was chosen by them as the most suitable acritarch for colour determinations because of its relatively simple morphology and large size. Based on the presence of degraded leiospheres in strata with CAI values of 2 – 2.5 (indicating peak temperatures of 50-90°C) they established a maximum thermal limit of 90°C for their AAI, suggesting leiospheres do not survive much higher temperatures. They inferred a 60°C minimum temperature for the strata from a range of data collected in the area. Legall *et al.* (1981) used visual estimation to determine the colour of leiospheres and to ensure consistency compared them to colour photographs representing each point. Their five point AAI is shown in Figure 4.1 along with a correlation of temperature and CAI values.

Bertrand *et al.* (1989) published a short abstract which stated for samples of equal rank, the acritarch alteration index should have lower values than the spore thermal alteration index. They also noted that acritarchs were better preserved than spores in samples of higher maturity.

Williams *et al.* (1998) studied Palaeozoic strata in western Newfoundland. Unlike Legall *et al.* (1981), Williams *et al.* (1998) used acritarch assemblages rather than a single genus as thermal maturity indicators. They believed that while there were different maturation paths for spores and acritarchs in immature strata, there was little difference within the oil window. Acritarch assemblages from Cambro-Ordovician rocks were calibrated against TAI data of spores found in nearby Carboniferous rocks. However, it is not clear from the publication how Williams *et al.* could be sure that the level of thermal maturity of the Cambro-Ordovician sequence was the same as the adjacent Carboniferous succession. They found that AAI values in the upper part of the oil window were lower than corresponding spore TAI but by the time the floor of the oil window was reached, spore

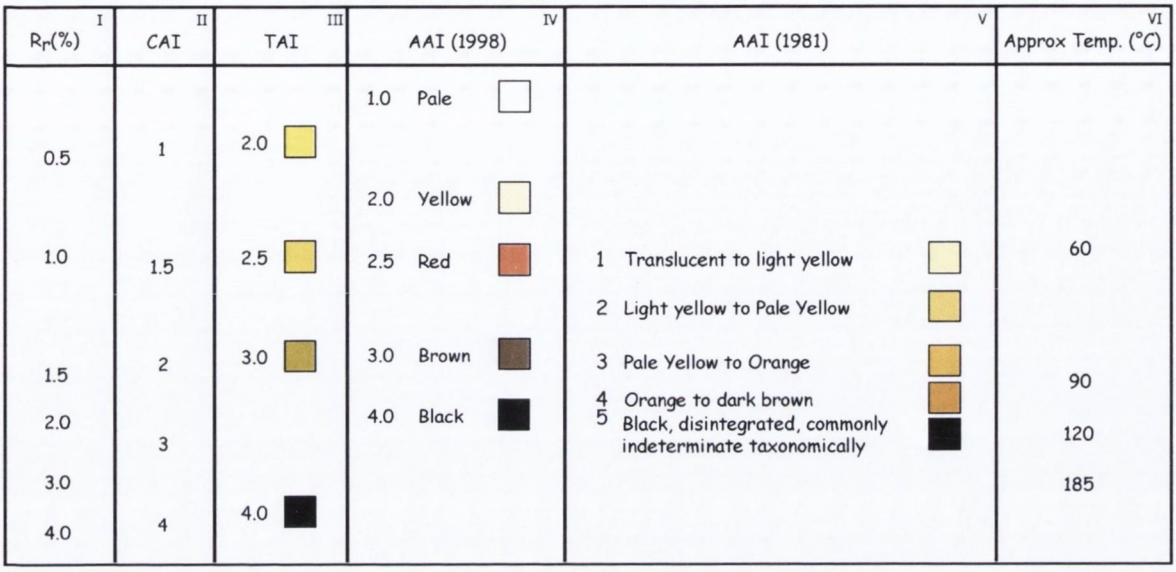

Figure 4.1: Correlation of various thermal maturity indicators after Legall *et al.* (1981) and Williams *et al.* (1998).

I: Random vitrinite reflectance data from Gentizis *et al.* (1996) in Williams *et al.* (1998)

II: Conodont Alteration Index data from Gentizis *et al.* (1996) in Williams *et al.* (1998)

III: Thermal Alteration Index data from Staplin (1977) in Williams *et al.* (1998), Colour values from Pearson (1984).

IV: Acritarch Alteration Index from Williams *et al.* (1998). Colour values are taken from their literal description as no colour chart was published.

V: Acritarch Alteration Index from Legall *et al.* (1981). Colour values taken from literal description (1, 5) and colour photographs (2, 3 and 4).

VI: Approximate temperature data from Legall *et al.* (1981) based on their assessment of conodont and kerogen colour, and regional studies of the southern Ontario area.

and acritarch colour were essentially equivalent. Their calibration of acritarch colour against other maturity indicators is shown in Figure 4.1.

4.5. COLOUR DETERMINATIONS

4.5.1. SAMPLE PREPARATION

Samples were processed using standard palynological techniques, as described in section 3.2.1. Sieved organic residue was pippetted onto No.1 thickness 22 x 40mm cover slips and allowed to dry overnight. Once water had evaporated from the cover slips, they were mounted onto 1 – 1.2mm thick 76 x 26mm slides using *Elvacite* mounting medium. A number of strewn slides were made for each sample. Once samples were mounted they were visually scanned to locate any *Veryhachium* or *Tasmanites* specimens. When a specimen was found, its location was recorded using an *England Finder* reference slide. Sample labels were placed to the right of each slide (see Figure 4.2). To locate any acritarch specimen listed in this study using an *England Finder* reference, the slide should be placed on the microscope stage with the label at the right hand side.

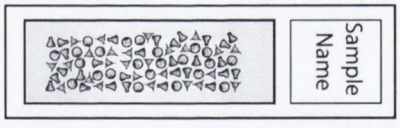

Figure 4.2: Sample labels were placed on the right of each strewn slide.

4.5.2. IMAGE ANALYSIS SYSTEM INTRODUCTION

The image analysis system used in this project utilised routines written by McCaughan (2002). Strewn slides were viewed using Leitz Dialux 20 transmitted light microscope with a Leitz NPL Fluotar L25/0.55 objective. Images of the selected acritarchs were captured using a JVC TK-C1380 colour video camera attached to the microscope's phototube. A Leitz Wild Heerbrugg power supply set to 9V and a 100W halogen light bulb were used to illuminate the system. Once a suitable palynomorph had been found, the field of view was captured by the colour video camera and converted to a digital image by

an Analogue to Digital Converter (ADC) within the Leica Q500IW imaging workstation (McCaughan 2002). The QWin image analysis program was used, together with routines written in the accompanying QUIPS macro programming facility, to analyse the image and determine the average RGB (Red, Green and Blue) intensity of the palynomorph.

4.5.3. Microscope Set up

Unlike some systems used to determine colour which rely on spectral measurements, the determination of RGB intensities is device dependent. Combinations of different microscopes, cameras and light sources will produce different RGB readings of the same object. Even using the same device to measure colour, there are day to day variations. To combat this problem a standardised routine, modified from that employed by McCaughan (2002) was carried out each time the system was used.

The camera and light source were switched on and allowed to warm up for half an hour before any measurements were made. The system was illuminated by a 100W halogen bulb with the voltage set to 9V. This light setting was chosen to provide the whitest background light and to produce the greatest spread of RGB values between dark and light acritarchs. Figure 4.3 shows the RGB values of four different coloured *Veryhachium* measured at different light settings, with and without neutral density filters, and with different camera shutter speeds.

McCaughan (2002) found that an inconsistent condenser/field diaphragm position was a major source of error in calibrating the system. As a result, he designed a procedure to ensure consistent positioning of these elements which was followed during this study. Using the x25 objective, the surface of a glass slide was brought into focus and the field diaphragm fully closed. The condenser stop screw was moved back and the condenser raised into its uppermost position using the vertical adjuster. The condenser stop screw was then used to lower the condenser slightly so that the edge of the field diaphragm appeared sharp. Using the centering screws, the image of the field diaphragm was centred on the cross hairs. Finally, the field diaphragm was opened until it disappeared just beyond the edge of the field of view.

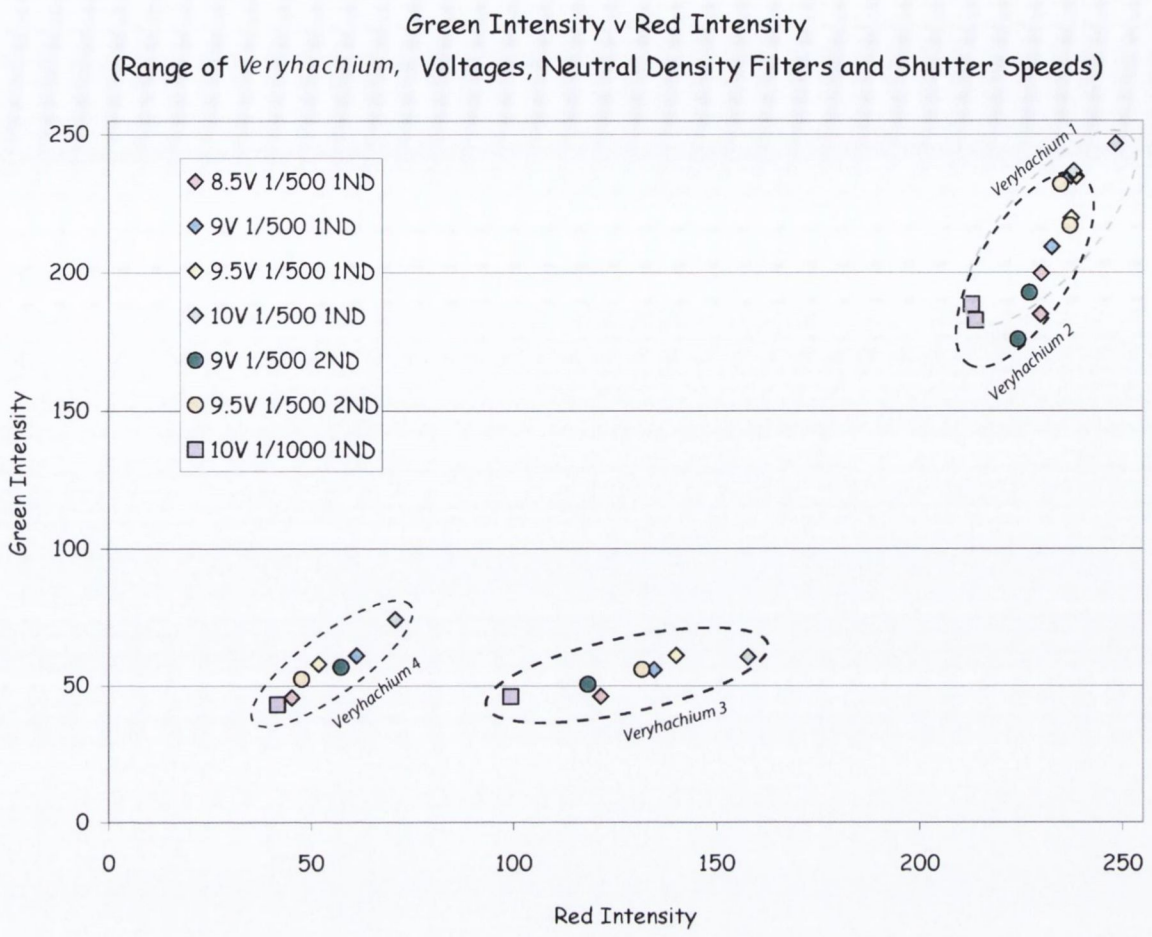

Figure 4.3a: Green intensity vs. red intensity of four *Veryhachium* specimens (shown below) under different lighting conditions. Camera shutter speed varied between 1/500 and 1/1000. Light source voltage ranged from 8.5V to 10V and either one or two neutral density filters (ND) were used. It was decided to use a combination of 2 neutral density filters, a shutter speed of 1/500 and a power supply set a 9V. This setting gave the greatest spread of red and green intensities between the four different *Veryhachium* (below) and distinguished between the two palest specimens without 'burning out' the images.

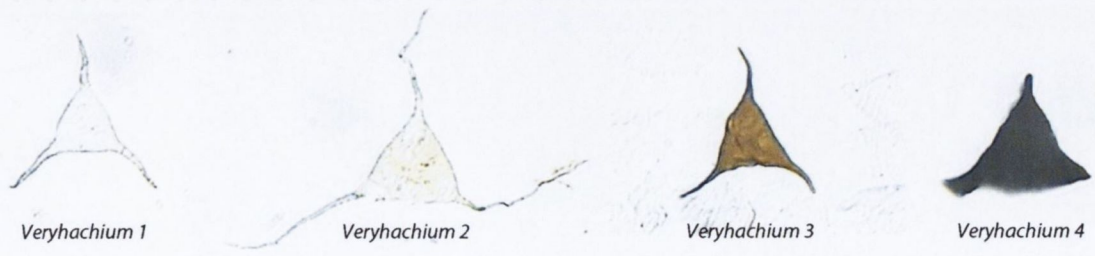

Figure 4.3b: Four *Veryhachium* specimens used to asses the suitability of a range of lighting conditions.

McCaughan (2002) used a well preserved spore as a standard and measured its RGB at each session. If there was any variation from his average value for the spore, the white balance of the camera was adjusted to compensate until the RGB determinations of the spore matched the average value. It was decided during this project not use the white balance of the camera to calibrate the system. Instead, the camera settings remained constant and a series of 'standards' were used to calibrate the system, independent of the white balance.

4.5.4. Camera Setup

Once the settings for the video camera used in the study were established, they remained constant for the duration of the study. From figure 4.8 it was decided that a shutter speed of 1/500 produced the greatest spread of RGB values for the four chosen *Veryhachium.* The white balance was not altered from the previous study (McCaughan 2002) (Figure 4.4) along with the other adjustable parameters.

4.5.5. Standards

Cokin translucent photographic filters were used as 'standards' for the image analysis system during this project, to compensate for daily variations. At the start of this project, 30 RGB determinations were made on 10 of these filters with different absorption colours to establish their respective RGB intensity values. This procedure is discussed in Chapter 5. The microscope was set up using the procedure described in detail section 4.5.3. and the system was allowed to warm up for half an hour. A blank palynological slide was placed on the microscope stage and its surface brought into focus. After the field diaphragm and condenser had been adjusted, a Cokin photographic filter was placed on the lamp housing (Figure 4.5). An 'image' of the filter was captured using the JVC TK-C1380 colour video camera and an RGB determination of the image was made using the Leica Qwin image analysis program. After each determination was carried out, the filter was moved and another determination was made. This was repeated until 30 determinations were made. The average of each of these 30 readings was used as the RGB intensity value of each 'standard'. This procedure was carried out for each of the Cokin filters used for this study.

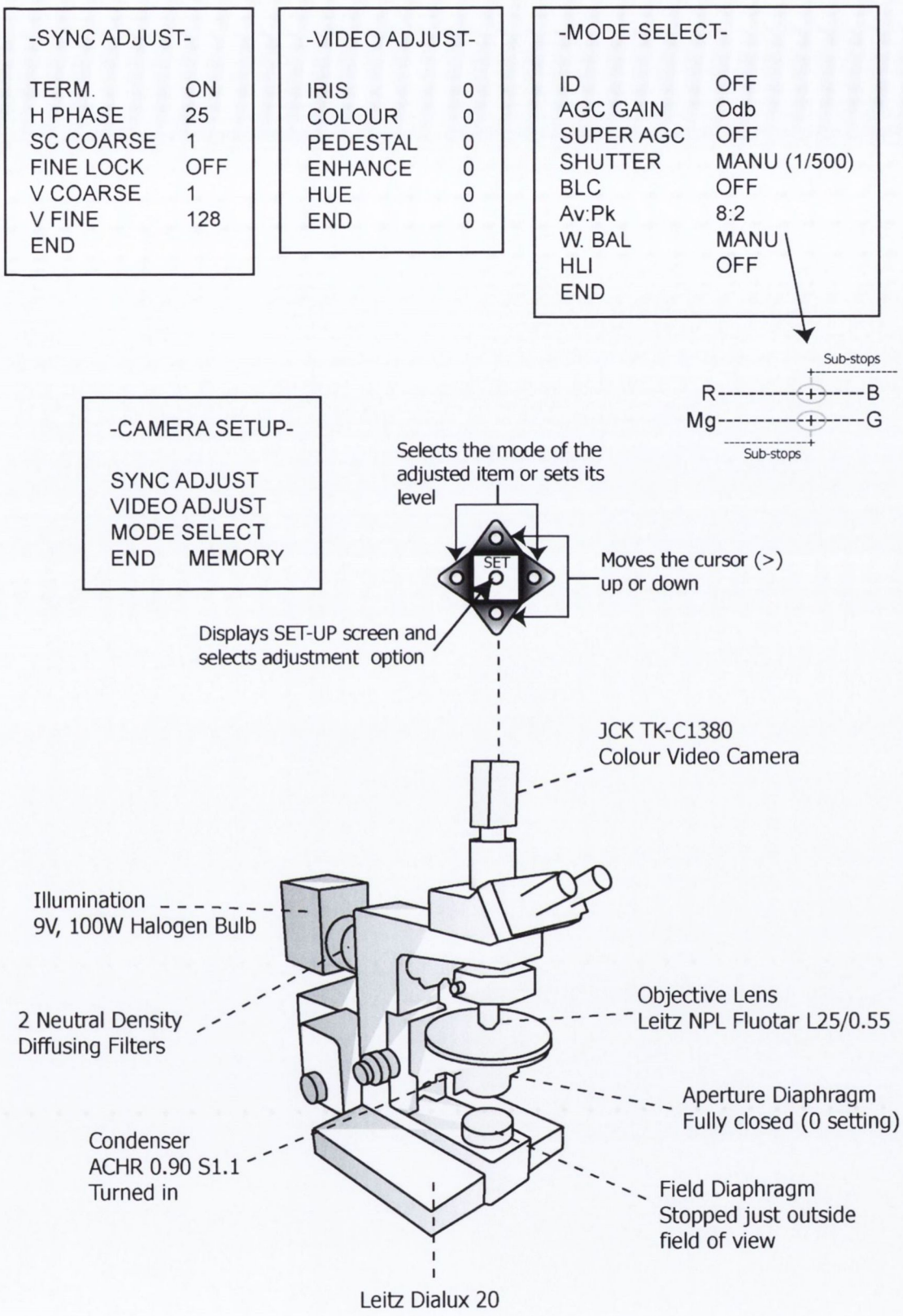

Figure 4.4: Diagram showing the microscope and camera settings used in this study (After McCaughan 2002). The camera settings remained constant throughout the project and the white balance was not altered from session to session.

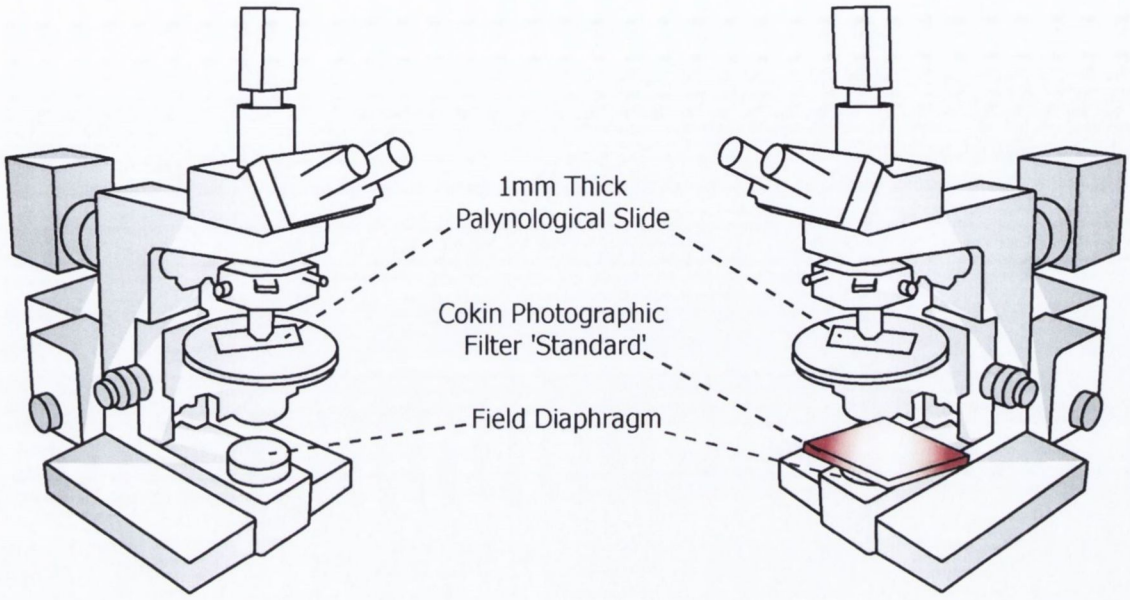

Figure 4.5: Schematic diagram of Leitz Wetzlar Dialux 20 Microscope showing position of colour 'standard', a Cokin photographic filter. The 'standard' rests on the microscope's field diaphragm housing. A 1mm thick glass slide is placed on the microscope's stage and the RGB measurement of the standard is taken with the surface of the glass slide in focus.

4.5.6. IMAGE ANALYSIS SYSTEM

The image analysis system used in this project was based on the *EasyColour.Q5R* routine written by McCaughan (2002) and runs on the Leica QWin image analysis program. Once the system had been set up under the conditions described in section 4.5.3. and 4.5.4., and an RGB determination made on each 'standard', palynomorph colour could then be determined.

Veryhachium and *Tasmanites* were located and focused under the microscope's eye pieces first. The microscope's field of view was then captured by the colour video camera and converted to a digital image by an Analogue to Digital Converter (ADC) within the Leica Q500IW imaging workstation (McCaughan 2002). The image of the palynomorph was saved to a folder. Using the *EasyColour.Q5R* routine (Figure 4.6a – 4.6d), pixels were selected from the image of the microfossil. The program then assigns an RGB value to each pixel and calculates the mean RGB value of all selected pixels. This is the RGB value recorded for the microfossil.

4.5.7. *VERYHACHIUM* MEASUREMENTS

When making RGB colour determinations on *Veryhachium*, blemishes and pyrite inclusions were avoided (Figure 4.7). Occasionally portions of the *Veryhachium* wall or eilyma have been thinned, where the vesicle has been damaged, or the excystment structure has ruptured. Pixels were only selected where the eilyma was intact. Because of the limited surface area of the three processes of *Veryhachium*, measurements were only made on the acritarch vesicle. Pyrite inclusions were commonly found within the *Veryhachium* vesicle. These areas were avoided, as were pixels within their immediate area as a yellow 'halo' could be seen around the site of the pyrite. Where acritarchs have become degraded due to intense thermal alteration, only portions of the vesicle that were still intact were selected.

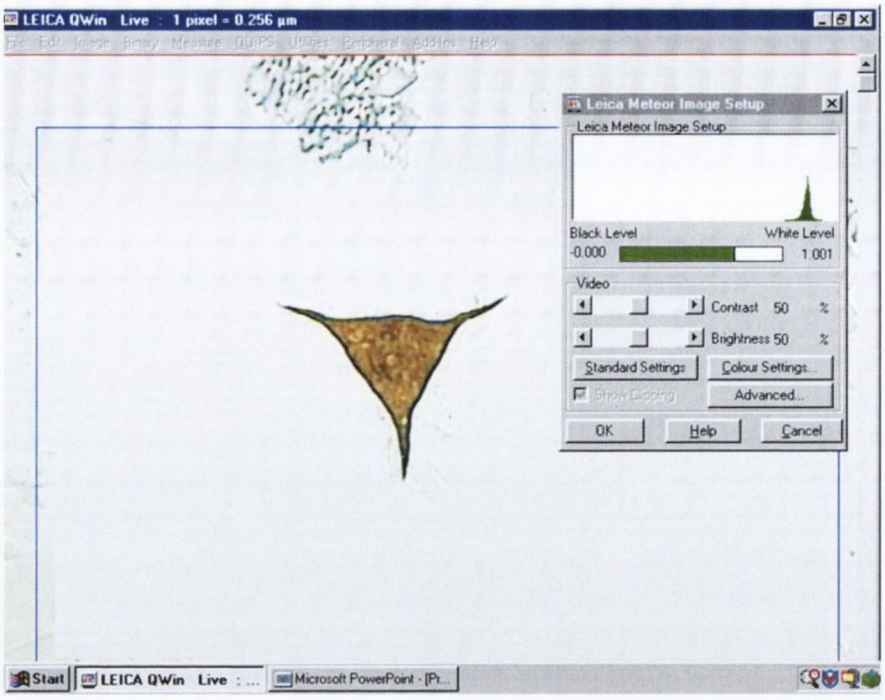

Figure 4.6a: **Image Setup**

The live image is focused on the screen and captured.

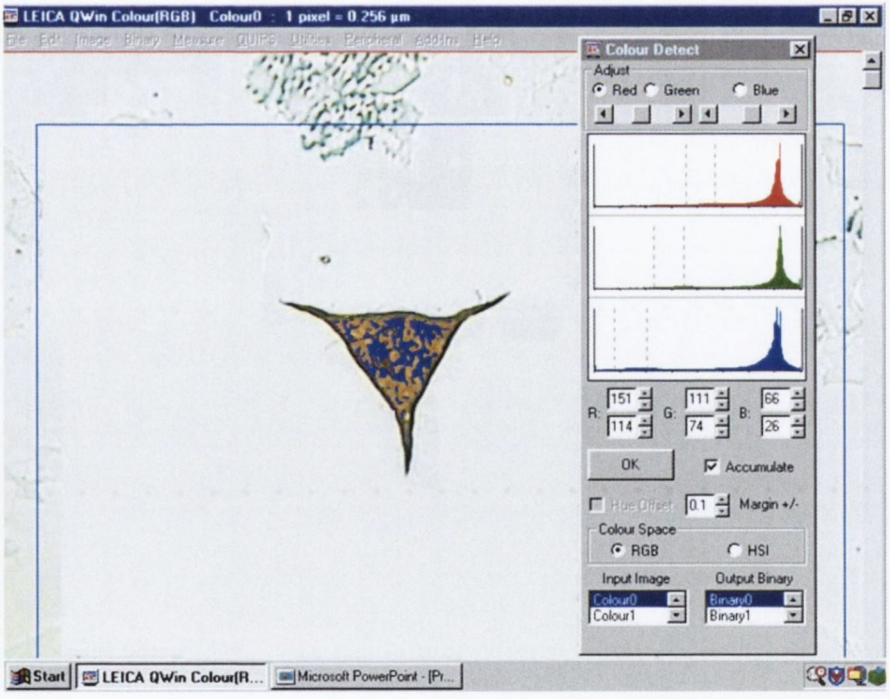

Figure 4.6b: **Colour Detect**

Pixels of interest are selected using the cursor. These pixels are accumulated until all pixels of interest are highlighted.

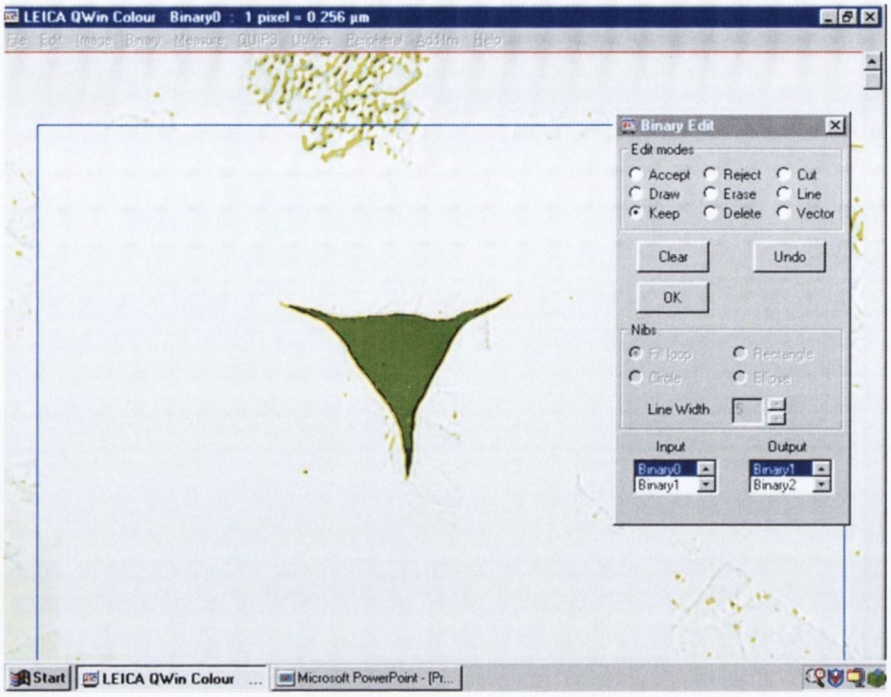

Figure 4.6c: **Binary Edit**

When pixels are selected at the 'colour detect' stage, often unwanted pixels are also highlighted. In the 'Binary Edit' window pixels of interest are kept (green) and all other pixels rejected (yellow).

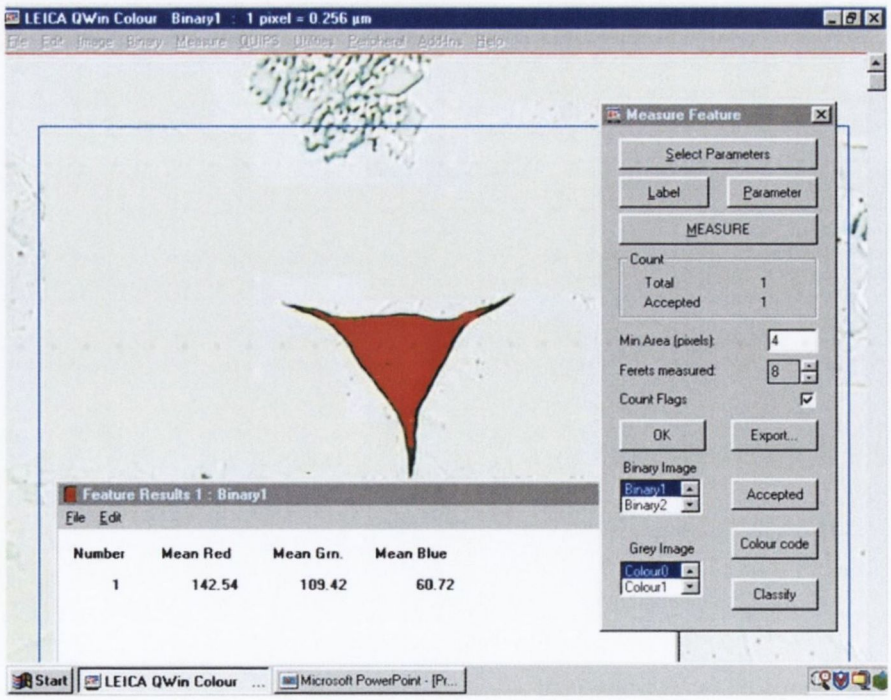

Figure 4.6d: **Measure Feature**

The average RGB of all pixels selected in the 'Binary Edit' window is calculated by the program. This is the RGB value recorded for the acritarch.

4.5.8. *TASMANITES* MEASUREMENTS

The colour of both the vesicle and the thinnest *Tasmanites* fold were measured in this study. Due to the size of some *Tasmanites* specimens investigated, it was not possible to capture the complete image of the palynomorph in one frame. It was also impossible to focus all parts of the *Tasmanites* at the same time (Figure 4.7). As a result, one image was used to select pixels for the vessicle measurement and another was used for the fold measurement. As discussed above, blemished areas or sites of pyrite inclusions were avoided. The thinnest fold of each *Tasmanites* was also measured. This was taken to be the lightest of the folds on the surface of the vesicle.

4.5.9. CORRECTION OF RESULTS

Using the RGB data from the 'standards' taken at the start of each session, the palynomorph RGB data were corrected using an Excel spreadsheet (Appendix IX Digital Data). By plotting the RGB data from the 'standards' taken at the beginning each session against the average RGB values established at the start of the study, day to day variations could be corrected (Figure 4.8). Each variable, red, green and blue, was adjusted separately.

4.5.10. QUALITATIVE FLUORESCENCE

A thorough description of the theory and application of fluorescence microscopy is given in Taylor *et al.* (1998) where the following account is taken from. Fluorescence is a form of luminescence, the emission of electromagnetic radiation as photons from a substance. This occurs following the absorption of energy in one of the various forms of electromagnetic or particulate radiation. The fluorescence of organic matter investigated in this study is a form of photoluminescence where excitation of photons is by light energy. Specific carbon bonds known as fluorophores are responsible for the absorption of high energy, short wavelength, radiation and emission of photons of electromagnetic radiation in the visible range. With increasing thermal maturity and break down of these carbon

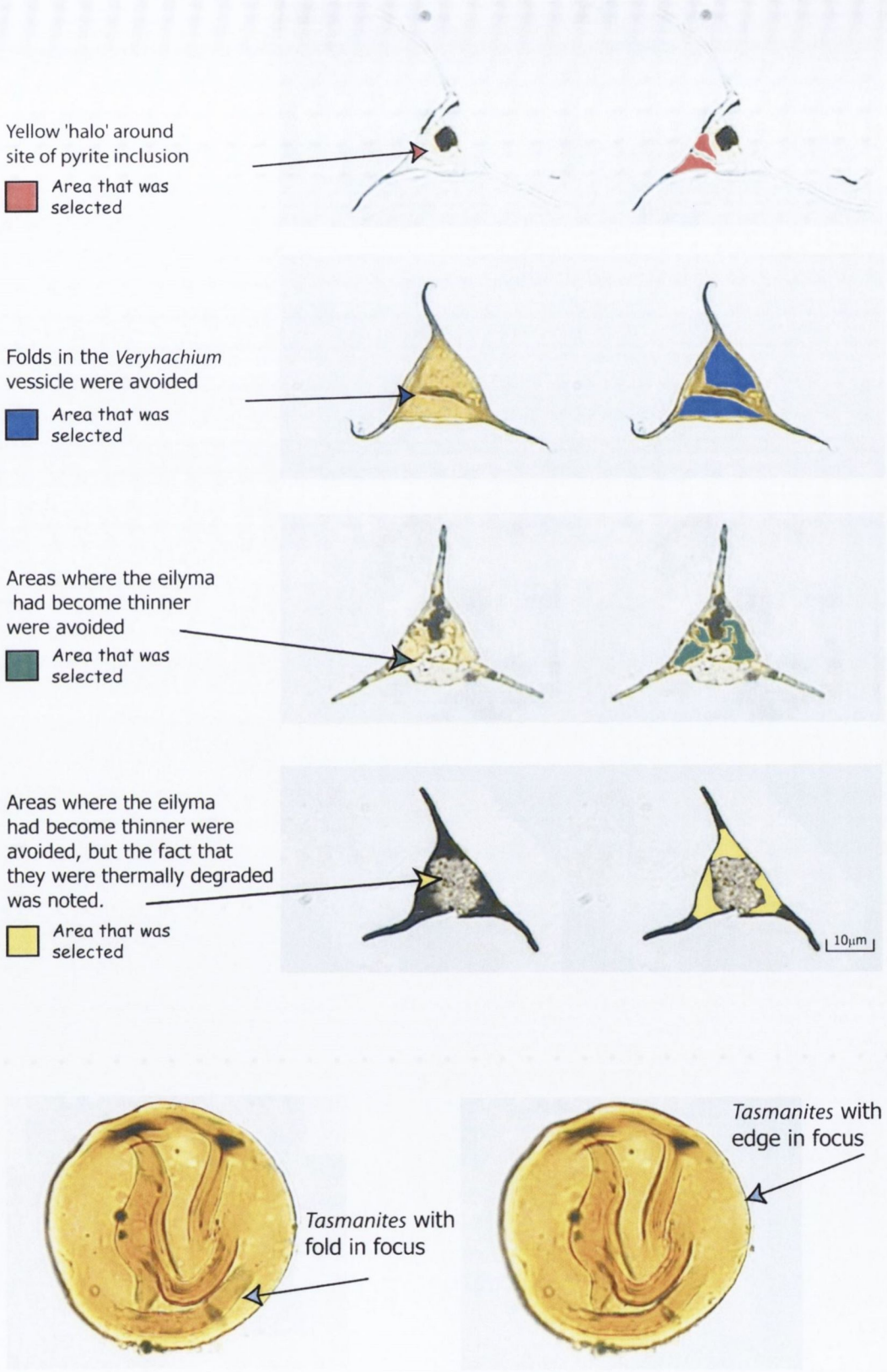

Figure 4.7: Guidelines of how the RGB determinations of *Veryhachium* specimens with variable surface features were determined. Also diagram showing a *Tasmanites* specimen with its thinnest fold in focus (left) and its wall in focus (right).

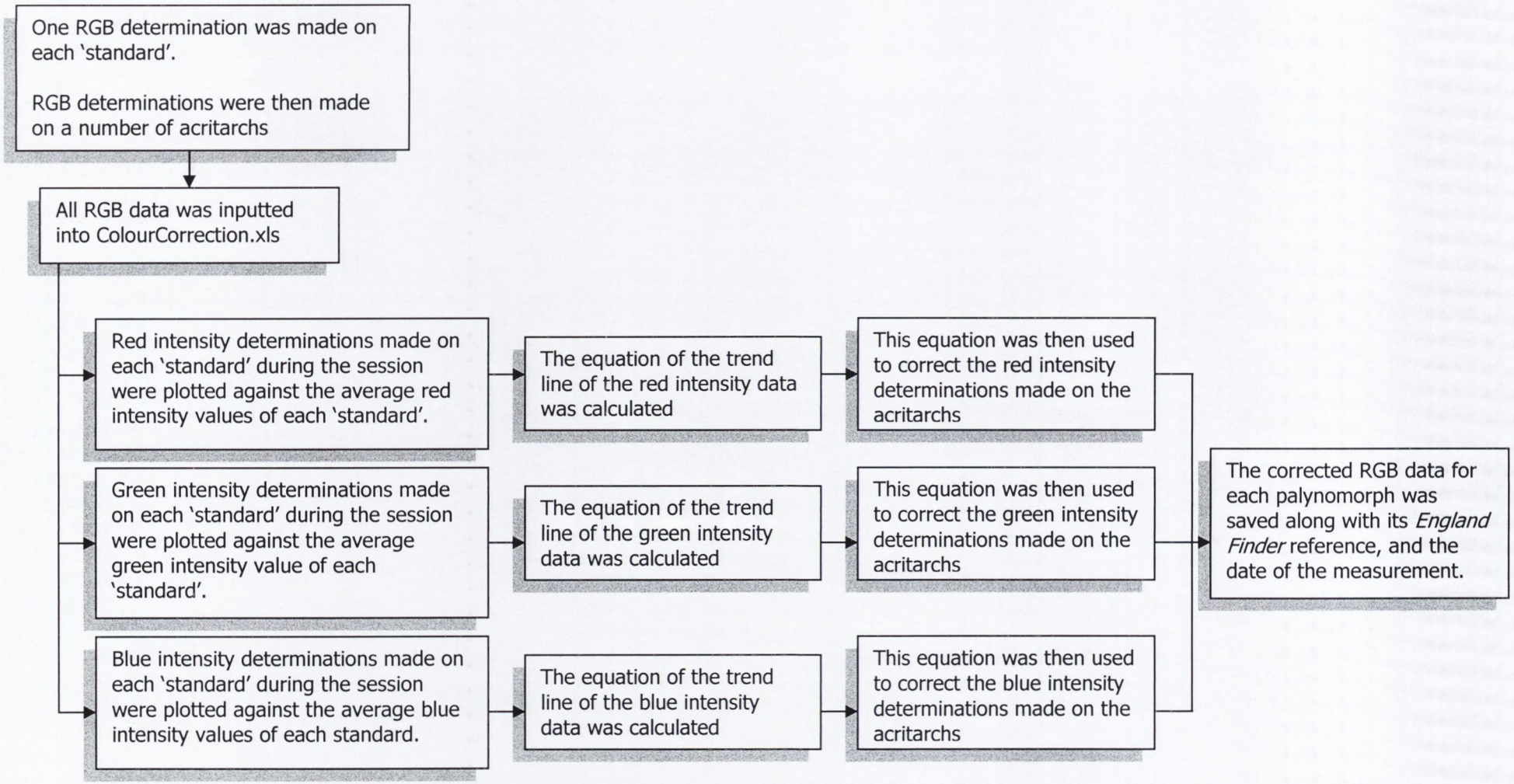

Figure 4.8: Flow chart showing each step used in correcting RGB data of acritarchs collected during one session (see Appendix IX Digital Data).

bonds, fluorescence becomes weaker and eventually ceases. In the case of pollen and spores, fluorescence ends at the floor of the oil window.

Only qualitative fluorescence determinations were made on acritarchs during the study; whether acritarchs within a sample fluoresced or not. The same palynological slides and microscope used for colour determinations were used for fluorescence studies. The microscope was fitted with a Leitz PLOEMOPAK 2.4 high-powered mercury vapour fluorescence illuminator, fitted with a Leitz H2 filter block (BP 390 – 490 excitation filter, RKP 510 dichroic mirror, LP 515 barrier filter). Using this system a violet and blue radiation (390 – 490nm) was produced.

The apparatus was switched on and allowed to warm up for 30 minutes before any observations were carried out. Palynomorphs were viewed using a Leitz NPL Fluotar L25/0.55 objective in a darkened room. After approximately 1 minute excitation of the organic matter, the presence or absence of fluorescence was recorded (Figure 4.12).

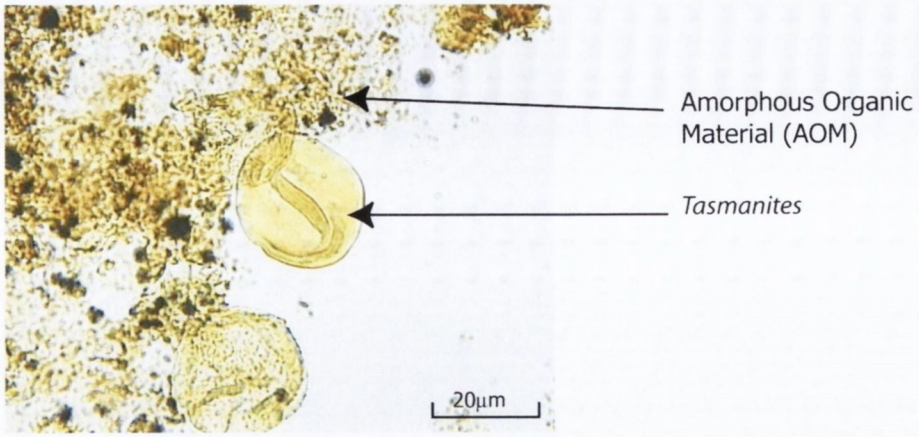

Figure 4.9: Photomicrograph showing *Tasmanites* specimen surrounded by amorphous organic material (AOM). Sample Pet3 E.F. Reference t52/2

Figure 4.10: *Veryhachium* specimen. Sample TL2 E.F. Reference v42

Figure 4.11: *Tasmanites* specimen. Sample P11 E.F. Reference u30/2

Figure 4.12: *Veryhachium* specimen in transmitted light (left) and fluorescing in ultra violet light (right). Field of view is 50µm.

CHAPTER 5
RGB DETERMINATIONS: CALIBRATION AND ERRORS

5.1. RGB COLOUR STANDARDS

5.1.1. INTRODUCTION

The RGB system is device dependent, with colour determinations made on the same substance using different cameras, light sources and image analysis programs producing different results (pers. comm. Fairchild 2005, Munsell Colour Science Laboratory). One of the aims of this project was to develop a system that could standardise measurements between different setups, to allow the widespread application of the RGB image analysis technique. There are no commercially available standards for the determination of RGB intensities of translucent materials. Materials suitable to use as 'standards' needed to fulfil certain conditions; it was important there was adequate quality control between different production runs of the material, that it was widely available, and was capable of producing a range of RGB values.

5.1.2. STANDARDS

Several different materials were investigated as possible 'standards'. Stained glass is available in a wide range of colours and produces a suitable spread of RGB values, but consistency between production runs could not be guaranteed. Individual palynomorphs, while often producing a suitable range of RGB intensities, could never be widely available. Neutral density filters were examined but only provided RGB intensities towards the lighter end of the scale. The most suitable material proved to be Cokin photographic filters. These filters are available in most camera outlets and are made of a type of high quality plastic known as 'organic glass' (www.cokin.com). A combination of nine Cokin photographic filters were used to produce a range of RGB values that were evenly distributed across the RGB scale, as well as one photographic filter of unknown origin ('pastel violet') (Figure 5.1).

Once the Cokin photographic filters were chosen as the most suitable 'standards' it was necessary to establish their mean RGB value. The microscope was set up under the conditions described in section 4.5.3. After the field diaphragm and condenser of the Leitz Dialux 20 transmitted light microscope were correctly positioned, a glass slide was placed on the microscope's stage and the surface of the glass was brought into focus. Each Cokin filter was placed in turn on the field diaphragm housing (Figure 5.2). An 'image' of the filter was captured and an RGB determination made.

Thirty determinations were made on each filter, which was moved slightly after each determination to ensure any variation in colour within the filter was taken into account. To avoid any effect of day to day variation, all of the 'standards' were measured thirty times during the same session. Table 5.1 lists the determinations made on three of the nine Cokin filters to demonstrate the spread between 30 readings. The means and standard deviations of the RGB intensities of each standard are shown in Figure 5.3, 5.4 and 5.5. The mean values for each 'standard' measured that day were used to calibrate all subsequent readings (Figure 5.6). Before any colour determinations were made on palynomorphs, one RGB measurement was made on every 'standard' at the beginning of a session. It should be noted that although there is an inspection of each production run of Cokin photographic filters they are not rigorously tested. They are not designed as scientific standards and make no claim to be.

Two different sets of Cokin filters were purchased to establish the colour difference between different production runs. The second set of filters was purchased two years after the first. The RGB data of the two sets were measured on the same set up, at the same time, and compared (Figure 5.7, 5.8 and 5.9). For all except the Cokin 003 filter, the difference between the sets was deemed to be minimal.

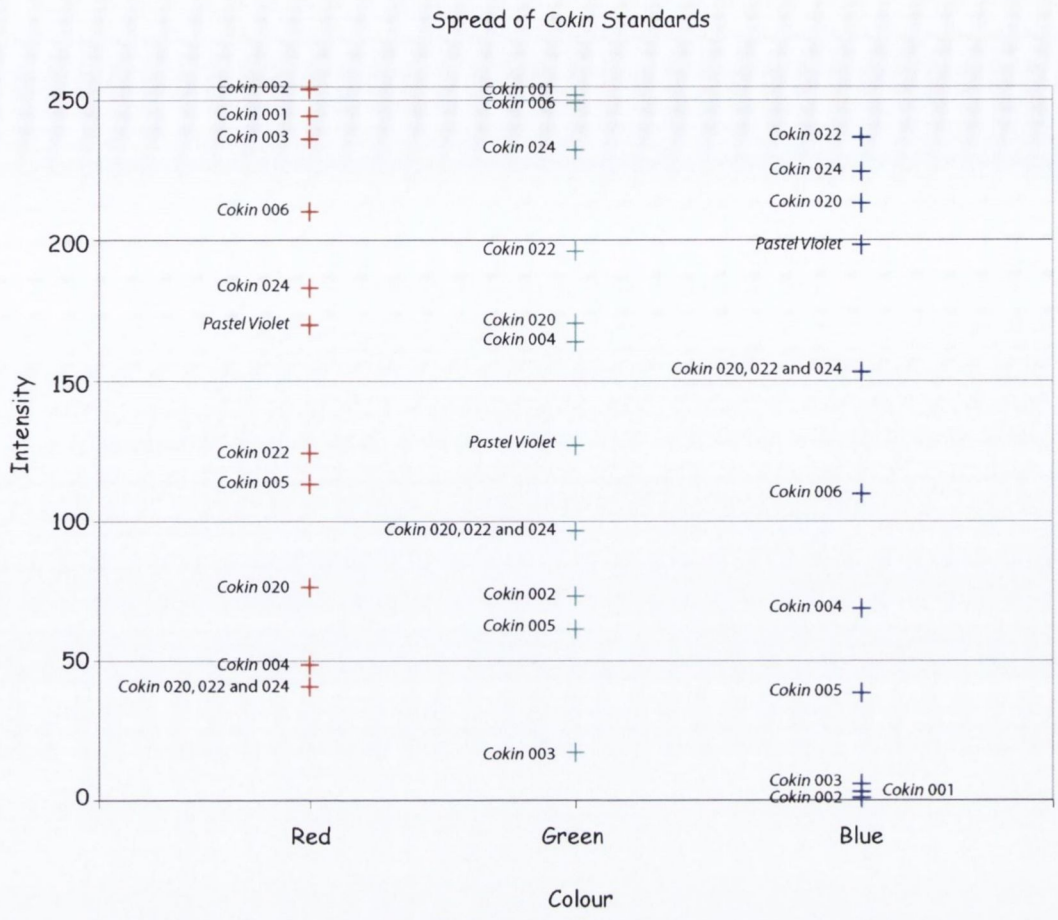

Figure 5.1: Plot showing the spread of RGB data for the Cokin photographic filters, with the name of each 'standard' attached. Ideally 'standards' would plot at each interval of 50; however the choice of standards is limited by the range of Cokin filters available.

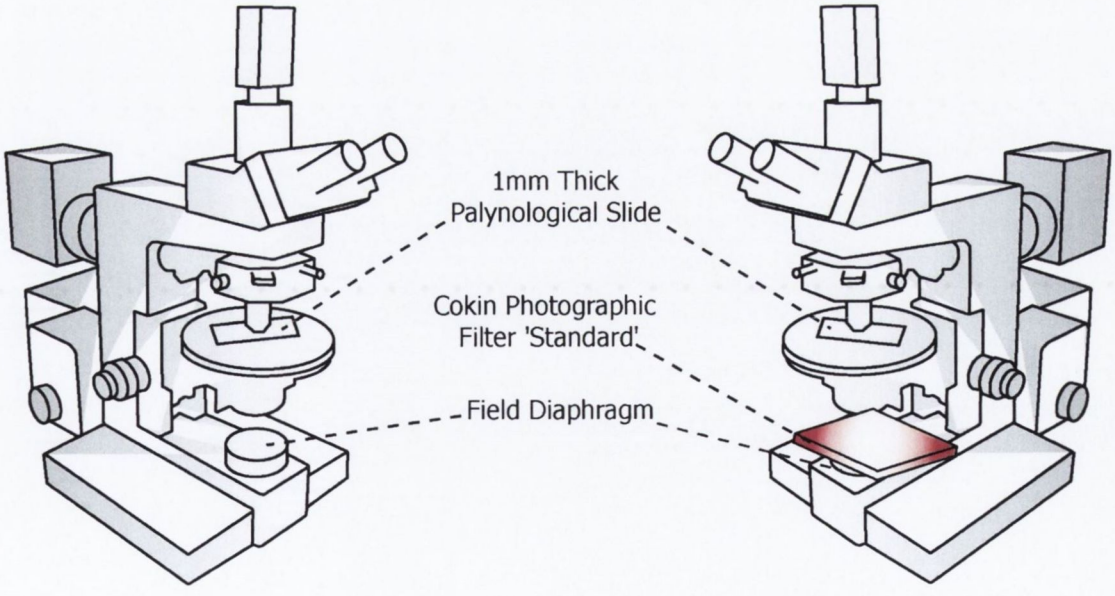

Figure 5.2: Schematic diagram of Leitz Wetzlar Dialux 20 Microscope showing position of colour 'standard', a Cokin photographic filter. The 'standard' rests on the microscope's field diaphragm housing. A 1mm thick glass slide is placed on the microscope's stage and the RGB measurement of the standard is taken with the surface of the glass slide in focus.

	Cokin 001 (Yellow)			Cokin 004 (Green)			Cokin 022 (Blue)		
No.	R	G	B	R	G	B	R	G	B
1	246	253	4	49	165	69	122	195	235
2	244	252	3	50	164	68	123	196	237
3	244	251	2	50	165	68	125	198	240
4	244	252	3	50	163	68	118	189	226
5	244	252	3	49	166	69	125	198	241
6	244	251	3	48	163	70	125	197	239
7	244	252	3	50	167	71	125	196	236
8	244	252	3	49	163	68	123	196	236
9	245	253	4	50	167	70	126	199	241
10	244	251	2	49	166	70	124	196	236
11	245	252	4	49	164	68	125	199	241
12	244	252	3	50	167	70	124	197	238
13	244	251	3	49	165	69	125	196	237
14	245	252	4	47	158	66	125	195	236
15	244	252	3	50	166	71	125	195	234
16	245	252	4	48	162	67	125	197	238
17	244	252	3	48	162	68	124	195	234
18	245	252	4	47	162	67	124	195	235
19	244	252	3	49	165	70	125	198	240
20	244	252	3	47	160	68	125	195	236
21	244	252	3	48	165	70	125	199	242
22	244	252	3	49	163	68	127	199	242
23	244	252	3	48	163	69	125	196	238
24	244	252	3	48	164	70	125	195	234
25	245	252	4	49	166	70	124	195	236
26	245	253	4	49	165	70	123	197	237
27	244	252	3	48	163	68	123	193	232
28	245	253	4	50	165	70	122	192	230
29	245	252	4	47	160	68	126	199	240
30	244	252	3	46	162	68	124	194	234
Mean	244	252	3	49	164	69	124	196	237
Std. Dev	1	1	0	1	2	1	2	2	4

Table 5.1: List of 30 RGB determinations, made on three of the nine Cokin 'standards'. These determinations were all taken on the same day, in rapid succession, using the same microscopic setting and lighting conditions described in section 4.5.3. Appendix III lists the 30 determinations made on each of the ten 'standards'.

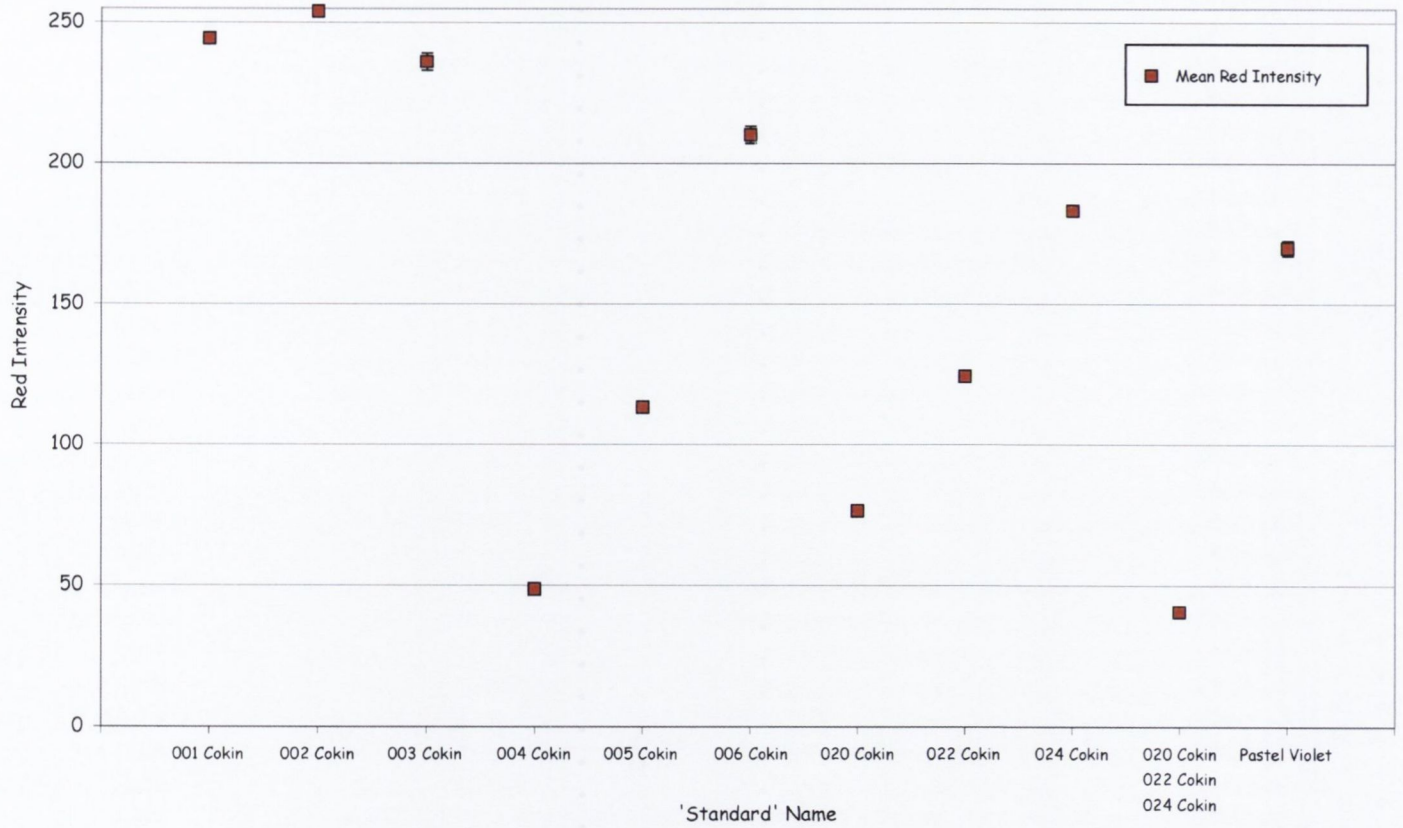

Cokin	Mean Red	Std. Dev
001 Cokin	244.35	0.66
002 Cokin	254.00	0.00
003 Cokin	236.16	3.14
004 Cokin	48.63	1.03
005 Cokin	113.27	0.96
006 Cokin	210.12	3.00
020 Cokin	76.46	0.69
022 Cokin	124.25	1.52
024 Cokin	183.15	1.18
020/022/024	40.82	0.76
Pastel Violet	169.83	2.66

Figure 5.3: Mean red intensities and standard deviations of 'standards' used in this project. Most standard deviations are too small to be seen clearly.

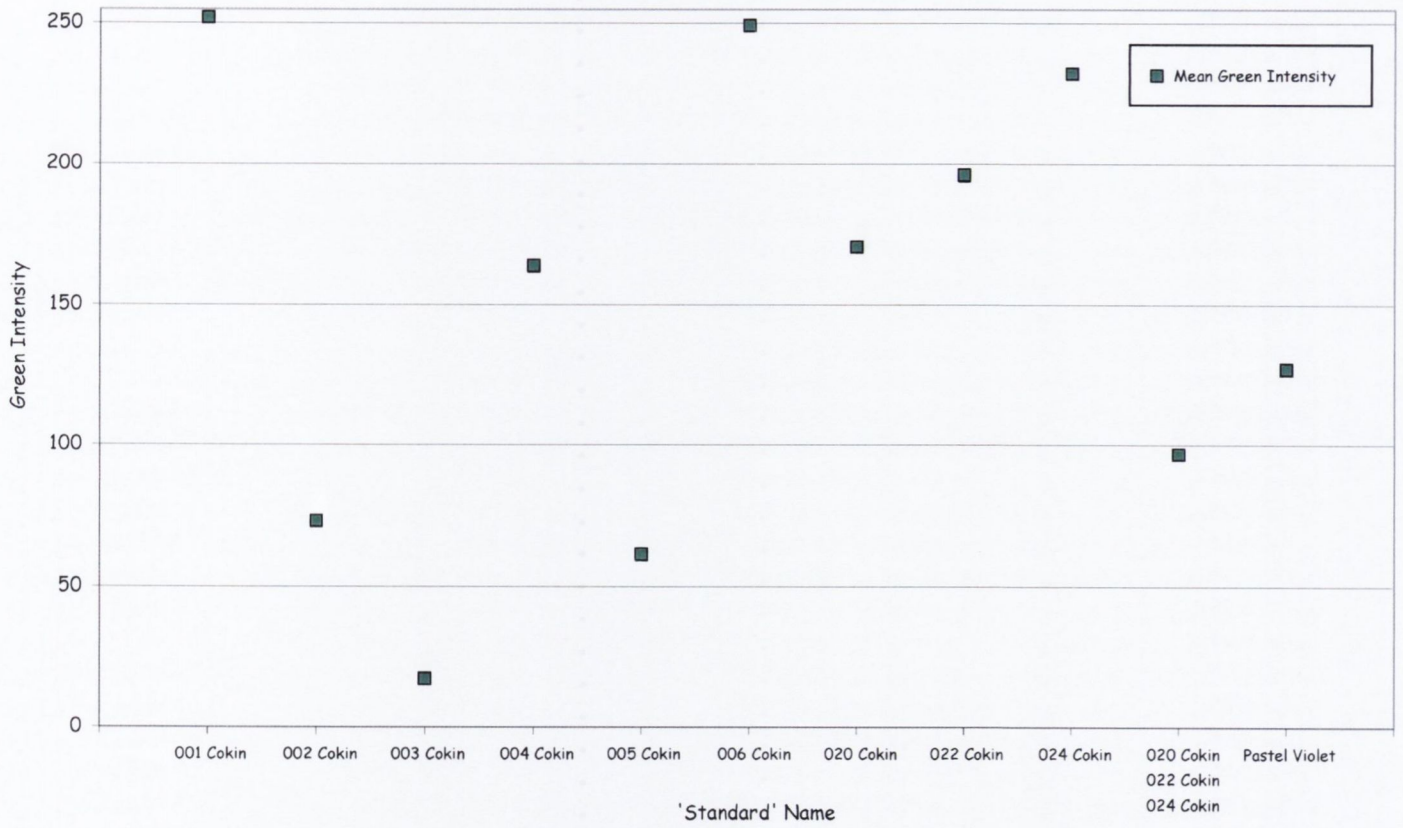

Cokin	Mean Green	Std. Dev
001 Cokin	251.96	0.50
002 Cokin	73.24	1.99
003 Cokin	17.21	0.48
004 Cokin	163.82	2.17
005 Cokin	61.41	0.43
006 Cokin	249.12	0.53
020 Cokin	170.54	1.83
022 Cokin	196.05	2.28
024 Cokin	232.14	1.37
020/022/024	96.69	1.42
Pastel Violet	126.99	1.32

Figure 5.4: Mean green intensities and standard deviations of 'standards' used in this project. Most standard deviations are too small to be seen clearly.

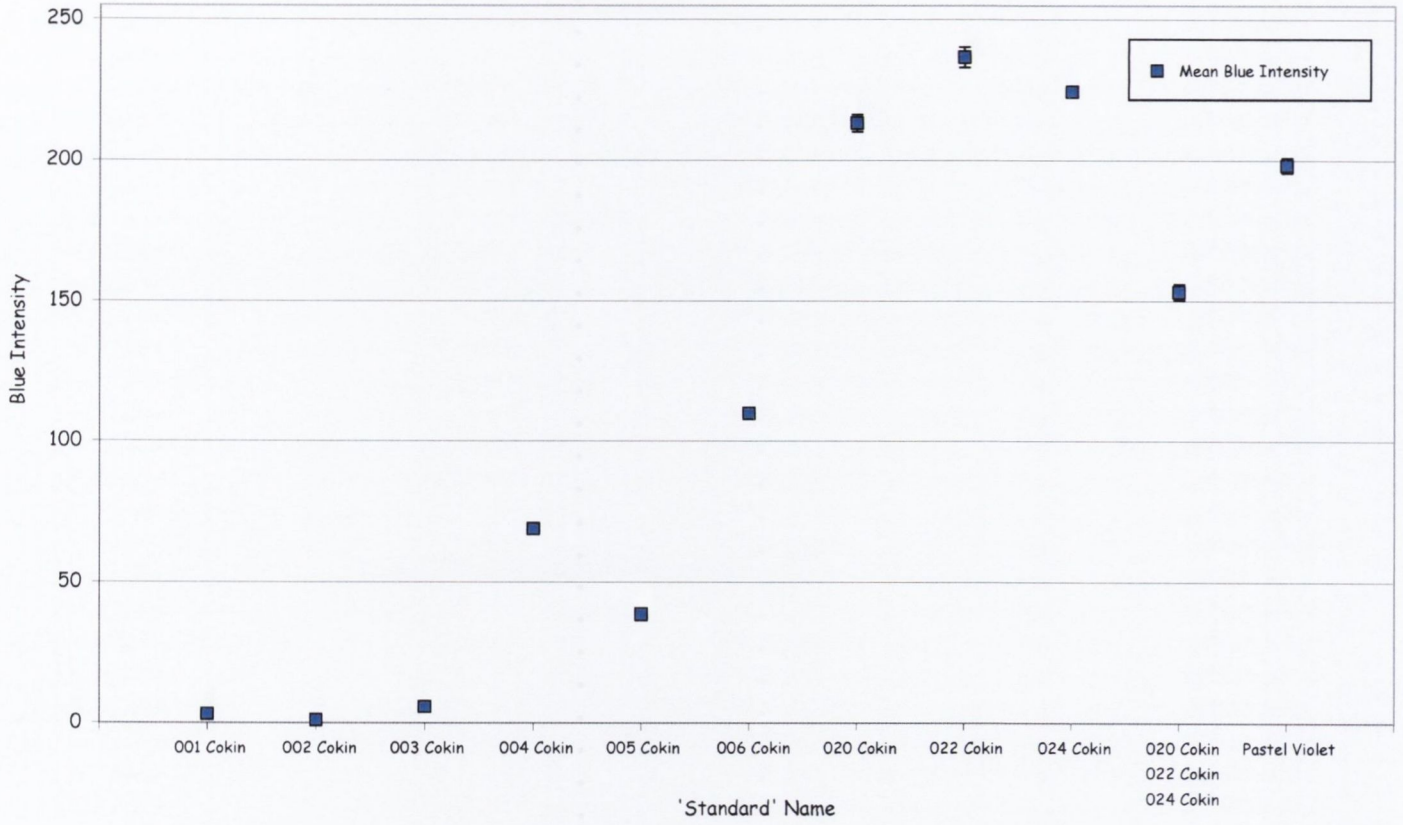

Cokin	Mean Blue	Std. Dev
001 Cokin	3.12	0.44
002 Cokin	1.00	0.00
003 Cokin	5.80	0.32
004 Cokin	68.86	1.12
005 Cokin	38.57	0.69
006 Cokin	109.92	1.80
020 Cokin	213.25	3.04
022 Cokin	236.74	3.57
024 Cokin	224.42	0.51
020/022/024	153.26	2.85
Pastel Violet	198.25	2.66

Figure 5.5: Mean blue intensities and standard deviations of 'standards' used in this project. Most standard deviations are too small to be seen clearly.

Cokin A 001
R: 244
G: 251
B: 3

Cokin A 005
R: 113
G: 61
B: 38

Cokin A 024
R: 183
G: 232
B: 224

Cokin A 002
R: 254
G: 73
B: 1

Cokin A 006
R: 210
G: 249
B: 109

'Pastel Violet'
R: 169
G: 126
B: 198

Cokin A 003
R: 236
G: 17
B: 5

Cokin A 020
R: 76
G: 170
B: 213

Cokin A 020, 022 and 024 together
R: 40
G: 96
B: 153

Cokin A 004
R: 48
G: 163
B: 68

Cokin A 022
R: 124
G: 196
B: 236

Figure 5.6: Diagram showing the 11 original 'standards' used in this study. The mean RGB value of each 'standard' is shown. This RGB value is based on the average of 30 determinations made on random areas of each standard under the described lighting conditions

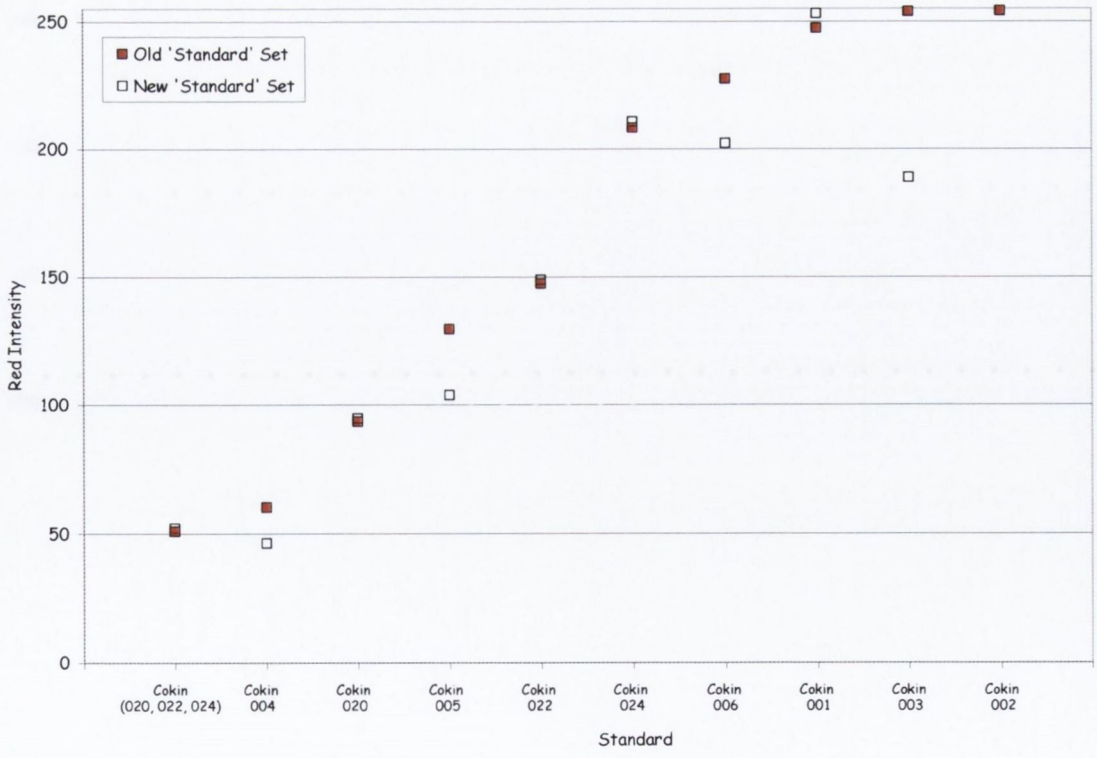

Figure 5.7: Red intensity of two different sets of Cokin filters, measured on the same setup at the same time. Most intensity values plot close to each other, but the two readings for Cokin 003 filter are significantly different.

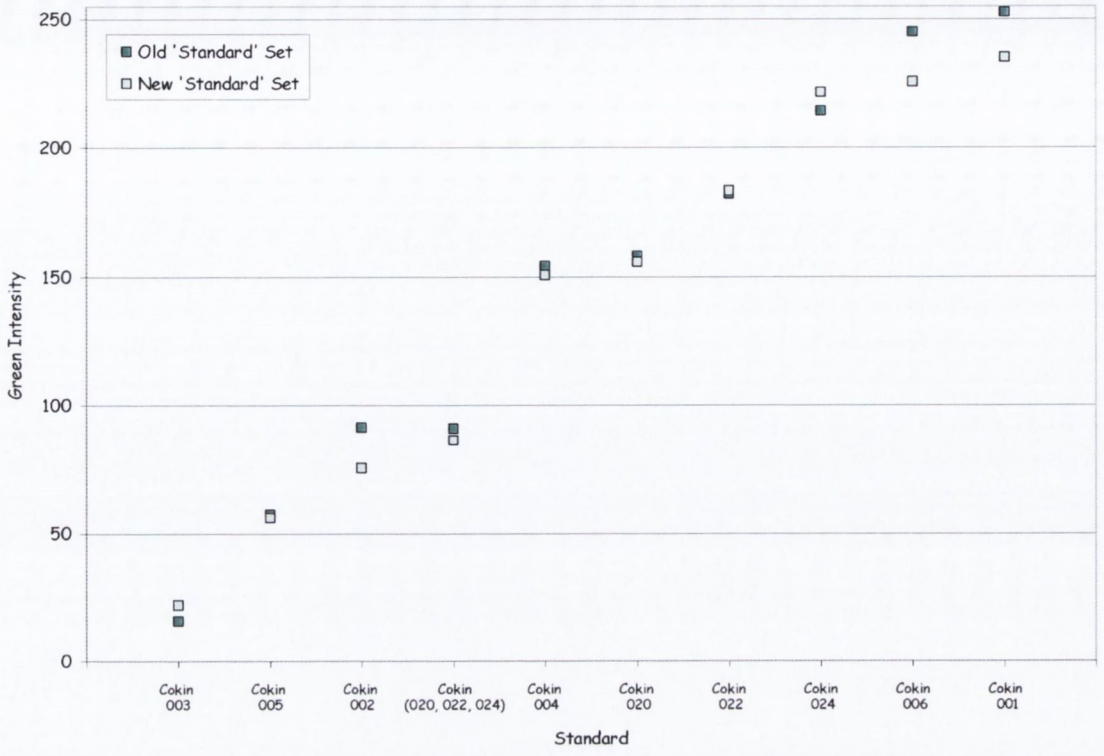

Figure 5.8: Green intensity of two different sets of Cokin filters, measured on the same setup at the same time.

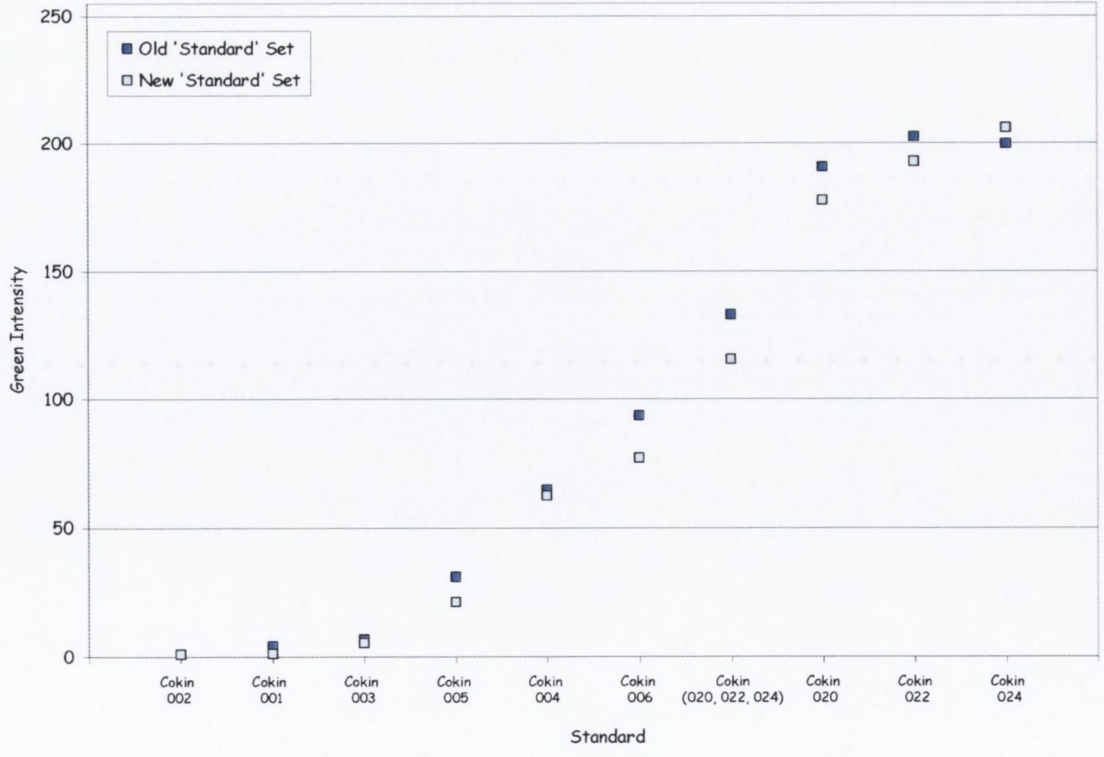

Figure 5.9: Blue intensity of two different sets of Cokin filters, measured on the same setup at the same time.

5.2. ERRORS ASSOCIATED WITH THE RGB SYSTEM

5.2.1. INTRODUCTION

If the use of colour image analysis of *Veryhachium* and *Tasmanites* is to be used by different workers, it is important to understand the range of errors related to differences in setups, users, and different sets of standards. In order to investigate this further, one sample (TL3) was measured by a number of different people, with different equipment, and at different times. The *Veryhachium* specimens investigated from sample TL3 are shown in Figure 5.10, 5.11 and 5.12. Due to time constraints, only a limited number of experiments were carried out. The following results represent a preliminary attempt at understanding the variations in RGB data determinations associated with different conditions.

5.2.2. GRADUAL VARIATIONS WITH TIME

As previously discussed, the image analysis system used in this project varied from day to day. Over a two year period, each time the system was used RGB determinations were made on the set of Cokin filters. To investigate the variation of the system with time all sets of 'standard' measurements were grouped into six month periods (Appendix IV). Daily 'standard' values measured in each six month period were then plotted against the original value for each 'standard' calculated at the beginning of the study. Trend lines were then calculated for each six month interval (Figure 5.13, 5.14 and 5.15).

From Figure 5.13, it is clear that over the two year period red intensity determinations of the 'standards' gradually decreased relative to the original measurements. Overall, the decrease is of the order of 1%. The spread of green intensity determinations over the four six month intervals (Figure 5.14) appears to show the greatest swing, up to 5% at certain points along the intensity scale. The measured green intensities become progressively lower with time. Unlike the red and green standard intensities, the blue intensity data show no regular variation with time (Figure 5.15).

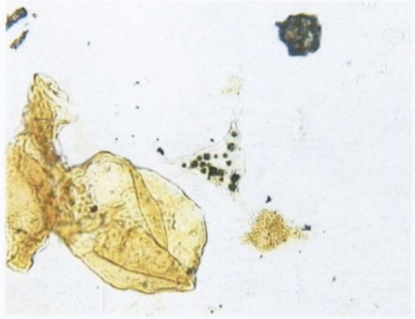

Veryhachium 1 - Sample TL3
E/F Reference: U37/4
Leica Microscope Reference: 372/958
(field of view 120μm)

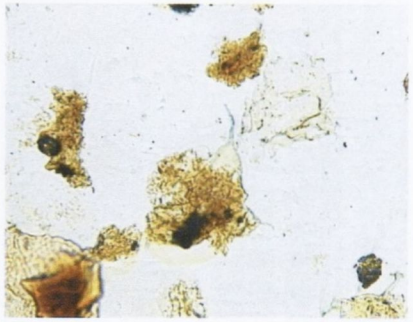

Veryhachium 4 - Sample TL3
E/F Reference: N46/4
Leica Microscope Reference: 458/1031
(field of view 120μm)

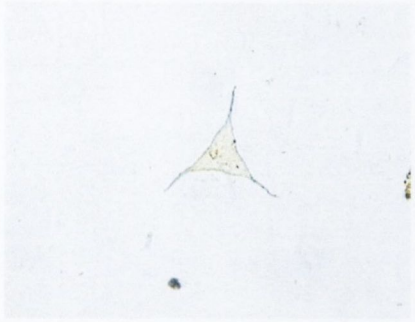

Veryhachium 2 - Sample TL3
E/F Reference: D40/2
Leica Microscope Reference: 400/1122
(field of view 120μm)

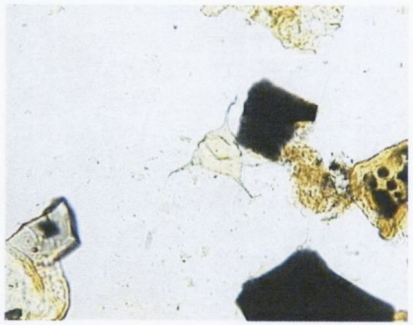

Veryhachium 5 - Sample TL3
E/F Reference: S47/2
Leica Microscope Reference: 468/987
(field of view 120μm)

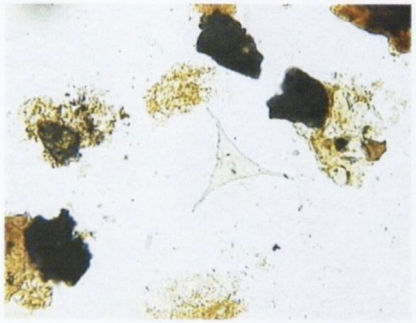

Veryhachium 3 - Sample TL3
E/F Reference: R42/2
Leica Microscope Reference: 420/994
(field of view 120μm)

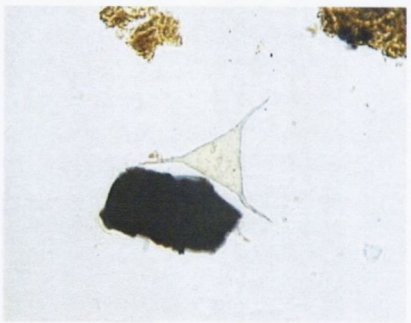

Veryhachium 6 - Sample TL3
E/F Reference: Y51/4
Leica Microscope Reference: 509/926
(field of view 120μm)

Figure 5.10: *Veryhachium* specimens (1-6) from sample TL3 (Slide 1) used to test variations in RGB determinations.

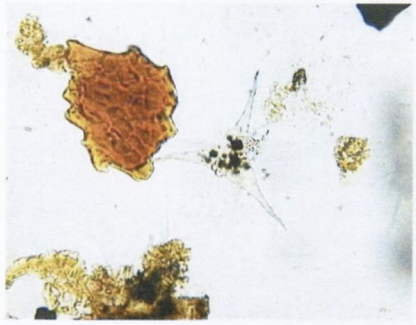

Veryhachium 7 - Sample TL3
E/F Reference: M56/3
Leica Microscope Reference: 549/1041
(field of view 120µm)

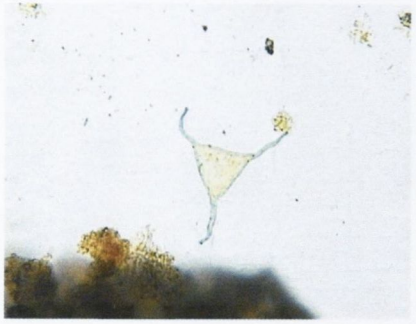

Veryhachium 8 - Sample TL3
E/F Reference: Q57/1
Leica Microscope Reference: 556/1005
(field of view 120µm)

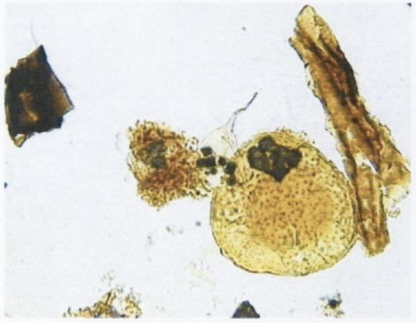

Veryhachium 9 - Sample TL3
E/F Reference: S57/2
Leica Microscope Reference: 564/989
(field of view 120µm)

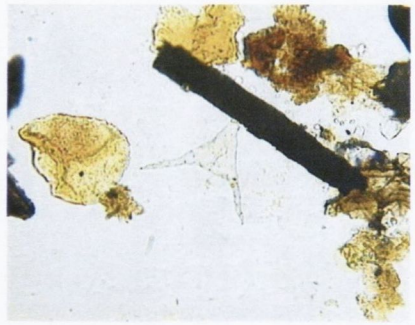

Veryhachium 10 - Sample TL3
E/F Reference: P59/3
Leica Microscope Reference: 577/1022
(field of view 120µm)

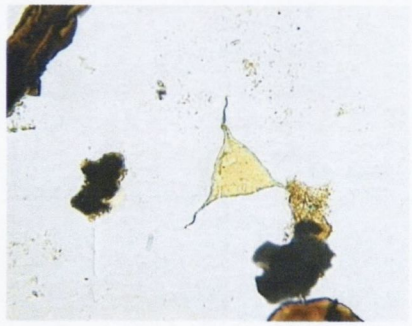

Veryhachium 11 - Sample TL3
E/F Reference: T61/3
Leica Microscope Reference: 597/973
(field of view 120µm)

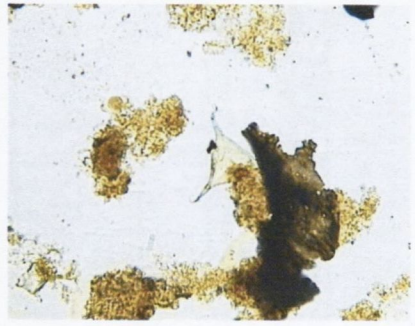

Veryhachium 12 - Sample TL3
E/F Reference: O61/4
Leica Microscope Reference: 602/1023
(field of view 120µm)

Figure 5.11: *Veryhachium* specimens (7-12) from sample TL3 (Slide 1) used to test variations in RGB determinations.

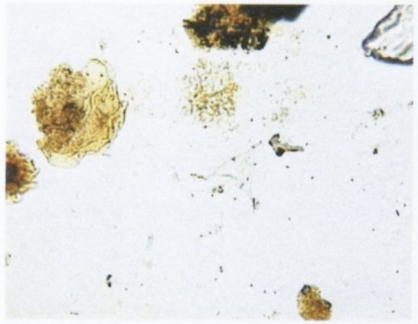

Veryhachium 13 - Sample TL3
E/F Reference: N62/2
Leica Microscope Reference: 609/1038
(field of view 120μm)

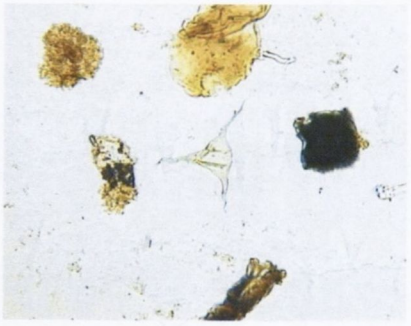

Veryhachium 16 - Sample TL3
E/F Reference: N72/1
Leica Microscope Reference: 702/1036
(field of view 120μm)

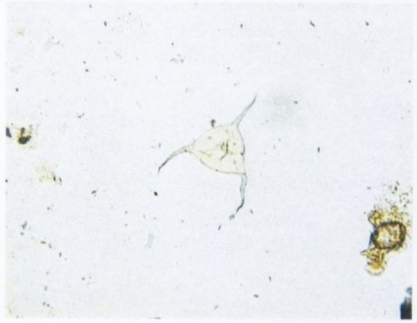

Veryhachium 14 - Sample TL3
E/F Reference: Q67
Leica Microscope Reference: 656/1002
(field of view 120μm)

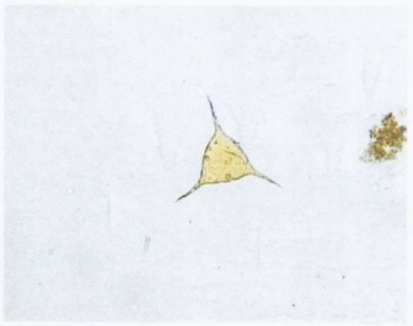

Veryhachium 17 - Sample TL3
E/F Reference: Y74/4
Leica Microscope Reference: 730/925
(field of view 120μm)

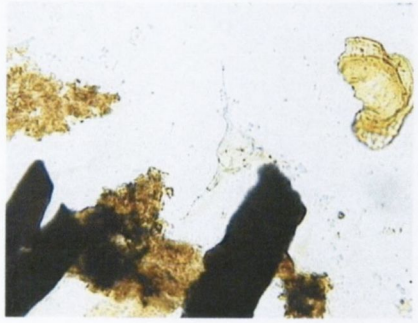

Veryhachium 15 - Sample TL3
E/F Reference: T71/2
Leica Microscope Reference: 698/982
(field of view 120μm)

Figure 5.12: *Veryhachium* specimens (13-17) from sample TL3 (Slide 1) used to test variations in RGB determinations.

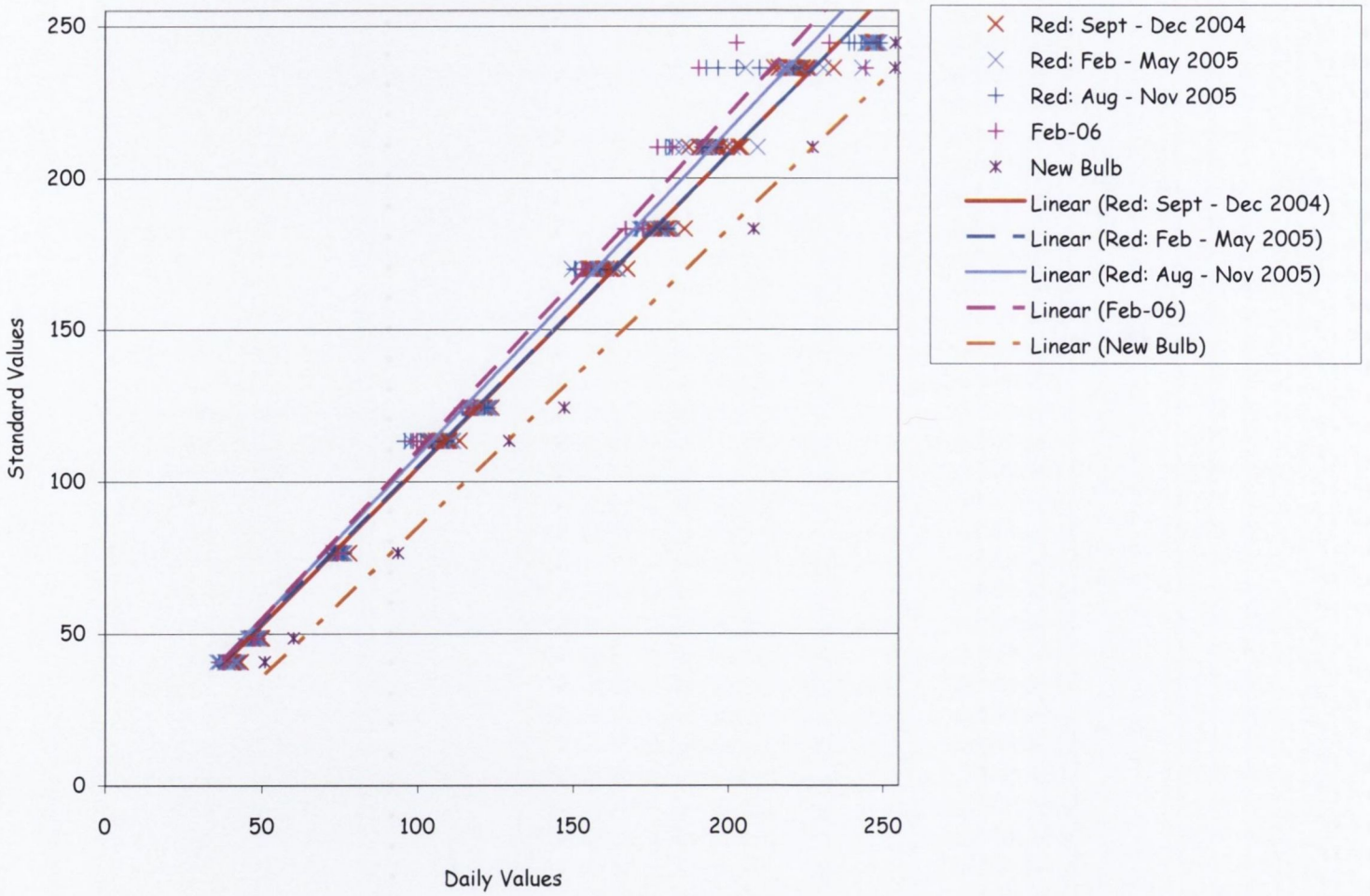

Figure 5.13: Daily 'standard' red intensities, grouped in six month intervals, plotted against the red intensities of the Cokin filters measured at the beginning of the study. With time, the daily red intensity values of the 'standards' decreases.

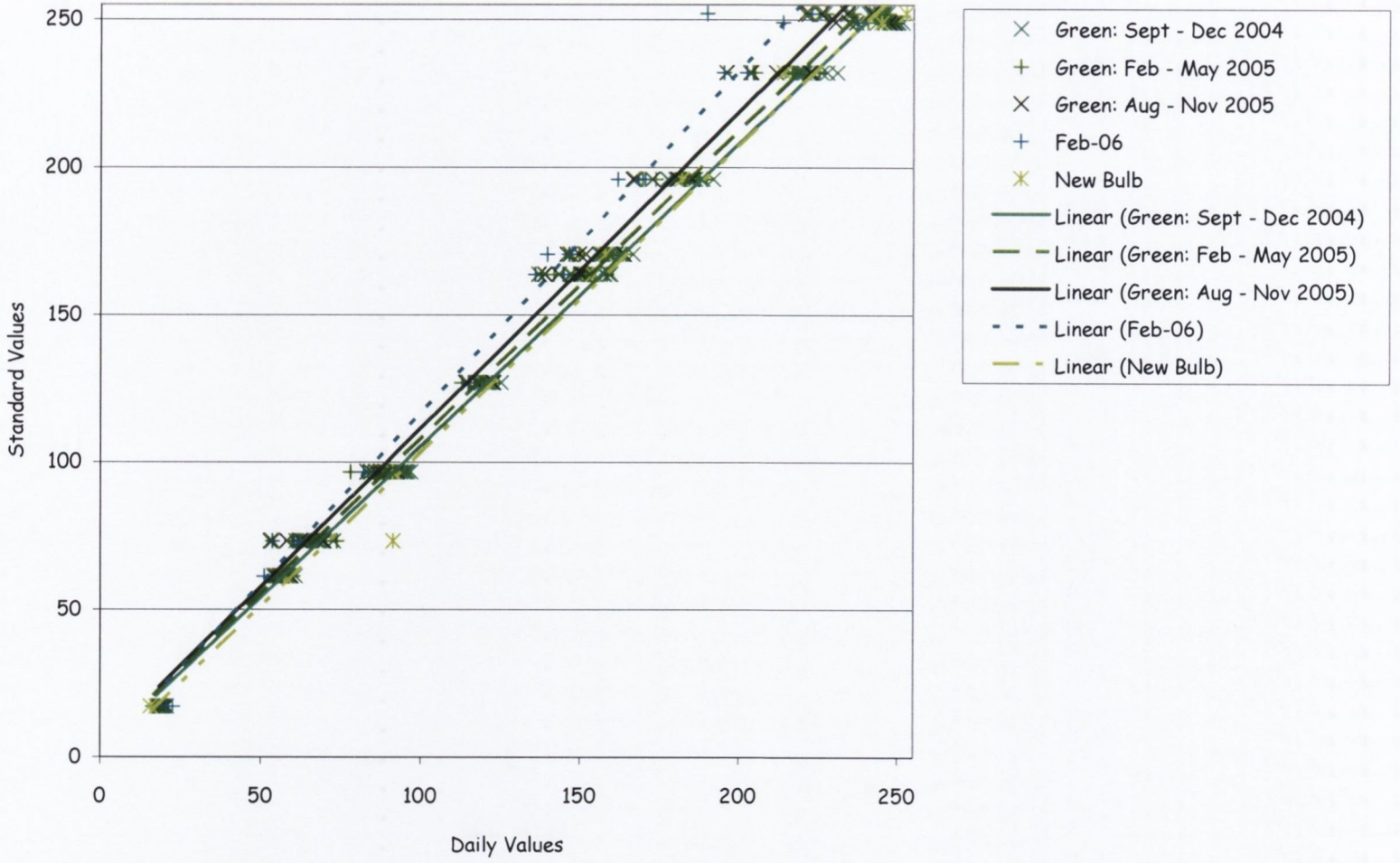

Figure 5.14: Daily 'standard' green intensities, grouped in six month intervals, plotted against the green intensities of the Cokin filters measured at the beginning of the study. With time, the daily green intensity values of the 'standards' decreases.

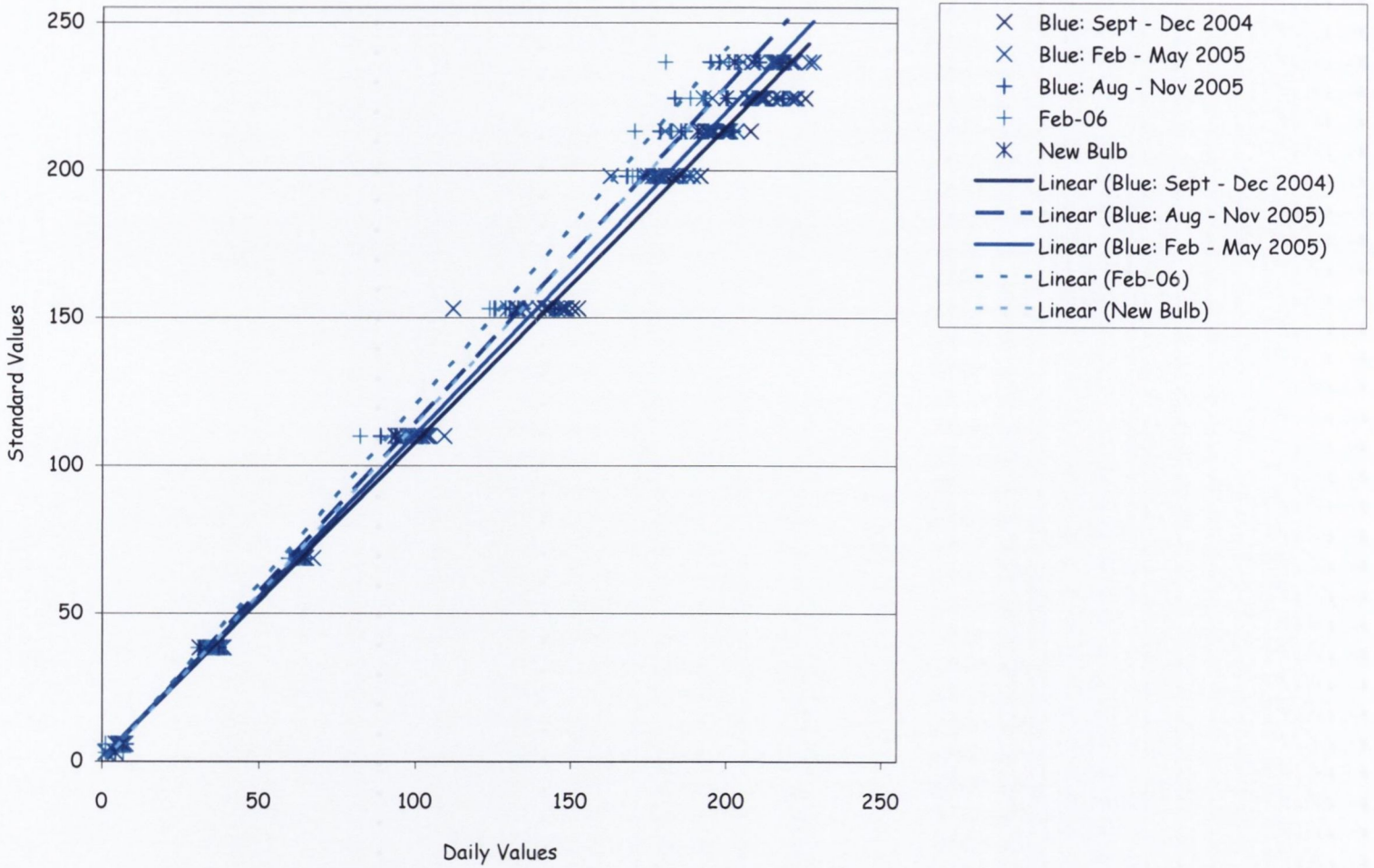

Figure 5.15: Daily 'standard' blue intensities, grouped in six month intervals, plotted against the blue intensities of the Cokin filters measured at the beginning of the study. With time, there is no discernable change of the daily measurement of blue intensity.

A possible explanation for this phenomenon may be change in the emission characteristics of the halogen bulb with time. A new bulb was fitted at the end of the study, and the standards measured again. The 'new bulb' data are also plotted on the graphs discussed above (Figure 5.13, 5.14 and 5.15). In the case of red and green intensity determinations, 'standard' readings are closer to those measured at the start of the study, with a newer bulb, than those measured towards the end of the project. With the blue intensity data no clear pattern is revealed. The variation of RGB determinations with time clearly demonstrates the need for a method to standardise results.

Having established the ten photographic filters as 'standards' for the system, it was important to test their effectiveness in correcting for daily variations within the equipment. RGB determinations were made on the same fifteen specimens of *Veryhachium* from sample TL3 on two different days, 13 months apart. The different sets of determinations were made by the same operator and using the Leica/Qwin setup as previously described. The RGB intensities measured on the two days are plotted relative to each other in Figure 5.16, 5.17 and 5.18. Note that the three sets of data, red, green and blue intensities are plotted at different scales to show the distribution of raw and corrected data more clearly.

The mean *Veryhachium* RGB intensity of sample TL3 was calculated for each day, from both corrected and raw data. The average RGB determination of these two sets of means was then calculated, along with standard deviation and relative standard deviation (standard deviation/mean x 100) (Table 5.2 and 5.3). In an ideal situation, without any gradual variation, the mean RGB determination of sample TL3 calculated on the different days would be the same, and the standard deviation of the means would be zero. As this is not the case, the standard deviation, and the relative standard deviation provide an indication of the spread between the two mean RGB determinations of sample TL3.

In theory, the two sets of corrected data should be closer to each other than the sets of raw data but this is clearly not so (Table 5.2). The relative standard deviations of the raw RGB intensities are all less than 1%, while the relative standard deviations of the corrected RGB intensities range from 4-8%.

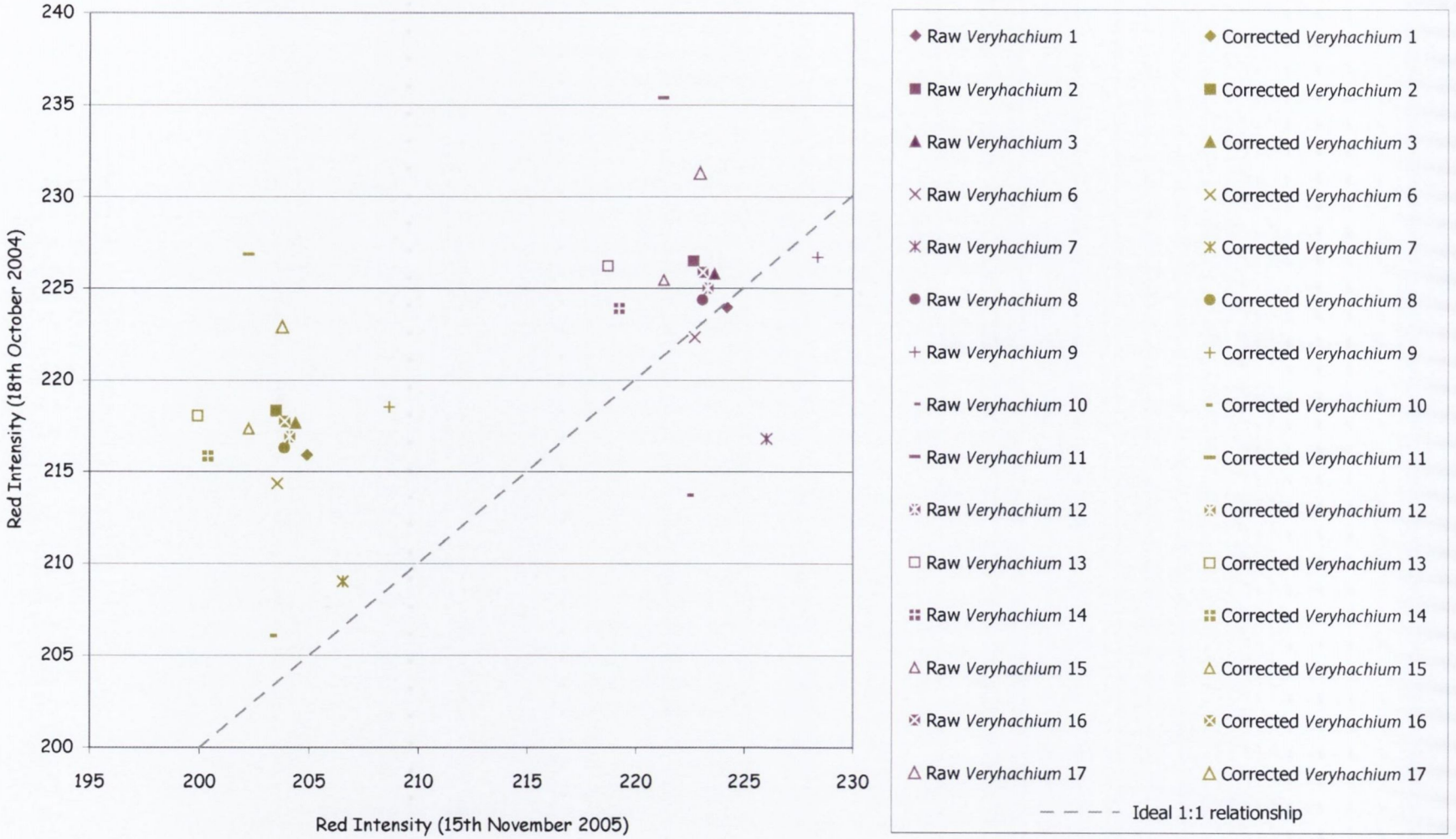

Figure 5.16: Red Intensity data gathered on the 18th October 2004 vs. red intensity data gathered on the same specimens on the 15th November 2005. The colour of each data point denotes if it is raw or corrected data. The shape of each data point refers to a specific *Veryhachium* specimen.

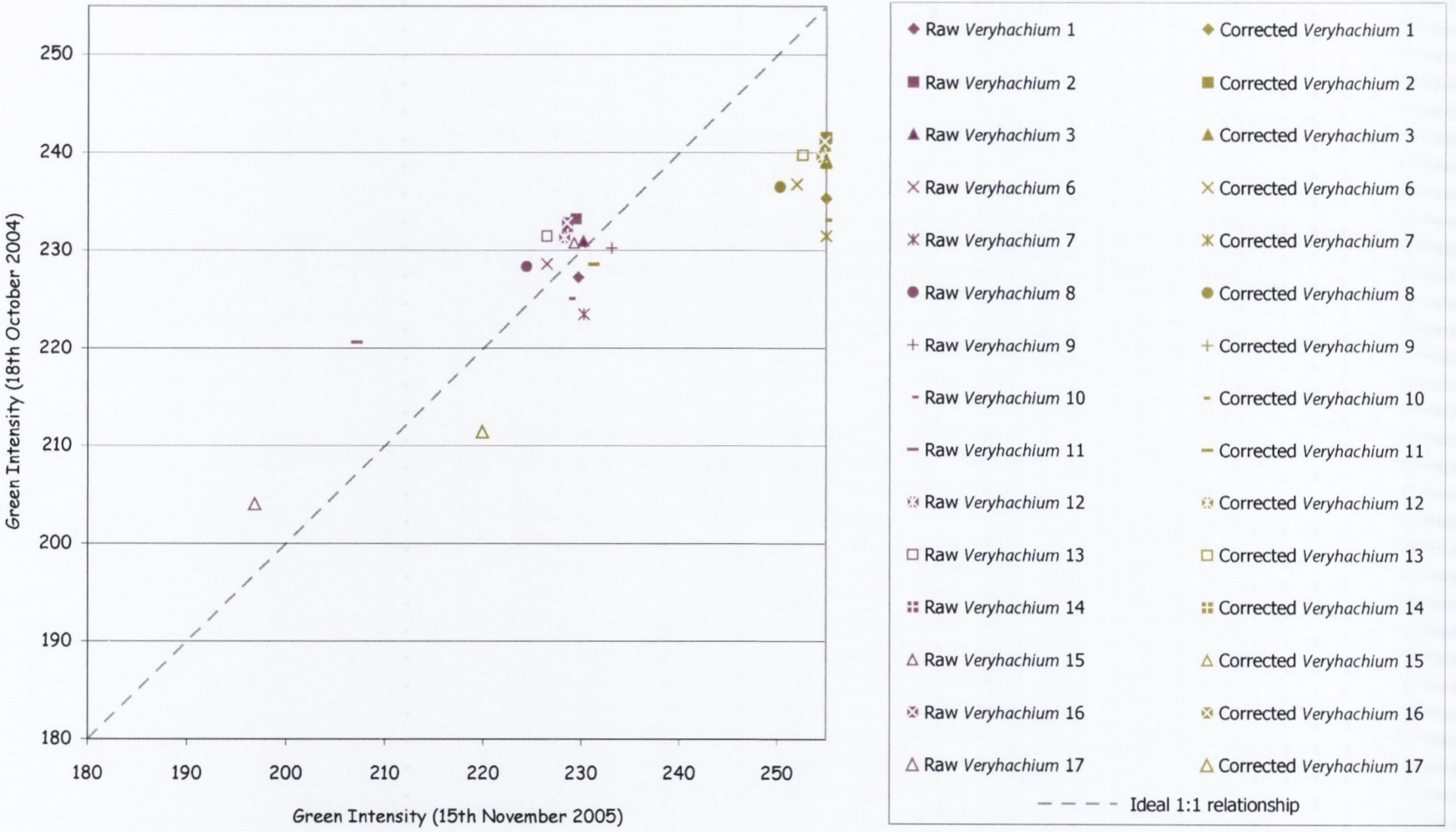

Figure 5.17: Green Intensity data gathered on the 18th October 2004 vs. green intensity data gathered on the same specimens on the 15th November 2005. The colour of each data point denotes if it is raw or corrected data. The shape of each data point refers to a specific *Veryhachium* specimen.

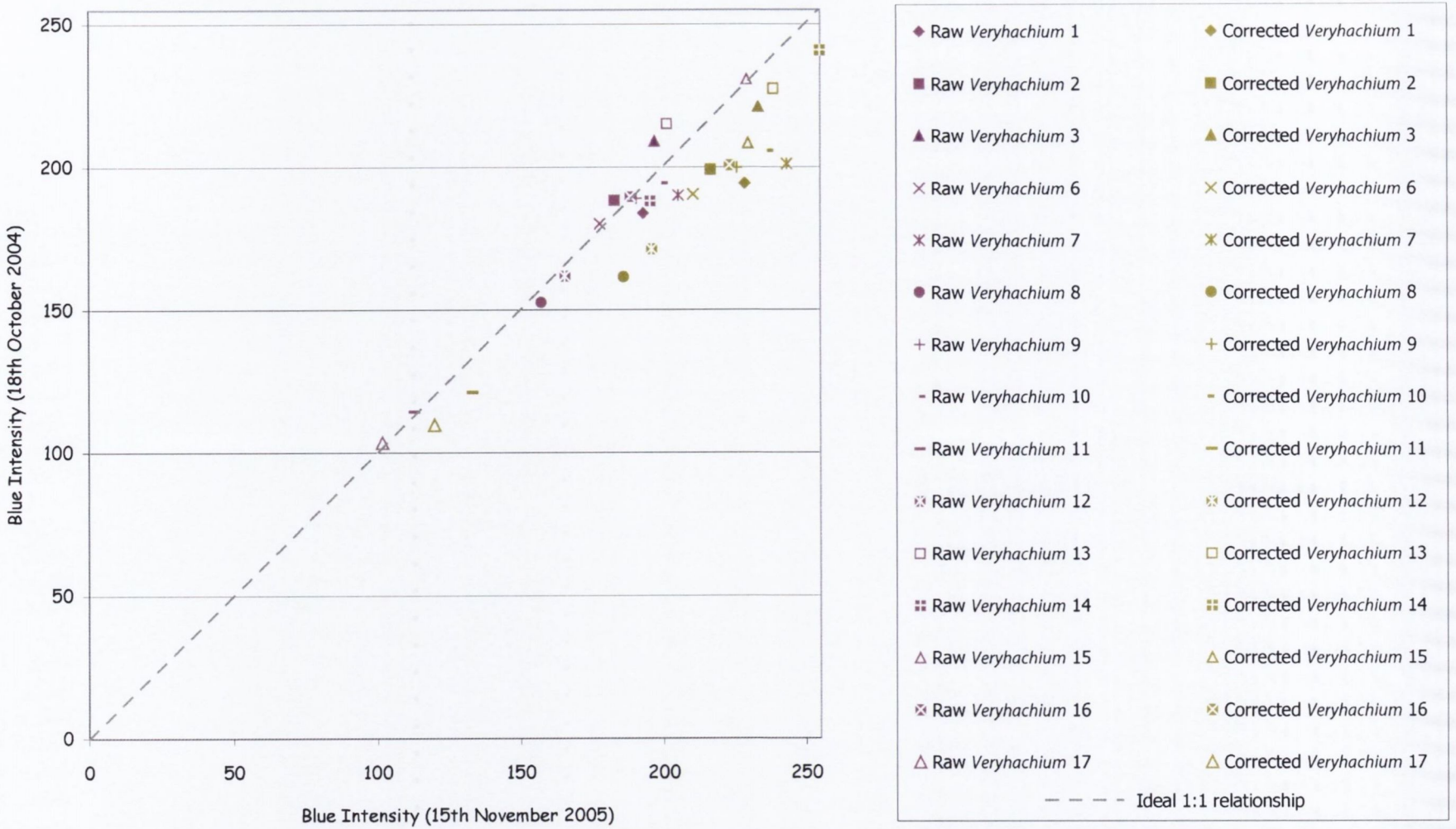

Figure 5.18: Blue Intensity data gathered on the 18th October 2004 vs. blue intensity data gathered on the same specimens on the 15th November 2005. The colour of each data point denotes if it is raw or corrected data. The shape of each data point refers to a specific *Veryhachium* specimen.

From these data, which are based on only two days, the case could be made that the system operates better without the use of 'standards'. However, from Figure 5.13, 5.14 and 5.15, it is clear that there is a systematic change in illumination settings and RGB determinations with time. While it appears that Cokin filters are not hugely successful as 'standards', it does not negate the need for some method to correct for the drift of data with time. In the absence of any other suitable material, these filters were used to calibrate all RGB data determinations made during this project.

Gradual Variations (Raw Data)	**Red**	**Green**	**Blue**
Mean RGB determination of TL3 (15th October 2004)	223	225	177
Mean RGB determination of TL3 (18th November 2005)	225	227	177
Average of the two means (15th Oct '04 and 18th Nov '05)	224	226	177
Std. Deviation of the two means	1	2	0
Relative Standard Deviation	0.60%	0.70%	0.10%

Table 5.2: Raw data collected by the same operator, on the same specimens, the same Leica/Qwin system on two different days.

Gradual Variations (Corrected Data)	**Red**	**Green**	**Blue**
Mean RGB determination of TL3 (15th October 2004)	204	250	210
Mean RGB determination of TL3 (18th November 2005)	217	236	187
Average of the two means (15^{th} Oct '04 and 18th Nov '05)	210	243	199
Std. Deviation of the two means	9	10	16
Relative Standard Deviation	4.40%	4.30%	8.10%

Table 5.3: Corrected data collected by the same operator, on the same specimens, the same Leica/Qwin system on two different days.

5.2.3. VARIATIONS BETWEEN OPERATORS

RGB determinations were made on the same seventeen specimens of *Veryhachium* from sample TL3 by four different operators. Each operator was given guidelines on where to make RGB determinations on each specimen (section 4.5.7.). The different sets of determinations were made on the same day, in quick succession, on the same Leica/Qwin setup as previously described. The data discussed here were not corrected. The only variable that changed was the operator.

The red intensity data gathered by each of the three novice operators were plotted against the red intensity determinations made by the author (Figure 5.19). There was no systematic difference between the different sets of data; there was not a tendency for one operator to make consistently higher or lower red intensity determinations compared to other operators. While the red intensity data gathered by the novice operators is spread over a larger range (218-240) compared to the author's data (218-228), the majority of data cluster around a small area (Figure 5.19).

Green intensity data were also plotted (Figure 5.20). Again, there is no systematic difference in the determinations made by different novice operators, as is also the case with blue intensity determinations (Figure 5.21)

The mean RGB intensity of sample TL3 calculated by each of the users is shown in Table 5.1. The average RGB intensity of these four means was also calculated as was the standard deviation. The standard deviation and relative standard deviation allow a crude quantification of the spread in data between the four users. In this case, the relative standard deviation of the red, green and blue determinations range from 4-8%. This suggests that the variation between operators using image analysis is less than the variation between operators using traditional visual estimation of colour. Batten (1981) suggested there could be up to half a point difference between operators using his 7 point colour scheme.

Variations between operators	**Red**	**Green**	**Blue**
Mean RGB determinations of sample TL3 (DC)*	226	227	181
Mean RGB determinations of sample TL3 (AB)*	226	228	171
Mean RGB determinations of sample TL3 (AH)*	227	228	180
Mean RGB determinations of sample TL3 (CD)	223	225	177

Average of the four operator means	226	227	177
Std. Deviation of the four operator means	2	1	5
Relative Standard Deviation (Std. Deviation/Mean*100)	0.76%	0.62%	2.5%

* indicates novice operator

Table 5.4: Raw data collected by different operators, on the same specimens, on the same day and using the same Leica/Qwin system.

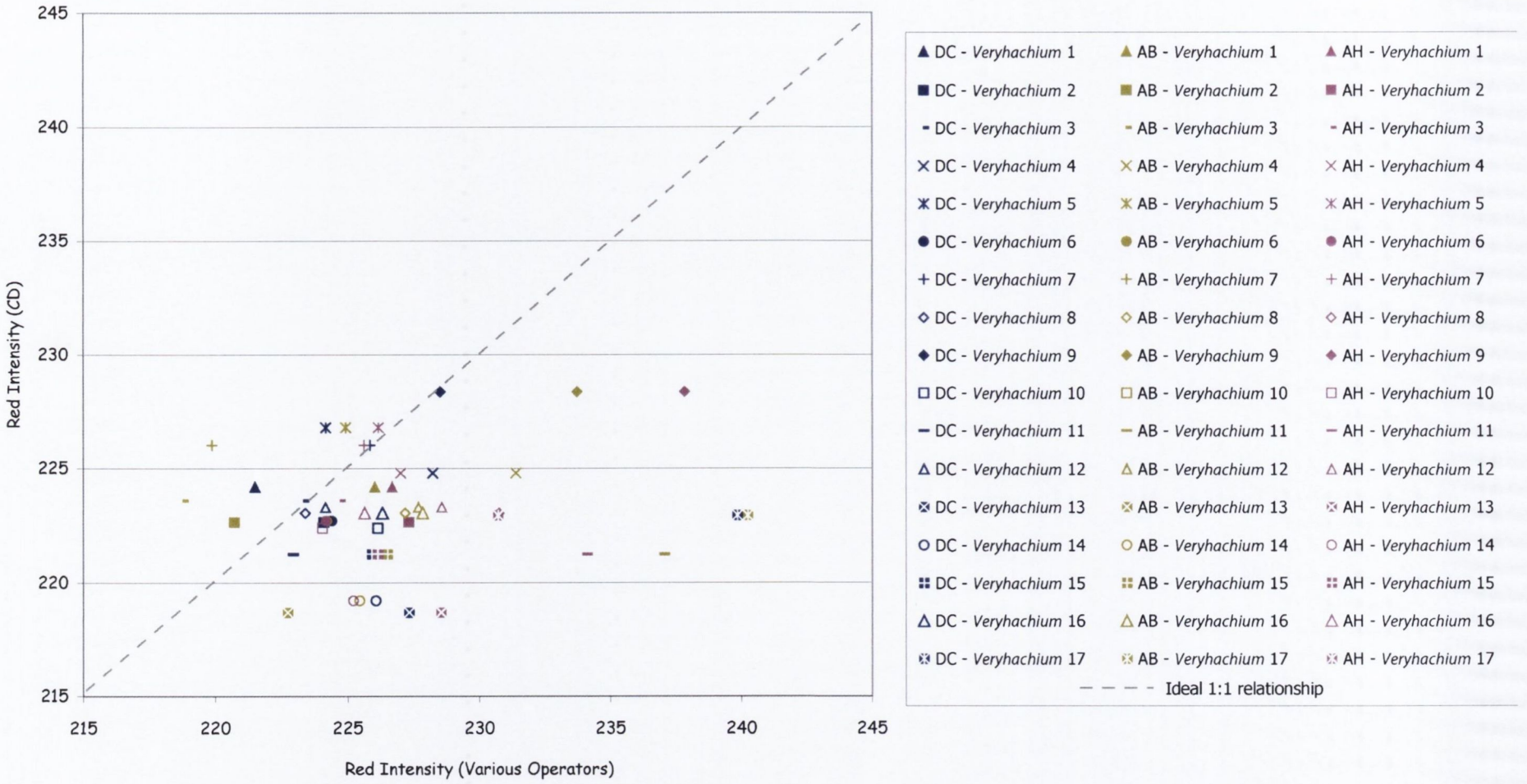

Figure 5.19: Red intensity determinations of seventeen *Veryhachium* specimens made by the author vs. red intensity determinations of the same seventeen *Veryhachium* made by different novice operators. The colour of each data point refers to the user. The shape of each data point refers to the individual *Veryhachium* specimen. The data were collected on the same day, using the same Leica/Qwin system and were not corrected.

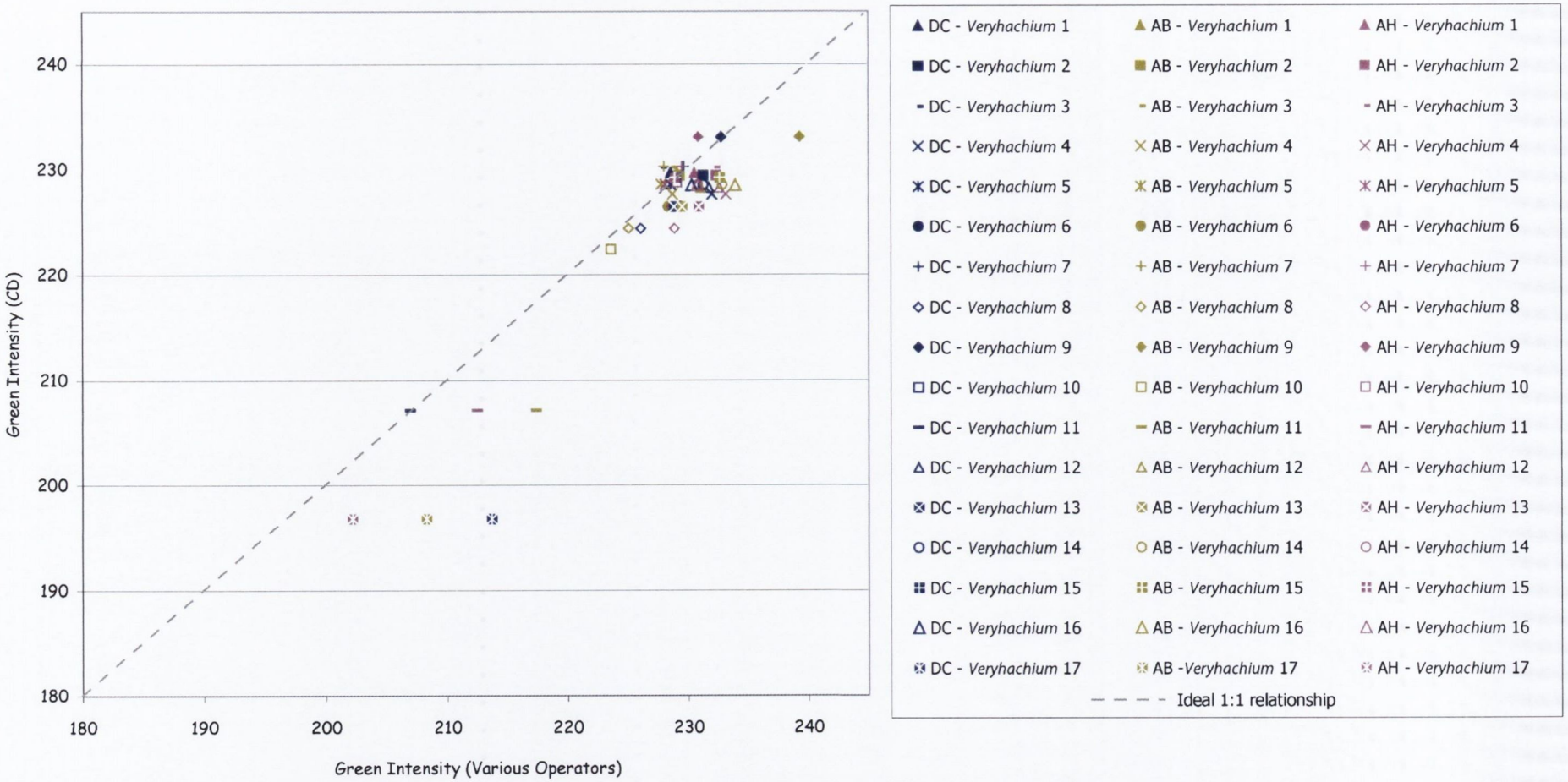

Figure 5.20: Green intensity determinations of seventeen *Veryhachium* specimens made by the author vs. green intensity determinations of the same seventeen *Veryhachium* made by different novice operators. The colour of each data point refers to the user. The shape of each data point refers to the individual *Veryhachium* specimen. The data were collected on the same day, using the same Leica/Qwin system and were not corrected.

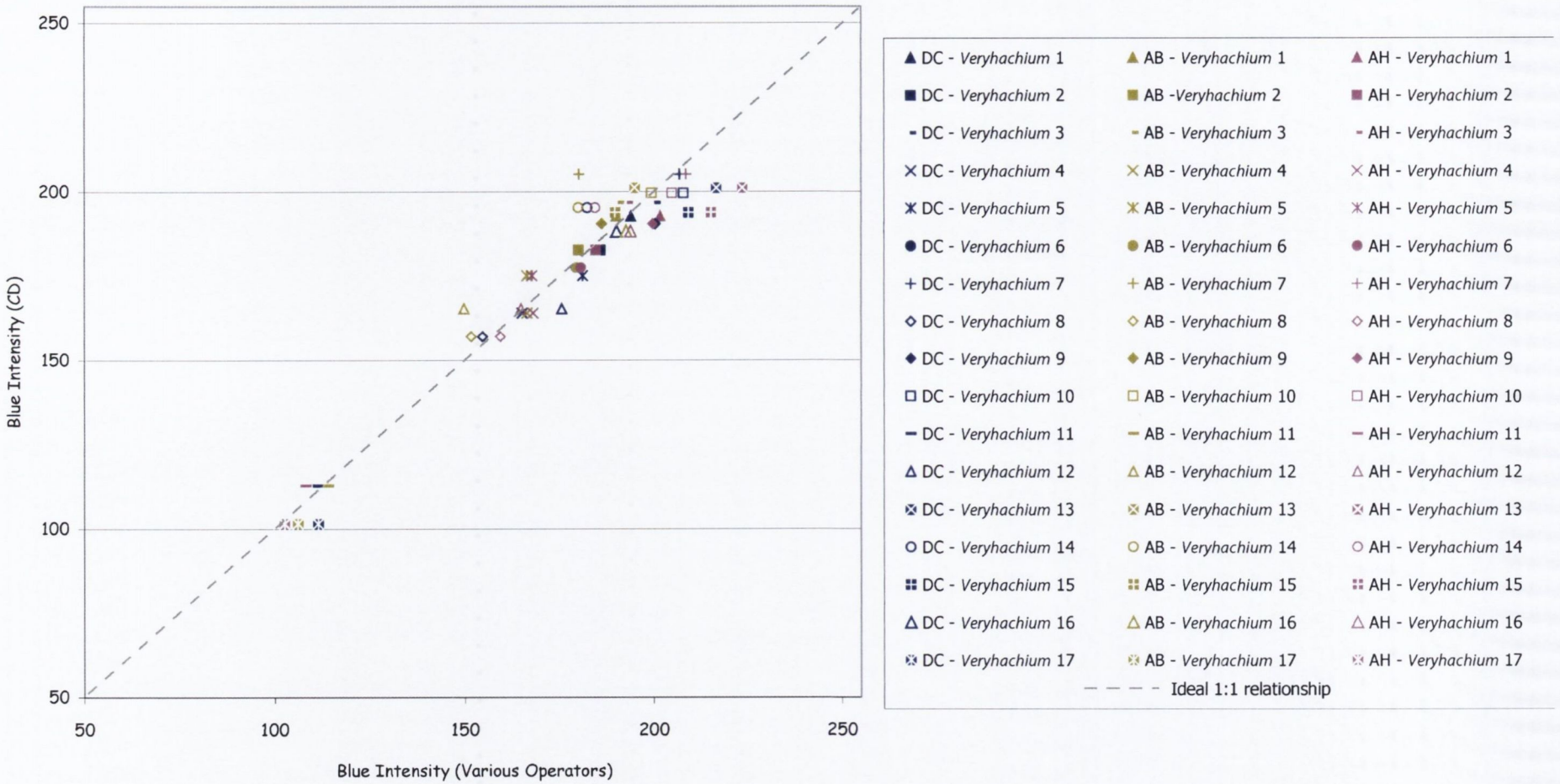

Figure 5.21: Blue intensity determinations of seventeen *Veryhachium* specimens made by the author vs. blue intensity determinations of the same seventeen *Veryhachium* made by different novice operators. The colour of each data point refers to the user. The shape of each data point refers to the individual *Veryhachium* specimen. The data were collected on the same day, using the same Leica/Qwin system and were not corrected.

5.2.4. VARIATIONS BETWEEN QWIN AND PHOTOSHOP DETERMINATIONS

The system used to assess colour in this study is part of an integrated image analysis system. This system may not be readily available to all workers, so an attempt was made to achieve similar results using Adobe Photoshop® CS. This program is an industry standard and is readily available in most laboratories. It is envisaged that a worker with a digital camera, a set of 'standards' and this program, should be able to achieve similar results in lieu of an image analysis system. Images captured using a colour video camera, as described previously, were opened in Adobe Photoshop® CS. Using the circular marquee tool, a suitable area was selected (section 4.5.7.) for colour determination. By choosing the 'histogram' option in the 'tools' menu, the average red, green and blue intensities of the selected area could be determined (Figure 5.22).

RGB determinations were made on the same fifteen specimens of *Veryhachium* from sample TL3 using the previously described Leica Qwin image analysis system, and Adobe Photoshop® CS. The determinations were made on the same captured images and as a result the data were not corrected to account for any differences in illumination. The RGB intensities determined using the two different systems are plotted relative to each other in Figure 5.23, 5.24 and 5.25. There was little difference between the two data sets with the relative standard deviations of the three intensities ranging from 0.4 - 1.6%. This is useful as Adobe Photoshop is a commonly used program and suggests that the method does not require expensive image analysis technology.

Variations between Qwin and Photoshop	**Red**	**Green**	**Blue**
Mean RGB determination of TL3 (Qwin Image Analysis)	225	227	177
Mean RGB determination of TL3 (Adobe Photoshop)	223	230	181
Average of the two means (Qwin and Photoshop)	224	229	179
Std. Deviation of the two means	1	2	3
Relative Standard Deviation	0.40%	0.90%	1.60%

Table 5.5: Raw data collected by the same operator, on the same specimens, from the same images using the Qwin image analysis program and Adobe Photoshop® CS.

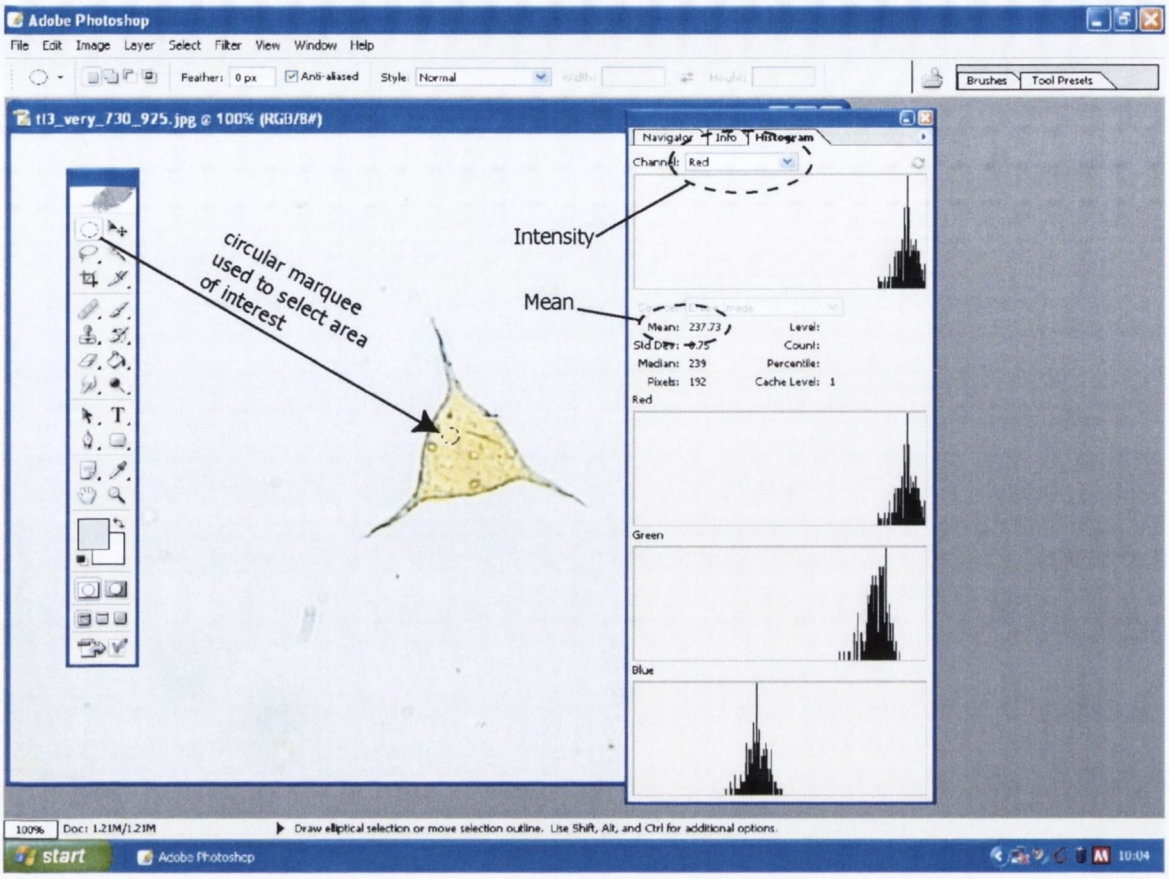

Figure 5.22: Screen shot of Adobe Photoshop CS window showing use of the circular marquee to select a suitable area on the *Veryhachium* specimen on which to make a colour determination. Also highlighted is the 'histogram' window which shows the average red, green, and blue intensities values for the area highlighted.

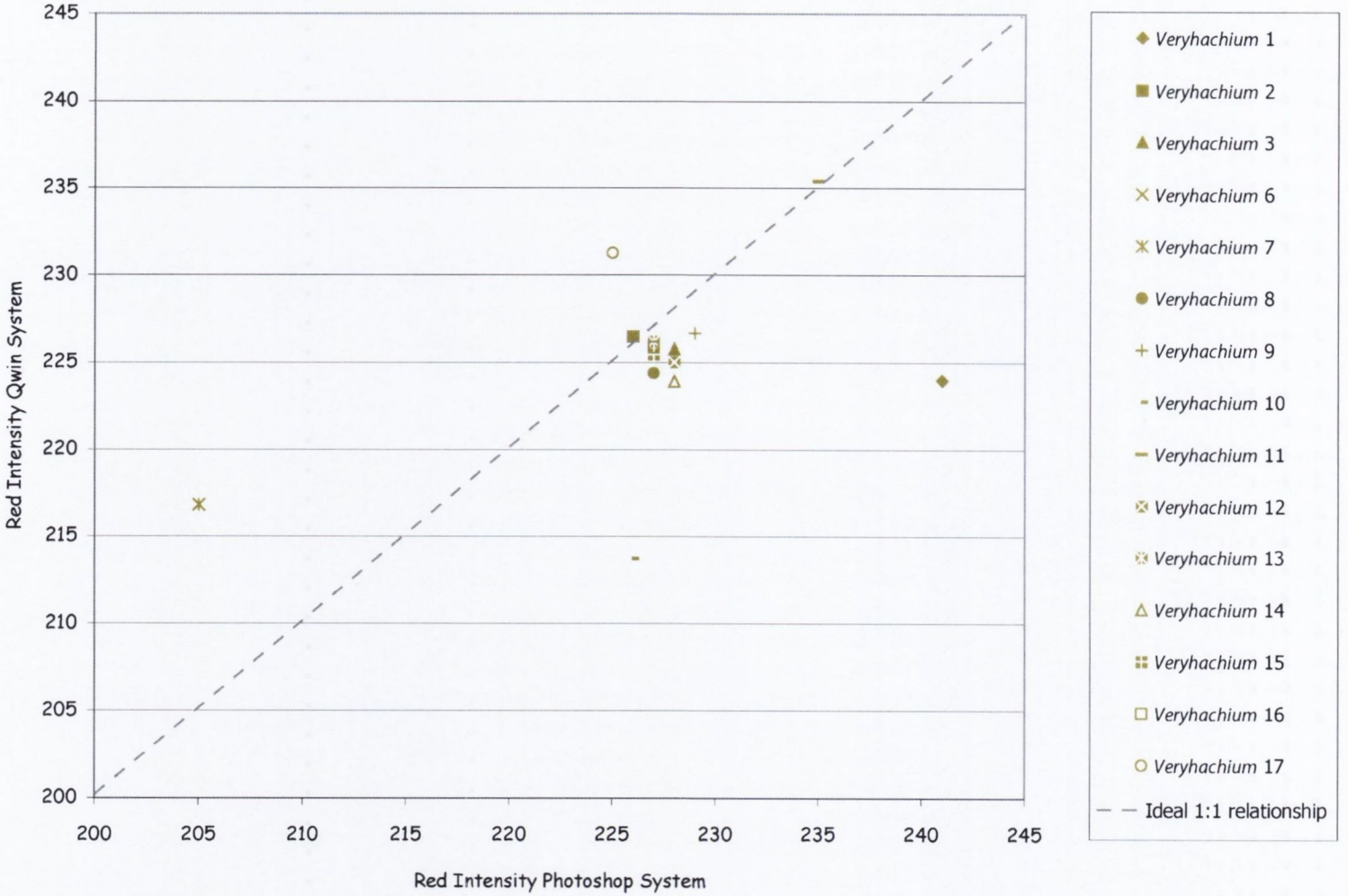

Figure 5.23: Red Intensity determinations made on 15 *Veryhachium* specimens using Adobe Photoshop CS vs. red intensity determinations made on the same images of the *Veryhachium* specimens using the Qwin image analysis system. This is raw data.

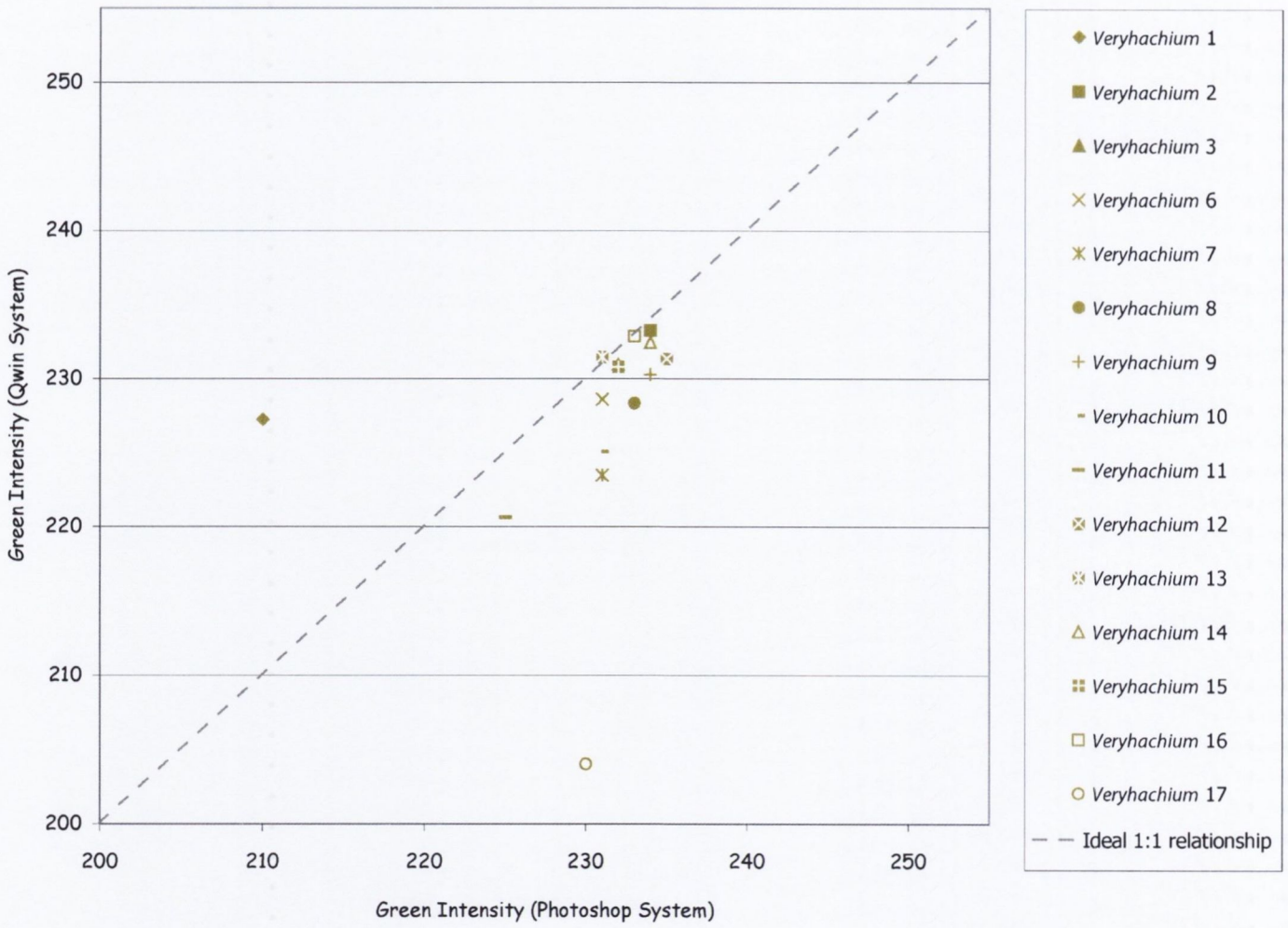

Figure 5.24: Green Intensity determinations made on 15 *Veryhachium* specimens using Adobe Photoshop CS vs. green intensity determinations made on the same images of the *Veryhachium* specimens using the Qwin image analysis system. This is raw data.

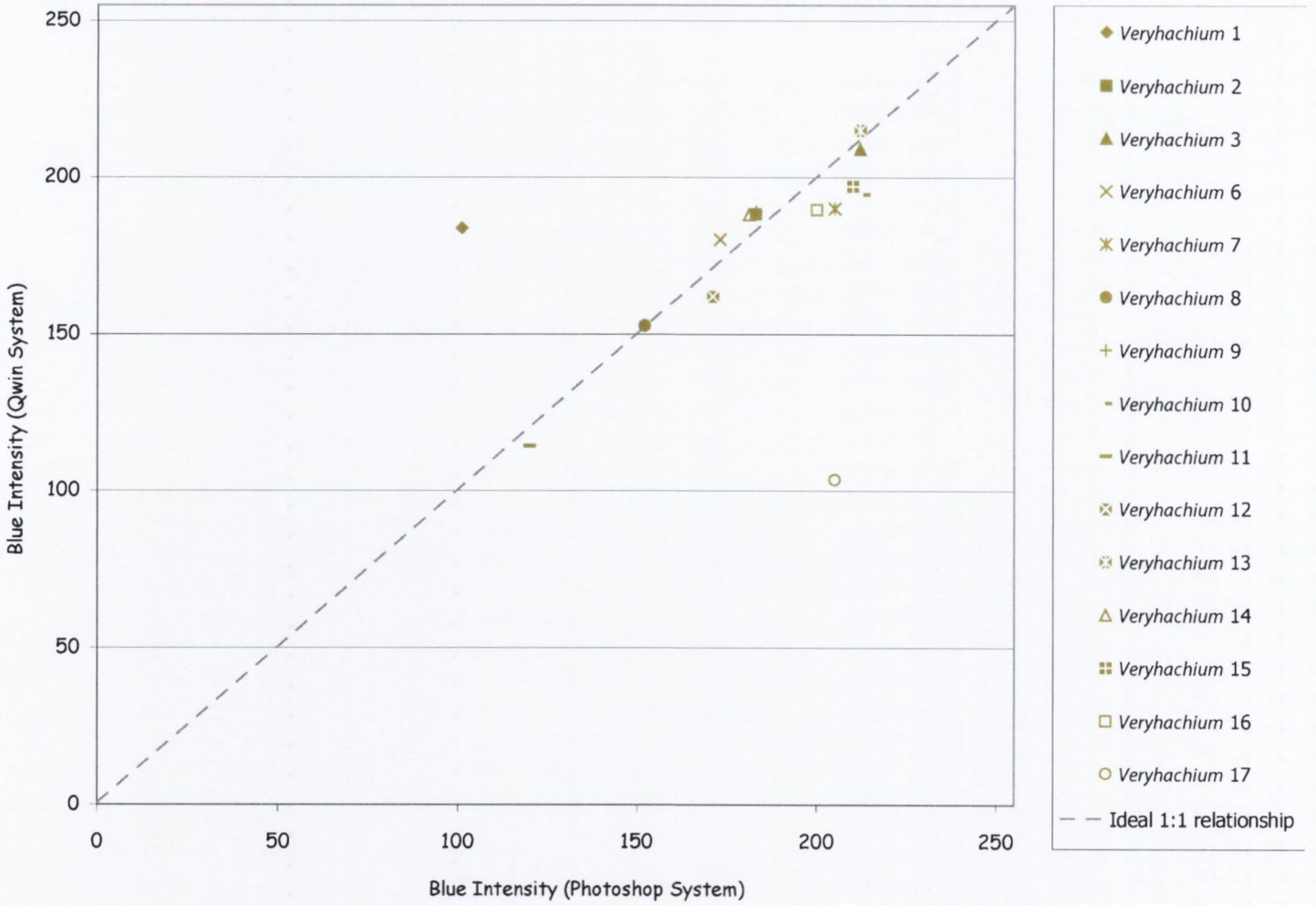

Figure 5.25: Blue Intensity determinations made on 15 *Veryhachium* specimens using Adobe Photoshop CS vs. blue intensity determinations made on the same images of the *Veryhachium* specimens using the Qwin image analysis system. This is raw data.

5.2.5. VARIATIONS BETWEEN DIFFERENT SETUPS

The most likely source of error for the image analysis method is the variation between different setups, i.e. different microscopes, cameras, light sources and image analysis programs. To investigate this, RGB determinations were made on the set of Cokin photographic filters using a Nikon Eclipse E600 microscope attached to a DXM 1200 Nikon colour camera with images analysed using Lucia Image™ 5.10. The RGB determinations made on this setup were plotted against the established RGB values of the 'standards' from the Leica/Qwin system (see Figure 5.26, 5.27 and 5.28).

It appears that the Nikon / Lucia system underestimates the red intensity values of the 'standards' relative to the Leica Qwin System (Figure 5.26). The equation of the regression line of this data was used to calibrate red intensity determinations made on *Veryhachium* in sample TL3 on the same Nikon / Lucia system. The Nikon / Lucia system also seems to underestimate the green intensity of the Cokin filters relative to the Leica Qwin System (Figure 5.27). Again, the equation of the regression line was used to calibrate *Veryhachium* green intensity determinations.

There is a relatively linear relationship between red and green intensity determinations made on the Leica/Qwin and Nikon/Lucia system. However, there is a poor correlation between blue intensity data gathered on the two different setups (Figure 5.28). It is unclear why there is such a difference between the three intensities.

Both the raw and corrected RGB determinations made on each *Veryhachium* specimen using the two different setups are plotted against each other in Figures 5.29, 5.30 and 5.31. The relative standard deviation between the mean RGB determination of sample TL3 made on the Leica/Qwin system and the Nikon/Lucia system is shown below (table 5.5 and 5.6). The raw data sets appear to be closer together than the corrected data. The highest relative standard deviation is connected to the corrected blue intensity data. This is clearly related to the poor correlation between the 'standards' measured on the two systems (Figure 5.31).

Raw Data	**Red**	**Green**	**Blue**
Mean RGB determination of TL3 (Leica/Qwin System)	226	227	174
Mean RGB determination of TL3 (Nikon/Lucia System)	210	229	166
Average of the two means	218	228	170
Std. Deviation of the two means	11	1	6
Relative Standard Deviation	5%	0.50%	4%

Table 5.6: Raw data collected by the same operator, on the same specimens using the Leica/Qwin system and the Nikon/Lucia System.

Corrected Data	**Red**	**Green**	**Blue**
Mean RGB determination of TL3 (Leica/Qwin System)	218	235	184
Mean RGB determination of TL3 (Nikon/Lucia System)	234	253	229
Average of the two means	226	244	207
Std. Deviation of the two means	11	13	32
Relative Standard Deviation	5%	5%	15%

Table 5.7: Corrected data collected by the same operator, on the same specimens using the Leica/Qwin system and the Nikon/Lucia System.

5.2.6. Conclusions

There was little variation between operators who used image analysis techniques to determine palynomorphs colour. Daily variations within the system do exist, as demonstrated by the systematic change in RGB determinations made on Cokin filters (Figure 5.13, 5.14 and 5.15). The use of 'standards' to compensate for this drift was of no value with relative standard deviations larger in corrected data than raw data. This pattern was also repeated in raw and corrected RGB data from different setups.

It appears that the Cokin filters cannot be used as 'standards' in the traditional sense. This is probably a result of several factors. Perhaps there were too few filters used and with the addition of more filters the regression lines used to raw data would be more tightly constrained. It is also possible that using a different regression method would improve the calibration technique. RGB determinations varied across the surface of the filter, although the relative standard deviation of 30 measurements made across the surface of each filter was less than 2%. The greatest source of variation in the Leica/Qwin system appears to relate to the age of bulb. The Cokin 'standards' do not compensate fully for this drift. Replacement of the halogen light bulb every six months might help to reduce the effect.

The filters do still act as a useful guide to the general variation from setup to setup. They may be of greater benefit as a tool to determine when the illumination of a setup is similar to the one used in this study. They could be used to calibrate the system, rather than the data. Further work is needed to determine if this is possible but it is beyond the scope of this project.

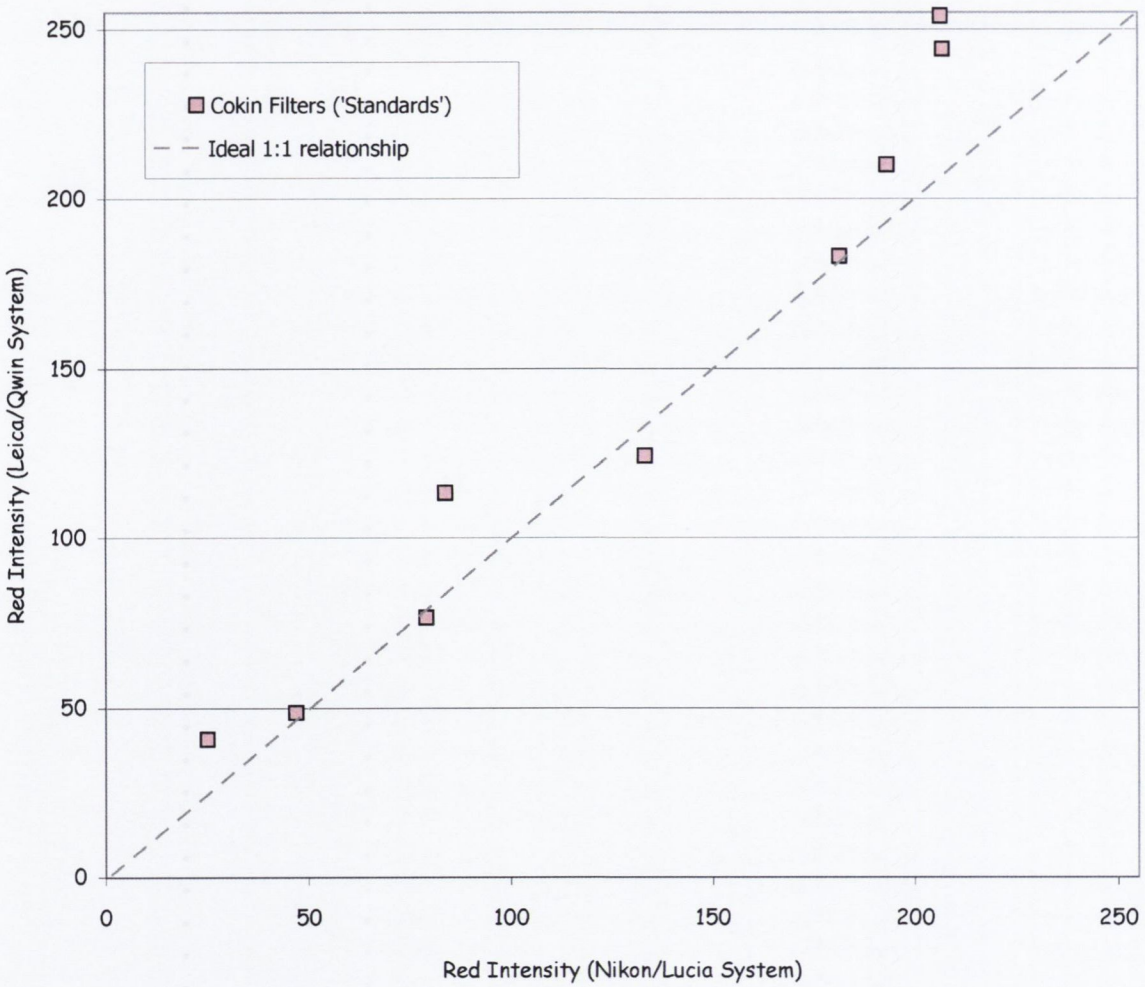

Figure 5.26: Red Intensity determinations made on the original set of Cokin photographic filters using the Leica/Qwin system vs. red intensity determinations made using the Nikon/Lucia system.

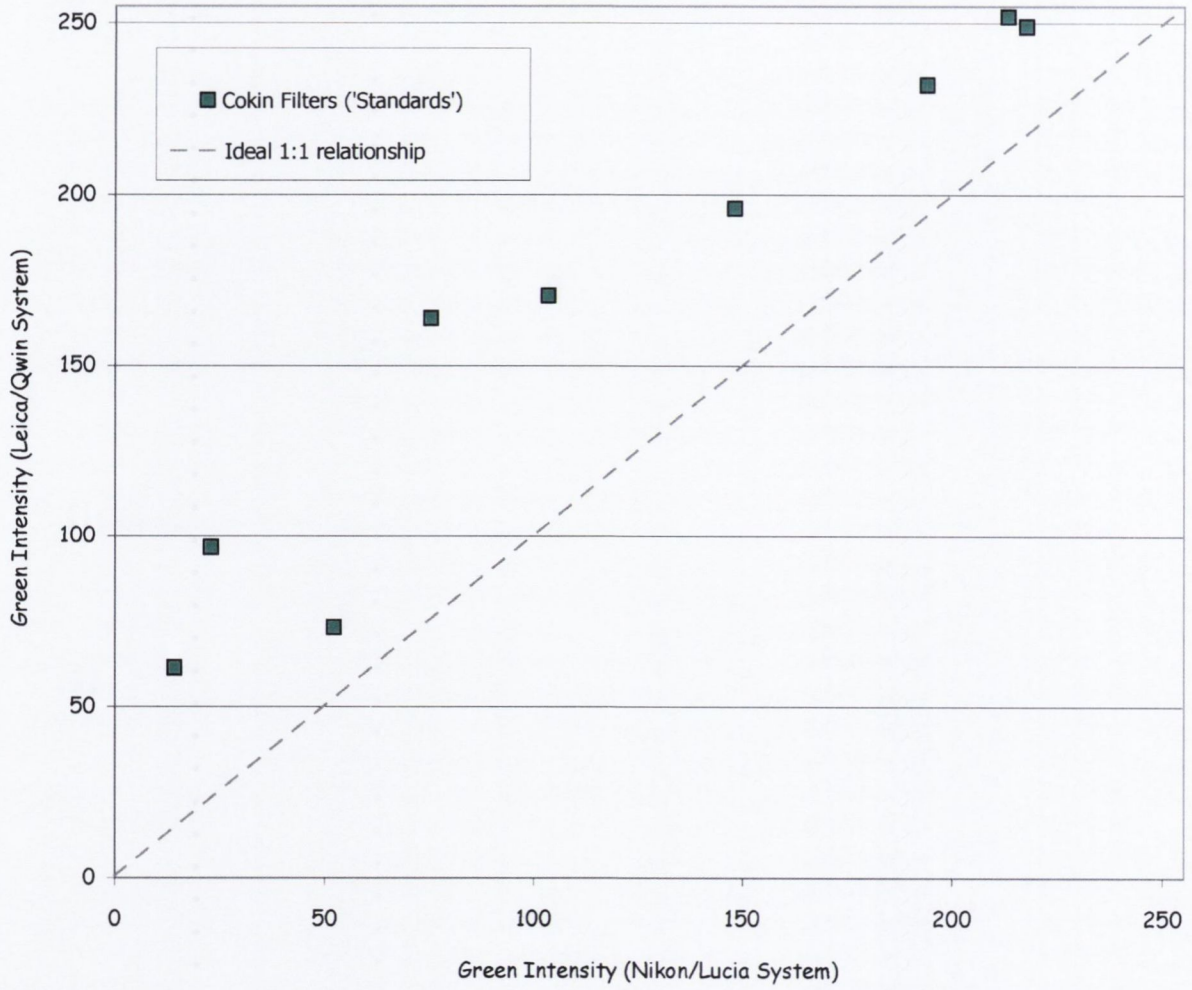

Figure 5.27: Green Intensity determinations made on the original set of Cokin photographic filters using the Leica/Qwin system vs. green intensity determinations made using the Nikon/Lucia system.

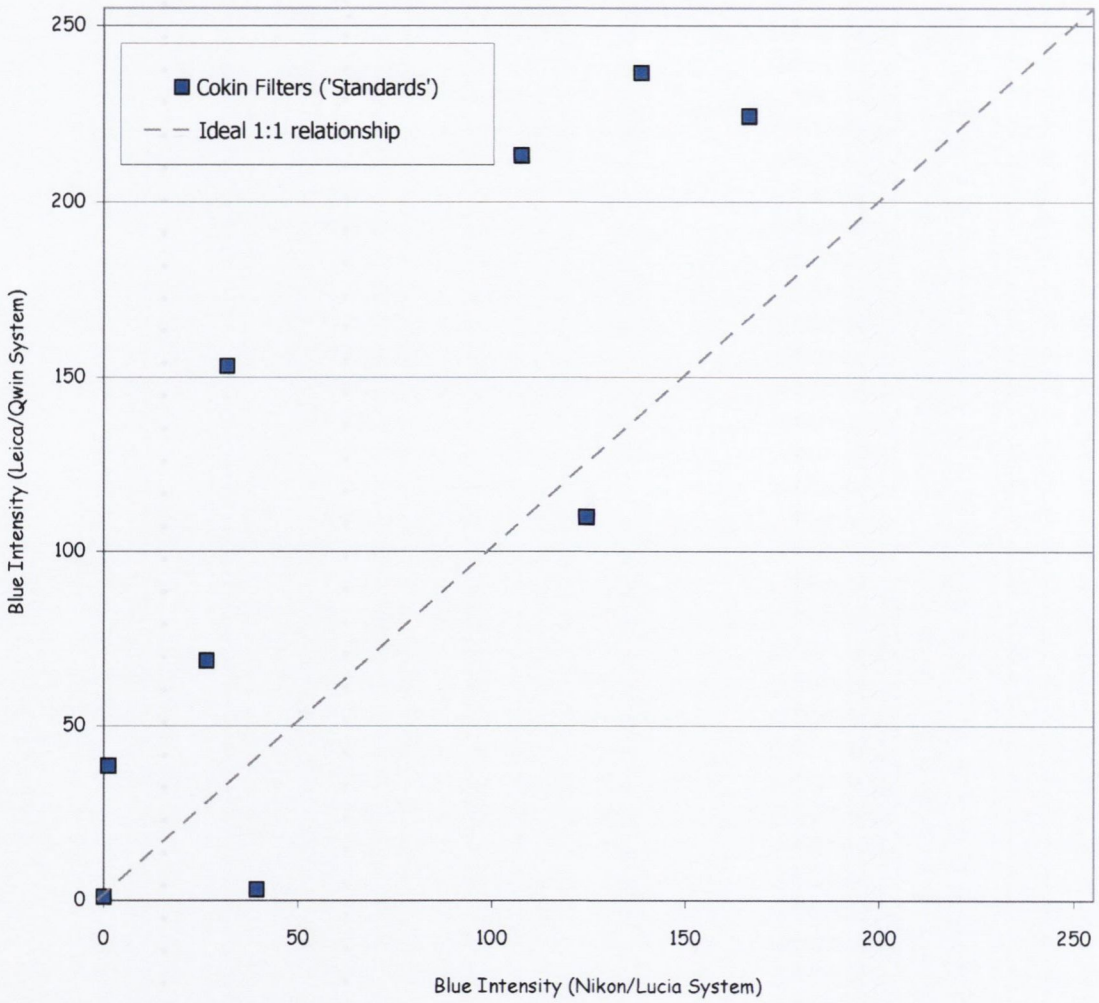

Figure 5.28: Blue Intensity determinations made on the original set of Cokin photographic filters using the Leica/Qwin system vs. blue intensity determinations made using the Nikon/Lucia system.

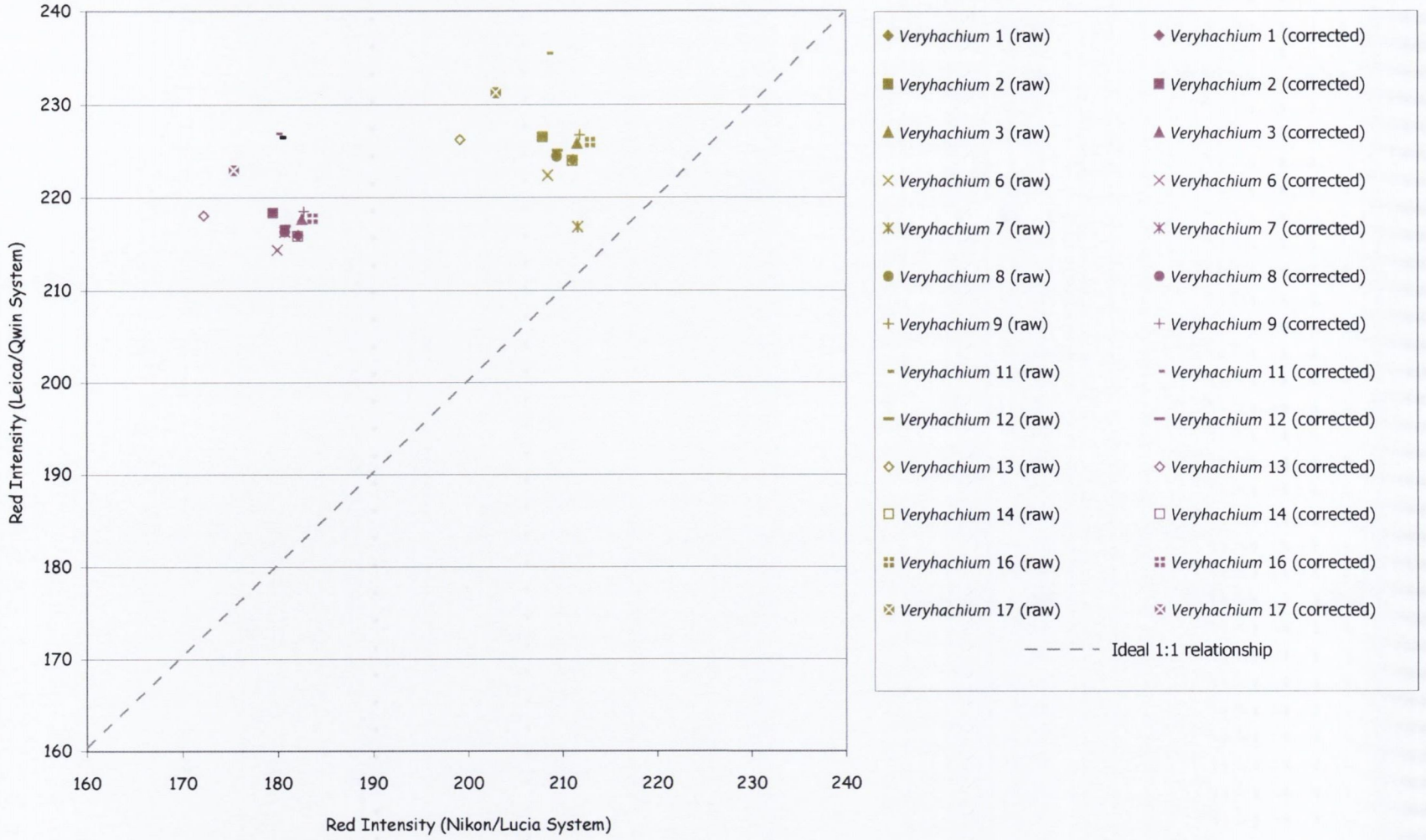

Figure 5.29: Red Intensity determinations made on 13 *Veryhachium* specimens using the Nikon/Lucia system vs. red intensity determinations made on the same specimens using the Leica/Qwin system. The colour of each data point denotes whether it is corrected or not. The shape of each data point refers to a specific specimen.

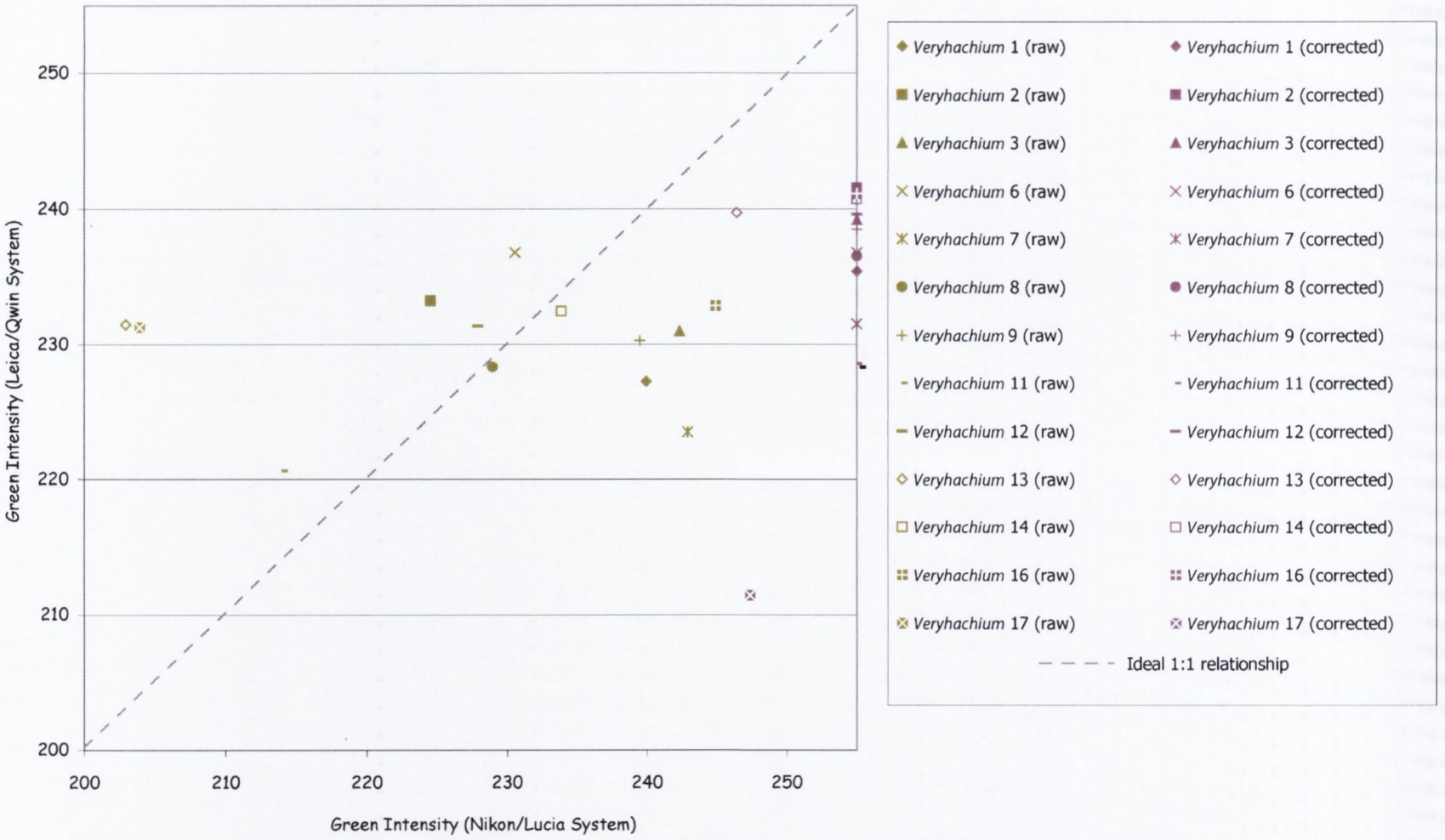

Figure 5.30: Green Intensity determinations made on 13 *Veryhachium* specimens using the Nikon/Lucia system vs. green intensity determinations made on the same specimens using the Leica/Qwin system. The colour of each data point denotes whether it is corrected or not. The shape of each data point refers to a specific specimen.

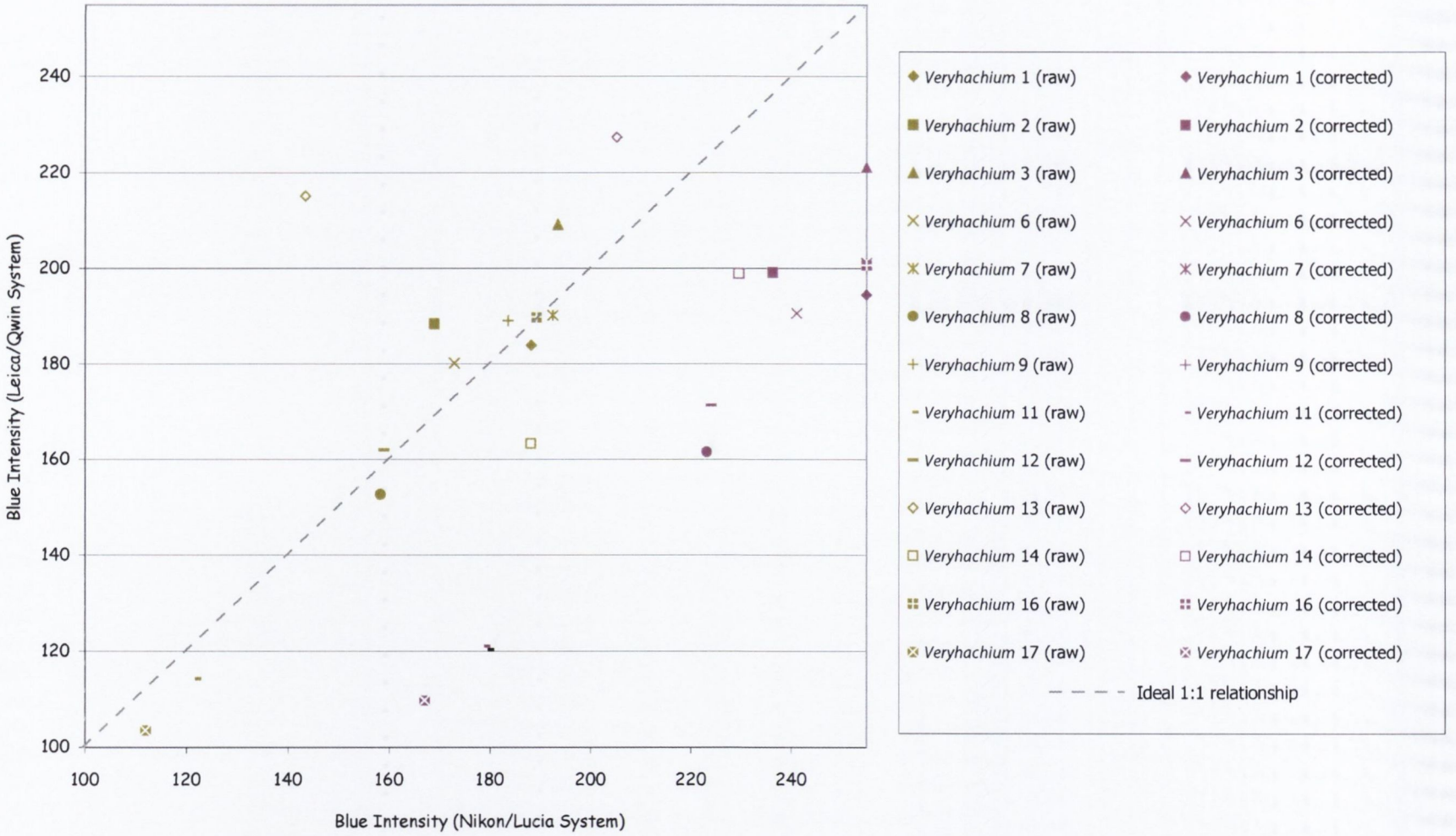

Figure 5.31: Blue Intensity determinations made on 13 *Veryhachium* specimens using the Nikon/Lucia system vs. blue intensity determinations made on the same specimens using the Leica/Qwin system. The colour of each data point denotes whether it is corrected or not. The shape of each data point refers to a specific specimen.

CHAPTER 6
RESULTS AND DISCUSSION

6.1. REFLECTANCE DETERMINATION RESULTS

6.1.1. FACTORS AFFECTING ACCURACY OF RESULTS

All reflectance results are given in Appendix II. The chitinozoa and vitrinite reflectance determinations of a sample are dependant on a number of factors. In an ideal situation, the value determined reflects the maturity of a sample, and is based on measurements made on indigenous particles. However, the inclusion of 'foreign' populations of vitrinite grains or chitinozoa in a sample, through caving or reworking, can lead to anomalous reflectance determinations. Caved grains are grains originating from the upper part of a borehole or well which have been incorporated into a cuttings sample taken from a deeper part of the borehole. Reworked grains are grains originally deposited in a sediment that was subsequently eroded and incorporated into a younger sediment. Only reworked grains that have been initially subjected to higher levels of maturity than the sediment they were subsequently deposited in will be identifiable. In order to assess the maturity level of a sample, it is important to filter out suspected caved and reworked populations from the data set.

In this study, identification of suspect particles was based on histogram shape. In a sample containing only an indigenous vitrinite or chitinozoa population, the reflectance values should be distributed normally about the mean (Figure 6.1). Samples which include caved grains usually produce bimodal histograms. The caved specimens generally plot to the left of the indigenous population, typically with low reflectance and smaller number of grains (Figure 6.2). Reworked material often plots to the right of an indigenous population, with a higher reflectance and a smaller number of grains (Figure 6.3). If these populations are not removed from the data set, they will alter the average vitrinite or chitinozoa reflectance of the sample. Data were removed only from samples where caving or reworking was clearly suggested by the histogram shape. The mean reflectance of the sample was recalculated after the anomalous readings had been removed (Figure 6.4). It should be noted that populations where 100% of the particles are either reworked or caved are

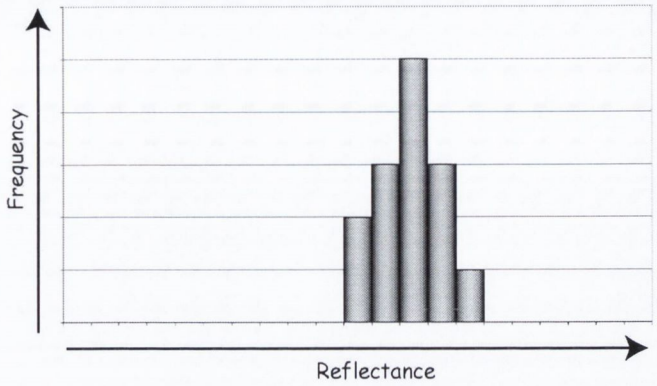

Figure 6.1: Idealised histogram of an indigenous vitrinite/chitinozoa population plotting reflectance against frequency. The data are distributed normally about the mean.

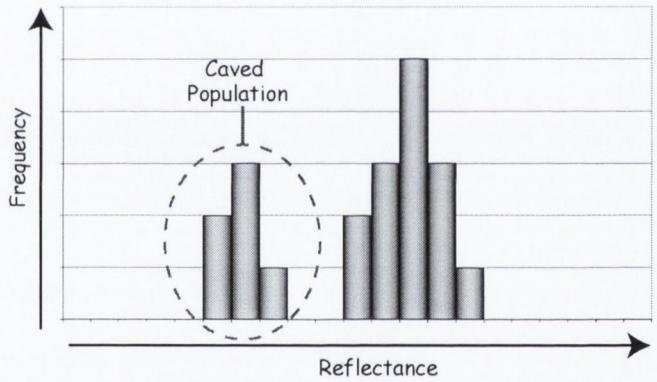

Figure 6.2: Idealised histogram of data set that contains an indigenous and caved population. The caved material has a lower reflectance than the indigenous population, and is smaller in number.

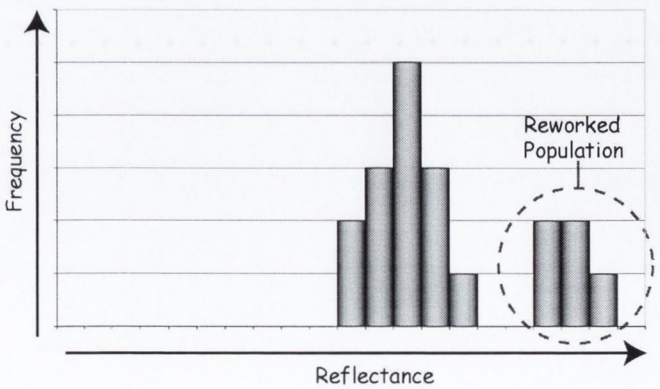

Figure 6.3: Idealised histogram of data set that contains an indigenous and reworked population. The reworked material has a higher reflectance than the indigenous population, and is smaller in number.

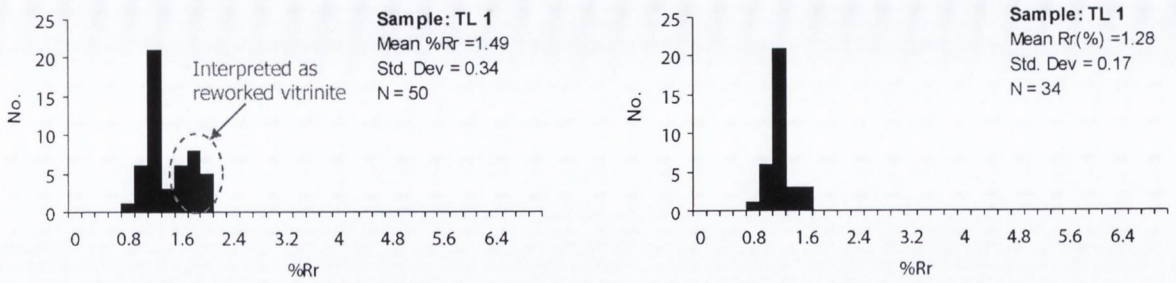

Figure 6.4: Example of reworked vitrinite that was selected and removed from sample TL1 on the basis of a bimodal histogram. Once the anomalous data were removed the mean random reflectance (%Rr) of the sample was recalculated.

obviously impossible to identify, except in the context of indigenous data from higher and lower in the section. Histograms for each sample used in this study are shown in Appendix II, along with the sample size, mean reflectance (after caved and reworked samples have been removed) and standard deviation. In general, the standard deviation of data was lower for chitinozoa reflectance populations than vitrinite reflectance data sets. Many samples investigated in this study contained only small vitrinite populations, with marine derived microfossils dominant. Although several slides were mounted for each sample, in some cases the number of grains measured was still less than the recommended 30 determinations (Barker *et al.* 1993).

6.2. RGB DETERMINATIONS RESULTS

6.2.1. CORRECTION OF RGB DETERMINATIONS

As discussed in Chapter 5, Cokin photographic filters were used to calibrate all colour measurements and correct for the effect of daily variations within the system. While this correction technique appeared the most suitable and user friendly method available, there were some inherent flaws. Over the two year period, corrected RGB intensities of paler *Veryhachium* specimens produced colours that obviously did not reflect the colour of the acritarch, some almost bright green (Figure 6.5). This appeared to be the result of the correction technique producing abnormally high green intensity values.

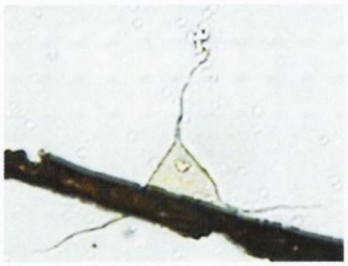

Sample	**Sun 7 *Very_h69_3***
Corrected Red	186
Corrected Green	245
Corrected Blue	224
Date of Measurement	18th August 2004

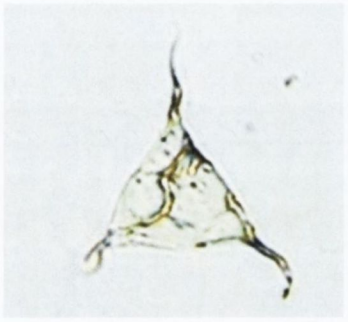

Sample	**Can 9 *Very_q38***
Corrected Red	204
Corrected Green	255
Corrected Blue	230
Date of Measurement	21st Feb 2005

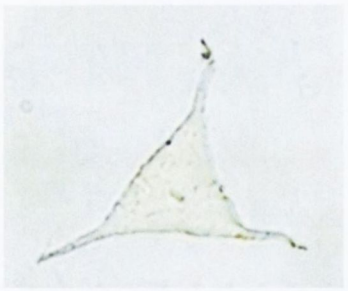

Sample	**TL 7 *Very_g43_1***
Corrected Red	204
Corrected Green	255
Corrected Blue	236
Date of Measurement	21st Feb 2005

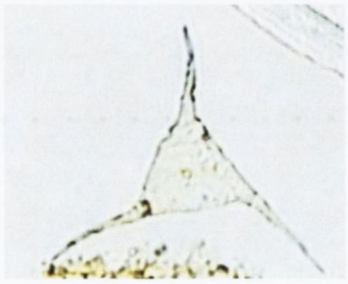

Sample	**P23 *Very_q46***
Corrected Red	210
Corrected Green	245
Corrected Blue	236
Date of Measurement	20th Nov 2005

Figure 6.5: Examples of anomalous corrected RGB intensities and photomicrographs of the specimens in question.

Because of the relatively large decrease of green intensity with time (see section 5.2.2.), the difference between raw and corrected values increases. The value of green intensity is limited to a maximum intensity of 255. This limit is not factored into the correction equation, which is simply a linear regression. As a result, the correction equation tends to overestimate the corrected green intensity value and produces green intensity values for pale *Veryhachium* in excess of 255. These excessive values of green intensity are replaced manually by an intensity value of 255. While this anomaly should not affect the data set, as all data has been subject to the same procedures, it does sometimes create slightly unrealistic synthetic colours for paler acritarchs.

6.2.2. *VERYHACHIUM* COLOUR DETERMINATIONS

Like reflectance measurements, the mean RGB colour determination of a *Veryhachium* population can be influenced by caved and reworked specimens. Again, histograms were used to identify 'foreign' populations within the data set. In the case of the red, green and blue histograms, caved (paler coloured) populations plot to the right of the indigenous population with higher intensities and a smaller sample size (Figure 6.7). Reworked (darker coloured) specimens plot to the left of the indigenous population with lower intensities and a smaller sample size (Figure 6.7). Because the spread of red, green and blue intensities varied with maturity, different (red, green or blue) histograms often produced two or more populations. In this study, caved or reworked specimens were identified on the basis that they plotted as separate populations in at least two of the three histograms. RGB histograms for each sample used in this study are shown in Appendix V, along with the sample size, mean intensity (after caved and reworked specimens have been removed) and standard deviation. In many samples investigated in this study, while *Veryhachium* was present, it was never common. Although several slides were mounted for each sample, in some cases the number of specimens measured was still less than the desired 30 determinations.

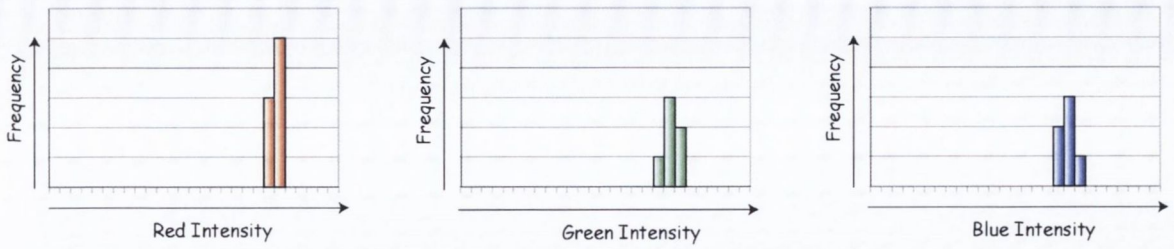

Figure 6.6: Idealised histogram of the red, green and blue intensities of an indigenous population. The intensities form one population, normally distributed about the mean.

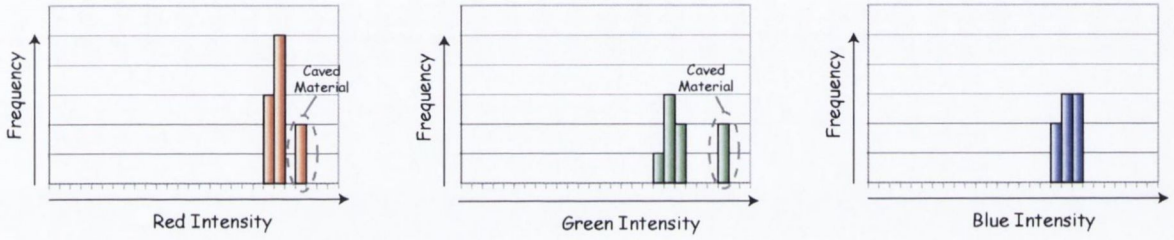

Figure 6.7: Idealised histogram of the red, green and blue intensities of an indigenous and caved population. Caved material is identified on the basis that in at least two out of the three histograms, the data plots as two separate populations. This material is generally lighter in colour than the indigenous population and as such plots to the right of the indigenous population.

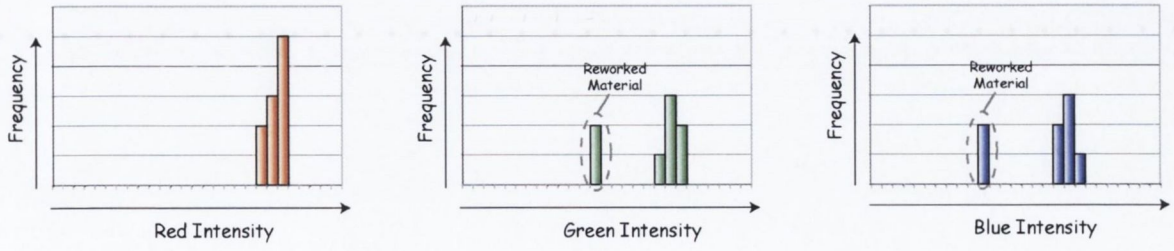

Figure 6.8: Idealised histogram of the red, green and blue intensities of an indigenous and reworked population. Reworked material is identified on the basis that in at least two out of the three histograms, the data plots as two separate populations. This material is generally darker in colour than the indigenous population and as such plots to the left of the indigenous population.

6.2.3. *TASMANITES* COLOUR DETERMINATIONS

Investigation of *Tasmanites* as a potential maturity indicator was based on the assumption that the colour of the microfossil becomes darker with increasing thermal maturity. It was also based on the assumption that all specimens start with the same colour and change at the same rate. However, unlike *Veryhachium* specimens, the morphology of *Tasmanites* specimens varies considerably within a single sample. The most noticeable difference amongst tasmanitids within a sample is the range of specimen diameters. Following observations on several samples, it appears that this variation in size has some bearing on the colour of the microfossils.

In general, smaller specimens were observed to be lighter in colour than larger specimens within the same sample (Figure 6.9). However, there were also rarer cases where smaller specimens were darker than larger specimens in the same sample. This phenomenon may be related to wall thickness, with smaller specimens generally having thinner walls and therefore lighter in colour than thicker walled specimens. Despite several attempts, it proved impossible to accurately determine the wall thickness of specimens in this study in an attempt to establish a correlation between body diameter and wall thickness. Specimens where walls were visible, were difficult to bring into sharp focus and make confident measurements of thickness. However, a graph published by Winslow (1962) shows considerable variation of wall thickness amongst different *Tasmanites* specimens (Figure 6.10).

When red, green and blue intensities are plotted against diameter for each sample, there is a varying amount of correlation (Figures 6.11 – 6.16). It appears that, in some cases at least, the diameter, or more likely the wall thickness of the specimen, influences the colour. This suggests that the mean red, green and blue intensities of *Tasmanites* within a sample will be influenced by the range of diameters of specimens measured, and which size is dominant, as well as the level of maturity.

Like chitinozoa, vitrinite, and *Veryhachium* populations, *Tasmanites* colour data may also include caved and reworked specimens. However, with the suspected influence of wall thickness on colour, it becomes difficult to determine caved and reworked specimens on the basis of colour alone. In order to confidently identify foreign populations in the data

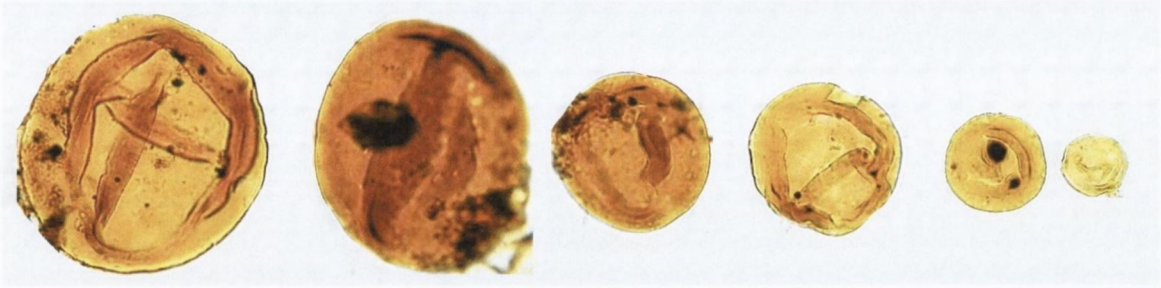

Sample P11

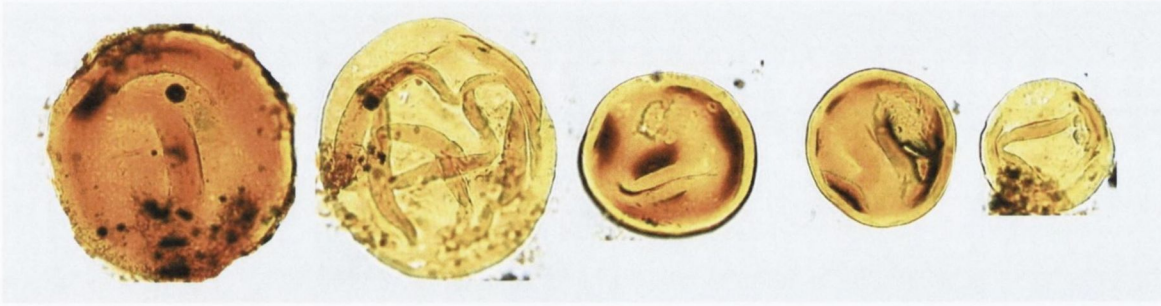

Sample Pet 3

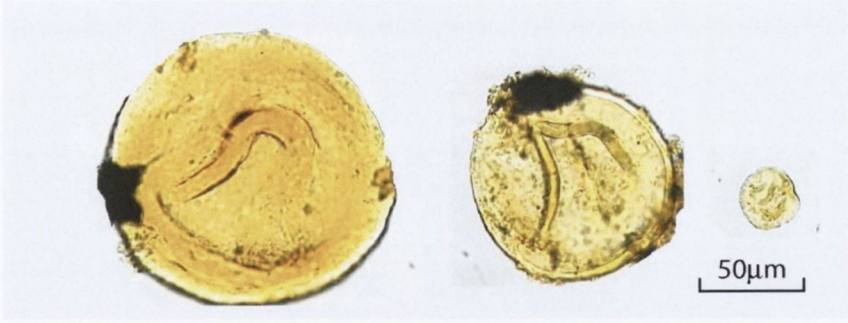

Sample CC3

Figure 6.9: Examples of *Tasmanites* taken from three samples, showing the variation in colour and size that can be found in a single sample. Note the general trend of darkening colour with increased diameter size.

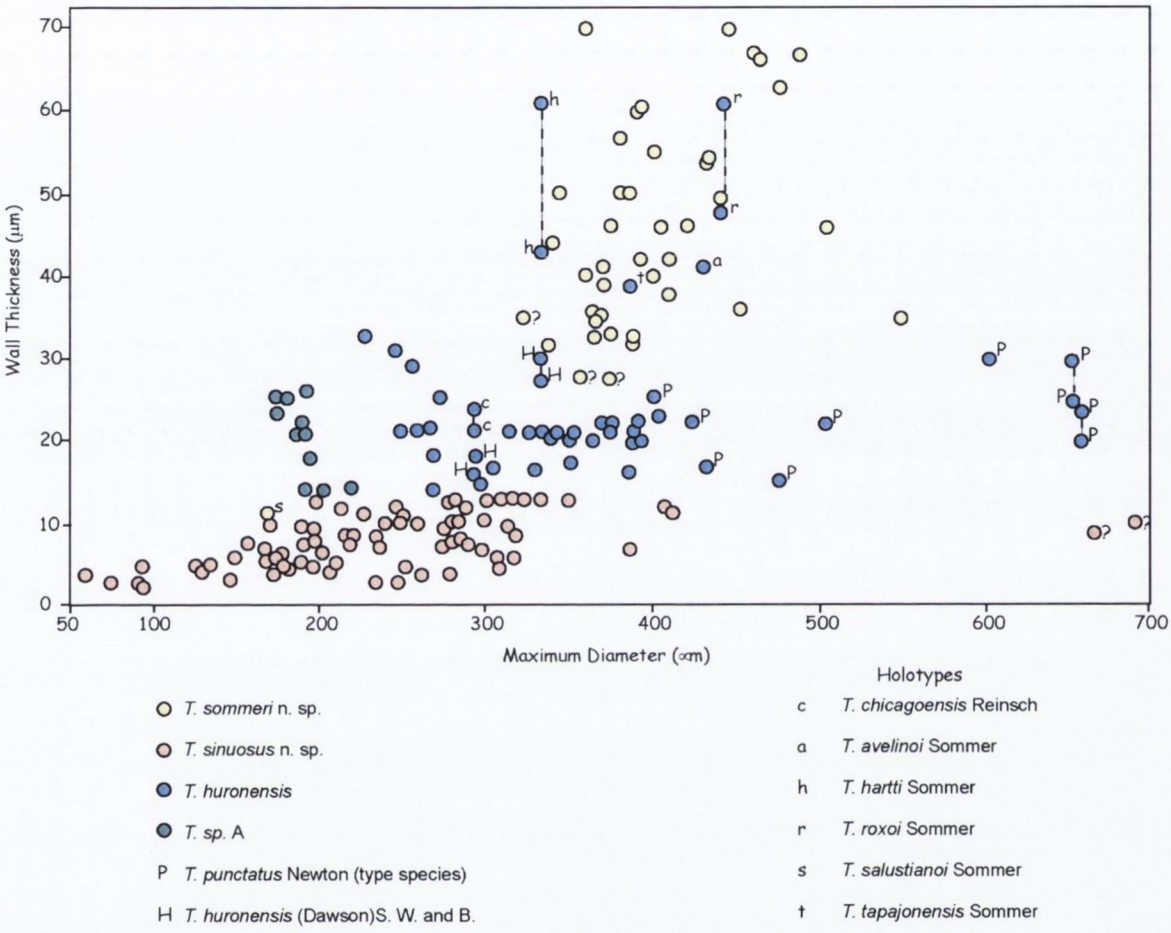

Figure 6.10: Previously published plot of wall thickness against maximum diameter of *Tasmanites* specimens. Dashed lines between identical symbols indicate that the measurement of the wall thickness of the specimen is uncertain within the indicated limits. A question mark beside a symbol indicates uncertain identity (Winslow 1962).

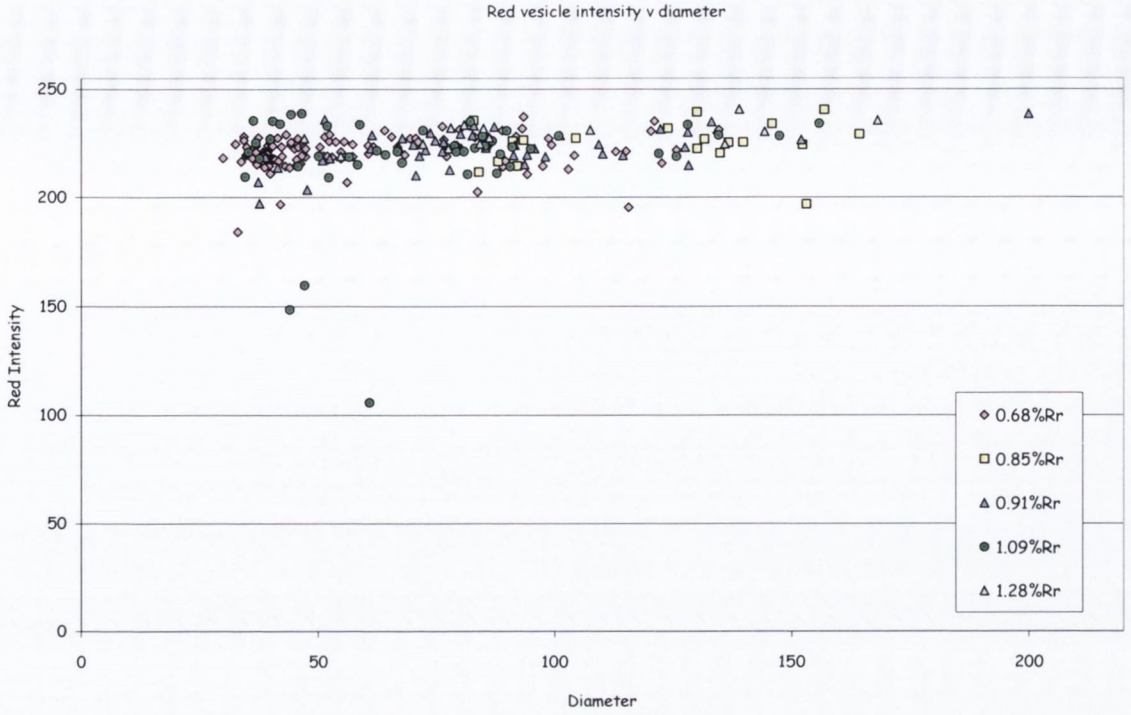

Figure 6.11: Plot of corrected red vesicle intensity against diameter for individual *Tasmanites* specimens. Specimens from samples of the same maturity are denoted by the same symbol. It appears that diameter has little influence on red intensity determinations of the body *Tasmanites*.

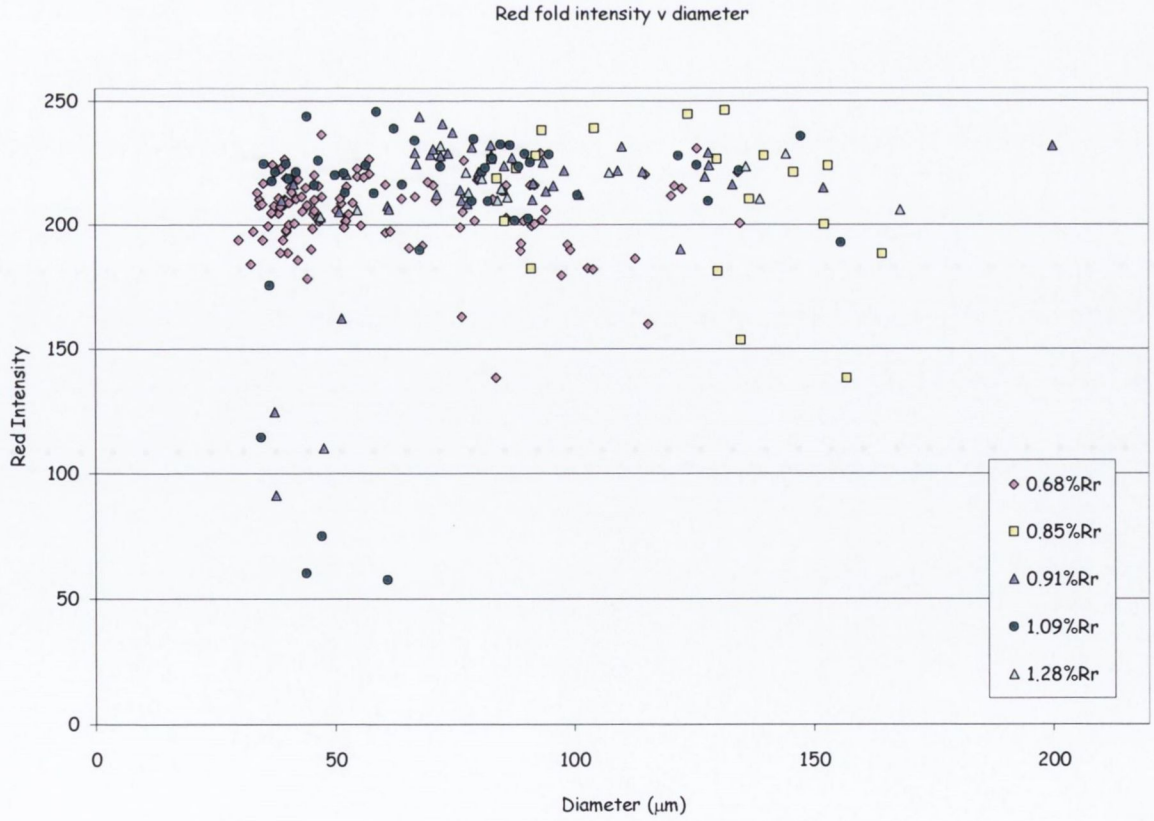

Figure 6.12: Plot of corrected red fold intensity against diameter for individual *Tasmanites* specimens. Specimens from samples of the same maturity are denoted by the same symbol. It appears that diameter has no clear influence on red intensity determinations of the fold *Tasmanites*.

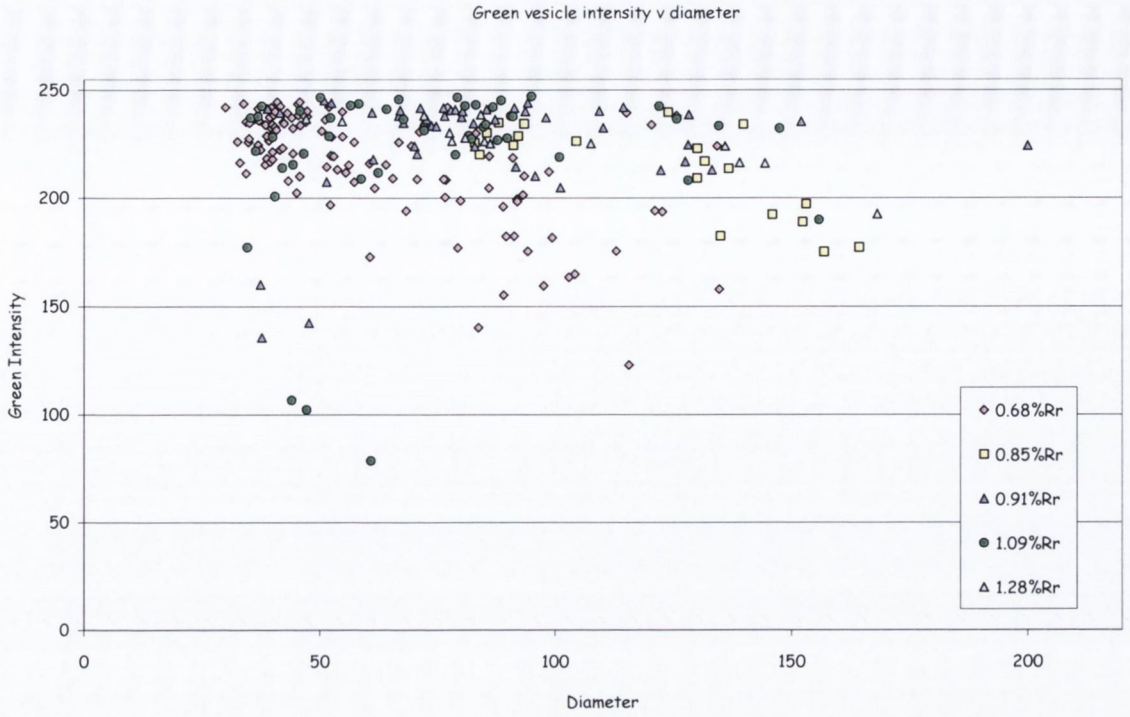

Figure 6.13: Plot of corrected green vesicle intensity against diameter for individual *Tasmanites* specimens. Specimens from samples of the same maturity are denoted by the same symbol. It appears that diameter has some influence on green intensity determinations of the body of *Tasmanites* with a general increase in spread of green intensity determinations with diameter.

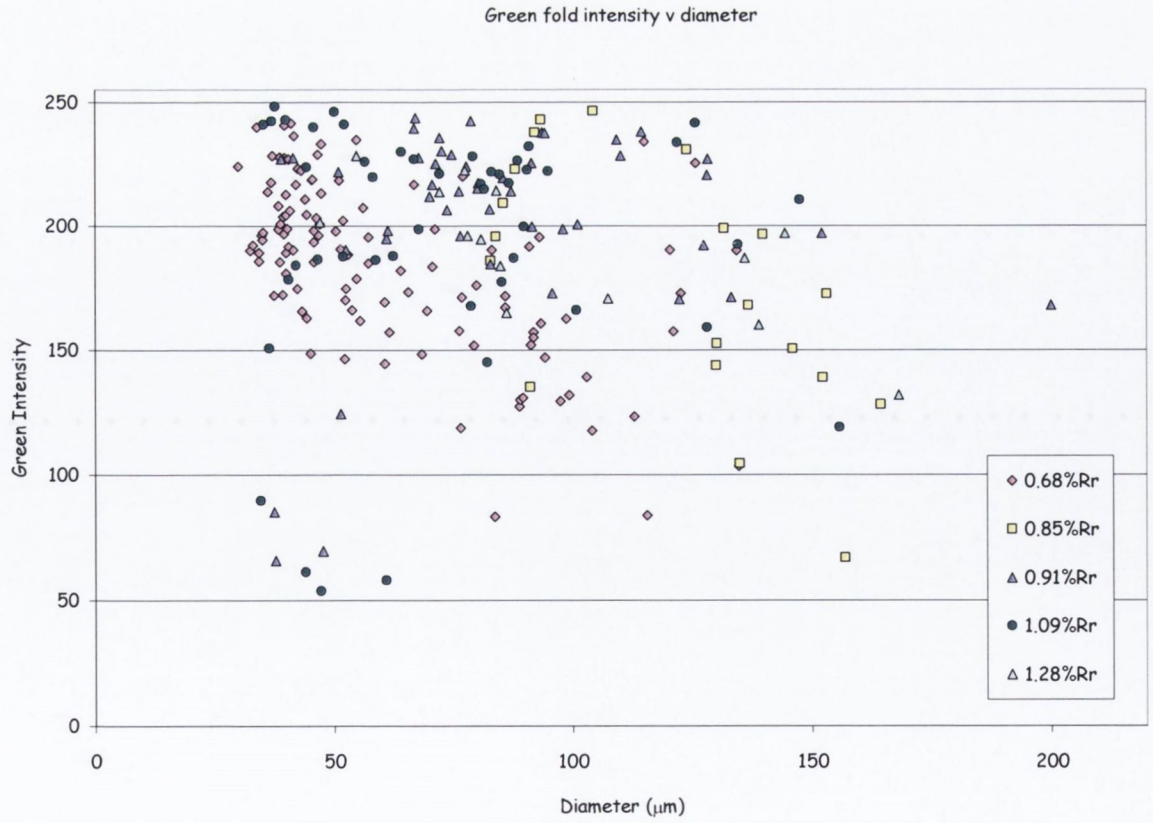

Figure 6.14: Plot of corrected green fold intensity against diameter for individual *Tasmanites* specimens. Specimens from samples of the same maturity are denoted by the same symbol. It appears that diameter has some influence on green intensity determinations of the fold of *Tasmanites* with a general decrease of green intensity determinations with increasing diameter.

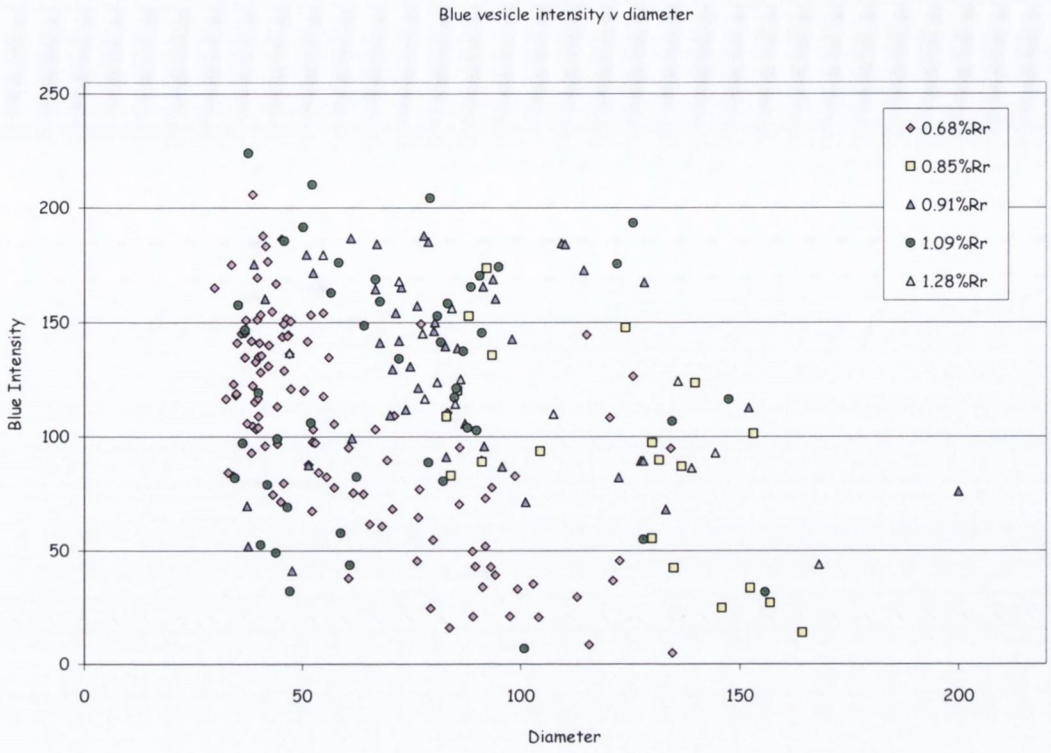

Figure 6.15: Plot of corrected blue vesicle intensity against diameter for individual *Tasmanites* specimens. Specimens from samples of the same maturity are denoted by the same symbol. It appears that diameter has some influence on blue intensity determinations of the body of *Tasmanites* with a general decrease in blue intensity determinations with increasing diameter.

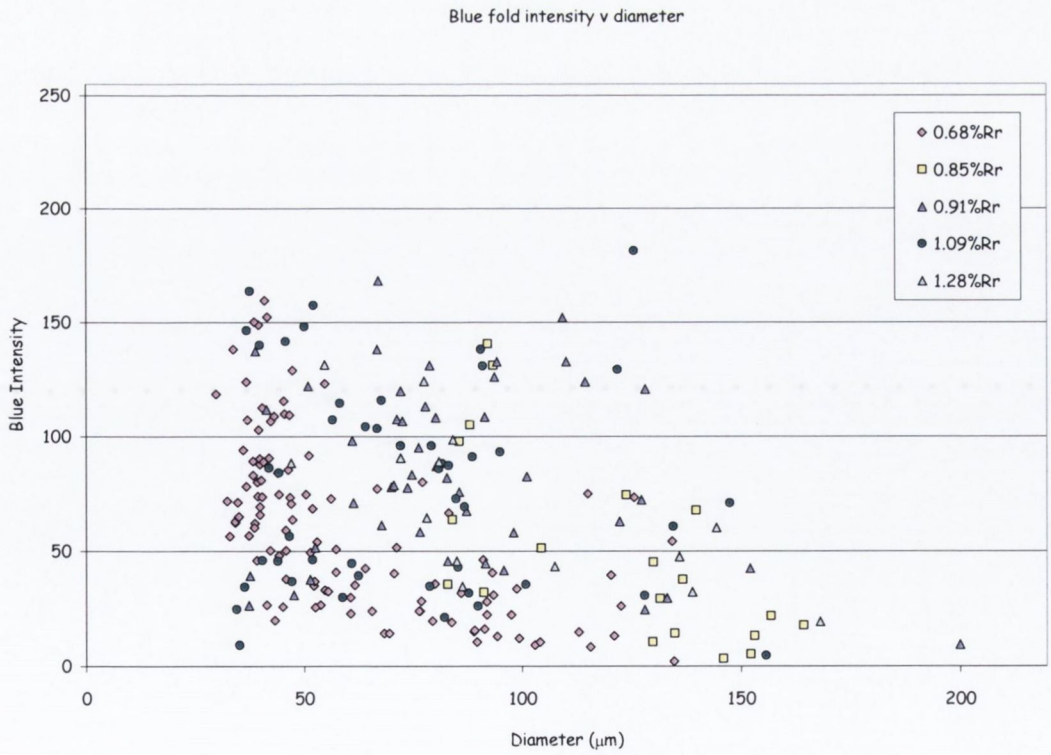

Figure 6.16: Plot of corrected blue fold intensity against diameter for individual *Tasmanites* specimens. Specimens from samples of the same maturity are denoted by the same symbol. It appears that diameter has some influence on blue intensity determinations of the fold of *Tasmanites* with a general decrease of blue intensity determinations with increasing diameter.

set it would be necessary to carry out taxonomic identification of the specimens, which is beyond the scope of this study. As a result of the apparent influence of specimen size on the colour of some *Tasmanites* specimens, it was decided that the average colour of *Tasmanites* within a sample was not a suitable variable to be calibrated as indicator of thermal maturity. It is possible that with further study the nature of the relationship between specimen size, colour and maturity could be established but due to time constraints, this work could not be carried out as part of this project.

6.3. RGB DETERMINATIONS AND MATURITY

6.3.1. CALIBRATION OF CORRECTED RGB DETERMINATIONS AGAINST VITRINITE REFLECTANCE

As discussed in section 6.2.3., it was decided that without further study, the value of *Tasmanites* colour data was of limited use as a maturity indicator because of the suspected influence of diameter and thickness on colour. As a result, only *Veryhachium* RGB intensities will be discussed further. The average red, green and blue intensities for indigenous *Veryhachium* from each sample were plotted against the average indigenous vitrinite reflectance value for the same sample (Figures 6.17 – 6.22). Ideally, the series of samples used should cover a wide range of maturities. Efforts were made to collect samples with a range of evenly spaced vitrinite reflectance values but it proved impossible to find any samples between 1.5 – 2.0%R_r.

In the Figures 6.17, 6.19 and 6.21 both well preserved samples and degraded samples were plotted together. For all intensities, the degraded samples plot off the apparent trend of the well preserved samples. The colour of well preserved samples represents the thermal alteration of the original eilyma, which has essentially remained intact. Because the walls of the degraded samples may also have been thinned, a different variable is measured. Thermal alteration darkens the colour of the eilyma, but thinning of the vesicle wall counteracts this. As a result, this thermal alteration scale was based on well preserved specimens of *Veryhachium* alone. Degraded samples were not included in the data set (Figure 6.31).

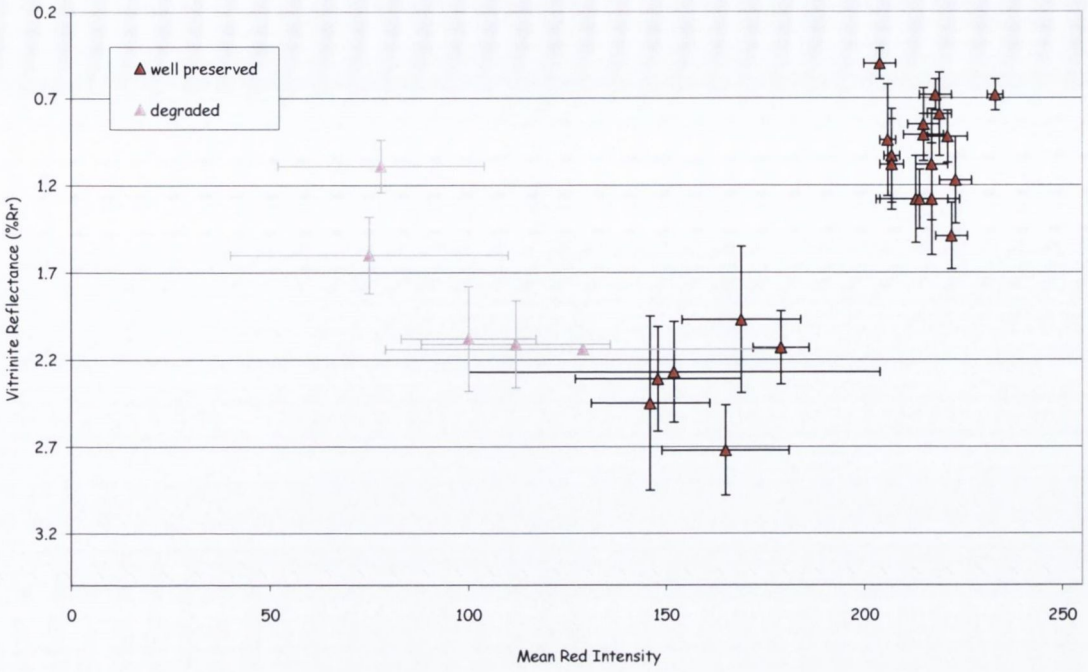

Figure 6.17: Average vitrinite reflectance of a sample vs. corrected average red intensity of *Veryhachium* specimens within the same sample. Standard deviations of the data are also plotted. Both determinations made on well preserved samples and degraded samples are shown, although only well preserved samples were used for calibration of the system.

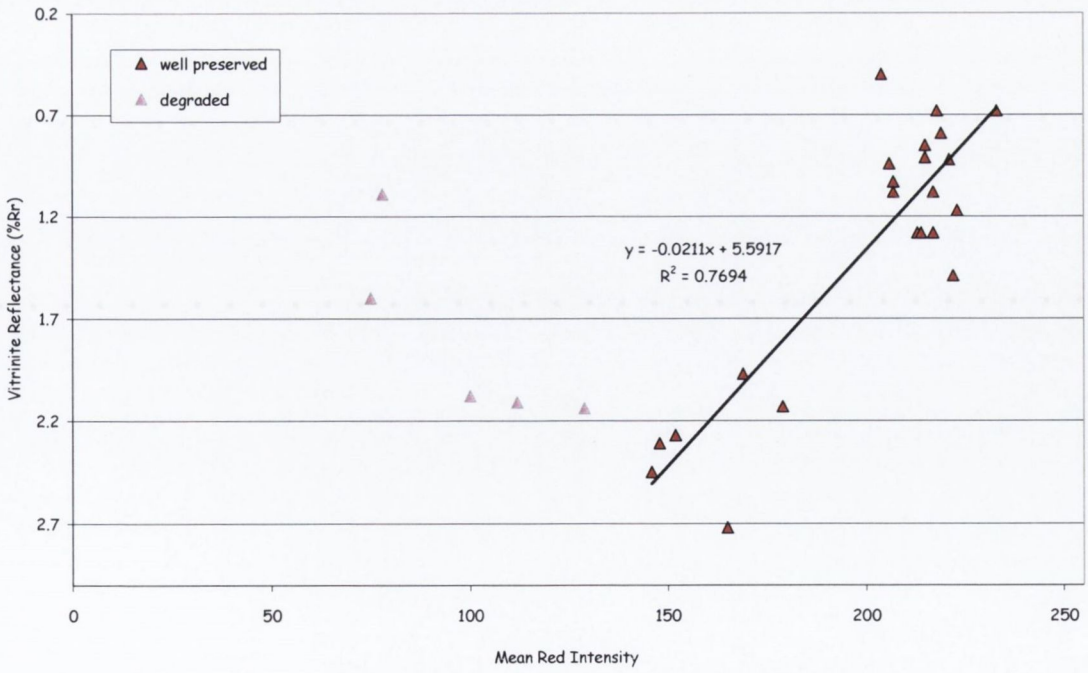

Figure 6.18: Average vitrinite reflectance of a sample vs. corrected average red intensity of *Veryhachium* specimens within the same sample. A trend line, extrapolated from the well preserved data set, is also shown, along with its R-squared value. This value implies that 77% of the spread of red intensity data can be explained by the vitrinite reflectance value of a sample.

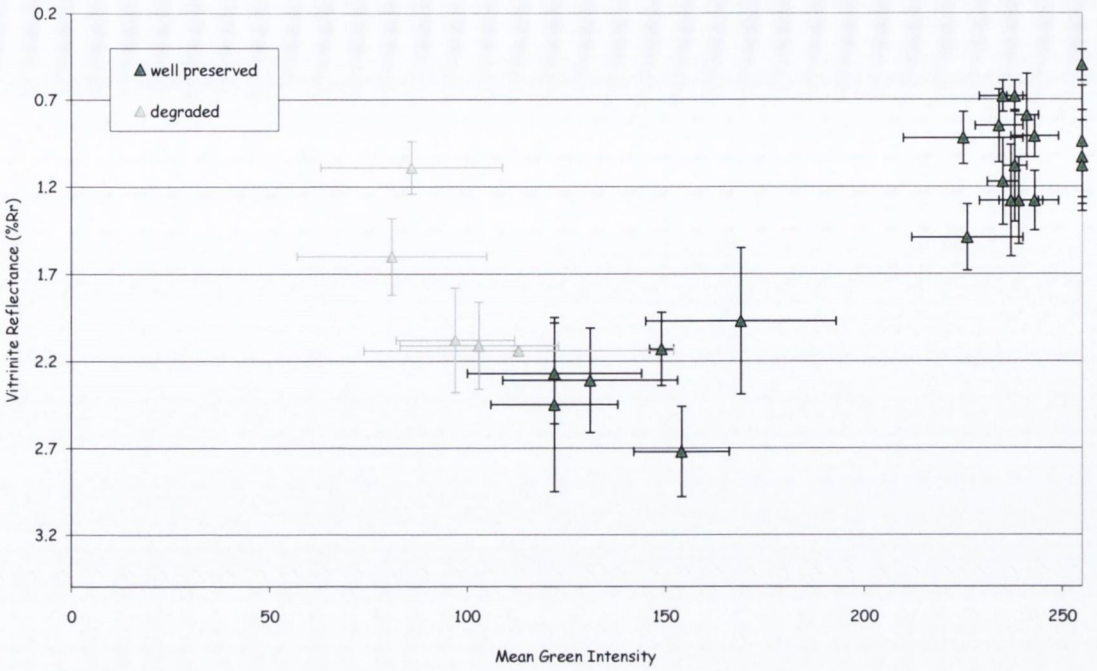

Figure 6.19: Average vitrinite reflectance of a sample vs. corrected average green intensity of *Veryhachium* specimens within the same sample. Standard deviations of the data are also plotted. Both determinations made on well preserved samples and degraded samples are shown, although only well preserved samples were used for calibration of the system.

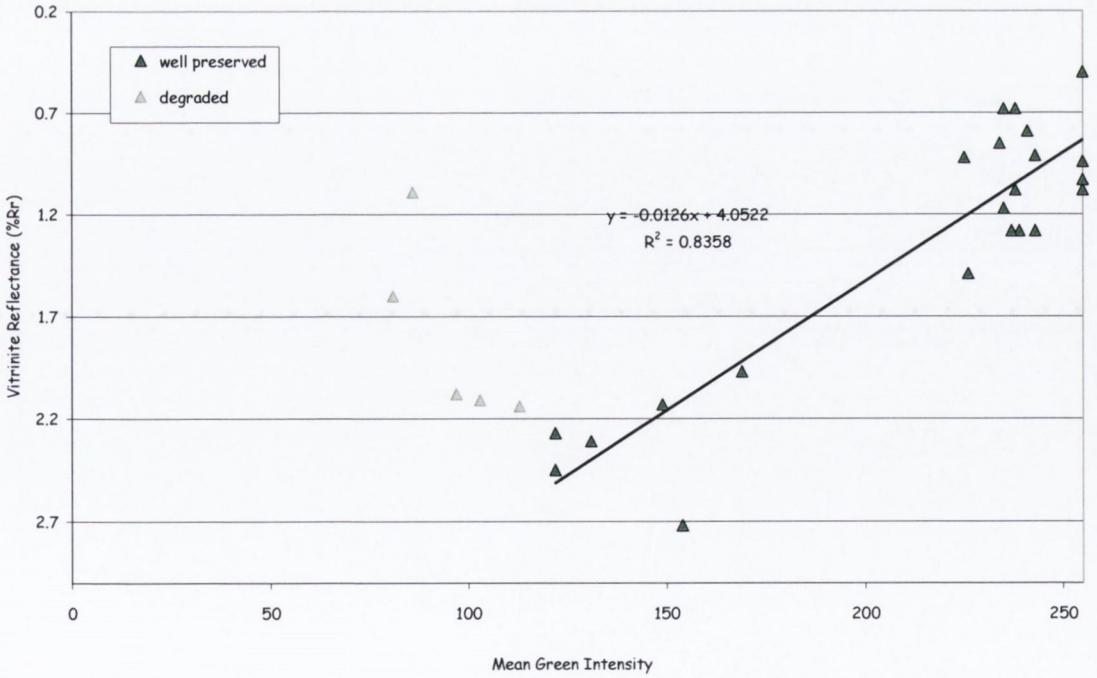

Figure 6.20: Average vitrinite reflectance of a sample vs. corrected average green intensity of *Veryhachium* specimens within the same sample. A trend line, extrapolated from the well preserved data set, is also shown, along with its R-squared value. This value implies that 84% of the spread of green intensity can be explained by the vitrinite reflectance value of a sample.

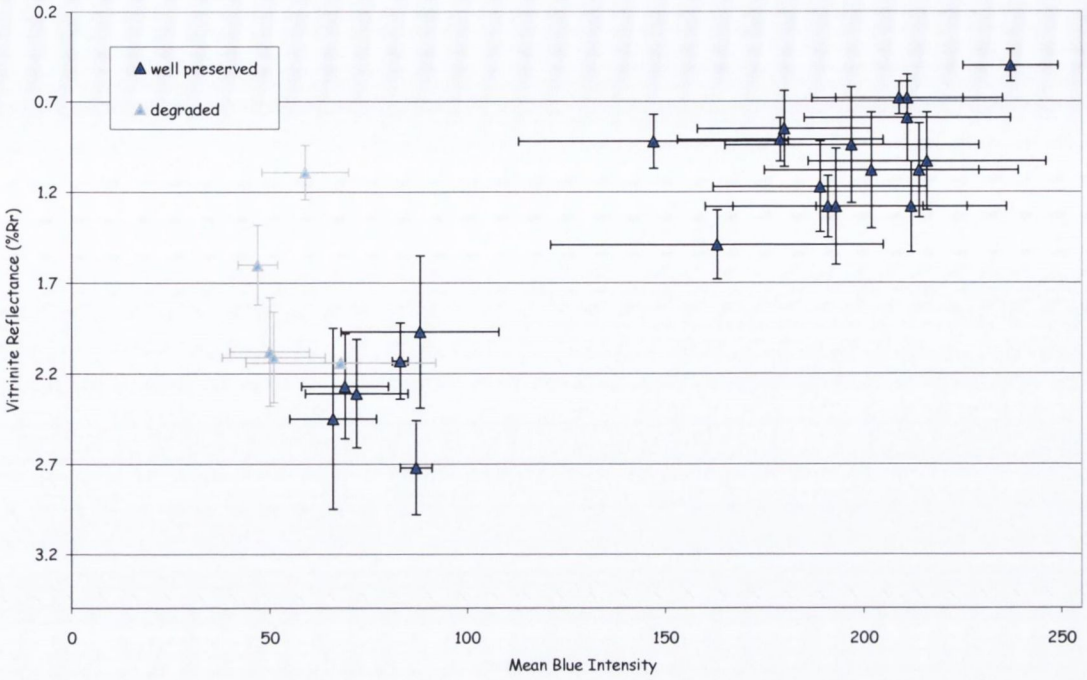

Figure 6.21: Average vitrinite reflectance of a sample vs. corrected average blue intensity of *Veryhachium* specimens within the same sample. Standard deviations of the data are also plotted. Both determinations made on well preserved samples and degraded samples are shown, although only well preserved samples were used for calibration of the system.

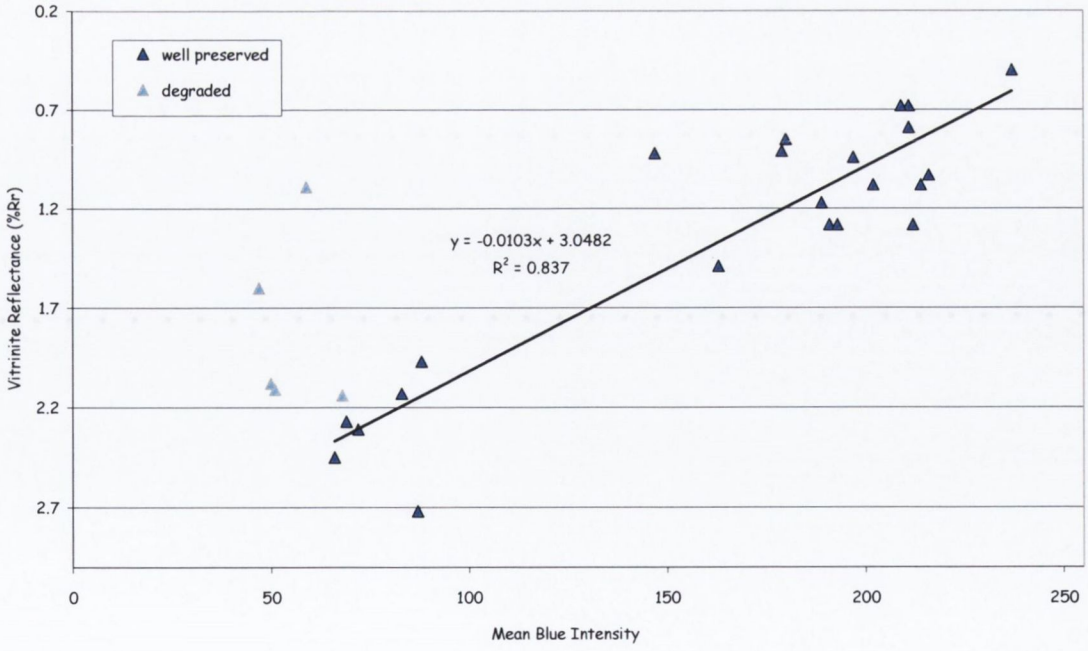

Figure 6.22: Average vitrinite reflectance of a sample vs. corrected average blue intensity of *Veryhachium* specimens within the same sample. A trend line, extrapolated from the well preserved data set, is also shown, along with its R-squared value. This value implies that 84% of the spread of blue intensity can be explained by the vitrinite reflectance value of a sample.

A linear regression was calculated for each data set of intensity and vitrinite reflectance. The correlation coefficient (R^2) for each regression is given in Table 6.1. This value is the percentage of spread of the data that can be explained by the linear regression.

Intensity	R^2 value	95% confidence interval	90% confidence interval
Red	0.7694	± 0.67% R_r	± 0.55% R_r
Green	0.8358	± 0.56% R_r	± 0.46% R_r
Blue	0.837	± 0.54% R_r	± 0.45% R_r

Table 6.1: R^2 value of the linear trend lines extrapolated for each intensity plotted against vitrinite reflectance. Also given are the limits of the 95% and 90% confidence interval for each channel.

All of the regressions proved to be significant. A 95% confidence interval was also calculated for each line. This value is the range in which, given x (an R, G, or B intensity), there is a 95% chance y (vitrinite reflectance) lies. It should be noted that these linear regressions and confidence intervals are based on only 22 samples. If this sample size was increased, it is likely that the span of a 95% confidence interval would decrease. All calculations used to find these confidence intervals are given in Appendix VIII. A worked example is shown below using average red, green and blue intensity to calculate a vitrinite reflectance equivalent value.

From Figures 6.17, 6.19 and 6.21, it is clear that the standard deviation of the average red, green and blue intensity varies with maturity. In lower maturity samples, the average red and green values of a sample are associated with smaller standard deviations than average blue values. This situation is reversed at higher levels of maturity. From Figure 6.23, it appears that standard deviation of average red and green intensities increases with decreasing values of intensity. Conversely, standard deviations of average blue values decrease with intensity. Using this plot, estimates of maturity based on the three different intensities can be ranked in terms of their reliability (Figure 6.24).

If the method was to be simplified using a single intensity as a maturity indicator, based on the R^2 value and limits of a 95% confidence interval, it would appear that average blue and green intensities are the most sensitive to changes in thermal maturity of a sample.

Worked Example

Average Intensity for *Veryhachium* from sample A:

Red	218
Green	234
Blue	211

From Figure 6.18:

Vitrinite Reflectance Equivalent = -0.0211(Average red intensity) + 5.5917

= -0.0211(218) + 5.5917

= 0.99% R_r ± 0.67% R_r (95% confidence interval)

= 0.99% R_r ± 0.55% R_r (90% confidence interval)

From Figure 6.20:

Vitrinite Reflectance Equivalent = -0.0126(Average green intensity) + 4.0522

= -0.0126(234) + 4.0522

= 1.10%R_r ± 0.56%R_r (95% confidence interval)

= 1.10%R_r ± 0.46%R_r (90% confidence interval)

From Figure 6.22:

Vitrinite Reflectance Equivalent = -0.0103(Average blue intensity) + 3.0482

= -0.0103(211) + 3.0482

= 0.87%R_r ± 0.55%R_r (95% confidence interval)

= 0.87%R_r ± 0.45%R_r (90% confidence interval)

Based on the R^2 values of the three correlations, blue and green are the most reliable. Chitinozoa reflectance data from this sample suggests a vitrinite reflectance equivalent value of 0.67%R_r ± 0.09.

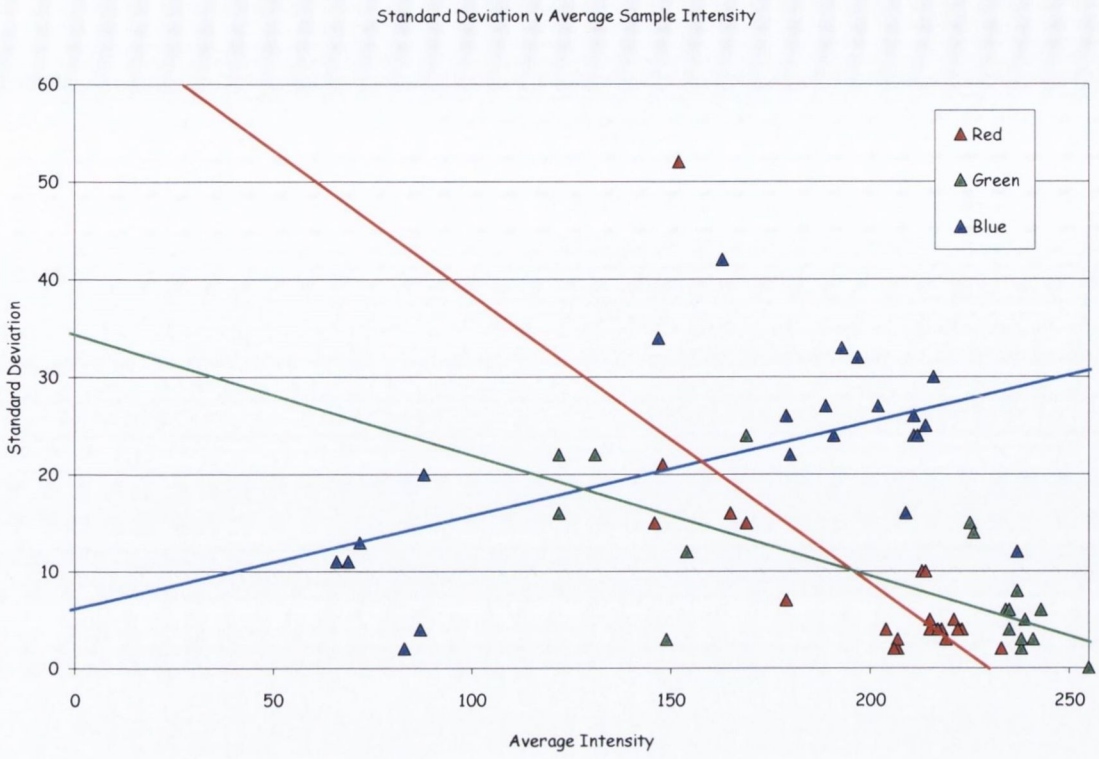

Figure 6.23: Average RGB intensity of a sample against the standard deviation of each intensity for that sample. As red and green intensity increases, the standard deviations decrease. Conversely, standard deviations of average blue values increase with intensity.

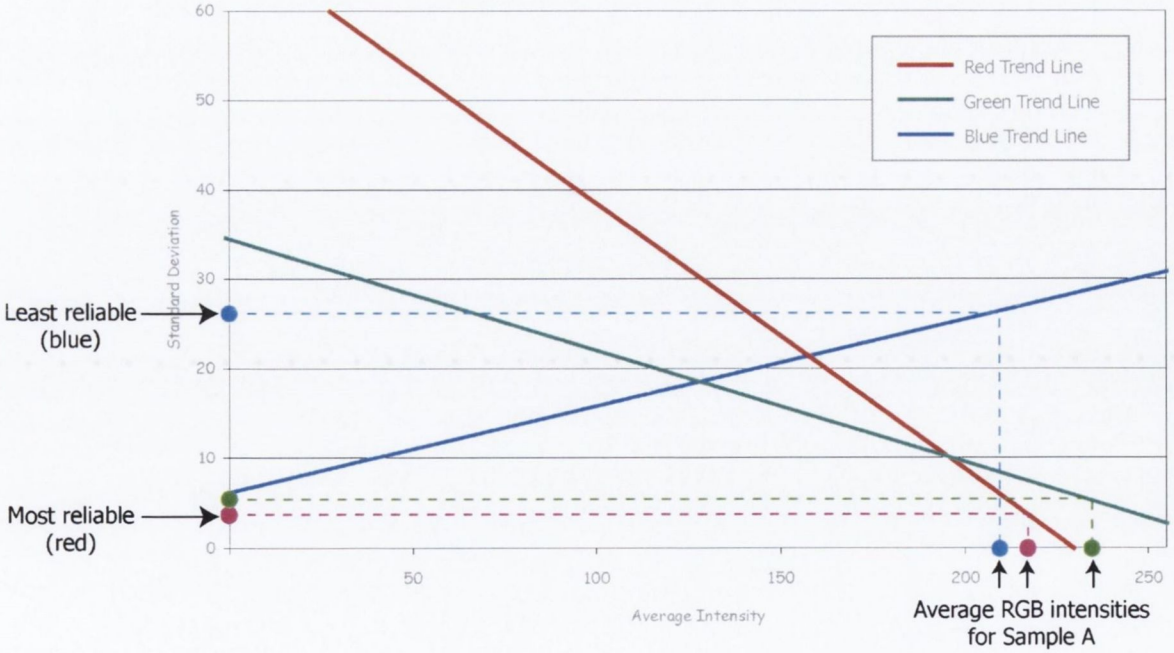

Figure 6.24: Plot used to determine the relative reliability of vitrinite reflectance equivalent values calculated from RGB intensities. It appears that the vitrinite reflectance equivalent value calculated from the average red intensity of the sample is the most reliable, followed by green and blue intensity calculations.

6.3.2. RGB INTENSITIES AS MATURITY INDICATORS

Using the vitrinite reflectance data for with each sample, the samples were classed as either mature (0.5 – 1.3%R_r) or post-mature (>1.3%R_r) with respect to the oil window (Taylor *et al.* 1998). In Figures 6.25, 6.26 and 6.27, average red, green and blue intensities are plotted in pairs. Also shown are fields of mature and post-mature samples based on vitrinite reflectance results. Reworked specimens identified and removed from individual sample data are also plotted. Although there are no maturity data associated with these specimens, they are useful in filling 'colour gaps'. In addition, all other average *Veryhachium* RGB intensities from samples with no associated maturity data were also plotted for comparison. In all three cases, a progressive maturation pathway can be observed (Figures 6.25, 6.26 and 6.27).

Also plotted, as a separate group, are degraded samples that were not used to calculate the linear regression of intensity with vitrinite reflectance. These plots (Figures 6.25, 6.26 and 6.27) suggest that the degraded samples are from post-mature samples. The data associated with the degraded samples are shown below (Table 6.2). It is not known why some samples become degraded, while other samples, from higher maturities, remain well preserved. It is possible that either the reflectance or intensities values of these samples are inaccurate due to caving or reworking. However, neither of these scenarios is suggested by the samples' histograms.

Name	%Rr	Std. Dev.	N	Red	Std. Dev.	Green	Std. Dev.	Blue	Std. Dev.	N
P25	1.09	0.15	26	78	26	86	23	59	11	4
RH19	1.6	0.22	21	75	35	81	24	47	5	12
VA118	2.08	0.3	6	100	17	97	15	50	10	11
VA115	2.11	0.25	14	112	24	103	20	51	13	19
JM5	2.14	Unknown	?	129	50	113	39	68	24	7

Table 6.2: Data table of samples with degraded *Veryhachium* (N = number of readings). A small amount of Sample JM was supplied by John Marshall. The vitrinite reflectance of this sample was determined by John Marshall in a previous thermal maturity study.

It is important to note that, although the samples are from different geographical locations, they still plot along a well defined trend line for each pair of colours. This implies that *Veryhachium* follows a consistent colour pathway regardless of where the sample came from (Figure 6.28 and 6.29).

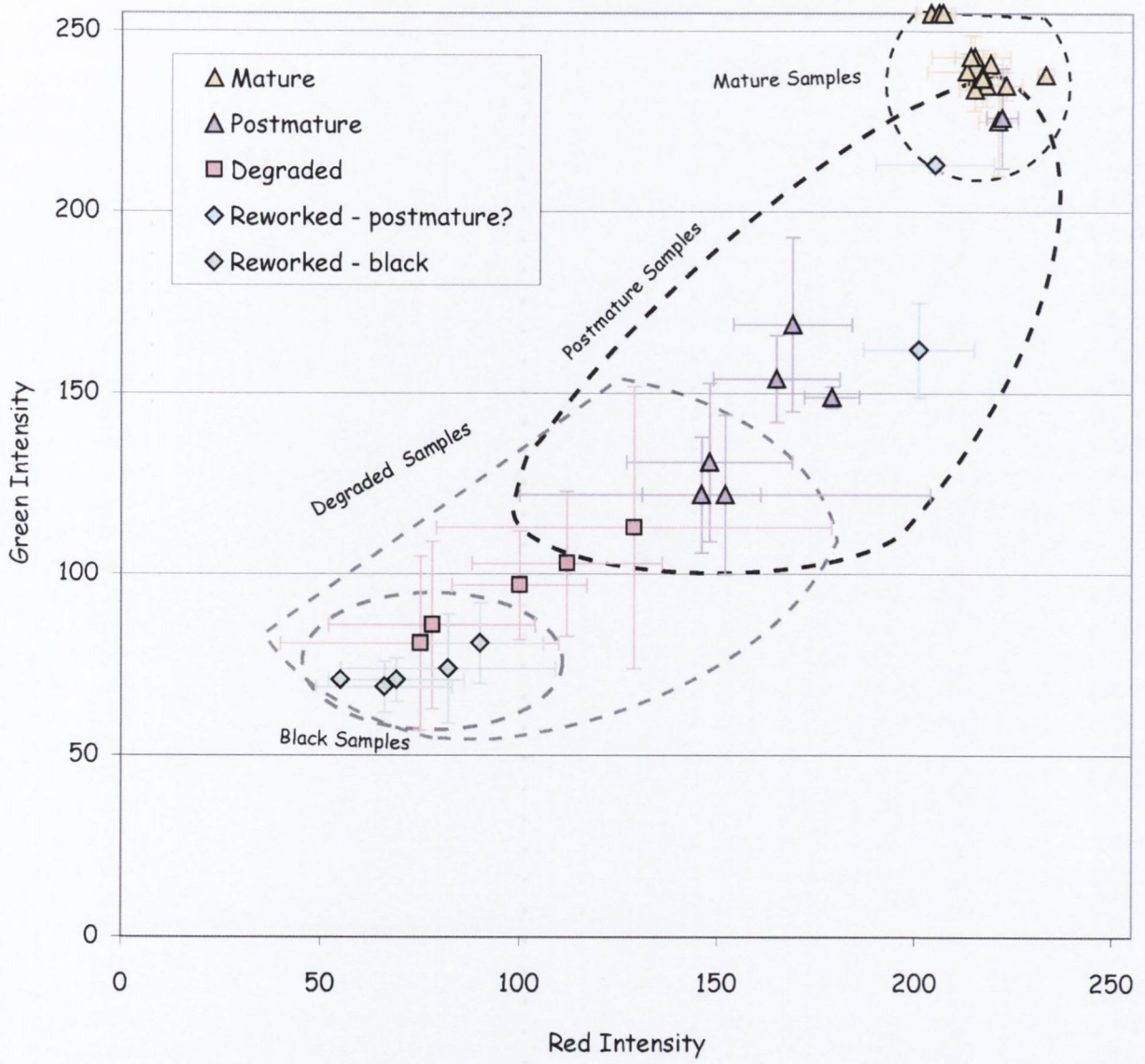

Figure 6.25: Average *Veryhachium* green intensity against average *Veryhachium* red intensity of all samples studied in this project. For those well preserved samples for which vitrinite reflectance data was collected, they have been divided into mature and post-mature samples with respect to the oil window. Degraded samples are grouped together. Those specimens identified as reworked are also plotted in order to fill 'colour gaps' and have been split into two groups; those samples that are clearly black, and those that still retain lighter colours.

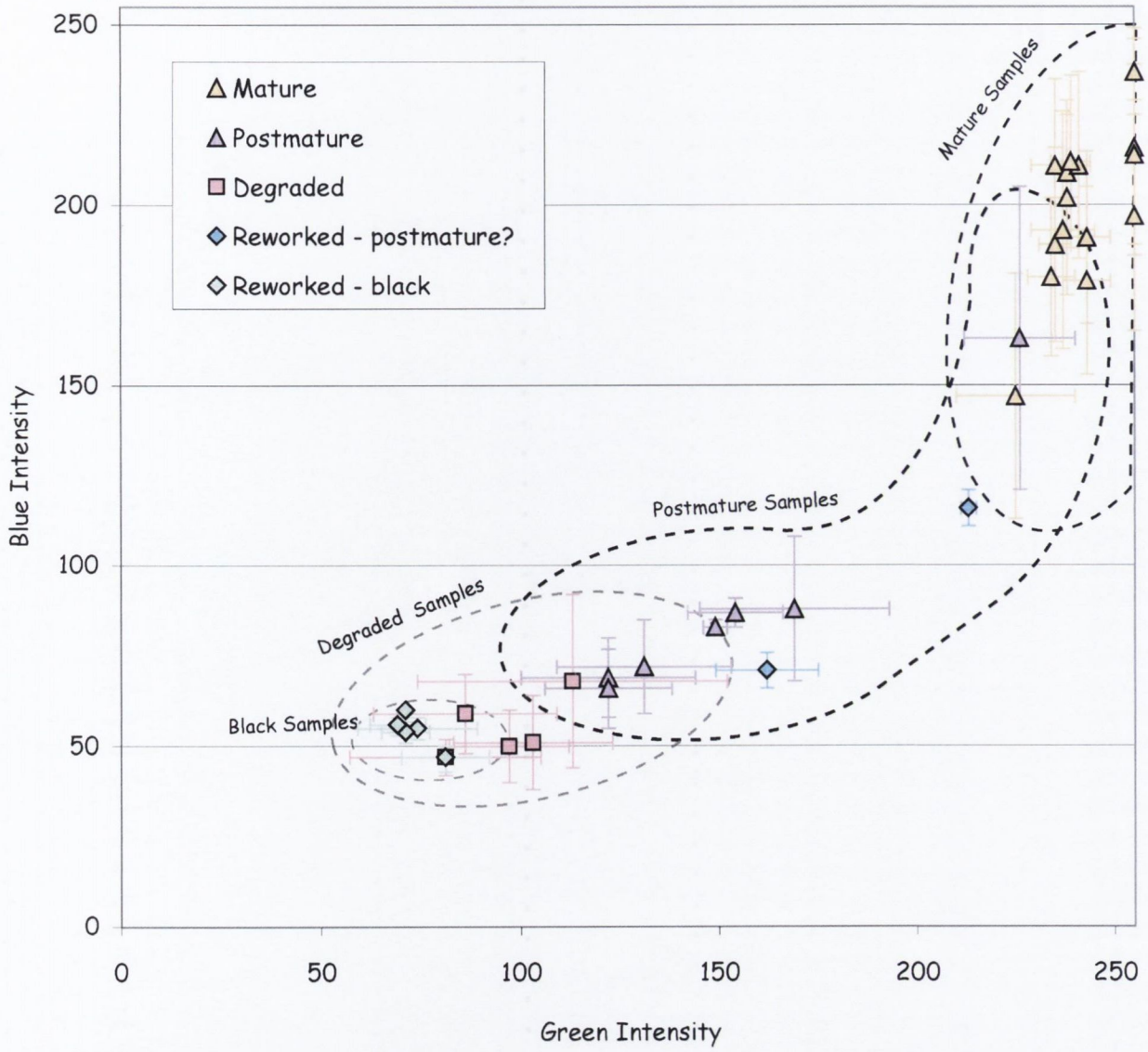

Figure 6.26: Average blue *Veryhachium* intensity against average green *Veryhachium* intensity of all samples studied in this project. For those well preserved samples for which vitrinite reflectance data was collected, they have been divided into mature and post-mature samples with respect to the oil window. Degraded samples are grouped together. Those specimens identified as reworked are also plotted in order to fill 'colour gaps' and have been split into two groups; those samples that are clearly black, and those that still retain lighter colours.

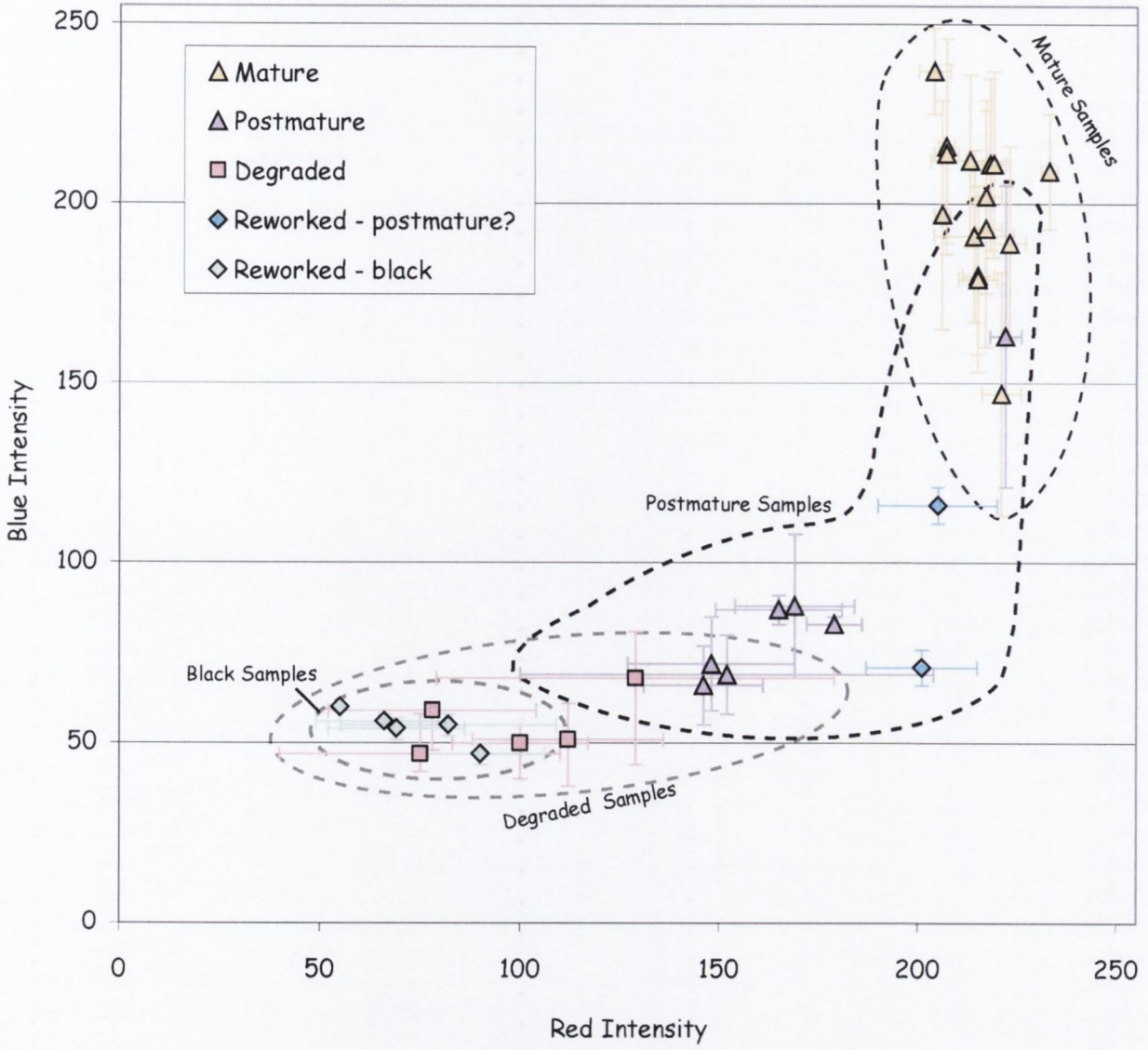

Figure 6.27: Average blue *Veryhachium* intensity against average red *Veryhachium* intensity of all samples studied in this project. For those well preserved samples for which vitrinite reflectance data was collected, they have been divided into mature and post-mature samples with respect to the oil window. Degraded samples are grouped together. Those specimens identified as reworked are also plotted in order to fill 'colour gaps' and have been split into two groups; those samples that are clearly black, and those that still retain lighter colours.

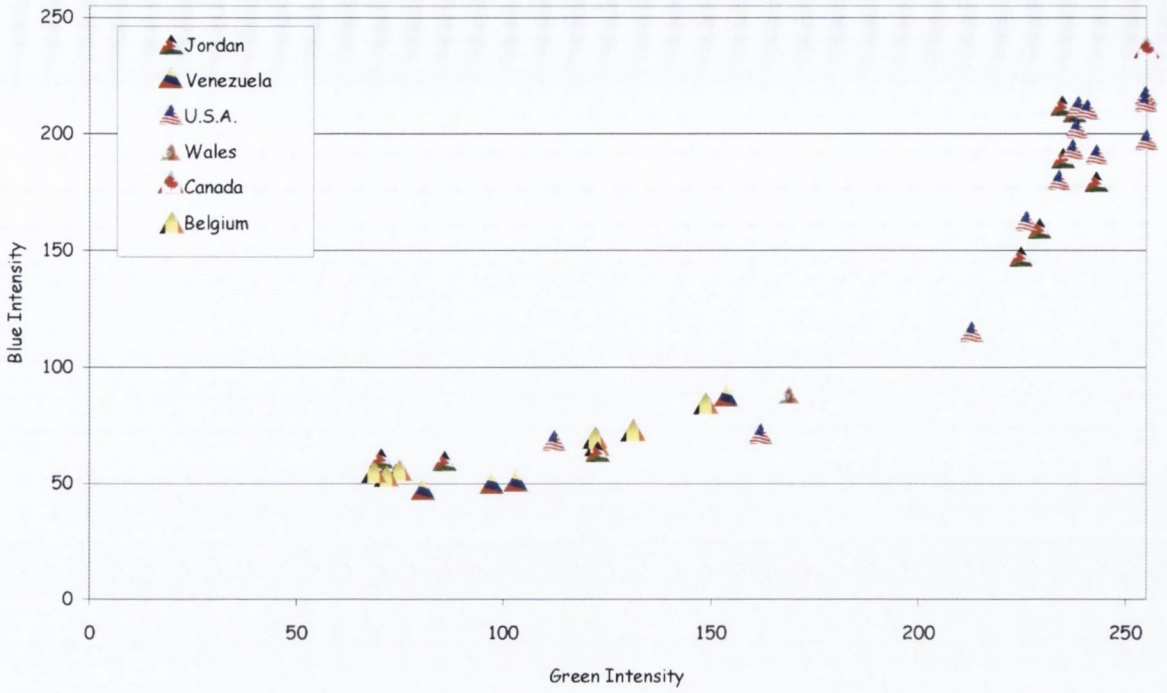

Figure 6.28: Average blue *Veryhachium* intensity against average green *Veryhachium* intensity. Data are grouped according to the country in which the samples were collected. It appears that regardless of geographical location, samples still plot on the same pathway.

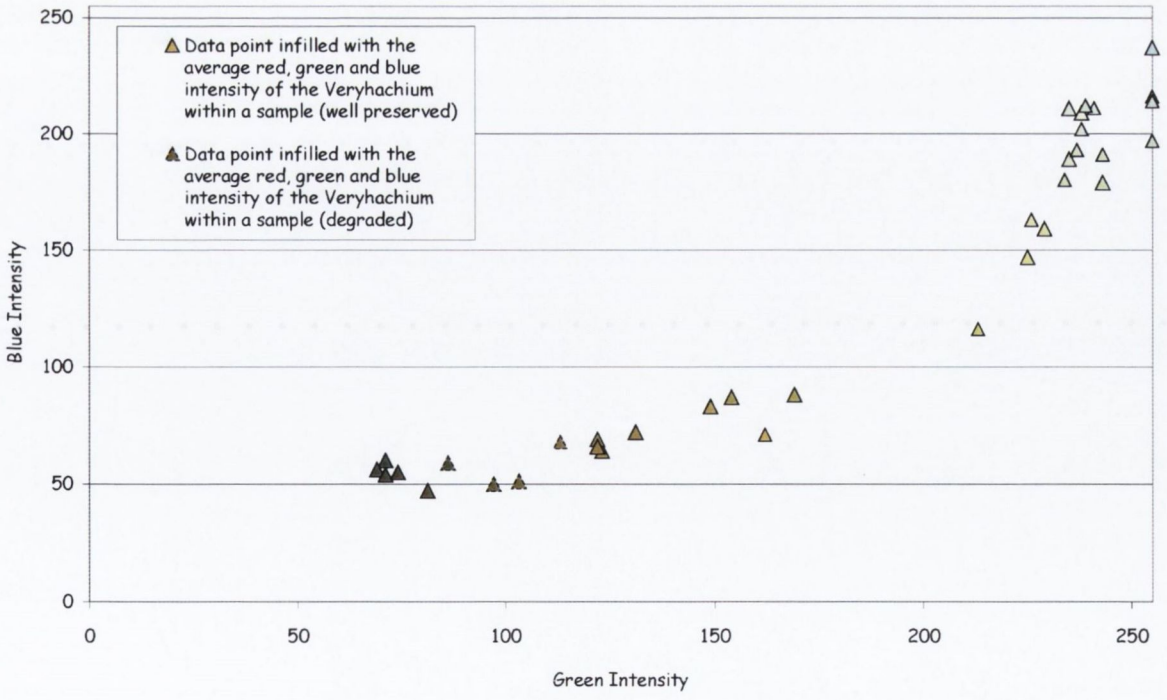

Figure 6.29: Average blue *Veryhachium* intensity against average green *Veryhachium* intensity. Data points are infilled with the average *Veryhachium* RGB intensities of the sample. It appears that this trend represents the maturation pathway of *Veryhachium*.

6.3.3. COMPARISON OF *VERYHACHIUM* AND SPORE COLOUR

Two sources were used to compare spore colour to acritarch colour. The Phillips Petroleum Company Pollen/Spore Colour 'Standard' (Pearson 1984) was scanned and its various spore colours sampled. A set of Robertson Research (UK) Spore Colour Index slides were lent by John Marshall. An RGB determination was made on an unornamented area of each spore using the image analysis system previously described (see section 4.5). Using Schwab's (1995) approximate calibration of various maturity indicators published in Batten (1996), it was possible to show a crude comparison between these alteration indexes and the change in *Veryhachium* colour with maturity based on this study.

From Figure 6.30, it is clear that while most spore colour change occurs within the oil window, *Veryhachium* colour appears to remain almost constant during this interval. It is not until after the floor of the oil window has been reached that significant *Veryhachium* colour change occurs. Yule *et al.* (1998), in their colour image analysis study of spores, found most spore colour change occurred rapidly over a small temperature interval. They interpreted this event as being directly related to the chemical breakdown of the spore wall to generate hydrocarbons. It represented the mature phase of their samples where spores moved from a stable yellow trend to a stable brown/black trend. *Veryhachium* specimens in this study have been shown not to change significantly in colour until after the floor of the oil window has been reached. This suggests the chemical breakdown of their walls occurs at a different stage than that of spore walls. This is most likely because of a difference in their physical or chemical composition.

6.3.4. COMPARISON OF *VERYHACHIUM* AND SPORE FLUORESCENCE

The floor of the oil window, 1.35%R_r, is a well known cut off point for spore fluorescence (Van Gijzel 1982). It appears that *Veryhachium* behaves slightly differently, with fluorescence observed in a sample with a vitrinite reflectance value of 1.49%. The cut off point for *Veryhachium* fluorescence appears to lie somewhere between 1.5 and 2%. It is not possible to restrict this point further without additional samples.

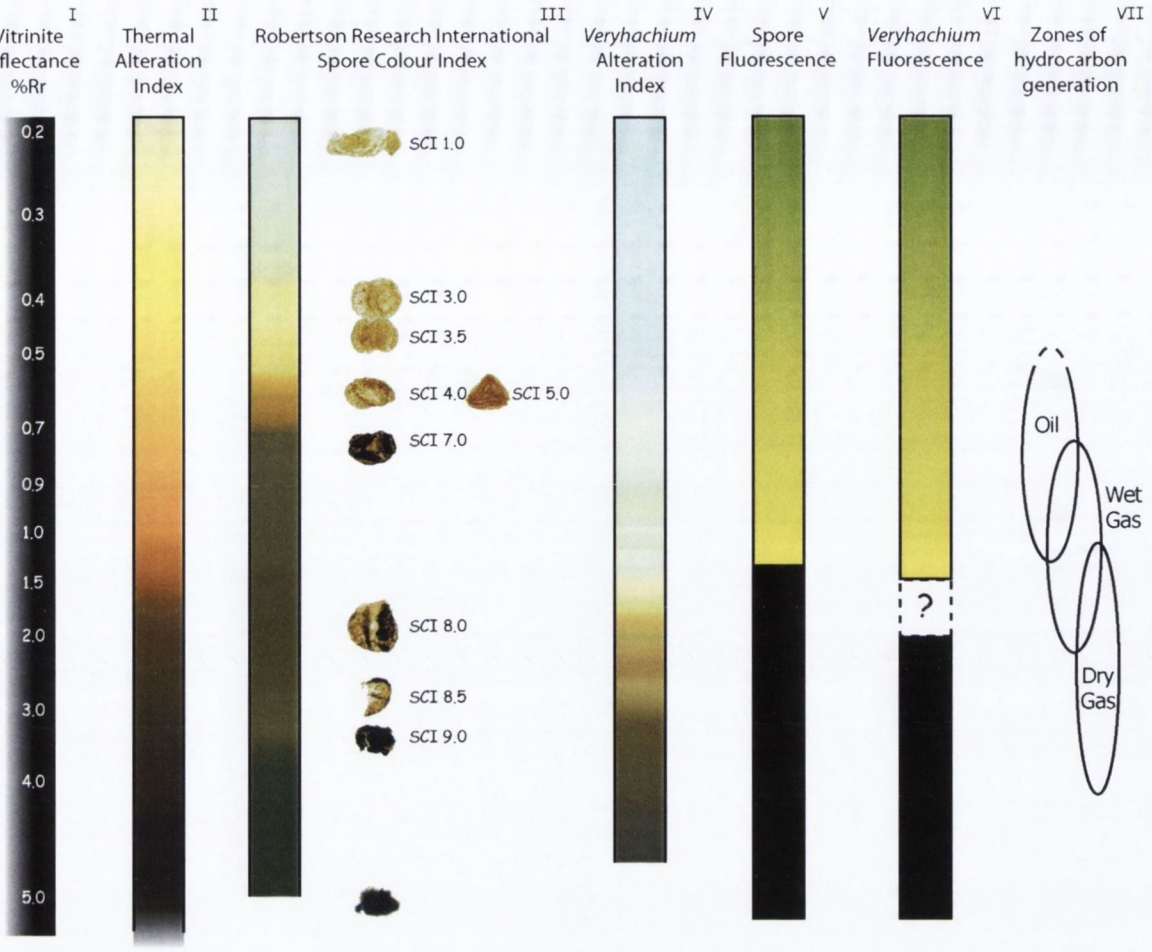

Figure 6.30: Approximate correlation of a range of thermal maturity indicators based mainly on a correlation by Schwab (1995) (published in Batten 1996). He used a technique known as ICA/SPD (Integrated Colour Analysis via Spectral Power Distribution) to correlate various sets of standard slides with each other and as well as vitrinite reflectance.

I Vitrinite reflectance values estimated by Schwab (1995) using a best fit polynomial curve on a hue/intensity plot of spores from samples of known vitrinite reflectances.

II Staplin's thermal alteration scale (TAI), correlated to vitrinite reflectance using Schwab's diagram. The colours shown are taken from Pearson (1984).

III Robertson Research International spore colour index (SCI) correlated to vitrinite reflectance values using Schwab's diagram. Colours shown are based on RGB determinations (this study) made on a set of standard slides supplied by John Marshall. Photomicrographs are taken from a set of standard slides supplied by John Marshall.

IV *Veryhachium* alteration index (this study).

V Spore fluorescence range (Van Gijzel 1982).

VI *Veryhachium* fluorescence range (this study).

VII Zones of hydrocarbon generation (Teichmüller 1987)

6.3.5. COMPARISON WITH PUBLISHED ACRITARCH ALTERATION INDEXES

Legall *et al.* (1981) first published an 'Acritarch Alteration Index' (AAI) based on *Leiosphaeridia* Eisenack 1958 emend Downie and Sarjeant 1963 whose colour was calibrated against the 'Conodont Alteration Index' (CAI). They established a maximum thermal limit of 90°C for their AAI, suggesting leiospheres do not survive much higher temperatures. They inferred a 60°C minimum temperature for the strata from a range of data collected in the area. Data from this study suggest that *Veryhachium* is useful as a maturity indicator beyond their maximum temperature of 90°C for *Leiosphaeridia*, with well preserved samples observed in samples with vitrinite reflectance values of 2.45% (207°C approx. Barker *et al.* (1994)).

Bertrand *et al.* (1989) published a short abstract which stated that for samples of equal rank, the acritarch colour was lighter than spore colour. They also noted that acritarchs were better preserved than spores in samples of higher maturity. This concurs with observations made during this study.

Williams *et al.* (1998) calibrated multi – taxon acritarch assemblages rather than single genus as thermal maturity indicators and stated that, while there were different maturation paths for spores and acritarchs in immature strata, there was little difference within the oil window. They found that AAI values in the upper part of the oil window were lower than corresponding spore TAI but by the time the floor of the oil window was reached, spore and acritarch colour were essentially equivalent. Their conclusion differs significantly from the results of this work, which found marked differences in colour still exist between spores and *Veryhachium* at the floor of the oil window. It is probable that this difference in conclusion is related to their use of assemblages as maturity indicators. During this study, it was noted in several samples that the colour of *Veryhachium* was often paler than other acritarchs like *Unellium* (Figure 6.32). If this is the case for other acritarch genera, it is likely that the ratio of one acritarch to another in an assemblage will affect the estimated colour of that assemblage.

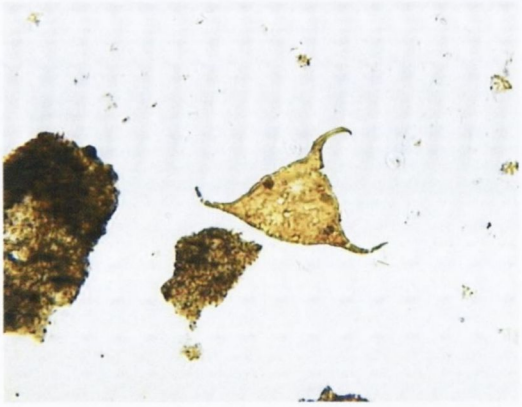

Slide Pet 16 E.F. reference s33/4

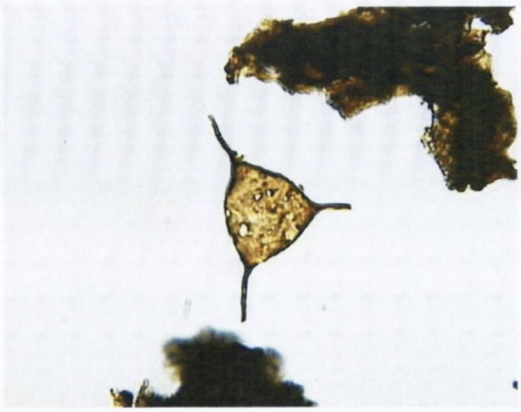

Slide Rh19 p12 E.F. reference w54/1

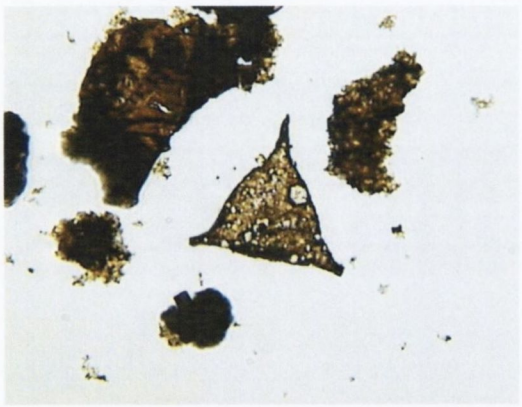

Slide Rh19 p15 E.F. reference o37/4

Slide P20 E.F. reference o40/2

Figure 6.31: Photomicrographs of degraded *Veryhachium* specimens unsuitable for RGB colour determinations. Note the colour of the eilyma is lighter in those areas that have been more degraded. Field of view is 123µm.

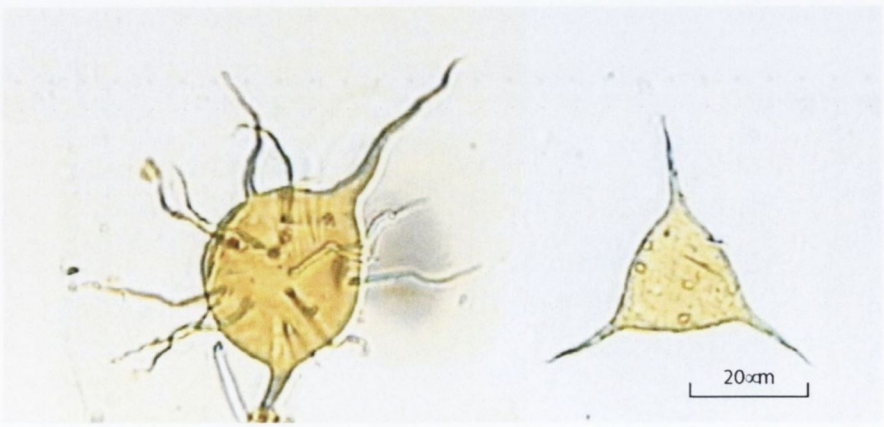

Figure 6.32: Photomicrograph of *Veryhachium* and *Unellium* from sample TL3 demonstrating the range in colour between different acritarchs in the same sample.

CHAPTER 7

APPLICATION OF THE METHOD: TWO CASE STUDIES

7.1. RISHA GAS FIELD, NORTH EAST JORDAN - PREVIOUS WORK

7.1.1. INTRODUCTION

The Risha Gas Field was discovered in 1987 by the Natural Resources Authority, Jordan. It is located in the eastern part of the Risha area (Lüning *et al.* 2005). Natural gas is produced from low porosity, fractured sandstone of the Ordovician Risha Formation (Lüning *et al.* 2005). The origin of the gas is not clear, with isotope data indicating a marine algal origin (Lüning *et al.* 2005). The gas produced is very dry, consisting of more than 90% methane and 'suggests a postmature source rock, with a vitrinite reflectance equivalent value of 2.0%' (Lüning *et al.* 2005).

The Upper Hot Shale Member of the Mudawwara Formation is a well known source rock throughout the region but is 'middle' mature (0.8 – 0.95%R_r) in well RH-3, suggesting that it is not the source of the gas (Lüning *et al.* 2005). The Lower Hot Shale Member of the Mudawwara Formation is found to the west of the Risha Gas Field, as well as western Iraq and northern Saudi Arabia. The Lower Hot Shale Member is thought to be a more likely source than the Upper Hot Shale Member with gas possibly migrating from a distance of 30 – 300km (Lüning *et al.* 2005). The postmature Upper Ordovician shales found in the area have also been suggested as a possible source (Lüning *et al.* 2005).

7.1.2. GEOLOGICAL HISTORY

The Risha Gas Field is located in N.E. Jordan Paleozoic Basin (Beydoun *et al.* 1994) (Figure 7.1). Jordan lies on the northwestern margin of the Arabian Peninsula and formed part of a Paleozoic shelf system that extended across northern Gondwana (Beydoun 1988, Beydoun *et al.* 1994, Konert *et al.* 2001, Lüning *et al.* 2005). The area formed a tectonically quiet passive margin (Konert *et al.* 2001, Lüning *et al.* 2005). Palaeozoic sediments filled the depressions and crustal sags of the Arabian region, including those located in present day Jordan, and thickened towards the east (Beydoun *et al.* 1994, Konert

et al. 2001). Late Palaeozoic regional tectonism resulted in epeirogenic movements and broad uplift of the region (Husseini 1992, Beydoun *et al.* 1994). This movement inverted Arabian basins and parts of their upper sequences were stripped (Beydoun 1988, Beydoun *et al.* 1994, Konert *et al.* 2001). Silurian rocks in the Risha area are overlain unconformably by Triassic sediments which thicken towards the west (Beydoun *et al.* 1994). During the Permian / Triassic period, the Turkish, Iranian and Afghan fragments of Gondwana were rifted from Arabia during a period of extensional tectonics resulting in the opening of the Neo-Tethys Ocean (Beydoun *et al.* 1994, Konert *et al.* 2001, Sharland *et al.* 2001). Igneous dykes and sills have been reported from various levels within the Triassic succession, and a 100m thick basalt unit was intersected in the Upper Triassic of well RH-2, in the north west of the Risha area (Shinaq 1996). Basins formed in Jordan during the Mesozoic and Cenozoic are dominantly rift related (Beydoun *et al.* 1994).

The Tertiary was marked by the opening of the Gulf of Aden and the Red Sea by extension and sea floor spreading. This extension, together with the rotation of Arabia, separated the Arabian Plate from the African Plate and sutured it to the European Plate (Beydoun *et al.* 1994, Mukhopadhyay *et al.* 1996). The north and north western margin of the Arabian Plate is the site of this continuing collision. The late Eocene was marked by uplift and erosion (Beydoun *et al.* 1994).

Intrusive rocks and dykes occur within the Palaeozoic, Triassic and Jurassic sections of northern Jordan.(Sadooni *et al.* 1998). A simplified cross section for the Risha area and a lithostratigraphic column are shown in Figures 7.2 and 7.3.

7.1.3. Source Rock

The following review of the possible source rocks for the Risha Gas Field is taken mainly from the detailed account of Lüning *et al.* (2005). During the latest Ordovician / early Silurian a major eustatic sea level rise occurred, as a result of the melting of an ice cap located in central Africa, and led to the widespread deposition of black shale. In Jordan this unit is known, in subsurface log nomenclature, as the Mudawwara Formation. This formation contains the main oil prone source rock of the Risha area (Keegan *et al.* 1991)

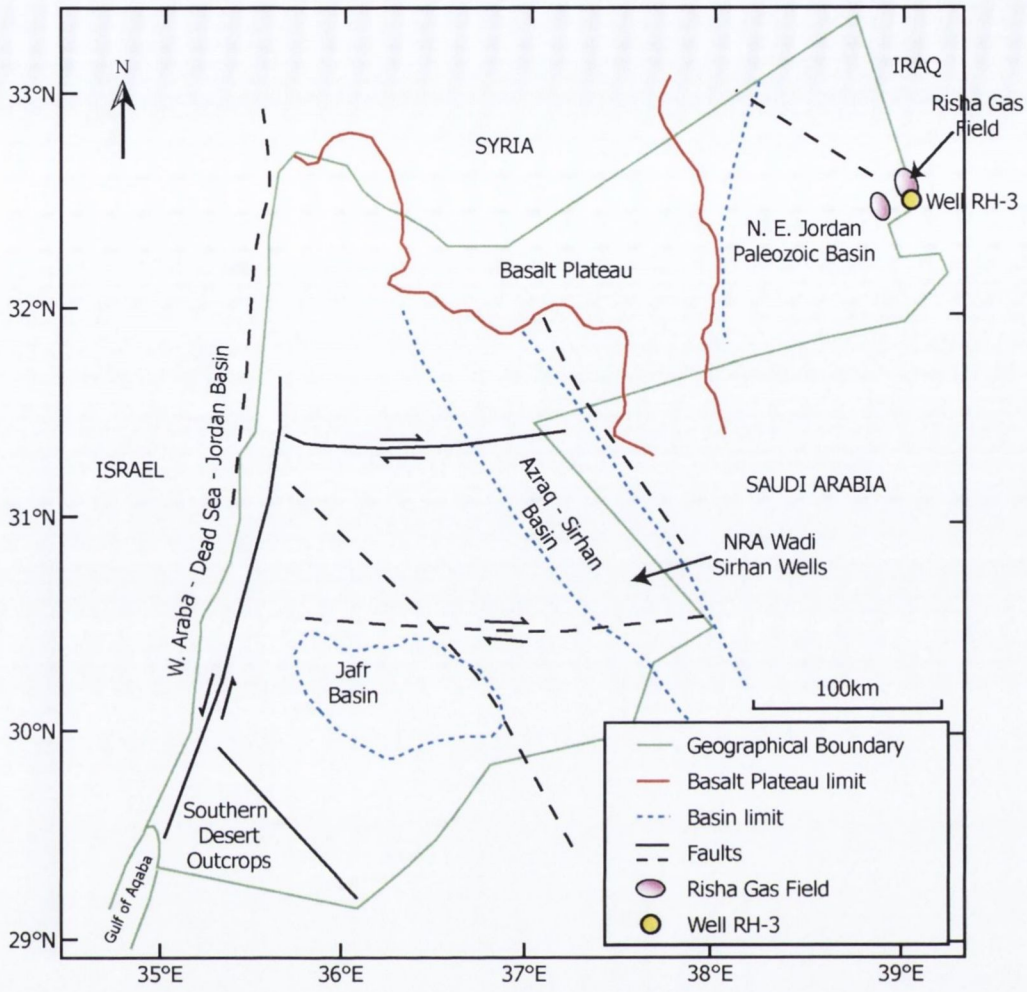

Figure 7.1: Simplified map of Jordan showing the main features of the area and the location of the Risha Gas Field (Beydoun *et al.* 1994).

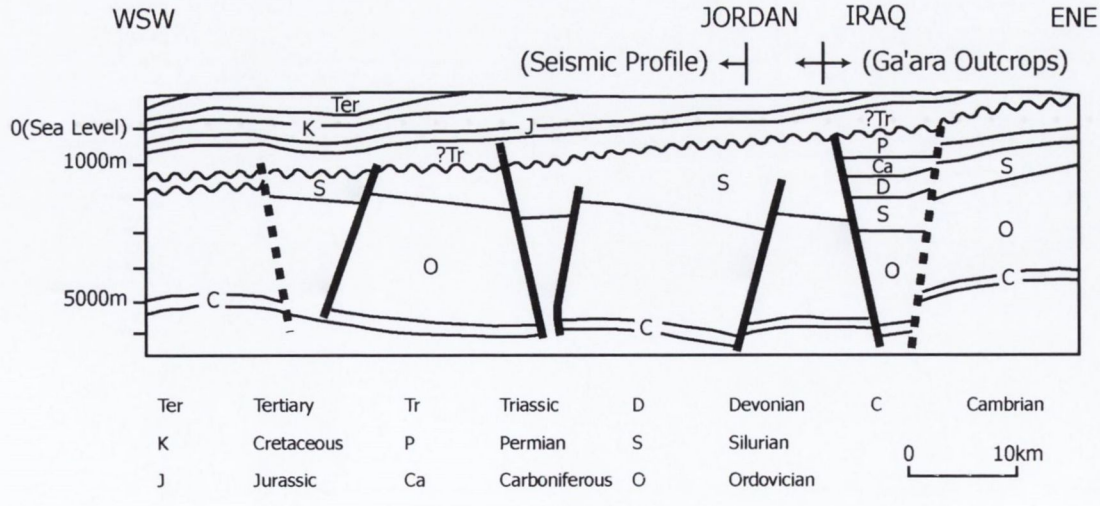

Figure 7.2: Simplified cross section of the north east Jordan, where the Risha Gas Field is located (Beydoun *et al.* 1994).

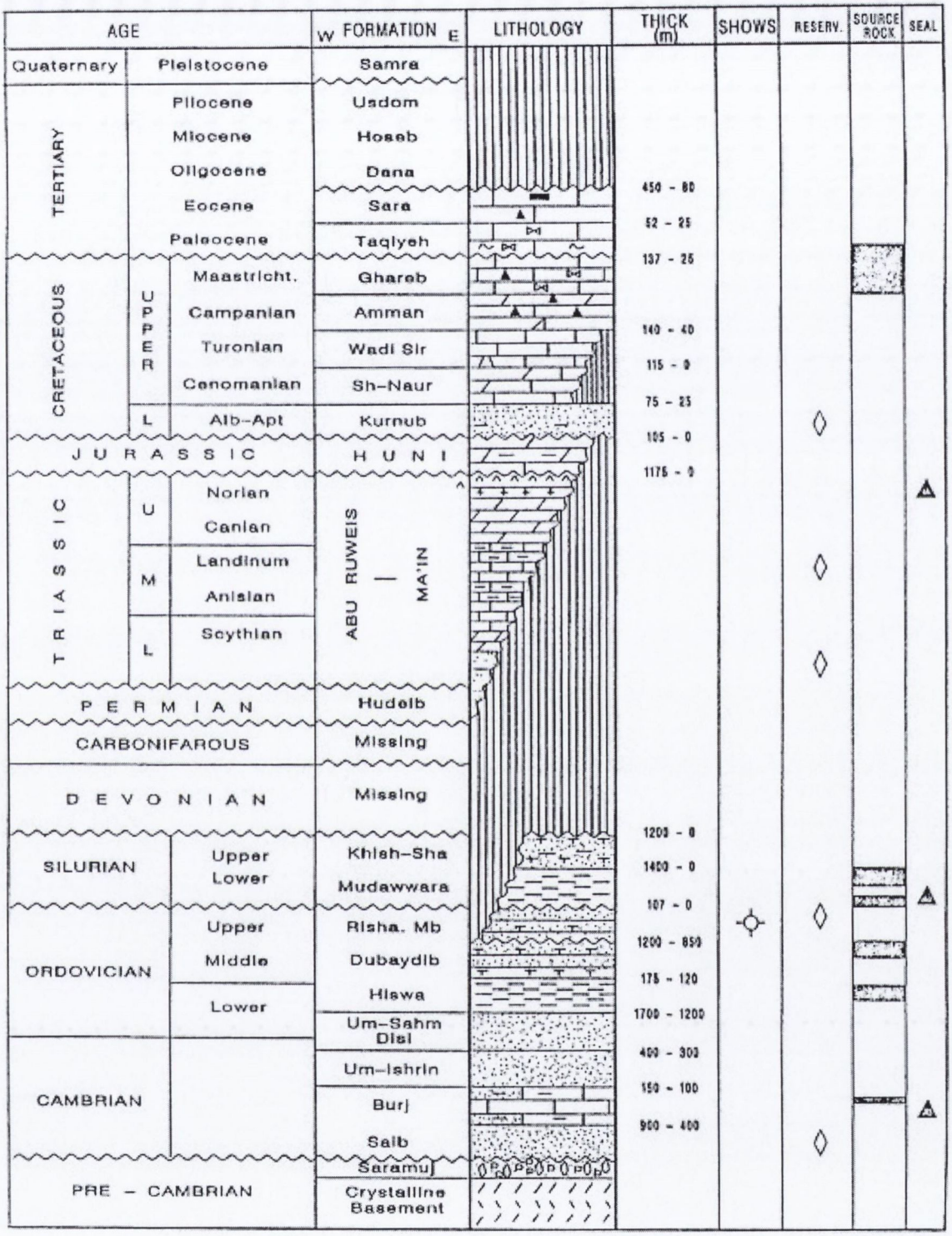

Figure 7.3: Lithostratigraphic column for the Risha area, north east Jordan (Petrel Resources Plc., 2005).

and is probably the main source for the gas accumulations in the area (Beydoun *et al.* 1994). The unit includes two distinctive organically rich shales known as the Upper and Lower Hot Shale members. The lower of these units, situated close to the base of the formation, is easily identified in well logs because of its high natural radioactivity. This member is found in all of south east Jordan, western Risha, eastern Wadi Sirhan and Jafr areas. It is not found in the Risha Gas Field or along the Iraqi border, where it is replaced by a sandstone facies.

Deposition within the Hot Shale unit is controlled mainly by the location of 'paleohighs' and 'paleodepressions' during the early Silurian. The location of these areas is controlled by latest Ordovician glacial relief and intraplate tectonics. At the time, eastern Risha formed a paleohigh, where as western Risha was the depocentre for the Lower Hot Shale Member. The sea level rise, which first triggered the deposition of the Lower Hot Shale Member, continued intermittently during the late Llandoverian and resulted in the onlap and toplap of organically-lean shales onto former paleohighs. The Mudawwara Formation increases in thickness to the north, from 100m in the Southern Desert outcrops, to 1000m in the Risha area.

The Upper Hot Shale Member of the Mudawwara Formation is developed in the Risha area, about 100m below the top of the formation. It is restricted mostly to the eastern Risha area, although it probably was deposited in western Risha but later removed during Hercynian uplift. The member commonly consists of two beds of radioactive shales (11 and 15m thick) separated by a 27m thick shale with normal gamma radiation values. It is seen in the Wadi Sirhan area to the south, but is absent in the Al Jafr area and Southern Desert outcrops. The Upper Hot Shale Member is thought to have been deposited during a double pulsed, large scale, anoxic event sometime during the Late Llandoverian and / or Wenlockian. It was only deposited in those areas dominated by hemipelagic, prodeltaic shale facies like the distal areas of Risha western Iraq. Other areas were dominated by the northward prograding delta.

The Ordovician Risha Formation also contains possible source rocks which may have contributed to the gas accumulation in the area. These organic rich shales are present over most of the Risha area. The Lower Ordovician Hiswa formation may also have been a source for some hydrocarbon production (Beydoun *et al.* 1994).

7.1.4. THERMAL MATURITY

With vitrinite absent, the determination of the thermal maturities of Ordovician and Lower Silurian sediments in Jordan is complicated (Lüning *et al.* 2005). Assessments are based on graptolite reflectance, chitinozoa colour, and pyrolysis derived temperatures of maximum hydrocarbon generation (T_{max}) (Lüning *et al.* 2005). In addition, palynomorph colour and fluorescence have been used as maturity indicators as well as chemical indicators such as Hydrogen Index (HI) and Carbon Preference Indices (CPI) (Paleoservices 1987a). These data are often reported in terms of approximate vitrinite reflectance equivalent values (Lüning *et al.* 2005).

The thermal maturity of Paleozoic sediments in Jordan increases northwards (Lüning *et al.* 2005). The Lower Hot Shale Member of the Mudawwara Formation has been classed as postmature with respect to the oil window in the western part of the Risha area (Lüning *et al.* 2005). The Upper Hot Shale Member is mature with respect to the oil window and has been assigned a vitrinite reflectance equivalent value of 0.8 – 0.95% in the Risha area (Lüning *et al.* 2005). In well RH-3, the maturity of the Paleozoic sediments increases from the mid oil window below the Triassic unconformity, to the start of the 'gas generation threshold' at 1900m in Lower Silurian sediments, to postmature with respect to the oil window in Late Ordovician sediments (Paleoservices 1987a). Shales and silts of the Lower Ordovician Hiswa Formation are postmature with vitrinite equivalent values of 2.0% (Beydoun *et al.* 1994).

7.1.5. TIMING OF HYDROCARBON GENERATION

Understanding the timing of hydrocarbon generation as well as fault movement and trap formation is critical in the location of a successful play in Jordan (Lüning *et al.* 2005). Two main phases of hydrocarbon generation are interpreted for the Risha area (Geotrack 2005, Lüning *et al.* 2005). The first major phase occurred during pre-Hercynian subsidence in the Carboniferous and was terminated by uplift (Lüning *et al.* 2005). It was during this period that the Paleozoic units reached their maximum paleotemperature. Cooling began between 400 – 240Ma (Geotrack 2005). An estimated 1900m of overburden was removed from the section following this Hercynian event (Paleoservices 1987a).

A less intense punctuated generation phase affected the Risha area between the Mesozoic and early Tertiary and was terminated by Jurassic/Cretaceous uplift (Geotrack 2005, Lüning *et al.* 2005, Paleoservices 1987a) and/or Miocene (Lüning *et al.* 2005, Paleoservices 1987a) uplift.

Any hydrocarbons generated during the first phase of subsidence and trapped within the Lower Paleozoic were liable to escape because of Hercynian deformation, when tectonic movement may have breached sealed structures (Konert *et al.* 2001, Lüning *et al.* 2005). In general, structures in the area are younger than the main pre – Hercynian generation phase (Lüning *et al.* 2005). In addition to the Hercynian event, Neogene tectonics may also have breached traps (Beydoun *et al.* 1994).

7.1.6. Kerogen Type and Organic Content

Total organic carbon content (TOC) is a measure of the organic carbon in a rock and is expressed as weight per cent (Miles 1994). The TOC of the Lower Hot Shale of the Mudawwara Formation in the Risha area does not generally exceed 4% (Lüning *et al.* 2005). To the south, in the Wadi Sirhan area, the TOC increases to a maximum of 7% and at the Southern Desert outcrop this value can be as high as 11% for the same unit (Lüning *et al.* 2005). The northerly decrease in TOC in this member is interpreted as the result of increased hydrocarbon generation in the north, reducing the amount of organic matter remaining in the source rock (Lüning *et al.* 2005).

Kerogen is the organic matter preserved within sedimentary rocks and three different types have been identified. Type I kerogen is algal dominated, type II kerogen is liptinitic and consists of zooplankton, phytoplankton with some algal detritus, while type III is humic, dominated by the lignin of higher woody plants (Tissot *et al.* 1974, Van Gijzel 1982). Different kerogens tend produce different hydrocarbons with type I kerogen often generating oil, type II oil and gas, and type III gas. The Lower Hot Shale Member is oil prone, dominated by type I/ type II kerogen (Lüning *et al.* 2005).

The Upper Hot Shale member of the Mudawwara Formation has a TOC value of 0.8 – 2.0% and generally consists of type I, oil prone, algal kerogen (Lüning *et al.* 2005). Like the Lower Hot Shale member, it is thought much of the oil prone potential of this unit in

the Risha area has been lost through primary migration and only depleted kerogen residue remains (Lüning *et al.* 2005).

The uppermost Ordovician shales of the Risha Formation have also been proposed as a possible source for hydrocarbon generation in the area (Lüning *et al.* 2005). The TOC value of this unit is 3%, but the remaining generating potential is low (Lüning *et al.* 2005). Like the upper and lower shale units previously discussed, it is likely the quality of this source rock was much better when it was first deposited (Lüning *et al.* 2005). In well RH-3, the maximum petroleum potential is found between 1322m – 1431m, which encompasses the upper 30m of the Ordovician Dubeidib Formation and the lower 76m of the Silurian Mudawwara Formation (Paleoservices 1987a).

7.1.7. Traps

The most common hydrocarbon traps in Jordan are related to horsts and tilted fault blocks, and/or drape structures located over deep seated fault blocks (Beydoun *et al.* 1994). Broad epeirogenic swells, with smaller low amplitude depocentres also form common traps in area (Beydoun *et al.* 1994).

Three different possible plays have been proposed by Lüning *et al.* for Jordan (2005). Their first play is based on the migration of hydrocarbons generated in the Upper and/or Lower Hot Shale members of the Mudawwara Formation laterally into Ordovician, or younger Triassic to Tertiary units across faults. Two fault types have been identified in the area: Paleozoic growth faults and post depositional Mesozoic to Tertiary faults. Their second play is described as a stratigraphic channel play, where upper Ordovician channel sands were charged by downward migrating hydrocarbons, sourced from the overlying Hot Shale. The final play relies on Upper Ordovician/ Lower Silurian paleohighs. The Lower Hot Shale was deposited in paleodepocentres, located near paleohighs where high energy sands were deposited. Lüning *et al.* (2005) suggest that hydrocarbons generated in the Lower Hot Shale charged the adjacent sandstone reservoirs and that the Risha Gas Field is a possible candidate for this type of play

7.1.8. GEOTHERMAL GRADIENTS

In north-east Jordan, present day geothermal gradients increase from 30°C/km in well RH-2 to over 50°C/km in well RH-3 to the east (Beydoun *et al.* 1994). This increase has been attributed to the insulating effects of the Silurian claystone which is absent in well RH-2, and 2100m thick in well RH-3 (Beydoun *et al.* 1994). The presence of young (7Ma) basalts may have had a local modifying effect on heat flow gradients (Beydoun *et al.* 1994). Maturation modeling carried out by the Natural Resources Authority of Jordan suggests that the higher gradients are a relatively young phenomenon and have been established over the past 100Ma (Beydoun *et al.* 1994). Elevated heat flow from Carboniferous – early Triassic times is suggested by apatite fission track data (Geotrack 2005). A 90Ma old apatite sample from RH-3 appears to show evidence of elevated heat flow which may be attributed to the effects of hot fluid flow (Geotrack 2005).

7.1.9. RESERVOIRS AND SEALS

In the Risha Gas Field, fractured sandstone from the Ordovician Risha Formation forms a reservoir for natural gas (Lüning *et al.* 2005). In Jordan, Cambrian and Ordovician sandstones generally vary in reservoir quality due to diagenesis and cementation by silica and/or volcanic derived clays (Beydoun *et al.* 1994). As in the case of the Risha Gas Field, fracturing has enhanced the quality of cemented quartz sandstones (Beydoun *et al.* 1994, Lüning *et al.* 2005).

Seals in the area generally consist of Paleozoic claystones and shales, where often the source rock acts as the seal (Beydoun *et al.* 1994, Konert *et al.* 2001). Triassic evaporates in Jordan have also acted as seals, as have Mesozoic source rocks (Beydoun *et al.* 1994).

7.2 RISHA GAS FIELD, NORTH EAST JORDAN

SAMPLES INVESTIGATED DURING THIS STUDY

7.2.1. INTRODUCTION

Both cuttings and core samples provided by Petrel Resources plc were investigated for this project (Tables 7.1, 7.3, 7.5, 7.7, 7.9, 7.11) . The samples studied were taken from the Silurian succession of well RH-3 in the Risha gas field, close to the Jordan/Iraq border. The samples were processed using standard palynological techniques as described in section 3.2.1. RGB determinations were made on the *Veryhachium* specimens in each sample and, where possible, chitinozoa reflectance (section 3.3.4) was also measured.

RGB intensity determinations were made on specimens of *Veryhachium* from each sample. The average RGB intensities are given for each sample, together with the standard deviation (Tables 7.2, 7.4, 7.6, 7.8, 7.10). Using these data, a vitrinite reflectance equivalent was calculated as described in section 6.3.1. The average *Veryhachium* RGB intensities were plotted on intensity-maturity graphs as described in section 6.3.2. The fluorescence of *Veryhachium* specimens under ultra violet/blue light was also recorded (section 4.5.10). Where possible, chitinozoa reflectance determinations were made on samples and the equivalent vitrinite reflectance calculated from Tricker *et al.* (1992).

7.2.2. SAMPLE P12

Well	RH-3	*Age*	Silurian
Depth	520m	*Formation*	Khishsha
Sample type	Cuttings		

Table 7.1: Details of Sample P12 provided by Petrel Resources plc.

	No. of readings	Mean Intensity	Standard Deviation	$\%R_r$ equivalent
Red	11	223	4	$0.88\%R_r \pm 0.67\%R_r$
Green	11	235	4	$1.09\%R_r \pm 0.56\%R_r$
Blue	11	189	27	$1.10\%R_r \pm 0.55\%R_r$

Table 7.2: Details of average red, green and blue intensities of *Veryhachium* in sample P12. Vitrinite reflectance equivalents calculated using the procedure described in section 6.3.1.

The average RGB intensity of *Veryhachium* specimens from sample P12 clearly plots in the same area as samples determined to be mature with respect to the oil window (see Figures 7.4, 7.5 and 7.6). The calculated vitrinite reflectance equivalent values and the fluorescence of the palynomorphs in ultra violet/blue light support the conclusion that this sample is mature with respect to the oil window.

A Paleoservices report (1987a) determined the Upper Silurian to Middle Silurian section of well RH-3 (398 - 1,220m) was mature with respect to the oil window. This interval includes sample P12.

7.2.3. SAMPLE P13

Well	RH-3	*Age*	Silurian
Depth	1155m	*Formation*	Khishsha
Sample type	Cuttings		

Table 7.3: Details of Sample P13 provided by Petrel Resources plc.

	No. of readings	Mean Intensity	Standard Deviation	$\%R_r$ equivalent
Red	46	222	2	$0.90\%R_r \pm 0.67\%R_r$
Green	46	237	4	$1.06\%R_r \pm 0.56\%R_r$
Blue	46	203	21	$0.95\%R_r \pm 0.55\%R_r$

Table 7.4: Details of average red, green and blue intensities of *Veryhachium* in sample P13. Vitrinite reflectance equivalents calculated using the procedure described in section 6.3.1.

The average RGB intensity of *Veryhachium* specimens from sample P13 clearly plots in the same area as samples determined to be mature with respect to the oil window (see Figures 7.4, 7.5 and 7.6). The calculated vitrinite reflectance equivalent values and the fluorescence of the palynomorphs under ultra violet light support the conclusion that this sample is mature with respect to the oil window.

A Paleoservices report (1987a) determined the Upper Silurian to Middle Silurian section of well RH-3 (398 – 1,220m) was mature with respect to the oil window. This interval includes sample P13. This report also contained vitrinite reflectance data for a sample close to P13, between 1160 – 1176m. Six determinations were made and the interval was assigned a vitrinite reflectance value of $0.88\%R_r$. While this determination also suggests

the sample is mature with respect to the oil window, the Middle Silurian age of the section (Paleoservices 1987b) casts doubt on whether the grains measured were vitrinite.

7.2.4. SAMPLE P11

Well	RH-3	*Age*	Silurian
Depth	1320 – 1333m	*Formation*	Mudawwara
Sample type	Cuttings		

Table 7.5: Details of Sample P11 provided by Petrel Resources plc.

	No. of readings	Mean Intensity	Standard Deviation	$\%R_r$ equivalent
Red	9	223	2	$0.88\%R_r \pm 0.67\%R_r$
Green	9	238	2	$1.05\%R_r \pm 0.56\%R_r$
Blue	9	209	16	$0.89\%R_r \pm 0.55\%R_r$

Table 7.6: Details of average red, green and blue intensities of *Veryhachium* in sample P11. Vitrinite reflectance equivalents calculated using the procedure described in section 6.3.1.

Chitinozoa reflectance determinations were made on this sample. The average chitinozoa reflectance for the sample was 0.87%, equivalent to $0.69\%R_r$ (Tricker *et al.* 1992). The average RGB intensity of *Veryhachium* specimens from sample P11 clearly plots in the same area as samples determined to be mature with respect to the oil window (see Figures 7.4, 7.5 and 7.6). The calculated vitrinite reflectance equivalent values, the fluorescence of the palynomorphs under ultra violet light, and chitinozoa reflectance determinations support the conclusion this sample is mature with respect to the oil window.

A Paleoservices report (1987a) determined the Middle to Lower Silurian section of well RH-3 (1,220 – 2,695m) was mature with respect to the oil window. In addition, it identified a major source rock succession between 1,265 – 1,696m that is mature with respect to the oil window. This interval includes sample P11. This report also contained vitrinite reflectance data for a core sample close to P11, at 1322m. Fifteen determinations were made and the interval was assigned a vitrinite reflectance value of $0.8\%R_r$. While this determination also suggests the sample is mature with respect to the oil window, the Middle Silurian age of the section (Paleoservices 1987b) casts doubt on whether the grains measured were vitrinite.

7.2.5. SAMPLE PET 3

Well	RH-3	*Age*	Silurian
Depth	1323 – 1330.2m	*Formation*	Mudawwara
Sample type	Core 3		

Table 7.7: Details of Sample Pet3 provided by Petrel Resources plc.

	No. of readings	Mean Intensity	Standard Deviation	$\%R_r$ equivalent
Red	16	218	4	$0.99\%R_r \pm 0.67\%R_r$
Green	16	237	3	$1.06\%R_r \pm 0.56\%R_r$
Blue	16	208	21	$0.90\%R_r \pm 0.55\%R_r$

Table 7.8: Details of average red, green and blue intensities of *Veryhachium* in sample Pet3. Vitrinite reflectance equivalents calculated using the procedure described in section 6.3.1.

The average chitinozoa reflectance for the sample was 0.86%, equivalent to $0.68\%R_r$ (Tricker *et al.* 1992). The average RGB intensities of *Veryhachium* specimens from sample Pet3 clearly plots in the same area as samples determined to be mature with respect to the oil window (see Figures 7.4, 7.5 and 7.6). The calculated vitrinite reflectance equivalent values, the fluorescence of the palynomorphs under ultra violet light, and chitinozoa reflectance determinations support the conclusion this sample is mature with respect to the oil window.

A Paleoservices report (1987a) determined the Middle to Lower Silurian section of well RH-3 (1,220 – 2,695m) was mature with respect to the oil window. In addition it identified a major source rock succession between 1,265 – 1,696m that is mature with respect to the oil window. This interval includes sample P11. This report also contained vitrinite reflectance data for a core sample close to P11, at 1322m. Fifteen determinations were made and the interval was assigned a vitrinite reflectance value of $0.8\%R_r$. While this determination also suggests the sample is mature with respect to the oil window, the middle Silurian age of the section (Paleoservices 1987b) casts doubt on whether the grains measured were vitrinite.

7.2.6. SAMPLE PET 6

Well	RH-3	*Age*	Ordovician
Depth	2599.33 – 2602.9m	*Formation*	Dubeidib
Sample type	Core 4		

Table 7.9: Details of Sample Pet6 provided by Petrel Resources plc.

This sample contained a small number of poorly preserved *Veryhachium* (Figure 7.7). All of the specimens located were degraded and thinned which made them unsuitable for RGB determinations. Those areas of the specimens that suffered the least alteration were darker in colour than any other *Veryhachium* observed in this well, and seem consistent with increasing levels of maturity with depth. None of the specimens observed fluoresced under ultraviolet light. The lack of fluorescence and the degraded nature of the palynomorphs suggest the sample is postmature with respect to the oil window.

A Paleoservices report (1987a) determined the Middle to Lower Silurian section of well RH-3 (1,220 – 2,695m) was mature with respect to the oil window. This interval includes sample Pet3. However, it was noted that the maturity of samples between 2,620 and 2,696m was close to the base of the oil window. This report also contained vitrinite reflectance data for core sample Pet6. Four determinations were made and the interval was assigned a vitrinite reflectance value of 3.7%R_r. While this determination suggests the sample is postmature with respect to the oil window, the Middle - Lower Silurian age of the section (Paleoservices 1987b) casts doubt on whether the grains measured were vitrinite. Having studied residue from this sample, it appears more likely that these reflectance determinations were made on chitinozoa fragments.

7.2.7. SAMPLE PET 9

Well	RH-3	*Age*	Ordovician
Depth	2856 – 2857m	*Formation*	Dubeidib
Sample type	Core 5		

Table 7.10: Details of Sample Pet9 provided by Petrel Resources plc.

Like Sample Pet 6, this sample also contained poorly preserved *Veryhachium* (Figure 7.8). Again, areas of the specimens that suffered the least degradation were darker in colour than any other *Veryhachium* observed in this well. None of the specimens observed fluoresced under ultraviolet light. The lack of fluorescence and the degraded nature of the palynomorphs suggest the sample is postmature with respect to the oil window.

The Paleoservices geochemical report (1987a) records a vitrinite reflectance value, based on 16 determinations, of 2.16%R_r from the interval 2710 – 2711m. While these data suggests the sample Pet9 (2856 – 2857m) may be post mature, given this sample is dated as Late Ordovician, it seems unlikely that these determinations were made on vitrinite grains.

7.2.8. Conclusions

The maturity of samples determined by *Veryhachium* RGB determinations and fluorescence was similar to results obtained by Paleoservices (1987) using a variety of other organic and chemical parameters. No reworking or caving was indicated by the RGB intensity histograms (Appendix V), although it has been previously reported in samples from this well (Paleoservices 1987a). Although no useful RGB determinations could be made on the degraded *Veryhachium* specimens in sample Pet 6 or Pet 9, the lack of fluorescence was still useful in determining the maturity of the sample.

The average RGB intensities of *Veryhachium* populations for each sample were plotted against depth (Figures 7.8, 7.9, 7.10 and 7.11) together with their standard deviation. Maturity level and fluorescence data are also shown. In the mature samples, RGB intensities change little with depth. This is consistent with previous results of this study where *Veryhachium* from samples mature with respect to the oil window tend to cluster together (Section 6.3). It would be useful to have a more complete data set that spanned a larger range of maturities, to investigate how RGB intensity varies with depth.

While this case study is limited to six samples, it points to the potential successful application of this technique in assessing the thermal maturity of sediments. In this setting, *Veryhachium* RGB determinations are arguably more reliable maturity indicators than Late Ordovician vitrinite grains.

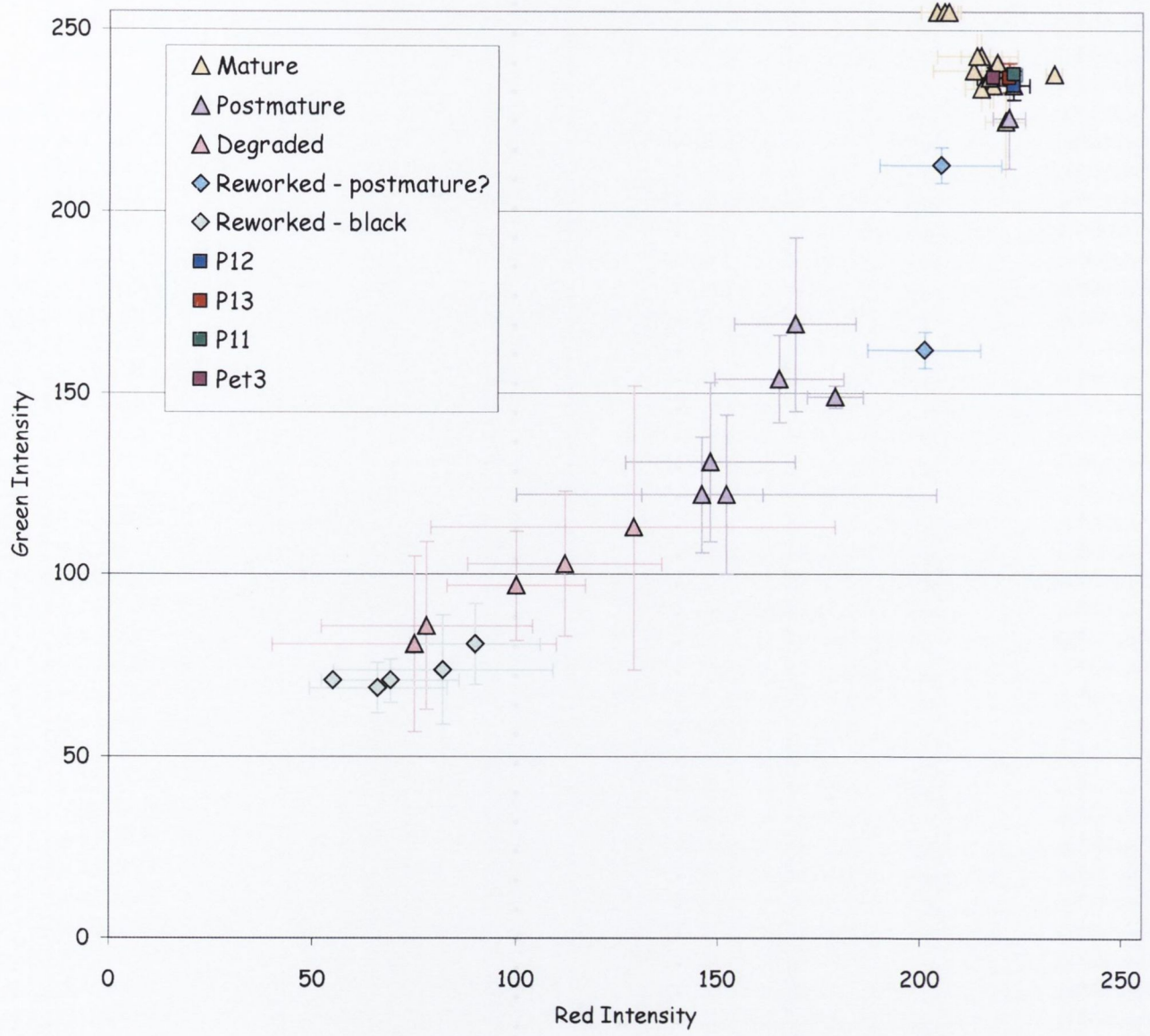

Figure 7.4: Average green *Veryhachium* intensity versus average red *Veryhachium* intensity for all samples investigated from well RH-3, Jordan.

Also plotted is the average green *Veryhachium* intensity versus average red *Veryhachium* intensity of all other samples studied in this project. For those well preserved samples for which vitrinite reflectance data were collected, they have been divided into mature and post-mature samples with respect to the oil window. Degraded samples are grouped together. Those specimens identified as reworked are also plotted in order to fill 'colour gaps' and have been split into two groups; those samples that are clearly black, and those that still retain lighter colours.

All well preserved samples from well RH-3 appear to plot in the 'mature with respect to the oil window' field. This plot is discussed further in section 6.3.2.

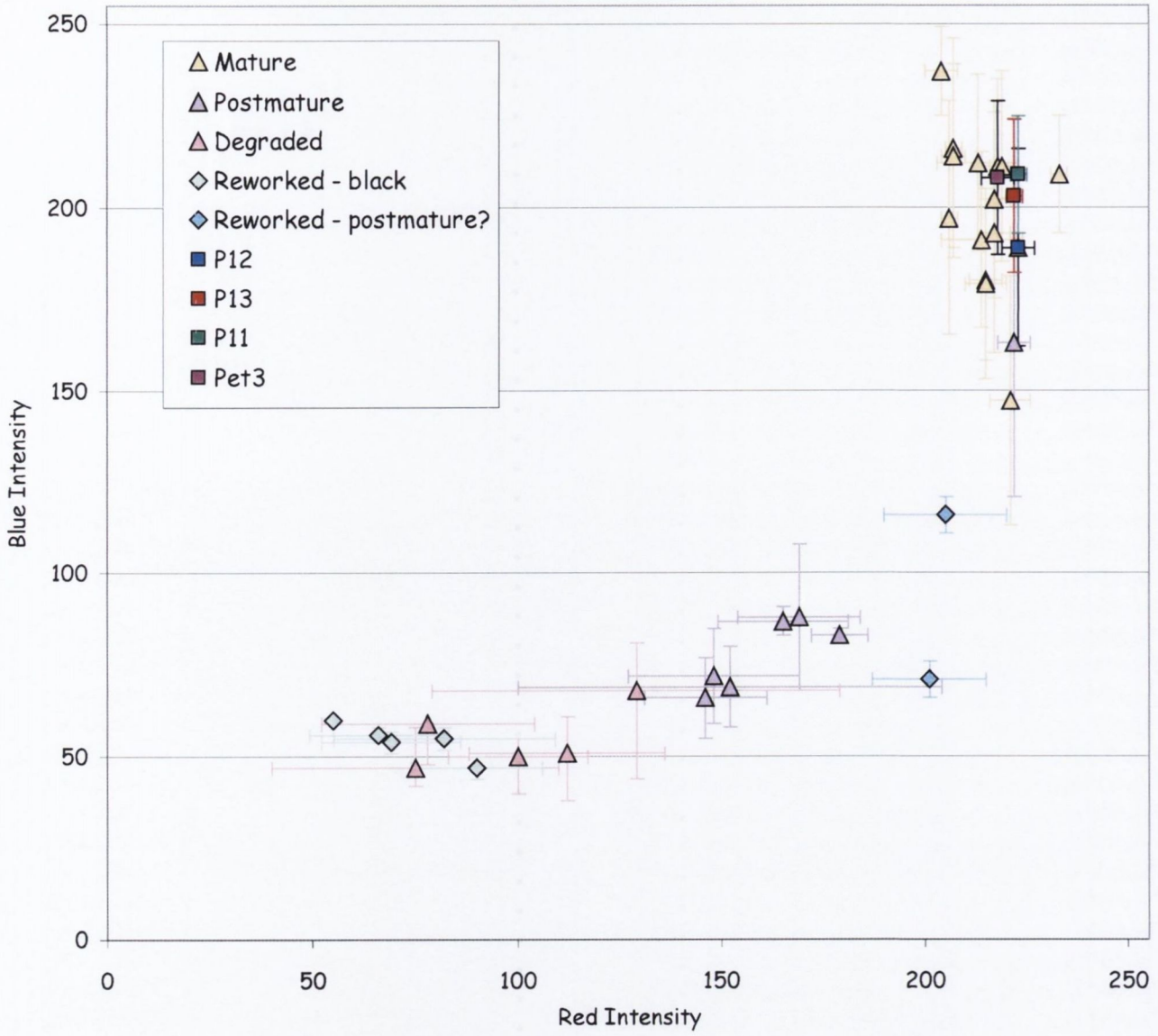

Figure 7.5: Average blue *Veryhachium* intensity versus average red *Veryhachium* intensity for all samples investigated from well RH-3, Jordan.

Also plotted is the average blue *Veryhachium* intensity versus average red *Veryhachium* intensity of all other samples studied in this project. For those well preserved samples for which vitrinite reflectance data were collected, they have been divided into mature and post-mature samples with respect to the oil window. Degraded samples are grouped together. Those specimens identified as reworked are also plotted in order to fill 'colour gaps' and have been split into two groups; those samples that are clearly black, and those that still retain lighter colours.

All well preserved samples from well RH-3 appear to plot in the 'mature with respect to the oil window' field. This plot is discussed further in section 6.3.2.

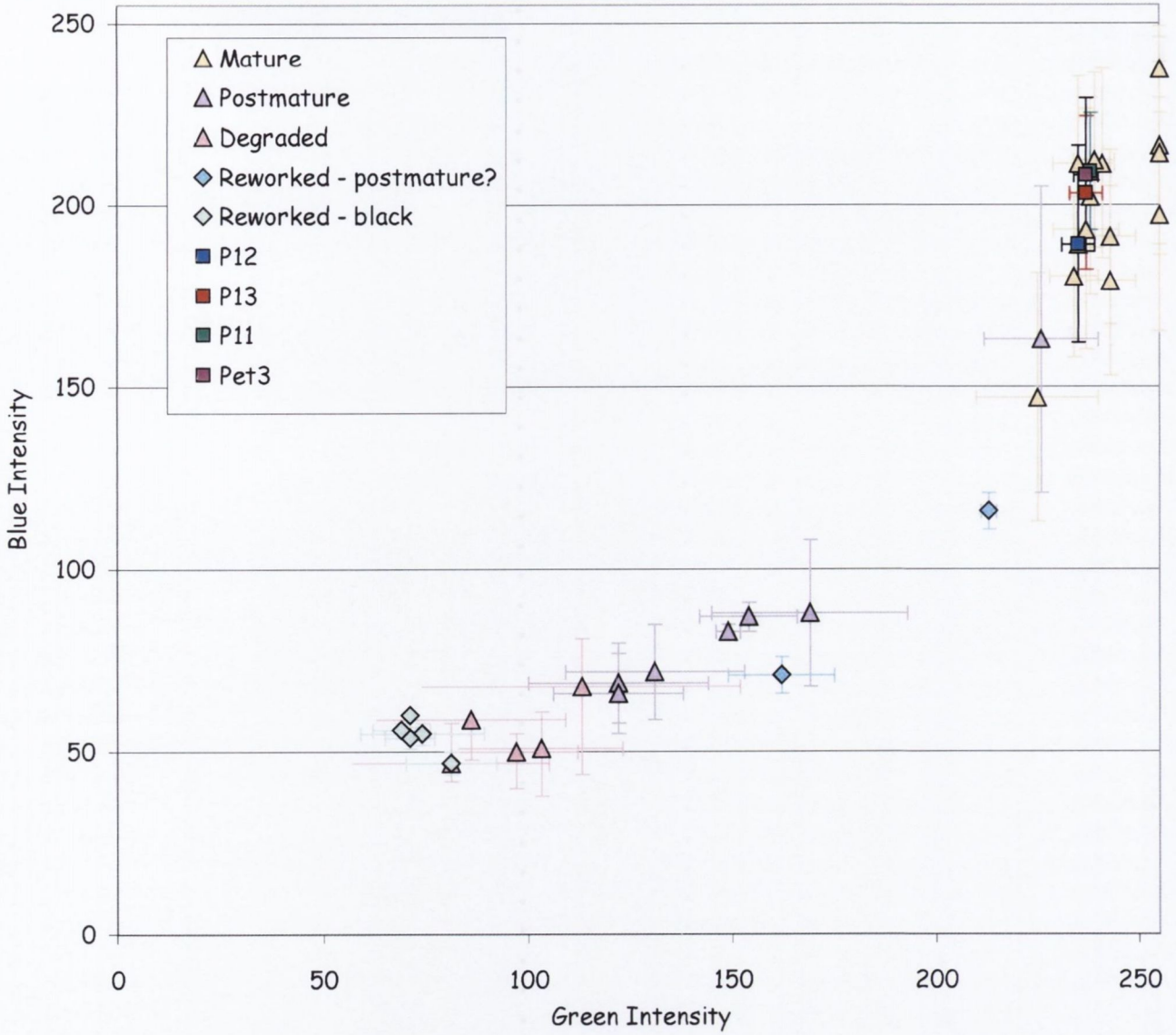

Figure 7.6: Average blue *Veryhachium* intensity versus average green *Veryhachium* intensity for all samples investigated from well RH-3, Jordan.

Also plotted is the average blue *Veryhachium* intensity versus average green *Veryhachium* intensity of all other samples studied in this project. For those well preserved samples for which vitrinite reflectance data were collected, they have been divided into mature and post-mature samples with respect to the oil window. Degraded samples are grouped together. Those specimens identified as reworked are also plotted in order to fill 'colour gaps' and have been split into two groups; those samples that are clearly black, and those that still retain lighter colours.

All well preserved samples from well RH-3 appear to plot in the 'mature with respect to the oil window' field. This plot is discussed further in section 6.3.2.

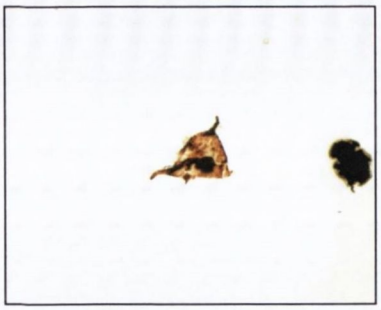

Degraded *Veryhachium* specimen
Sample: Pet 6 (Slide 1)
E/F Ref. C34/4
(field of view 100µm)

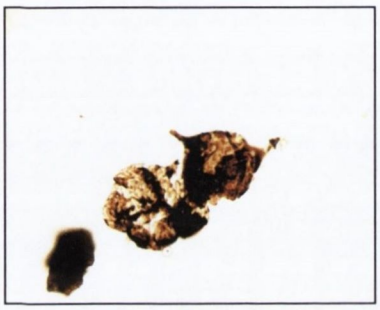

Degraded *Veryhachium* specimen
Sample: Pet 6 (Slide 1)
E/F Ref. S35/2
(field of view 100µm)

Degraded *Veryhachium* specimen
Sample: Pet 9 (Slide 1)
E/F Ref. K73/3
(field of view 100µm)

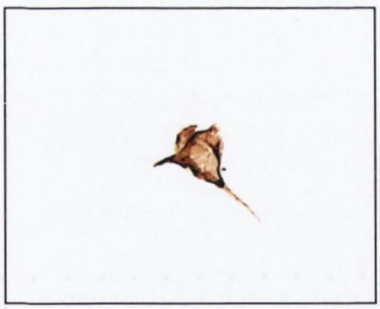

Degraded *Veryhachium* specimen
Sample: Pet 9 (Slide 1)
E/F Ref. J49/2
(field of view 100µm)

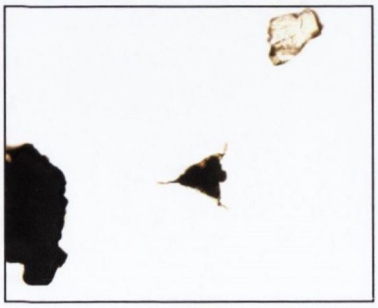

Veryhachium with pyrite
Sample:Pet 9 (Slide 1)
E/F Ref.F73/1
(field of view 100µm)

Figure 7.7: *Veryhachium* specimens from sample Pet 6 and Pet 9

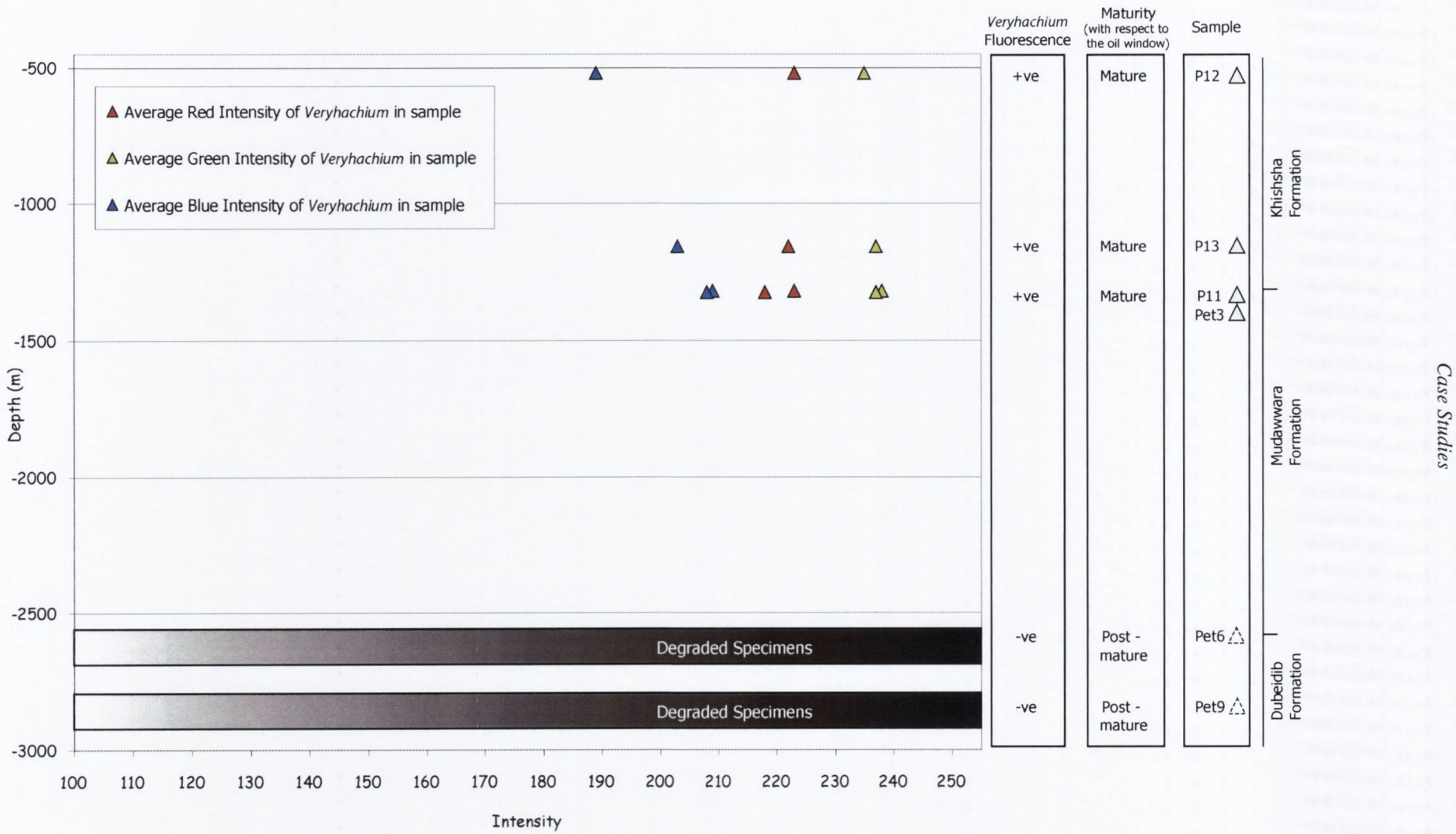

Figure 7.8: Summary of maturity data collected for well RH-3 during this project, including average RGB intensities of the *Veryhachium* of each sample plotted versus depth.

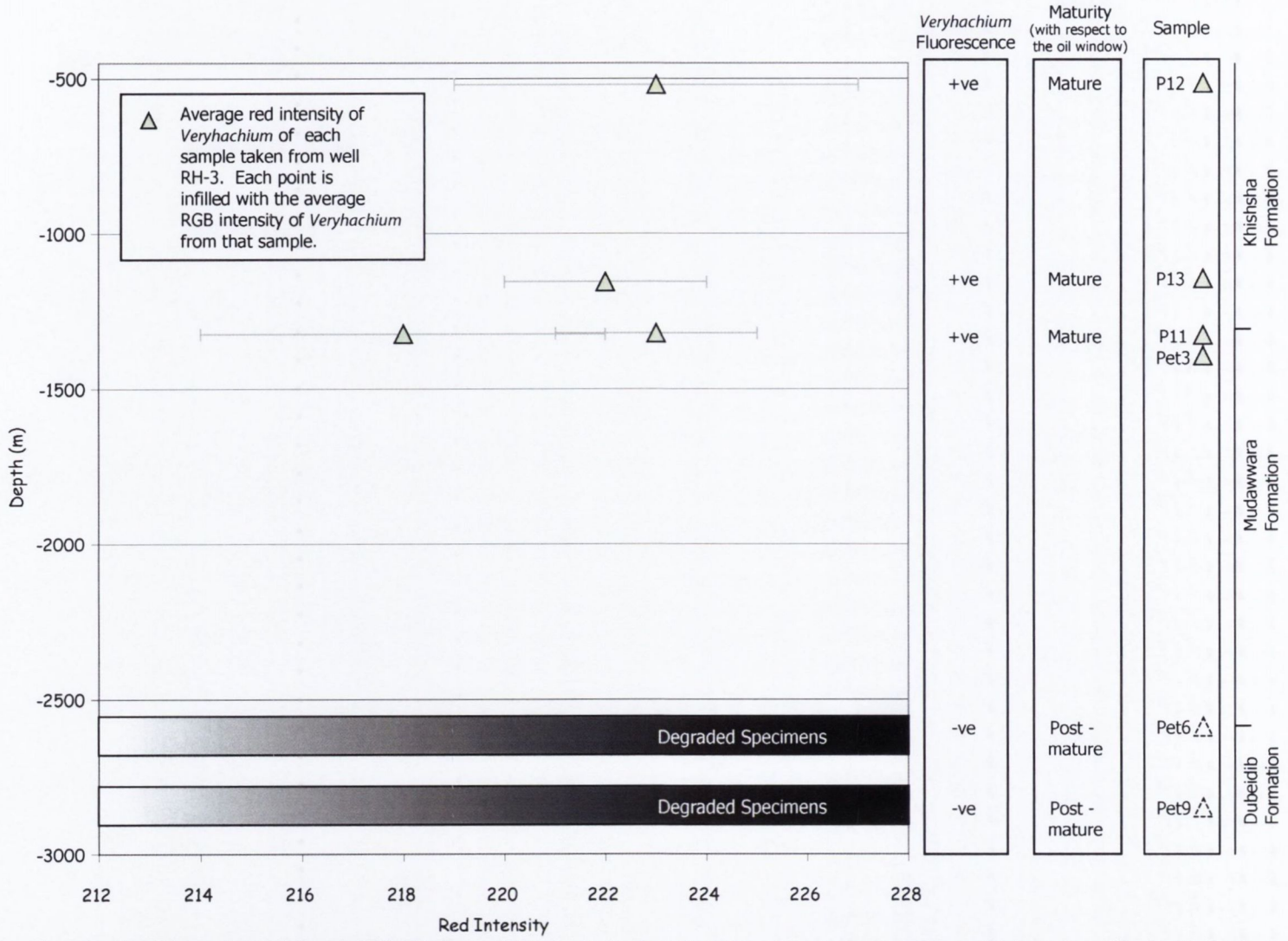

Figure 7.9: Summary of maturity data collected for well RH-3 during this project, detailing the change in average red intensity with depth (note scale).

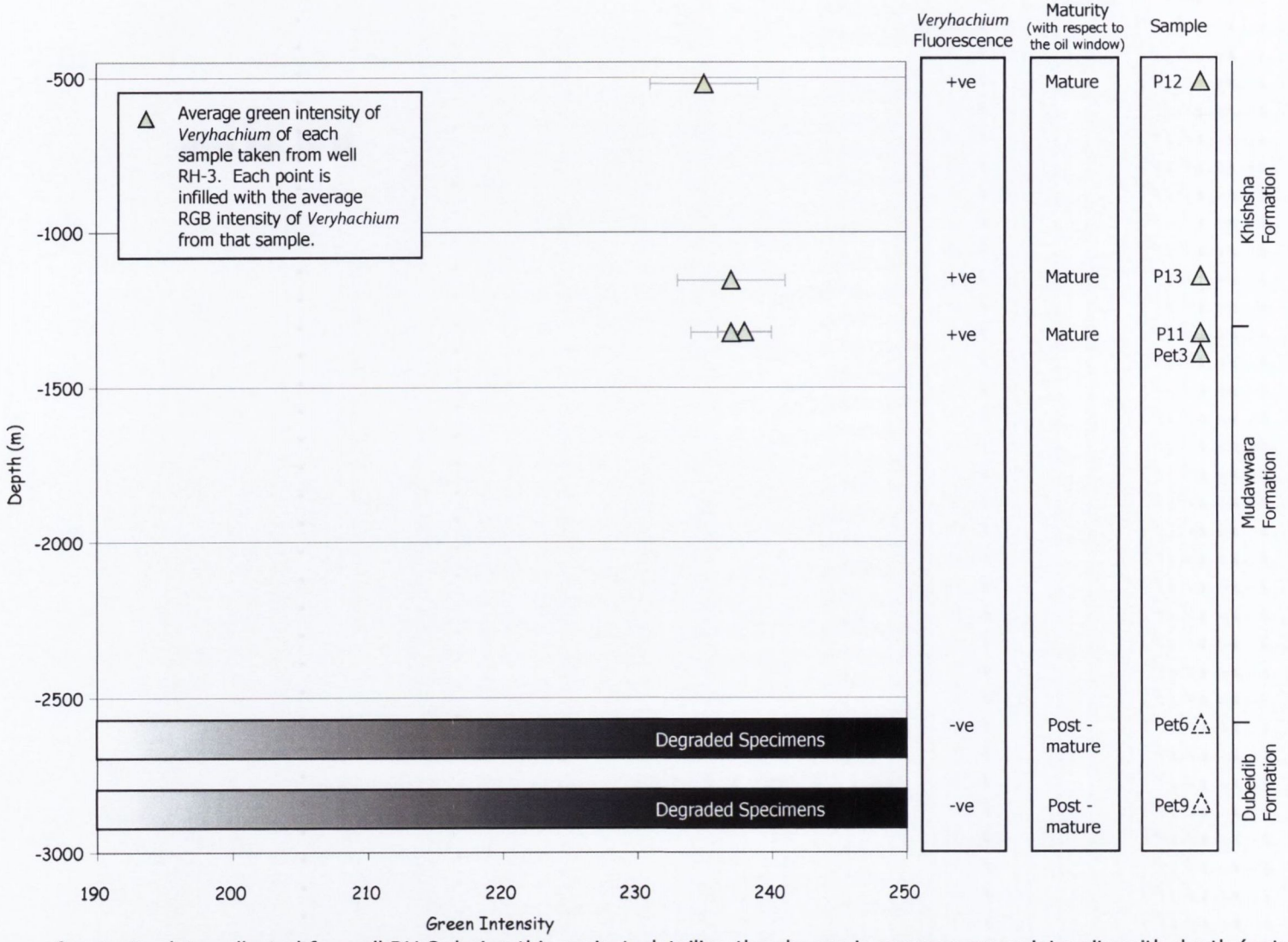

Figure 7.10: Summary of maturity data collected for well RH-3 during this project, detailing the change in average green intensity with depth (note scale).

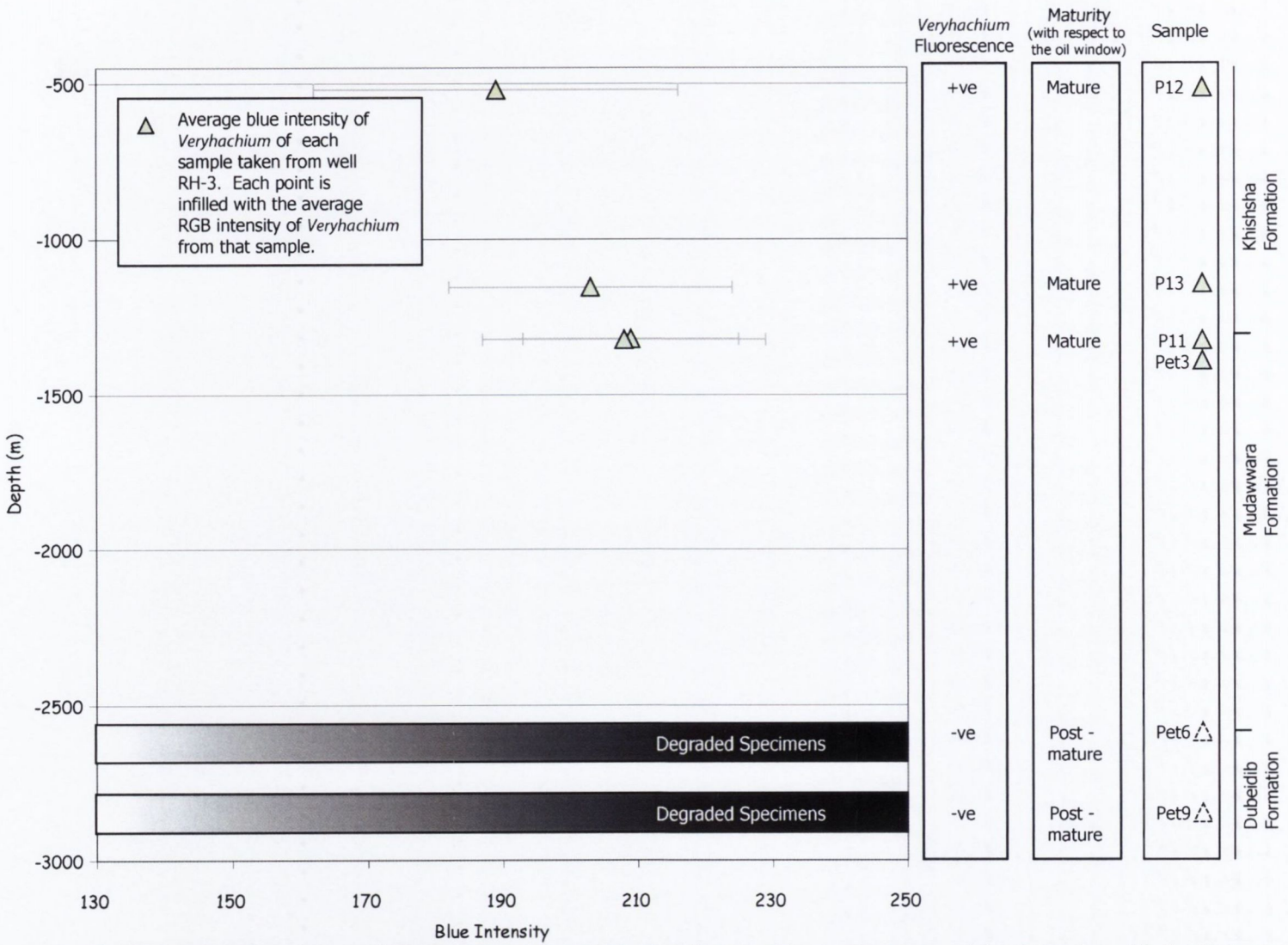

Figure 7.11: Summary of maturity data collected for well RH-3 during this project, detailing the change in average blue intensity with depth (note scale).

7.3. REWORKING IN THE ITACUA FORMATION, BOLIVIA

7.3.1. INTRODUCTION

A sample from the Upper Devonian Itacua Formation, collected by Andy Racey (BG Exploration and Production), was investigated during this project. The presence of reworked palynomorphs within the section (Clayton 2003) made it of interest to this project. The sample studied was taken 'near Bermejo, 1½ hours drive west of Santa Cruz.', just at the base of the Itacua Formation.

The sample is located within the Santa Cruz. – Tarija Province of Bolivia, part of the Sub Andean Foreland Fold and Thrust Belt (Lindquist 1998). The unit forms part of the Paleozoic intracontinental Chaco – Tarija Basin (Lindquist 1998). During the Mississippian, diamictites were deposited in a glaciomarine environment in this backarc basin (Zapata *et al.* 2005). Reworking of palynomorphs in diamictite units of similar age to the Itacua Formation in the Madre de Díos Basin in northern Bolivia have been linked to a Devonian/Carboniferous glacial event (Vavrdova 1996).

Sample 'Bolivia 3', is dominated by acritarchs and prasinopyhtes with only a few miospores recorded (Clayton 2003). Miospores restricted to the latest Devonian, *Retispora lepidophyta* and *Vallatisporites pusillites,* are found along side the earlier Devonian *Cristatisporites triangulatus* (Clayton 2003). Reworked acritarchs are also present with Givetian – Frasnian examples including *Quadrisporites* cf. *granulatus* and *Dactylofusa fastidiona* recorded (Clayton 2003). Both the reworked miospores and acritarchs discussed above are indistinguishable from the later examples on the basis of colour or state of preservation (Clayton 2003). However, the colour of abundant *Veryhachium* specimens within the sample does show some variation.

The RGB intensities of 50 *Veryhachium* specimens were determined to establish whether a reworked population could be identified. Histograms of the three intensities are shown in Figures 7.12, 7.13 and 7.14. All histograms show a clear left tail which suggests while the dominant population is pale in colour, there is a small input of darker specimens. From this histogram data alone, a reworked population of at least four specimens can be confidently identified, and another two specimens are likely to be reworked. These six specimens clearly plot in a population separate from the majority of the *Veryhachium*

studied in this sample (Figures 7.15, 7.16 and 7.17). Colour is the only feature which identifies these specimens as reworked and without the use of colour analysis, they would not be documented.

While these six reworked specimens were identified using RGB determinations, it is likely that other reworked *Veryhachium* cannot be recognised on the basis of colour alone. As already discussed, those palynomorphs known to be reworked, on the basis of their stratigraphic range, show no variation in colour to the younger latest Devonian examples. It is reasonable to expect the same its true for any Middle and Late Devonian *Veryhachium* present in the sample.

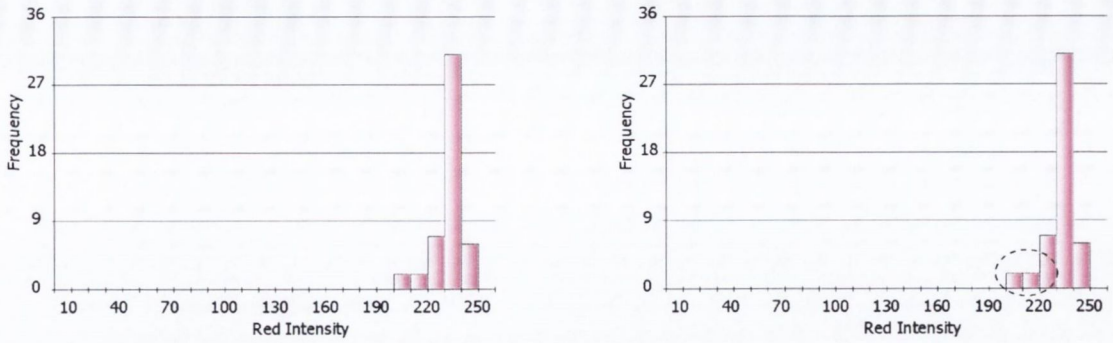

Figure 7.12: Distribution of the red intensity values of *Veryhachium* in Bolivia 3. Note that reworked specimens have been identified on the basis of green and blue intensity data (below).

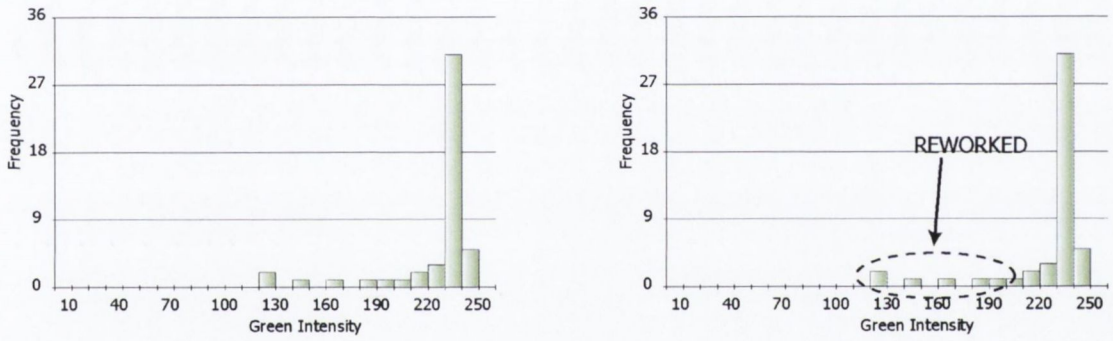

Figure 7.13: Distribution of the green intensity values of *Veryhachium* in Bolivia 3. The large spread of this population is unusal and indicates reworking.

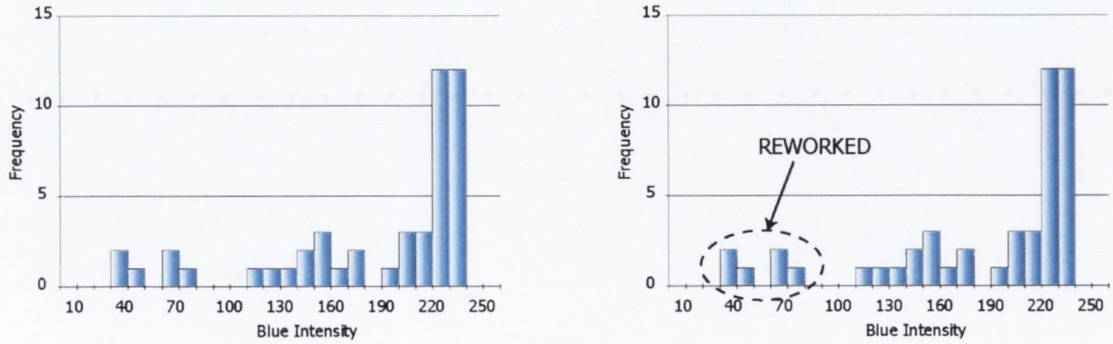

Figure 7.14: Distribution of the blue intensity values of *Veryhachium* in Bolivia 3. Blue intensity data tends to have the largest spread of values and it is not unusal to observe a bimodal distribution of blue intensity data. However, the highlighted population in this histogram corrosponds with outliers in the green intensity population data and so is probably reworked.

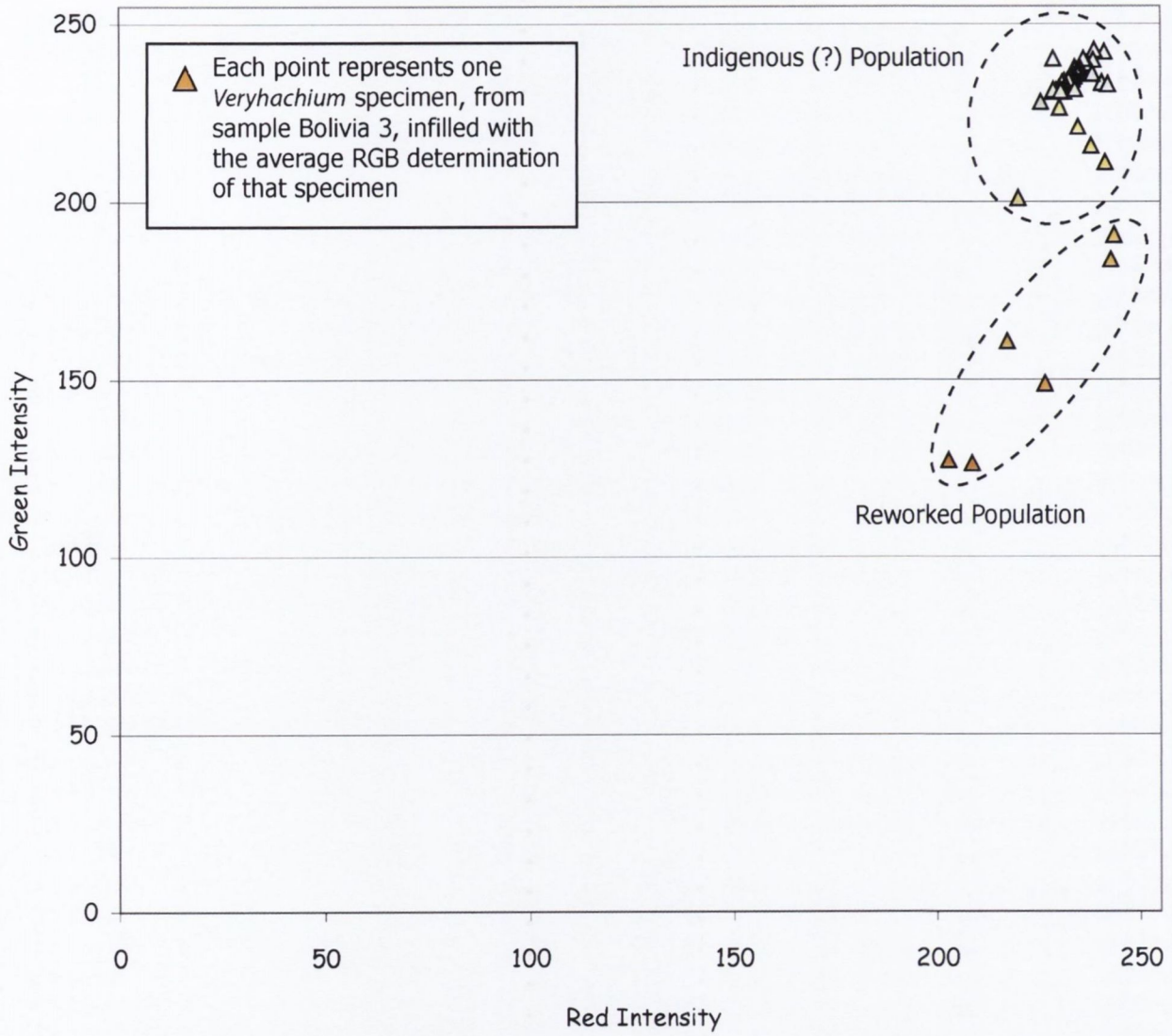

Figure 7.15: Average green intensity of *Veryhachium* specimens in Bolivia 3 versus average red intensity. Each data point has been infilled with the average RGB intensity of that specimen. Two populations are identified;a clearly reworked, darker, smaller population and a larger, lighter coloured population. This larger population may be indigenous to the sample, or may represent a different reworked population, or a combination of both.

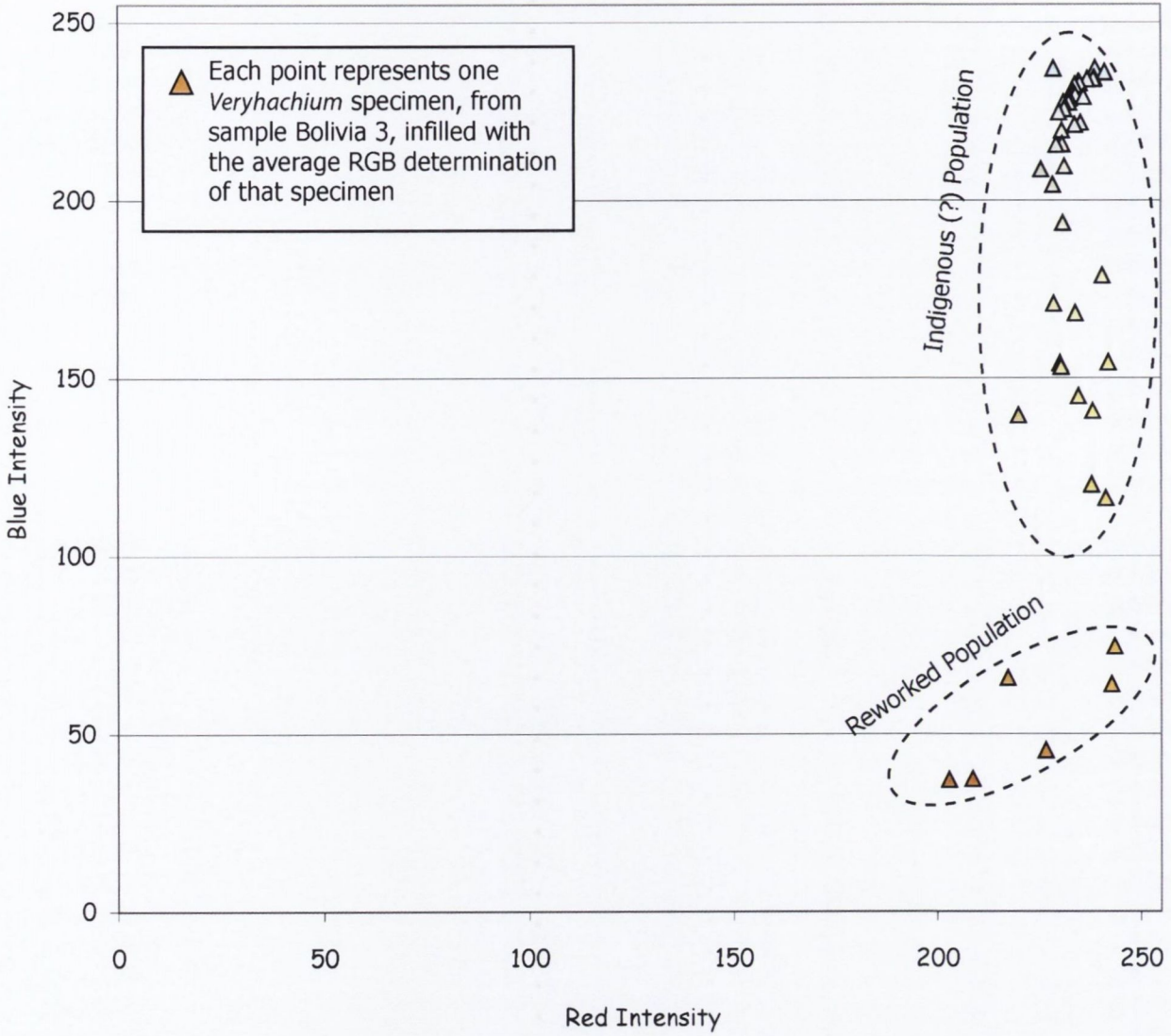

Figure 7.16: Average blue intensity of *Veryhachium* specimens in Bolivia 3 versus average red intensity. Each data point has been infilled with the average RGB intensity of that specimen. Two populations are identified;a clearly reworked, darker, smaller population and a larger, lighter coloured population. This larger population may be indigenous to the sample, or may represent a different reworked population, or a combination of both.

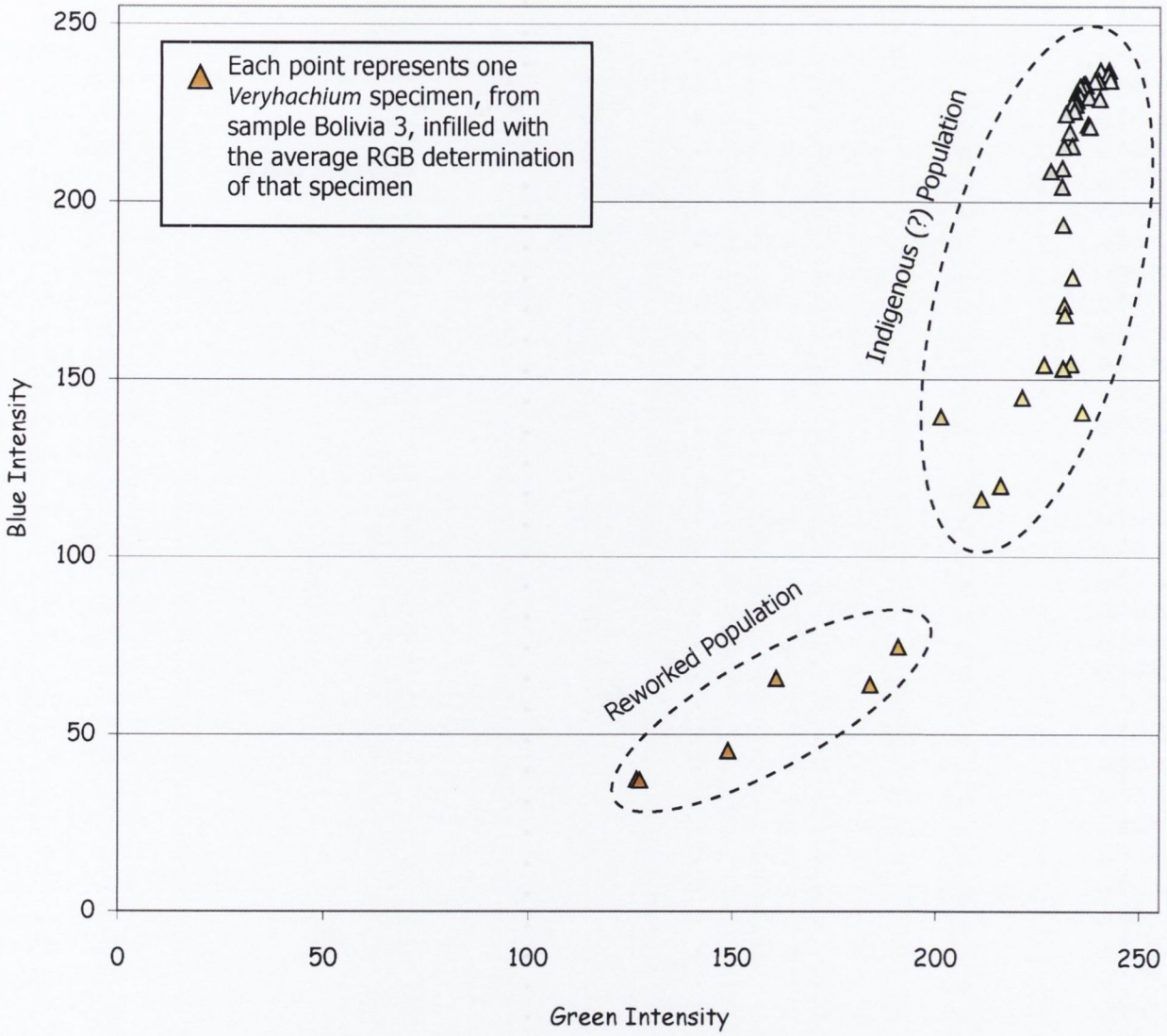

Figure 7.17: Average blue intensity of *Veryhachium* specimens in Bolivia 3 versus average green intensity. Each data point has been infilled with the average RGB intensity of that specimen. Two populations are identified;a clearly reworked, darker, smaller population and a larger, lighter coloured population. This larger population may be indigenous to the sample, or may represent a different reworked population, or a combination of both.

CHAPTER 8
CONLUSIONS AND FURTHER WORK

8.1. IMAGE ANALYSIS

Using image analysis to determine palynomorphs colour is a less subjective technique than traditional visual estimation.

RGB data gathered by both novice and experienced operators show little variation.

The RGB system is partially device dependant.

'Standards' developed to correct for variations within and between systems were of only limited success calibrating data.

The illumination properties of the microscope's halogen bulb change significantly over time affecting RGB determinations.

Variations between RGB determinations made using Qwin image analysis program and those made using Adobe Photoshop ® CS were minimal.

8.2. THERMAL MATURITY AND *VERYHACHIUM/TASMANITES* COLOUR

The colour of *Tasmanites* specimens appeared to be influenced by both the thermal maturity of the samples and the morphology of the specimen.

RGB determinations of well preserved *Veryhachium* colour were successfully calibrated against vitrinite reflectance data.

Green and blue *Veryhachium* intensity determinations are more sensitive to changes in maturity levels than red intensity.

RGB determinations of well preserved *Veryhachium* specimens can be used to calculate a vitrinite reflectance equivalent value.

Veryhachium RGB intensities follow clear maturation pathways, changing colour in samples postmature with respect to the oil window.

Spore colour is generally darker than *Veryhachium* colour at most thermal maturity levels.

8.3. Maturity Case Study

The maturity level of samples determined using *Veryhachium* colour concurred with the levels described in a Paleoservices report (1987).

8.3. Reworking Case Study

RGB data were used to successfully identify two different *Veryhachium* populations: a larger paler indigenous population and a smaller darker reworked population.

8.4. FURTHER WORK

The widespread application of the image analysis technique is dependant on the ability to understand and compensate for the variation in RGB determinations between different setups. The development of standards to calibrate data collected using different systems is one method which needs further investigation. The possibility of adjusting microscope, camera and illumination settings to produce similar RGB determinations from different setups also needs to be explored.

The correlation of vitrinite reflectance data and *Veryhachium* RGB determinations described in this study is based on only 22 sets of readings. No suitable samples were found with vitrinite reflectance values between 1.5 – 2.0%R_r. The larger the dataset used to correlate *Veryhachium* colour with vitrinite reflectance, the more reliable the calibration will be. It is important that additional determinations are made and incorporated into the dataset.

Further investigation into the effect that diameter and wall thickness has on the colour of *Tasmanites* vesicles is necessary if this palynomorph is to be used as a thermal maturity indicator. Experimental heating of tasmanite donated to this project is currently taking place in an attempt to learn more about the nature of this relationship.

References

Ager, D.V., (1980) *The Geology of Europe*. McGraw-Hill Book Company (UK) Limited, Maidenhead.

Al - Ameri, T.K., (1986) Observations on the wall structure and the excystment mechanism of acritarchs. *Journal of Micropalaeontology*, **52**, 27 - 35.

Alonso, J.L., Suarez, A., Rodríguez Fernández, Farias, P., Villegas, F. J., (1990) Mapa Geologico de España: La Pola de Gordón 103/ 13-7.

Arouri, K.R., Greenwood, P. F. and Walter, M. R., (2000) Biological affinities of Neoproterozoic acritarchs from Australia: microscopic and chemical characterisation. *Organic Geochemistry*, **31**, 75 - 89.

Barker, C.E., Goldstein, R. H., (1990) Fluid-inclusion technique for determining maximum temperature in calcite and its comparison to the vitrinite reflectance geothermometer. *Geology*, **18**(10), 1003-1006.

Barker, C.E., Pawlewicz, M. J., (1986) The correlation of vitrinite reflectance with maximum temperature in humic organic matter. In: G. Buntebarth, Stegena, L. (Ed.), *Paleogeothermics, Lecure Notes in Earth Science 5*. Springer, Berlin.

Barker, C.E., Pawlewicz, M. J., (1993) An empirical determination of the minimum number of measurements needed to estimate the mean random vitrinite reflectance of disseminated organic matter. *Organic Geochemistry*, **20**(6), 643 - 651.

Barker, C.E., Pawlewicz, M. J., (1994) Calculation of vitrinite reflectance from thermal histories and peak temperature: a comparison of methods. In: P.K.a.D. Mukhopadhyay, W. G. (Ed.), *Vitrinite Reflectance as a Maturity Parameter, 570, American Chemical Society Symposium series* pp. 216 - 229.

Barnard, P.C., Cooper, B. S. and Fisher, M. J., (1976) Organic maturation and hydrocarbon generation in the Mesozoic sediments of the Sverdrup basin, Arctic Canada. In: *4th International Palynological Conference*, pp. 581 - 588, Lucknow.

Batten, D.J., (1976) Use of transmitted light microscopy of sedimentary organic matter for evaluation of hydrocarbon source potential. In: *4th International Palynology Conference*, Lucknow.

Batten, D.J., (1981) Palynofacies, organic maturation and source potential for petroleum. In: J. Brooks (Ed.), *Organic maturation studies and fossil fuel exploration* pp. 201-223. Academic Press, London.

Batten, D.J., (1996) Palynofacies and Petroleum Potential. In: J. Jansonius, McGregor D. C. (Ed.), *Palynology: Principles and Applications, 3* pp. 1065 - 1078. American Association of Stratigraphic Palynologists Foundation, Salt Lake City.

Berry, C.M., Morel, E., Mojica, J., Villarroel, C., (2000) Devonian plants from Colombia, with discussion of the geological and palaeogeographical context. *Geological Magazine*, **137**(3), 257-268.

Bertrand, R., (1990) Correlations among the reflectances of vitrinite, chitinozoans, graptolites and scolecodonts. *Organic Geochemistry*, **15**, 565 - 574.

Bertrand, R., Achab, A., (1989) Equivalences between the reflectance of vitrinite, zooclasts (chitinozoans, graptolites and scolecondonts) and the color alteration of palynomorphs (spores and acritarchs). *Palynology*, **13**, 280.

Bertrand, R., Heroux, Y., (1987) Chitinozoan, Graptolite, and Scolecodont Reflectance As An Alternative to Vitrinite and Pyrobitumen Reflectance in Ordovician and Silurian Strata, Anticosti Island, Quebec, Canada. *AAPG Bulletin*, **71**(8), 951-957.

Beydoun, Z.R., (1988) *The Middle East: Regional geology and petroleum resources.* Scientific Press Ltd., Reading.

Beydoun, Z.R., Futyan, A. R. I., Jawzi, A. H., (1994) Jordan Revisited: Hydrocarbons habitat and potential. *Journal of Petroleum Geology*, **17**(2), 177-194.

Bezys, R.K., & Risk, M. J., (1990) The Long Rapids Formation: an Upper Devonian black shale in the Moose River Basin, northern Ontario. *Canadian Journal of Earth Sciences*, **27**(2).

Bless, M.J.M., (1991) Eustatic sea level and depth of a Late Cretaceous epicontinental sea: an example from NW Europe. *Geologie en Mijnbouw*, **70**(4), 339-347.

Brasier, M.D., (1980) *Microfossils.* Chapman and Hall, Ipswich.

Burnham, A.K., Sweeney, J. J, (1989) A chemical kinetic model of vitrinite maturation and reflectance. *Geochimica et Cosmochimica Acta*, **53**, 2649 - 2657.

Carr, A.D., Williamson, J. E., (1989) The relationship between aromaticity, vitrinite reflectance and maceral composition of coals: Implications for the use of vitrinite reflectance as a maturation parameter. *Organic Geochemistry*, **16**(1-3), 313-323.

Chesnut, D.R., (1996) Geologic framework for the coal-bearing rocks of the Central Appalachian Basin. *International Journal of Coal Geology*, **31**, 55-66.

Christensen, T., (1962) Alger. In: M. Bocher, Lange, M. and Sorenson, T. (Ed.), *Botanik 2 (Systematick Botanik)* pp. 1 - 178.

Clayton, G., (2003) Report on the palynology of thre samples from the Bermejo area, Bolivia.

Colbath, G.K., Grenfell, H. R., (1995) Review of biological affinities of Paleozoic acid-resistant, organic-walled eukaryotic algal microfossils (including "acritarchs"). *Review of Palaeobotany and Palynology*, **86**, 287-314.

Coleman, U., (1991) Palynology and intercontinental correlation of Upper Devonian and Lower Mississippian rocks from Kentucky and Indiana, U.S.A. In: *Department of Geology, Ph.D.* Trinity College, Dublin.

Conkin, J.E., Conkin, B. M., Walton, M. M. and Neff, E. D., (1981) Devonian and Early Mississippian smaller foraminiferans of southern Indiana and northwestern Kentucky. In: T.G. Roberts (Ed.), *GSA Cincinnati '81 Field Trip Guidebooks, 1* pp. 258. American Geological Institute.

Coogan, A.H., Heimlich, R. A., Malcuit, R. J., Bork, K. B. and Lewis, T. L., (1981) Early Mississippian deltaic sedimentation in central and northeastern Ohio. In: T.G. Roberts (Ed.), *GSA Cincinnati '81 Fieldtrip Guidebooks Volume II: Economic geology, structure*, 2 pp. 150.

Cooper, B.S., (1978) Estimation of the maximum temperatures attained in sedimentary rocks. In: G.D. Hobson (Ed.), *Developments in Petroleum Geology -1*. Applied Science Publishers Ltd., London.

Dalla Torre, M., Ferreiro Mahlmann, R., and Ernst, W. G., (1997) Experimental study on the pressure dependence of vitrinite maturation. *Geochimica et Cosmochimica Acta*, **61**(14), 2921-2928.

Dallmeyer, R.D., Martínez García, E., (1990) Pre-Mesozoic geology of Iberia, pp. 416. Springer-Verlag, Berlin; New York.

Davies, J.R., McNestry, A., Waters, R. A., (1991) Paleoenvironments and palynofacies of a pulsed transgression: the late Devonian and early Dinantian (Lower Carboniferous) rocks of southeast Wales. *Geological Magazine*, **128**(4), 355-380.

Davis, J.C., (2002) *Statistics and Data Analysis in Geology*. Wiley, New York: Chichester.

Dawson, J.W., (1888) *The geological history of plants*. Paul Kegan, London.

Deflandre, G., Deflandre M., (1964) Notes sure les acritarches. *Rev. Micropaleont.*, **7**(2), 111 - 114.

Dehandschutter, B., Vandycke, S., Sintubin, M., Vandenberghe, N., Wouters, L., (2005) Brittle fractures and ductile shear bands in argillaceous sediments: inferences from Oligocene Boom Clay (Belgium). *Journal of Structural Geology*, **27**, 1095-1112.

Delcambre, B., Pingot, J. L., (1993) Hastiere Dinant 53/7-8 Carte Geologique de Wallonie. Echelle: 1/25,000. Notice Explicative, pp. 73.

Deunff, J., (1954) *Veryhachium*, genre nouveau d'hystrichospheres du Primaire. *Compte Rendu Sommaire de Seances de la Societe Geologique de France*, **13**, 305 - 307.

Diver, W.L., Peat, C. J., (1979) On the interpretation and classification of Precambrian organic-walled microfossils. *Geology*, **7**, 401 - 404.

Dow, G.W., O'Connor, D. I., (1982) Kerogen maturity and type by reflected light microscopy applied to petroleum exploration, *How to assess maturation and paleotemperature: Short course number 7, Society of Economic Paleontologists and Mineralogists* pp. 289.

Downie, C., (1960) *Deunffia* and *Domasia,* new genera of hystrichospheres. *Micropaleontology*, **6**(2), 197 - 202.

Downie, C., (1963a) 'Hystrichospheres' (acritarchs) and spores of the Wenlock Shales (Silurian) of Wenlock, England. *Palaeontology*, **6**(4), 625 - 652.

Downie, C., (1967) The geological history of the microplankton. *Review of Palaeobotany and Palynology*, **1**, 269 - 281.

Downie, C., (1973) Observations on the nature of the acritarchs. *Palaeontology*, **16**, 239 - 259.

Downie, C., Evitt, W. R. and Sarjeant, W. A. S., (1963b) Dinoflagellates, hystrichosphers, and the classification of the acritarchs. *Stanford University Publications, Geological Sciences*, **7**, 1 - 16.

Eisenack, A., (1931) Neue Mikrofossilien des baltischen Silurs I. *Palaont. Z.*, **13**(1 - 2), 74 - 118.

Eisenack, A., (1958) *Tasmanites* Newton 1875 and *Leiosphaeridia* n.g. als Gattungen der Hystrichosphaeridea. *Palaeontographica A*, **110**(1 - 19).

Epstein, A.G., Epstein, J. B. and Harris, L. D., (1977) Conodont Color Alteration - an Index to Organic Metamorphism. *U. S. Geological Survey Professional Paper*, **995**.

Evitt, W.R., (1963a) A discussion and proposals concerning fossil dinoflagellates, hystrichospheres, and acritarchs. *Proceedings of the National Academy of Sciences*, **49**, 298 - 302.

Evitt, W.R., (1963b) A discussion and proposals concerning fossil dinoflagellates, hystrichospheres, and acritarchs. *Proceedings of the National Academy of Sciences*, **49**, 158 - 164.

Evitt, W.R., (1969) Dinoflagellates and other organisms in palynological preparations. In: R.H.a.S. Tschudy, R. A. (Ed.), *Aspects of palynology* pp. 439 - 479. Wiley - Interscience, New York.

Fang, H., Jianyu, C., (1992) The cause and mechanism of vitrinite reflectance anomalies. *Journal of Petroleum Geology*, **15**(4), 419-434.

Fensome, R.A., Williams, Graham L., Barss, M. Sedley, Freeman, Janette M., Hill, Jean M., (1991) Alphabetical listing of acritarch and fossil prasinophyte species. *Contributions Series - American Association of Stratigraphic Palynologists*, **26**, 111.

Fielitz, W., & Mansy, J., (1999) Pre- and synorogenic burial metamorphism in the Ardenne and neighbouring area (Rhenohercynian zone, central European Variscides). *Tectonophysics*, **309**, 227 - 256.

Fisher, M.J., Barnard, P. C., Cooper, B. S., (1980) Organic maturation and hydrocarbon generation in the Mesozoic sediments of the Sverdrup Basin, Arctic Canada. In: *Proceedings of the 4th International Palynological Conference, Lucknow (1976 - 77), 2*, pp. 581-588.

Forero Suarez, A., (1970) El Paleozoico Superior del flanco oriental de la Cordillera Central. *Geologia Colombiana*, **7**, 139-145.

Forero Suarez, A., (1990) The basement of the Eastern Cordillera, Colombia: An allochthonous terrane in northwestern South America. *Journal of South American Earth Sciences*, **3**(2/3), 141-153.

Forir, M.H., (1900) Carte Geologique de la Belgique Houyet-han-sur-Lesse. No 185 (planchettes 1-2 de la feuille LIX de la carte topographique).

Gentzis, T., de Freitas, T., Goodarzi, F., (1996) Thermal maturity of Lower Paleozoic sedimentary successions in Arctic Canada. *American Association of Petroleum Geologists Bulletin*, **80**, 1065 - 1084.

Geotrack, (2005) Thermal history reconstruction in well RH-3, RH-4 and WS-6 and fourteen outcrop samples from Jordan, based on AFTA, ZFTA and VR data. *Geotrack Report #903*.

Grayson, J.F., (1975) Relationship of palynomorph translucency to carbon and hydrocarbons in clastic sediments. In: B. Alpern (Ed.), *Petrographie de la matiere organique des sediments, relations avec la paleotemperature et le potential petrolier* pp. 261 - 273. Centre National de la Recherche Scientifique. Paris.

Gutjahr, C.C.M., (1966) Carbonization of pollen grains and spores and their application. *Leidse Geologische Medelingen*, **38**, 1 - 30.

Guy - Ohlson, D., (1988) Developmental Stages in the Life Cycle of Mesozoic *Tasmanites*. *Botanica Marina*, **31**, 447 - 456.

Guy - Ohlson, D., (1996) Chapter 7B. Prasinophycean algae. In: J.a.M.D.C. Jansonius (Ed.), *Palynology: principles and applications*, *1* pp. 181 - 189. American Association of Stratigraphical Palynologists Foundation.

Hamad, S., (1987) Composite log of RH-3, Risha field, Jordan. Natural Resources Authority.

Hanne, D., White, N., Butler, A. & Jones, S., (2004) Phanerozoic vertical motions of Hudson Bay. *Canadian Journal of Earth Sciences*, **41**(10).

Hart, G.F., (1986) Origin and classifications of organic matter in clastic systems. *Palynology*, **10**, 1-24.

Harvey, C., (2001) Palynology and coal analysis of the Devonian Campo Chico Formation, western Venezuela. In: *Centre for PalynologyUniversity of Sheffield, UK*. University of Sheffield, Sheffield.

Helson, S., (1995) Burial history of the Palaeozoic strata in Belgium as revealed by conodont colour alteration data and thickness distributions. *Geologische Rundschau*, **84**(4), 738 - 748.

Heroux, Y., Chagnon, A., Bertrand, R., (1979) Compilation and correlation of major thermal maturation indicators. *AAPG Bulletin*, **63**(12), 2128-2144.

Hillier, S., Marshall, J., (1988) A rapid technique to make polished thin sections of sedimentary organic matter concentrates. *Journal of Sedimentary Petrology*, **58**, 754 - 755.

Hooker, J., (1852) On the spheroidal bodies, resembling seeds, from the Ludlow Bone Bed. *Quarterly Journal of the Geological Society London*, **9**(1), 12.

Huang, W., (1996) Experimental study of vitrinite maturation: effects of temperature, time, pressure, water and hydrogen index. *Organic Geochemistry*, **24**(2), 233-241.

Husseini, M.I., (1992) Upper Paleozoic tectono-sedimentary evolution of the Arabian and adjoining plates. *Journal of the Geological Society, London*, **149**, 419-429.

I.C.C.P., (1998) The new vitrinite classification (ICCP System 1994). *Fuel*, **77**(5), 349 - 358.

Jux, U., (1968) Uber den Feinbau der Wandung bei *Tasmanites* Newton. *Palaeontographica B*, **124**, 112 - 124.

Jux, U., (1975) Phytoplankton aus dem mittleren oberdevon (nehden-stufe) des Südwestlichen Bergischen Landes (Rheinisches Schiefergebirge). *Palaeontographica Abt. B*, **149**, 113-138.

Keegan, J.B., Rasul, S. M., Shaheen, Y., (1991) of the lower Palaeozoic, Cambrian to Silurian, sediments of the Hashemite Kingdom of Jordan. *Review of Palaeobotany and Palynology*, **66** ((3-4)), 167-180.

Kenis, I., Muchez, P., Verhaert, G., Boyce, A. and Sintubin, M, (2005) Evolution during burial and Variscan deformation in the Lower Devonian rocks of the High Ardenne slate belt (Belgium); sources and causes of high-salinity and C-O-H-N fluids. *Contributions to Mineralogy and Petrology*, **150**(1), 102-118.

Kepferle, R.C., Roen, J. B., de Witt, W. Jr., Maynard, J. B., Ettensohn, F. R. and Barron, L. S., (1981) Chattanooga and Ohio Shales of the southern Appalachian Basin. In: T.G. Roberts (Ed.), *GSA Cincinnati '81 Field Trip Guidebooks*, *2* pp. 150. American Geological Institute.

Koch, J., Gunther, M., (1995) Relationship between random and maximum vitrinite reflectance. *Fuel*, **74**(11), 1687 - 1691.

Konert, G., Afifi, A. M., Al-Hajri, S. A., de Groot, K., Al Naim, A. A., Droste, H. J., (2001) Paleozoic stratigraphy and hydrocarbon habitat of the Arabian Plate. In: T. Marlan W., Jack C., Morgan, William A. (Ed.), *Petroleum provinces of the twenty-first century, AAPG Memoir, 74* pp. 483-515.

Krausel, R., (1941) Die Sporokarpien Dawsons, eine neue Thallophyten - Klasse des Devons. *Palaeontographica B*, **86**(4 - 6), 28 - 34.

Larsen, G.E., (1992) ODNR Division of Geological Surcey Core Record. File No. 3256.

Larsen, G.E., (1994) Reconnaissance bedrock geology of the Blakeslee, Ohio, quadrangle.

Legall, F.D., Barnes, C. R. and MacQueen, R., (1981) Thermal maturation, burial history and hotspot development, Paleozoic strata of Southern Ontario - Quebec, from conodont and acritarch colour alteration studies. *Bulletin of Canadian Petroleum Geology*, **29**(4), 492 - 539.

Lin, R., (1995) An interlaboratory comparsion of vitrinite reflectance measurment. *Organic Geochemistry*, **22**(1), 1-9.

Lindquist, S., (1998) The Santa Cruz - Tarija Province of Central South America: Los Monos - Machareti Petroleum System. *U. S. Geological Survey Open-File Report 99-50-C.*

Lo, H.B., (1988) Photometric methods for measuring the thermal maturity on strew-mounted kerogen slides. *Organic Geochemistry*, **12**(4), 303 - 307.

Loeblich Jr., A.R., Tappan, H., (1969) Acritarch excystment and surface ultrastructure, with descriptions of some Ordivician taxa. *Revista Espanola de Micropaleontologia*, **1**(1), 45 - 57.

Lüning, S., Shahin, Y. M., Loydell, D., Al-Rabi, H. T., Masri, A., Tarawneh, B., Kolonic, S., (2005) Anatomy of a world-class source rock: Distribution and depositional model of Silurian organic-rich shales in Jordan and implications for hydrocarbon potential. *AAPG Bulletin*, **89**(10), 1397-1257.

Madler, K., (1963) Die figurierten organischen Bestandteile der Posidonienschiefer. *Beih. Geol. Jb.*, **58**, 287 - 406.

Marshall, J.E.A., (1990) Determination of Thermal Maturity. In: P.R. Briggs. E. G. and Crowther (Ed.), *Palaeobiology, A Synthesis* pp. 511 - 515. Blackwell Science Ltd., Cambridge.

Marshall, J.E.A., (1991) Quantitative spore colour. *Journal of the Geological Society, London*, **148**, 223 - 233.

Martin, F., (1981) Acritarches du Famennien Inferieur a Villers-sur-Lesse (Belgique); Lower Famennian acritarchs from Villers-sur-Lesse, Belgique. *Bulletin de l'Institut Royal des Sciences Naturelles de Belgique. Sciences de la Terre*, **52**(2), 49-55.

Martin, F., (1993) Acritarchs: a review. *Biological Reviews*, **68**, 475 - 538.

McCaughan, G.A., (2002) Recognition of abnormal thermal histories of Jurassic source rocks from integrated analyses of vitrinite reflectance and organic matter colour/fluorescence. In: *Department of Geology, Ph.D.*, pp. 217. Trinity College Dublin, Dublin.

McGregor, D.C., & Camfield, M., (1976) Upper Silurian? to middle Devonian spores of the Moose River Basin, Ontario. *Geological Survey of Canada Bulletin*, **263**.

McNestry, A., (1989) The palynology of non marine to marine sequences of Devonian to Carboniferous age from Ireland and South Wales. In: *Department of Geology*. Trinity College, Dublin.

Miles, J.A., (1994) *Illustrated glossary of petroleum geochemistry*. Oxford University Press Inc., New York.

Miller, M.A., (1996) Chapter 11. Chitinozoa. In: J.a.M.D.C. Jansonius (Ed.), *Palynology: Principles and Applications*, *1* pp. 307 - 336. American Association of Stratagraphic Palynologists Foundation, Utah.

Molyneux, S.G., Manger, W. L. and Owens, B., (1984) Preliminary account of late Devonian palynomorph assemblages from the Bedford Shale and Berea Sandstone Formations of central Ohio, U.S.A. *Journal of Micropalaeontology*, **3**(2), 41 - 51.

Morrow, D.W., Issler, D. R., (1993) Calculation of Vitrinite Reflectance from Thermal Histories: A comparison of some methods. *AAPG Bulletin*, **77**(4), 610-624.

Muir, M.D., Sarjeant, W. A. S., (1971) An annotated bibliography of the Tasmanaceae and of related living forms (Algae: Prasinophyceae), *Microfossiles organiques du Paleozoique 3 Acritarches* pp. 60 - 111. Commission Internationale de Microflore du Paleozoique, Paris.

Mukhopadhyay, A., Al-Sulaimi, J., Al-Awadi E., Al-Ruwaih F., (1996) An overview of the Tertiary geology and hydrogeology of the northern part of the Arabian Gulf region with special reference to Kuwait. *Eath-Science Reviews*, **40**, 259-295.

Newton, E.T., (1875) On Tasmanite and Australian White Coal. *Geological Magazine*, **2**(8), 337 - 342.

Noger, M.C., (1988) Geologic Map of Kentucky. U.S. Geological Survey.

Norris, G., Sarjeant, W. A. S., (1965) A descriptive index of genera of fossil Dinophyceae and Acritarcha. *Palaeontological Bulletin, Wellington*, **40**, 72.

Obermajer, M., Fowler, M. G., Goodarzi, F. and Snowdon, L. R., (1996) Assessing thermal maturity of Palaeozoic rocks from reflectance of chitinozoa as constrained by gechemical indicators: an example from southern Ontario, Canada. *Marine and Petroleum Geology*, **13**(8), 907 - 919.

Orton, E., (1883) A source of bituminous matter of the black shales of Ohio. In: *Proceedings of the American Association of Advanced Science*, pp. 373 - 384, 31st Meeting, Montreal.

Paleoservices, (1987a) Well: RH-3 Petroleum Geochemical Report (Interval 130m - 4,005m (T.D. 4,204m)).

Paleoservices, (1987b) Well RH-3, Stratigraphical/Paleontological final report (Interval 10m - 4,203m).

Pashin, J.C., (1992) Paleoecology and sedimentology of the dysaerobic Bedford fauna (Late Devonian), Ohio and Kentucky (USA). *Palaeogeography, Palaeoclimatology, Palaeoecology*, **91**(1-2), 21-34.

Pearson, D.L., (1984) Pollen/Spore Color 'Standard'. *Phillips Petroleum Company, Exploration Projects Section.*

Pepper, J.F., de Witt, W. Jr., Demarest, D. F., (1954) Geology of the Bedford Shale and Berea Sandstone in the Appalachian Basin. *U. S. Geological Survey Professional Paper*, **P 0259**.

Playford, G., (1977) Lower to middle Devonian acritarchs of the Moose River Basin, Ontario. *Geological Survey of Canada Bulletin*, **279**.

Playford, G., (2002) *Acritarchs and Prasinophyte phycomata: A short course.* AASP Foundation Contributions Series No. 41.

Playford, G., Dettmann, M. E., (1996) Chapter 8. Spores. In: J. Jansonius, McGregor D. C. (Ed.), *Palynology: Principles and Applications*, *1* pp. 227-261. American Association of Stratigraphic Palynologists Foundation.

Qteishat, A., (1989) Composite log of WS-6 well, Sirhan Field, Jordan. Natural Resources Authority.

Quinlan, G.M., Beaumont, C., (1984) Appalachian thrusting, lithospheric flexure, and the Paleozoic stratigraphy of the Eastern Interior of North America. *Canadian Journal of Earth Sciences*, **21**, 973-996.

Ralph, T.S., (1865) Observations on the microscopical characters presented by a mineral (Dysodil) from Tasmania. *Transactions of the Royal Society Victoria*, **6**, 7.

Rejebian, V.A., Harris, A. G., Huebner, J. S., (1987) Conodont color and textural alteration: An index to regional metamorphism, contact metamorphism, and hyrdrothermal alteration. *Geological Society of America Bulletin*, **99**, 471-479.

Revill, A.T., Volkman, J. K., O'Leary, T., Summons, R. E., Boreham, C. J., Banks, M. R., Denwer, K., (1994) Hydrocarbon biomarkers, thermal maturity, and depositional setting of tasmanite oil shales from Tasmania, Australia. *Geochimica et Cosmochimica Acta*, **58**(18), 3803-3822.

Roberts, T.G., (1981a) GSA Cincinnati '81 Fieldtrip Guidebooks Volume 1: Stratigraphy, sedimentology, *1*, pp. 258. American Geological Institute.

Roberts, T.G., (1981b) GSA Cincinnati '81 Fieldtrip Guidebooks Volume 2: Economic geology, structure, *2*, pp. 150. American Geological Institute.

Root. S. and Onasch, C.M., (1999) Structure and tectonic evolution of the transitional region between the central Appalachian foreland and interior cratonic basins. *Tectonophysics*, **305**, 205 - 223.

Rostrepo, J.J., Toussaint, J. F., (1988) Terranes and continental accretion in the Colombian Andes. *Episodes*, **11**(3), 189-193.

Sadooni, F.N., Dalqamouni, A, (1998) Geology and petroleum prospects of Upper Triassic sediments, Jordan. *Marine and Petroleum Geology*, **15**(8), 783-801.

Sanford, B.V., & Grant, A. C., (1990) New findings relating to the stratigraphy and structure of the Hudson Platform, Current research; Part D, Interior Plains and

Arctic Canada--Recherches en cours; Partie D, Plaines interieures et region arctique du Canada. *Paper - Geological Survey of Canada*, **90 - 1D**.

Sanford, B.V., & Norris, A. W., (1975a) Devonian Stratigraphy of the Hudson Platform, Part 1: Stratigraphy and Economic Geology. *Geological Survey of Canada Memoir*, **379**, 124.

Sanford, B.V., & Norris, A. W., (1975b) Devonian Stratigraphy of the Hudson Platform, Part II: Outcrop and Subsurface Sections. *Geological Survey of Canada Memoir*, **379**, 248.

Sanford, B.V., Norris, A. W, (1973) The Hudson Platform. In: R.G. McCrossan (Ed.), *The future petroleum provinces of Canada, their geology and potential: Canadian Society of Petroleum Geology Memoir no. 1* pp. 387-409.

Sarjeant, W.A.S., Stancliffe, R. P. W., (1994) The *Micrhystridium* and *Veryhachium* complexes (Acritarcha: Acanthomorphitae and Polygonomorphitae): a taxonomic reconsideration. *Micropaleontology*, **40**(1), 1 - 79.

Schopf, J.M., Wilson, L. R. and Bentall, R., (1964) An annotated synopsis of Paleozoic fossil spores and the definition of generic groups. *Rep. Invest. Ill. St. Geol. Surv.*, **91**, 1 - 73.

Schumacher, G.A., (1995) Reconnaissance bedrock geology of the Chillicothe East, Ohio, quadrangle. Ohio Division of the Geological Survey.

Selley, R.C., (1998) *Elements of petroleum geology*. Academic Press, San Diego, California; London.

Shinaq, R., (1996) Subsurface Triassic sediments in Jordan: Stratigraphic and depositional characteristics, and hydrocarbon potential. *Journal of Petroleum Geology*, **19**(1), 57-76.

Slucher, E.R., (1997) Bedrock geology of the Sunbury, Ohio, quadrangle. Ohio Division of the Geological Survey.

Smith, P.M.R., (1983) Spectral Correlation of Spore Coloration Standards. In: J. Brooks (Ed.), *Petroleum Geochemistry and Exploration of Europe*, *Geological Society Special Publication No. 12* pp. 289 - 294. Blackwell Scientific Publications, Oxford.

Sommer, F.W., (1956) South American Paleozoic Sporomorphae without haptotypic structures. *Micropaleontology*, **2**(2), 175 - 181.

Sommer, F.W., (1960) Controversias sistematicas acerca do genero *Tasmanites*. In: *Anais. Acad. bras. Cienc.*, *3*, pp. XV - XVI.

Stach, E., Mackowsky, M.-TH., Teichmüller, M., Taylor, G. H., Chandra, D. and Teichmüller, R., (1982) *Stach's Textbook of Coal Petrology*. Gebrüder, Berlin.

Staplin, F.L., (1969a) Sedimentary organic matter, organic metamorphism and oil and gas occurrence. *Bulletin of Canadian Petroleum Geology*, **17**, 47 - 66.

Staplin, F.L., (1969b) Sedimentary organic matter, organic metamorphism, and oil and gas occurrence. *Bulletin of Canadian Petroleum Geology*, **17**(1), 47-66.

Staplin, F.L., (1977) Interpretation of thermal history from colour of particulate organic matter - a review. *Palynology*, **1**, 9 - 18.

Staplin, F.L., (1982) Determination of Thermal Alteration Index from color of exinite (pollen, spores). *How to Assess Maturation and Paleotemperatures, Society of Economic Paleontologists and Mineralogists, Short Course Number Seven.*

Staplin, F.L., Jansonius, J. and Pocock, S. A. J., (1965) Evaluation of some acritarchous Hystrichosphere genra. *Neues Jahrbuch fuer Geologie und Palaeontologie. Abhandlungen*, **123**, 167 - 201.

Strother, P.K., (1996) Acritarchs. In: J.a.M.D.C. Jansonius (Ed.), *Palynology: principles and applications, 1* pp. 81 - 106. American Association of Stratigraphic Palynologists Foundation.

Talyzina, N.M., Moczydlowska, M., (2000) Morphological and ultrastructural studies of some acritarchs from the Lower Cambrian Lukati Formation, Estonia. *Review of Palaeobotany and Palynology*, **112**, 1 - 21.

Tappan, H., (1980) *The paleobiology of plant protists*. W. H. Freeman & Co., San Francisco.

Taugourdeau-Lantz, J., (1979) Les Tasmanacees, kystes de Prasinophyceae fossiles; The Tasmanaceae, fossil cysts of Prasinophyceae. *Bulletin des Centres de Recherches Exploration-Production Elf-Aquitaine*, **3**(2), 833-841.

Taylor, G.H., Teichmüller, M., Davis, A., Diessel, C. F. K., Littke, R. and Robert, P., (1998) *Organic Petrology*. Gebrüder Borntraeger, Berlin.

Teichmüller, M., (1987) Recent advances in coalification studies and their application to geology. In: A.C. Scott (Ed.), *Coal and Coal-bearing Strata: Recent Advances, Geological Society Special Publication No. 32* pp. 332. Blackwell Scientific Publications.

Timofeyev, B.V., (1966) *Investigations of ancient microplankton suites*, Moscow, Leningrad.

Tissot, B., Durand, B., Espitalie, J., Combaz, (1974) Influence of Nature and Diagenesis of Organic Matter in Formation of Petroleum. *AAPG Bulletin*, **58**(3), 499-506.

Traverse, A., (1988) *Paleopalynology*. Unwin Hyman Ltd., London.

Tricker, P.M., Marshall, J. E. A. and Badman, T. D., (1992) Chitinozoan reflectance: a Lower Palaeozoic thermal maturity indicator. *Marine and Petroleum Geology*, **9**(3), 302 - 307.

Ujiie, Y., (2001) Brightness of pollen as an indicator of thermal alteration by means of a computer-driven image processsor: statistical thermal alteration index (stTAI). *Organic Geochemistry*, **32**, 127 - 141.

Van de Laar, J.G.M., David, P., (1998) Determination of spore colour alteration by means of colour image analysis. *Review of Palaeobotany and Palynology*, **103**, 41 - 44.

Van Gijzel, P., (1982) Characterization and identification of kerogen and bitumen and determination of thermal maturation by means of qualitative and quantitative microscopical techniques, *How to assess maturation and paleotemperatures, Society of Economic Paleontologists and Mineralogists, Short Course Number Seven.*

Vandenberghe, N., Laenen, B., Van Echelpoel, E., Lagrou, D., (1997) Cyclostratigraphy and climatic eustasy. Example of the rupelian stratotype. *Comptes Rendus de l'Académie des Sciences - Series IIA - Earth and Planetary Science*, **325**(5), 305-315.

Vavrdova, M., Bek, J., Dufka, P., Isaacson, P. E., (1996) Palynology of the Devonian (Lochkovian to Tournaisian) sequence, Madre de Díos Basin, northern Bolivia. *Věstník Českého geologického ústavu*, **71**(4), 333-348.

Wall, D., (1962) Evidence from Recent plankton regarding the biological affinites of *Tasmanites* Newton, 1875 and *Leiosphaeridia* Eisenack, 1958. *Geological Magazine*, **99**(4), 353 - 362.

Wall, D., Downie, C., (1963) Permian hystrichospheres from Britain. *Palaeontology*, **5**(4), 770 - 784.

Wallace, P., (1972) The geology of the Palaeozoic rocks of the south-western part of the Cantabrian Cordillera, North Spain. *Proceedings of the Geologists' Association*, **83**, 57-95.

Ward, C., (1984) Coal Geology and Coal Technology, pp. 345. Blackwell Scientific Publications, Singapore.

Wethered, E., (1886) On the occurrence of spores of plants in the Lower Limestone Shales of the Forest of Dean Coalfield and in the Black Shales of Ohio, United States. In: *Proc. Cotteswold Nat. Fld. Club, 8*, pp. 167 - 173.

Wetzel, O., (1933) Die organischerSubstanzerhaltenen Mikrofossilien des baltischen Kreide-Feuersteins mit einem sediment-petrographischen und stratigraphischen Anahng. *Palaeontographica, Abteilung A*, **78**, 1 - 110.

Wicander, R., (2002) Acritarchs: Proterozoic and Paleozoic enigmatic organic-walled microfossils. In: *Instruments, Methods and Missions for Astrobiology IV, Proceedings of The International Society for Optical Engineering, 4495* (Ed. by R.B. Hoover, Levin, G. V., Paepe, R. R., Rozanov, A. Y.), pp. 331-340, San Diego.

Wilkins, R.W.T., Wilmshurst, J. R., Hladky, G., Ellacott, M. V. and Buckingham, C.P., (1995) Should fluorescence alteration replace vitrinite reflectance as a major tool

for thermal maturity determination in oil exploration. *Organic Geochemistry*, **22**(1), 191-209.

Williams, S.H., Burden, E. T., and Mukhopadhyay, (1998) Thermal maturity and burial history of Paleozoic rocks in western Newfoundland. *Canadian Journal of Earth Sciences*, **35**, 1307 - 1322.

Winslow, M.R., (1962) Plant spores and other microfossils from the Upper Devonian and Lower Mississippian rocks of Ohio. *U. S. Geological Survey Professional Paper*, **364**, 1 - 93.

Woodcock, N., Strachan, R., (2000) Geological History of Britain and Ireland, pp. 423. Blackwell Science Ltd., Cambridge.

Yule, B., Roberts, S., Marshall, J. E. A. and Milton, J. A., (1998) Quantitative spore colour measurement using colour image analysis. *Organic Geochemistry*, **28**(3/4), 139 - 149.

Zapata, A., Sanchez, A., Segundo Carrasco, V., Cardona, A, Jorge Galdos, H., Fredy Cerron, Z., Semper, T., (2005) The Lower Carboniferous of the western edge of Gondwana in Peru and Bolivia: Distribution of sedimentary basins and associated magmatism. In: *Extended abstracts: 6th International Symposium on Andean Geodynamics*, Barcelona.

APPENDIX I

SAMPLES

All palynological and polished resin slides are stored in the Department of Geology, Trinity College, Dublin. Unless otherwise stated, all remaining rock samples are also stored in Trinity College.

Sample Wales 1 was donated by the British Geological Survey, sample number MPA 24131. Remaining rock residue and palynological slides are stored by the British Geological Survey.

Sample Name	*TCD Number*		*Slide Type*	
Bolivia 3	T.C.D. 56735	T.C.D. 56735a	Bolivia 3 1	Palynological Slide
Can9	T.C.D. 56736	T.C.D. 56736A	Can9 (1)	Palynological Slide
		T.C.D. 56736B	Can9 (2)	Palynological Slide
		T.C.D. 56736C	Polished Resin Slide	
CC3	T.C.D. 56737	T.C.D. 56737A	CC3 (1)	Palynological Slide
		T.C.D. 56737B	CC3 (2)	Palynological Slide
		T.C.D. 56737C	CC3 (3)	Palynological Slide
		T.C.D. 56737D	CC3 (4)	Palynological Slide
		T.C.D. 56737E	Polished Resin Slide	
JM5	T.C.D. 56738	T.C.D. 56738A	JM5 (1)	Palynological Slide
		T.C.D. 56738B	JM5 (2)	Palynological Slide
P11	T.C.D. 56739	T.C.D. 56739A	P11 (1)	Palynological Slide
		T.C.D. 56739B	Polished Resin Slide	
		T.C.D. 56739C	Polished Resin Slide	
		T.C.D. 56739D	Polished Resin Slide	
P12	T.C.D. 56740	T.C.D. 56740A	P12 (1)	Palynological Slide
		T.C.D. 56740B	Polished Resin Slide	
P13	T.C.D. 56741	T.C.D. 56741A	P13 (1)	Palynological Slide
P14	T.C.D. 56742	T.C.D. 56742A	P14 (1)	Palynological Slide
		T.C.D. 56742B	Polished Resin Slide	
P22	T.C.D. 56743	T.C.D. 56743A	P22 (1)	Palynological Slide
		T.C.D. 56743B	Polished Resin Slide	
P23	T.C.D. 56744	T.C.D. 56744A	P23 (1)	Palynological Slide
		T.C.D. 56744B	Polished Resin Slide	
P24	T.C.D. 56745	T.C.D. 56745A	P24 (1)	Palynological Slide
P25	T.C.D. 56746	T.C.D. 56746A	P25 (1)	Palynological Slide
		T.C.D. 56746B	Polished Resin Slide	
		T.C.D. 56746C	Polished Resin Slide	
		T.C.D. 56746D	Polished Resin Slide	
PET3	T.C.D. 56747	T.C.D. 56747A	PET3 (1)	Palynological Slide
		T.C.D. 56747B	Polished Resin Slide	
		T.C.D. 56747C	Polished Resin Slide	
		T.C.D. 56747D	Polished Resin Slide	
PET6	T.C.D. 56748	T.C.D. 56748A	PET6 (1)	Palynological Slide
		T.C.D. 56748B	PET6 (2)	Palynological Slide
		T.C.D. 56748C	Polished Resin Slide	
		T.C.D. 56748D	Polished Resin Slide	
PET9	T.C.D. 56749	T.C.D. 56749A	PET9 (1)	Palynological Slide
Rh19-p12	T.C.D. 56750	T.C.D. 56750A	Rh19-p12 (1	Palynological Slide
		T.C.D. 56750B	Rh19-p12 (2	Palynological Slide
		T.C.D. 56750C	Polished Resin Slide	
Sun 3	T.C.D. 56751	T.C.D. 56751A	Sun 3 (1)	Palynological Slide
		T.C.D. 56751B	Sun 3 (2)	Palynological Slide
		T.C.D. 56751C	Sun 3 (3)	Palynological Slide
		T.C.D. 56751D	Sun 3 (5)	Palynological Slide
		T.C.D. 56751E	Sun 3 (6)	Palynological Slide

Sample Name	*TCD Number*		*Slide Type*
Sun 3 (contd.)		T.C.D. 56751F	Sun 3 (7) Palynological Slide
		T.C.D. 56751G	Polished Resin Slide
		T.C.D. 56751H	Polished Resin Slide
Sun 7	T.C.D. 56752	T.C.D. 56752A	Sun 7 (1) Palynological Slide
		T.C.D. 56752B	Sun 7 (2) Palynological Slide
		T.C.D. 56752C	Sun 7 (3) Palynological Slide
		T.C.D. 56752D	Sun 7 (6) Palynological Slide
		T.C.D. 56752E	Polished Resin Slide
TL1	T.C.D. 56753	T.C.D. 56753A	TL1 (1) Palynological Slide
		T.C.D. 56753B	TL1 (2) Palynological Slide
		T.C.D. 56753C	TL1 (3) Palynological Slide
TL2	T.C.D. 56754	T.C.D. 56754A	TL2 (1) Palynological Slide
		T.C.D. 56754B	TL2 (2) Palynological Slide
		T.C.D. 56754C	TL2 (3) Palynological Slide
		T.C.D. 56754D	TL2 (4) Palynological Slide
		T.C.D. 56754E	TL2 (5) Palynological Slide
		T.C.D. 56754F	Polished Resin Slide
TL3	T.C.D. 56755	T.C.D. 56755A	TL3 (1) Palynological Slide
		T.C.D. 56755B	TL3 (2) Palynological Slide
TL7	T.C.D. 56756	T.C.D. 56756A	TL7 (1) Palynological Slide
		T.C.D. 56756C	TL7 (2) Palynological Slide
		T.C.D. 56756B	TL7 (3) Palynological Slide
		T.C.D. 56756D	Polished Resin Slide
V4	T.C.D. 56757	T.C.D. 56757A	V4 (1) Palynological Slide
		T.C.D. 56757B	V4 (2) Palynological Slide
		T.C.D. 56757C	Polished Resin Slide
		T.C.D. 56757C	Polished Resin Slide
V5	T.C.D. 56758	T.C.D. 56758A	V5 (1) Palynological Slide
		T.C.D. 56758B	Polished Resin Slide
V7	T.C.D. 56759	T.C.D. 56759A	V7 (1) Palynological Slide
		T.C.D. 56759B	V7 (2) Palynological Slide
		T.C.D. 56759C	V7 (3) Palynological Slide
		T.C.D. 56759D	Polished Resin Slide
		T.C.D. 56759E	Polished Resin Slide
V8	T.C.D. 56760	T.C.D. 56760A	V8 (1) Palynological Slide
		T.C.D. 56760B	V8 (2) Palynological Slide
		T.C.D. 56760B	Polished Resin Slide
Va115	T.C.D. 56761	T.C.D. 56761A	Va115 (1) Palynological Slide
		T.C.D. 56761B	Polished Resin Slide
Va118	T.C.D. 56762	T.C.D. 56762A	Va118 (1) Palynological Slide
		T.C.D. 56762B	Polished Resin Slide
Va47	T.C.D. 56763	T.C.D. 56763A	Va47 (1) Palynological Slide
		T.C.D. 56763B	Va47 (2) Palynological Slide
		T.C.D. 56763C	Polished Resin Slide
Wales 1	T.C.D. 56764	T.C.D. 56764A	Wales 1 (1) Palynological Slide
		T.C.D. 56764B	Wales 1 (3) Palynological Slide

Sample Name	*TCD Number*		*Slide Type*
Wales 1 (Contd.)		T.C.D. 56764C	Wales 1 (4) Palynological Slide
		T.C.D. 56764D	Wales 1 (5) Palynological Slide
		T.C.D. 56764E	Wales 1 (6) Palynological Slide
		T.C.D. 56764F	Polished Resin Slide
WC11	T.C.D. 56765	T.C.D. 56765A	WC11 (1) Palynological Slide
		T.C.D. 56765B	WC11 (2) Palynological Slide
		T.C.D. 56765C	Polished Resin Slide
		T.C.D. 56765D	Polished Resin Slide
WC15	T.C.D. 56766	T.C.D. 56766A	WC15 (1) Palynological Slide
		T.C.D. 56766B	WC15 (2) Palynological Slide
		T.C.D. 56766C	WC15 (3) Palynological Slide
		T.C.D. 56766D	WC15 (4) Palynological Slide
		T.C.D. 56766E	WC15 (5) Palynological Slide
		T.C.D. 56766F	Polished Resin Slide
		T.C.D. 56766G	Polished Resin Slide
WC17	T.C.D. 56767	T.C.D. 56767A	WC17 (1) Palynological Slide
		T.C.D. 56767B	WC17 (2) Palynological Slide
		T.C.D. 56767C	Polished Resin Slide
		T.C.D. 56767D	Polished Resin Slide

APPENDIX II

VITRINITE AND CHITINOZOA REFLECTANCE HISTOGRAMS

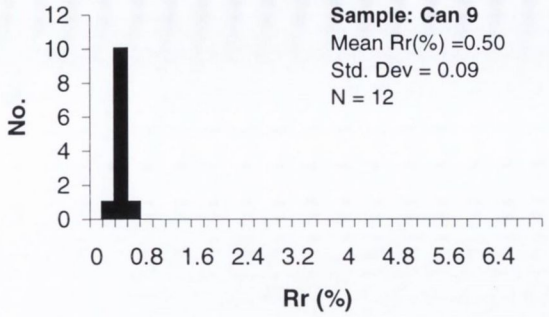
Sample: Can 9
Mean Rr(%) =0.50
Std. Dev = 0.09
N = 12
No.
Rr (%)

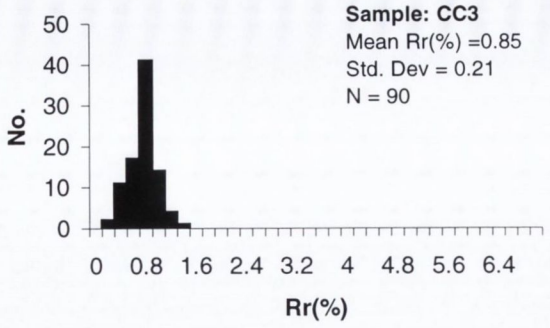
Sample: CC3
Mean Rr(%) =0.85
Std. Dev = 0.21
N = 90
No.
Rr(%)

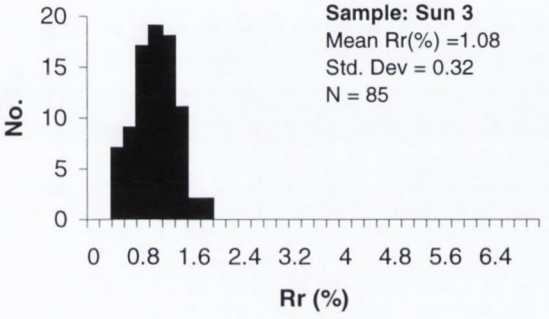
Sample: Sun 3
Mean Rr(%) =1.08
Std. Dev = 0.32
N = 85
No.
Rr (%)

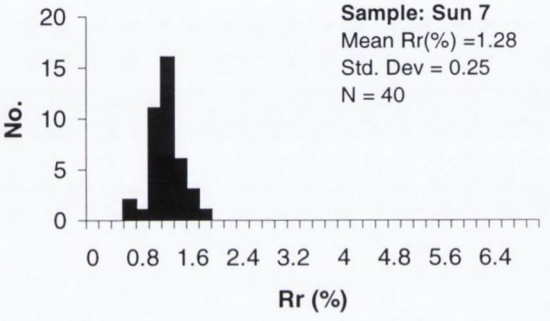
Sample: Sun 7
Mean Rr(%) =1.28
Std. Dev = 0.25
N = 40
No.
Rr (%)

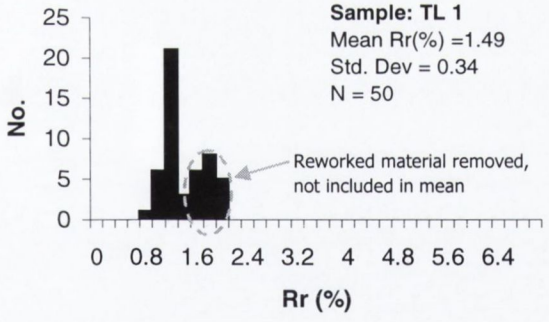
Sample: TL 1
Mean Rr(%) =1.49
Std. Dev = 0.34
N = 50
Reworked material removed,
not included in mean
No.
Rr (%)

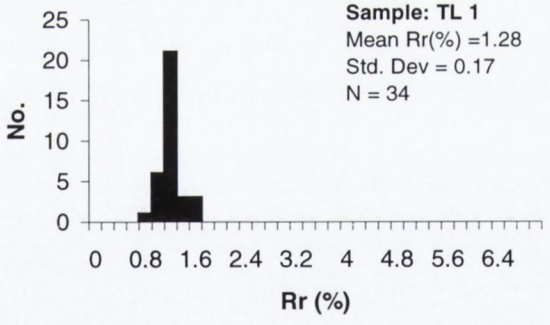
Sample: TL 1
Mean Rr(%) =1.28
Std. Dev = 0.17
N = 34
No.
Rr (%)

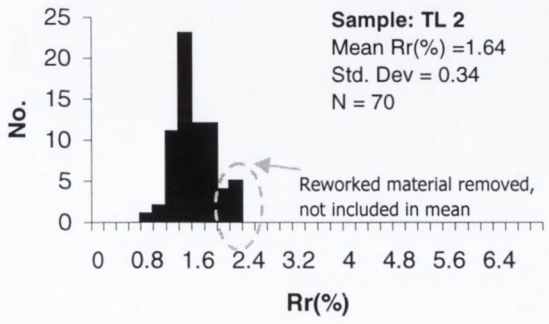
Sample: TL 2
Mean Rr(%) =1.64
Std. Dev = 0.34
N = 70
Reworked material removed,
not included in mean
No.
Rr(%)

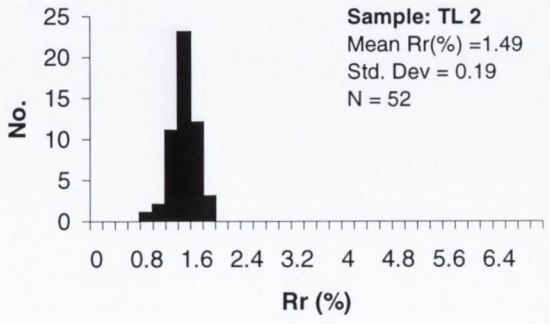
Sample: TL 2
Mean Rr(%) =1.49
Std. Dev = 0.19
N = 52
No.
Rr (%)

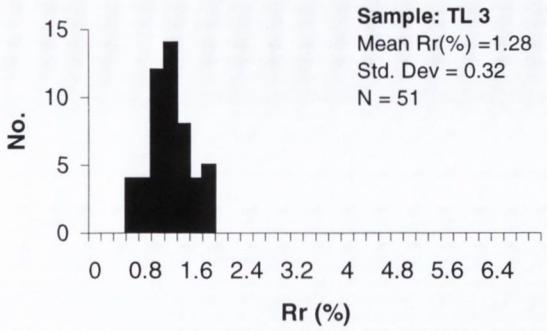
Sample: TL 3
Mean Rr(%) =1.28
Std. Dev = 0.32
N = 51
No.
Rr (%)

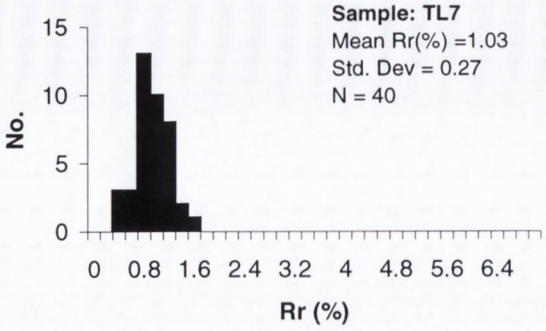
Sample: TL7
Mean Rr(%) =1.03
Std. Dev = 0.27
N = 40
No.
Rr (%)

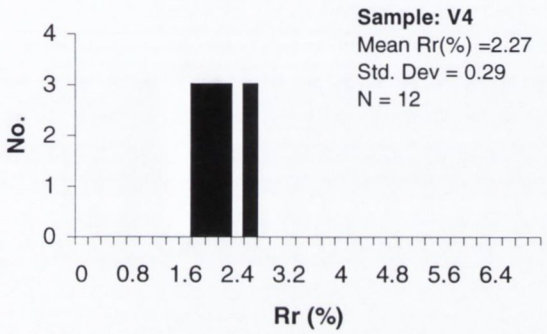
Sample: V4
Mean Rr(%) =2.27
Std. Dev = 0.29
N = 12
No.
Rr (%)

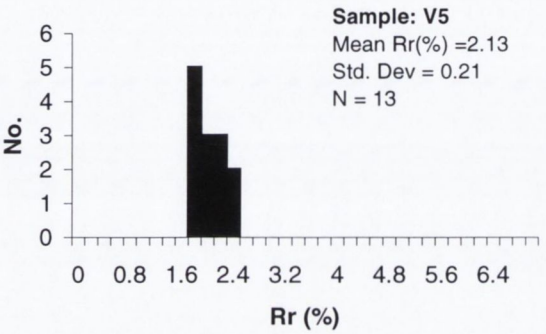
Sample: V5
Mean Rr(%) =2.13
Std. Dev = 0.21
N = 13
No.
Rr (%)

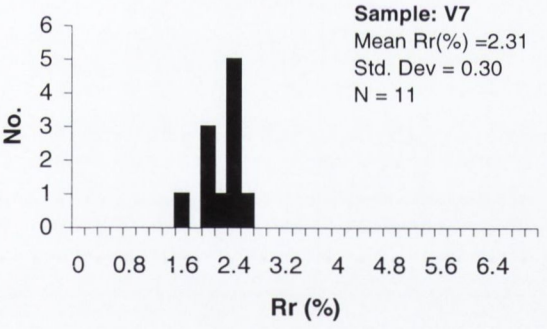
Sample: V7
Mean Rr(%) =2.31
Std. Dev = 0.30
N = 11
No.
Rr (%)

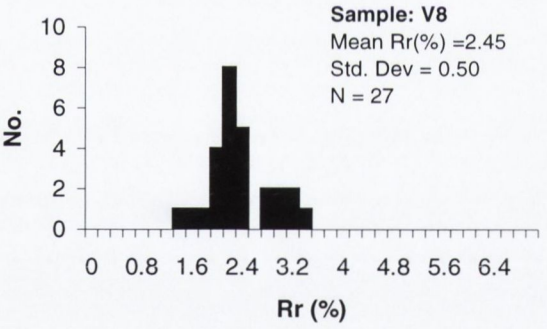
Sample: V8
Mean Rr(%) =2.45
Std. Dev = 0.50
N = 27
No.
Rr (%)

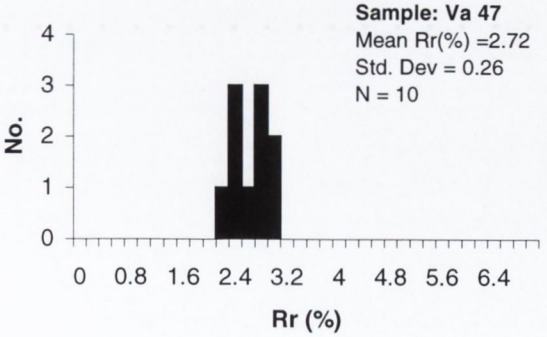
Sample: Va 47
Mean Rr(%) =2.72
Std. Dev = 0.26
N = 10
No.
Rr (%)

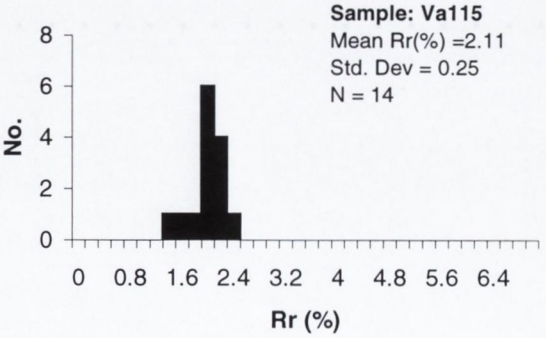
Sample: Va115
Mean Rr(%) =2.11
Std. Dev = 0.25
N = 14
No.
Rr (%)

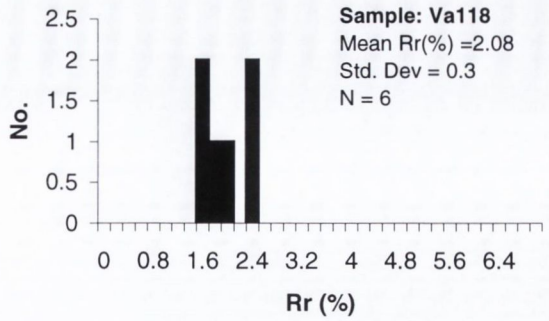
Sample: Va118
Mean Rr(%) =2.08
Std. Dev = 0.3
N = 6
No.
Rr (%)

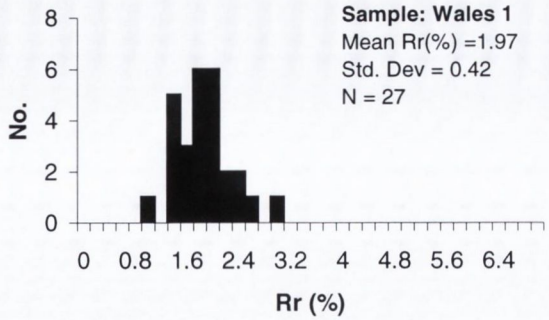
Sample: Wales 1
Mean Rr(%) =1.97
Std. Dev = 0.42
N = 27
No.
Rr (%)

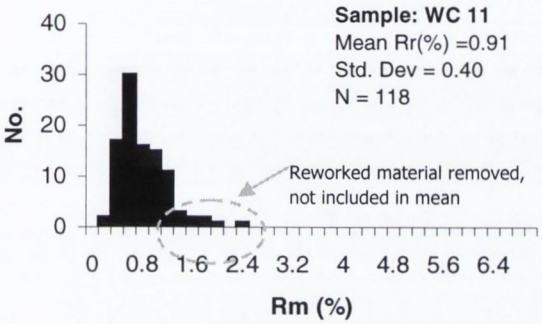
Sample: WC 11
Mean Rr(%) =0.91
Std. Dev = 0.40
N = 118
Reworked material removed,
not included in mean
No.
Rm (%)

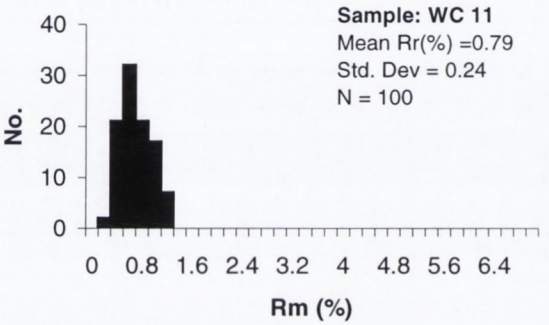
Sample: WC 11
Mean Rr(%) =0.79
Std. Dev = 0.24
N = 100
No.
Rm (%)

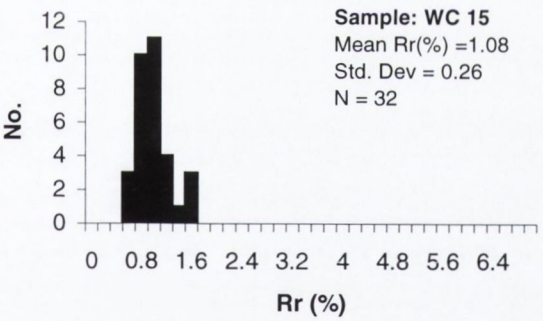
Sample: WC 15
Mean Rr(%) =1.08
Std. Dev = 0.26
N = 32
No.
Rr (%)

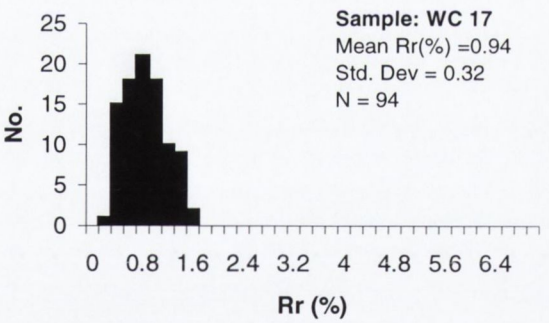
Sample: WC 17
Mean Rr(%) =0.94
Std. Dev = 0.32
N = 94
No.
Rr (%)

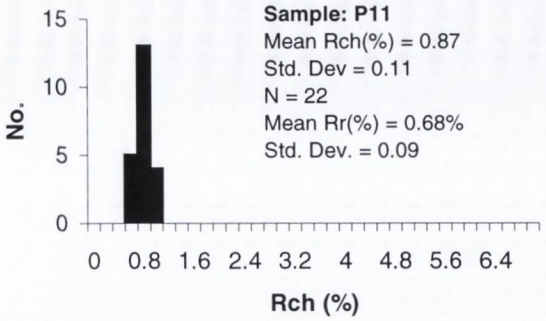
Sample: P11
Mean Rch(%) = 0.87
Std. Dev = 0.11
N = 22
Mean Rr(%) = 0.68%
Std. Dev. = 0.09
No.
Rch (%)

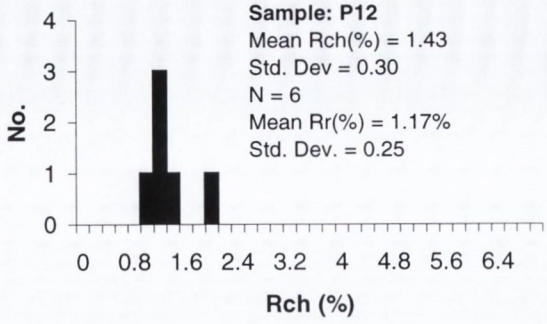
Sample: P12
Mean Rch(%) = 1.43
Std. Dev = 0.30
N = 6
Mean Rr(%) = 1.17%
Std. Dev. = 0.25
No.
Rch (%)

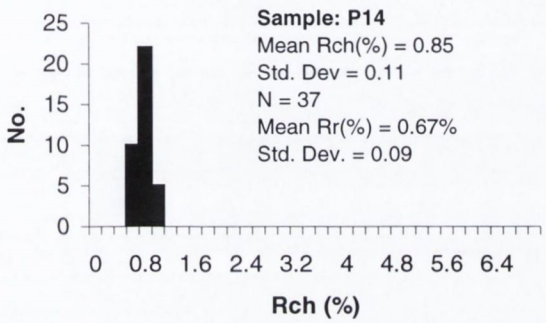
Sample: P14
Mean Rch(%) = 0.85
Std. Dev = 0.11
N = 37
Mean Rr(%) = 0.67%
Std. Dev. = 0.09
No.
Rch (%)

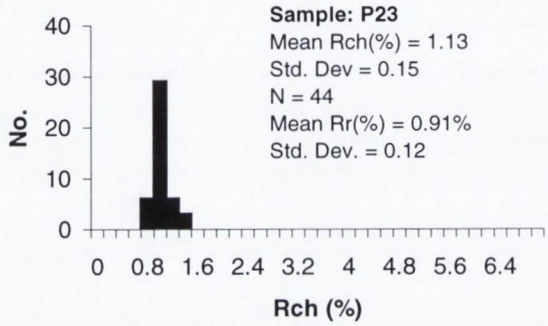
Sample: P23
Mean Rch(%) = 1.13
Std. Dev = 0.15
N = 44
Mean Rr(%) = 0.91%
Std. Dev. = 0.12
No.
Rch (%)

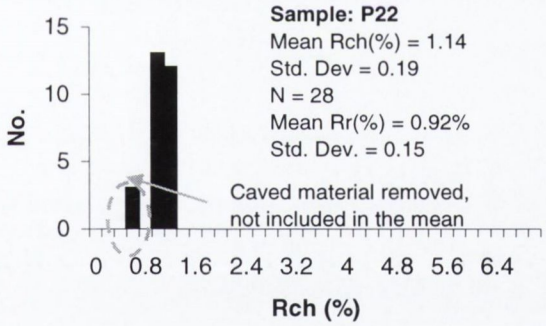
Sample: P22
Mean Rch(%) = 1.14
Std. Dev = 0.19
N = 28
Mean Rr(%) = 0.92%
Std. Dev. = 0.15
Caved material removed,
not included in the mean
No.
Rch (%)

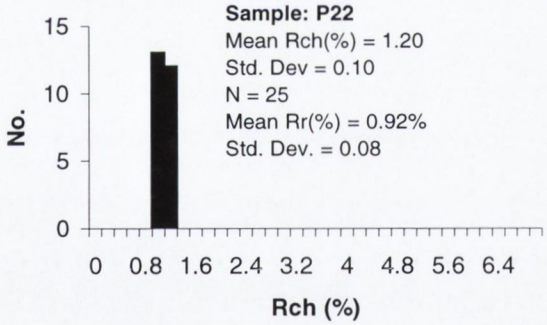
Sample: P22
Mean Rch(%) = 1.20
Std. Dev = 0.10
N = 25
Mean Rr(%) = 0.92%
Std. Dev. = 0.08
No.
Rch (%)

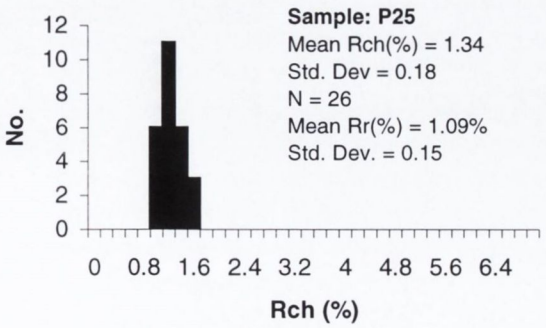
Sample: P25
Mean Rch(%) = 1.34
Std. Dev = 0.18
N = 26
Mean Rr(%) = 1.09%
Std. Dev. = 0.15
No.
Rch (%)

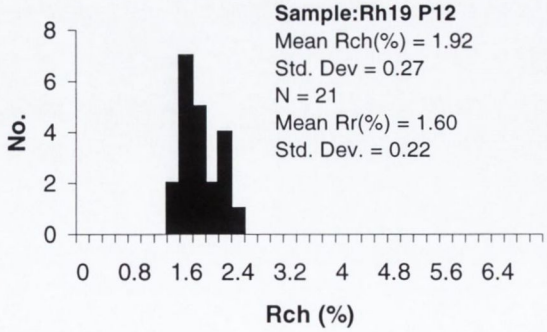
Sample:Rh19 P12
Mean Rch(%) = 1.92
Std. Dev = 0.27
N = 21
Mean Rr(%) = 1.60
Std. Dev. = 0.22
No.
Rch (%)

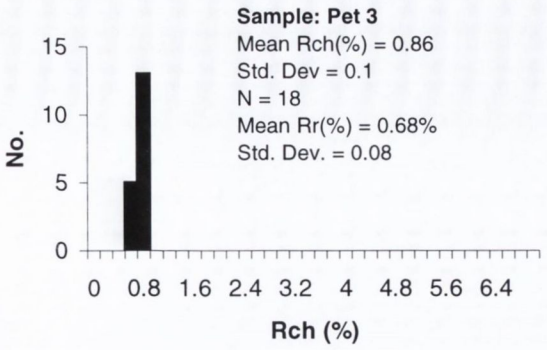
Sample: Pet 3
Mean Rch(%) = 0.86
Std. Dev = 0.1
N = 18
Mean Rr(%) = 0.68%
Std. Dev. = 0.08
No.
15
10
5
0
0 0.8 1.6 2.4 3.2 4 4.8 5.6 6.4
Rch (%)

APPENDIX III

RGB DETERMINATIONS OF COKIN PHOTOGRAPHIC FILTERS ('STANDARDS')

30 RGB determinations were made on each photographic filter under the conditions described in section 4.5.3. All readings were made on the same day. Each filter was moved slightly between determinations.

001 Cokin Photographic Filter

Number	Red	Green	Blue
1	245.51	252.61	3.77
2	243.73	251.54	2.7
3	243.78	251.04	2.47
4	244.1	252.05	3.03
5	244.31	252.12	3.14
6	243.62	251.31	2.57
7	244.04	252.06	3.04
8	243.76	251.71	2.8
9	245.26	252.71	3.78
10	243.83	250.69	2.34
11	245.11	252.46	3.56
12	243.83	251.65	2.77
13	243.81	251.14	2.52
14	245.1	251.65	3.69
15	244.29	252.12	3.14
16	245.3	252.43	3.6
17	243.62	251.65	2.72
18	245.13	252.43	3.58
19	244.13	252.04	3.06
20	243.95	251.84	2.89
21	243.95	251.99	3.01
22	244	251.92	2.97
23	243.64	251.59	2.68
24	243.94	251.97	3
25	245.15	252.46	3.59
26	245.03	252.51	3.56
27	243.58	251.94	2.87
28	245.4	252.59	3.75
29	245.18	252.49	3.62
30	244.42	252.23	3.26

Mean	244.35	251.96	3.12
Std. Dev	0.66	0.50	0.44

002 Cokin Photographic Filter

Number	Red	Green	Blue
1	254	73.79	1
2	254	69.23	1
3	254	72.74	1
4	254	73.25	1
5	254	73.19	1
6	254	70.77	1
7	254	71.14	1
8	254	71.57	1
9	254	72.25	1
10	254	72.57	1
11	254	72.91	1
12	254	72.72	1
13	254	70.97	1
14	254	69.23	1
15	254	72.79	1
16	254	73.13	1
17	254	73.8	1
18	254	70.86	1
19	254	73.98	1
20	254	76.53	1
21	254	73.95	1
22	254	73.95	1
23	254	74.49	1
24	254	77.25	1
25	254	74.03	1
26	254	76.16	1
27	254	73.32	1
28	254	75.17	1
29	254	75.94	1
30	254	75.63	1

Mean	254.00	73.24	1.00
Std. Dev	0.00	1.99	0.00

003 Cokin Photographic Filter

Number	Red	Green	Blue
1	237.62	16.94	5.66
2	237.51	16.88	5.27
3	239.89	16.79	5.13
4	243.41	16.19	5.41
5	237.12	17	6.05
6	234.16	17.45	6.07
7	239.92	16.45	5.95
8	232.22	17.59	5.66
9	239.71	16.75	5.96
10	234.65	17.68	5.58
11	239.4	16.87	5.66
12	236.32	17.28	5.62
13	237.3	17.04	6.24
14	239.92	16.44	6.52
15	232.98	17.76	5.78
16	232.85	17.88	5.98
17	237.69	16.87	5.75
18	234.78	17.58	5.78
19	233.45	17.63	5.48
20	231.65	17.86	6.29
21	233.94	17.33	6.14
22	236.63	17.38	5.57
23	234.98	17.4	5.77
24	236.8	17.14	5.8
25	234.89	17.64	5.58
26	238.79	16.89	5.77
27	239.91	16.45	5.48
28	230.41	17.8	5.79
29	234.53	17.33	6.33
30	231.46	17.86	5.98

Mean	236.16	17.21	5.80
Std. Dev	3.14	0.48	0.32

004 Cokin Photographic Filter

Number	Red	Green	Blue
1	48.87	164.61	68.75
2	49.74	163.63	68
3	49.6	164.99	68.47
4	49.61	163.12	68.42
5	49.15	165.55	69.37
6	47.75	163.4	69.54
7	49.85	167.13	70.53
8	48.96	162.9	68.14
9	49.85	167.45	70.47
10	48.78	165.89	70.02
11	48.73	164.18	68.29
12	49.96	166.59	69.95
13	49.06	165.04	69.4
14	47.45	158.07	66.34
15	49.83	165.63	70.52
16	47.83	161.8	66.83
17	47.82	162.17	68.25
18	47.34	161.55	67.33
19	48.95	164.87	69.69
20	47.4	160.33	67.6
21	47.83	164.88	70.15
22	48.66	162.85	67.89
23	48.49	162.96	68.6
24	48.24	164.46	69.81
25	49.41	166.11	69.72
26	49.06	165	69.7
27	48.47	162.95	68.36
28	49.59	164.92	69.6
29	47.25	160.09	67.84
30	45.5	161.56	68.13

Mean	48.63	163.82	68.86
Std. Dev	1.03	2.17	1.12

005 Cokin Photographic Filter

Number	Red	Green	Blue
1	112.07	60.86	38.69
2	112.18	60.87	38.5
3	112.92	61.41	39.93
4	113.31	62.1	38.99
5	113.83	61.62	40.18
6	114.46	61.62	39.11
7	112.47	60.98	37.65
8	114.06	61.91	39.1
9	113.85	61.46	38.09
10	112.74	61.37	38.76
11	114.69	61.38	38.39
12	114.35	61.53	38.47
13	112.83	61.35	38.31
14	114.54	61.21	37.24
15	112.82	60.89	37.78
16	112.27	61.18	38.37
17	113.51	61.3	38.75
18	112.31	61.32	37.7
19	113.88	61.77	39.7
20	114.41	61.68	38.52
21	112.35	61.38	38.31
22	114.82	61.82	38.2
23	113.33	61.67	38.61
24	112.63	60.48	37.57
25	112.1	61.11	38.14
26	112.14	60.81	38.33
27	113.95	62.01	39.3
28	114.64	62.51	39.45
29	112.93	61.51	38.06
30	111.68	61.08	38.8

Mean	113.27	61.41	38.57
Std. Dev	0.96	0.43	0.69

006 Cokin Photographic Filter

Number	Red	Green	Blue
1	209.58	249.09	108.35
2	216.47	248.15	113.51
3	211.19	248.68	110.04
4	208.95	249.28	108.68
5	211.63	248.82	110.73
6	209.78	249.15	108.53
7	210.32	248.95	109.24
8	215.75	248.22	112.32
9	206.14	249.73	108.79
10	208.14	248.97	110.05
11	204.75	249.86	108.68
12	208.27	249.4	108.51
13	214.27	249.4	111.8
14	207.06	249.92	105.5
15	209.07	249.52	108.67
16	213.53	248.49	111.82
17	208.02	249.22	110.65
18	210.71	248.9	110.09
19	213.27	248.71	111.77
20	212.48	248.77	111.7
21	209.89	248.97	111.73
22	209.41	249	110.84
23	212.43	250.32	107.14
24	210.5	249	109.45
25	210.51	248.84	110.21
26	211.81	248.53	111.54
27	211.93	248.53	111.87
28	204.51	249.71	109.31
29	205.53	249.91	107.19
30	207.58	249.47	108.74

Mean	210.12	249.12	109.92
Std. Dev	3.00	0.53	1.80

020 Cokin Photographic Filter

Number	Red	Green	Blue
1	77.09	168.04	210.12
2	76.51	166.38	207.17
3	75.51	172.75	217.11
4	76.88	169.45	211.35
5	75.32	170.62	212.97
6	75.37	169.1	209.62
7	75.74	170.43	214.34
8	76.76	172.03	216.18
9	76.99	172.45	217
10	76.86	168.96	208.98
11	76.21	172.31	216.2
12	76.65	169.07	211.48
13	77.27	171.77	213.62
14	77.9	171.78	214.26
15	76.64	167.32	207.67
16	76.27	169.29	211.65
17	76.81	173.19	217.69
18	75.85	172.12	213.64
19	75.64	167.83	209.46
20	76.11	170.46	212.46
21	75.29	171.18	213.82
22	76.6	168.1	210.5
23	76.69	171.81	215.87
24	76.59	172.65	218.36
25	77.39	170.49	212.88
26	76.29	170.79	214.13
27	75.49	171.26	215.69
28	77.28	170.15	211.75
29	76.43	171.21	214.77
30	77.34	173.06	216.85

Mean	76.46	170.54	213.25
Std. Dev	0.69	1.83	3.04

022 Cokin Photographic Filter

Number	Red	Green	Blue
1	122.48	194.56	234.67
2	123.49	196.14	237.09
3	124.95	198.24	240.1
4	118.34	189.15	226.3
5	125.49	198.27	240.64
6	124.78	197.29	239.34
7	125.45	195.91	236.31
8	123.18	195.85	235.66
9	126.03	199.09	240.59
10	123.68	196.37	236.26
11	124.62	198.62	241.14
12	124.24	196.91	238.25
13	125	196	237.38
14	124.71	195.17	235.74
15	124.64	194.77	234.18
16	125.19	196.8	237.54
17	124.11	195.01	234.48
18	123.91	194.79	234.51
19	125.04	198.4	240.16
20	124.73	194.98	235.96
21	124.85	198.89	241.8
22	126.72	198.76	242.09
23	124.84	196.3	238.47
24	124.99	195.24	234.35
25	124.16	194.78	236.01
26	123.37	197.04	237.45
27	122.75	192.73	231.79
28	122.23	192.23	230.09
29	125.78	199.32	240.18
30	123.8	193.78	233.55

Mean	124.25	196.05	236.74
Std. Dev	1.52	2.28	3.57

024 Cokin Photographic Filter

Number	Red	Green	Blue
1	182.69	231.66	224.58
2	183.24	232.66	224.67
3	182.05	230.37	223.95
4	182.36	231.09	224.04
5	183.95	232.78	224.38
6	183.17	233.18	224.8
7	180.89	229.74	223.59
8	184.05	233.19	224.41
9	181.65	231.01	223.25
10	182.86	231.64	224.25
11	181.61	229.66	223.17
12	182.65	229.16	224.1
13	183.97	232.43	224.75
14	183.25	232.76	224.53
15	183.78	233.06	225.01
16	183.41	233.16	224.38
17	185.1	234.5	224.99
18	182.44	231.57	224.99
19	182.29	232.16	225.13
20	182.49	231.52	223.76
21	184.17	233.26	224.55
22	183.26	232.58	224.34
23	182.3	231.35	224.45
24	186.14	234.45	224.48
25	183.05	231.86	224.44
26	182.28	231.57	224.74
27	185.44	234.08	224.95
28	182.78	231.94	224.59
29	182.44	231.55	224.22
30	184.74	234.23	225.17

Mean	183.15	232.14	224.42
Std. Dev	1.18	1.37	0.51

020, 022 and 024 Cokin Photographic Filters

Number	Red	Green	Blue
1	40.38	97.66	153.8
2	41.04	98.41	156.18
3	40.86	96.97	152.94
4	39.92	95.69	151.08
5	40.43	95.99	151.58
6	40.96	97.84	155.06
7	40.55	96.2	151.96
8	40.28	95.37	149.81
9	41.28	97.26	154.36
10	40.21	96.75	152.13
11	40.71	96.96	153.39
12	40.32	94.88	150.33
13	40.8	96.29	151.44
14	40.41	96.88	153.47
15	39.96	94.64	149.2
16	40.51	96.21	152.9
17	39.92	97.01	153.32
18	40.71	95.33	151.28
19	41.01	96.16	151.34
20	40.29	94.83	150.59
21	40.16	95.13	151.57
22	41.08	96.25	152.14
23	41.09	96.23	153.43
24	40.23	94.4	150.58
25	40.65	96.76	152.21
26	41.27	97.59	154.97
27	42.99	99.89	160.3
28	41.94	99.09	158.62
29	42.54	99.17	158.32
30	42.2	98.8	159.37

Mean	40.82	96.69	153.26
Std. Dev	0.76	1.42	2.85

'Pastel Violet' photographic filter, unknown brand

Number	Red	Green	Blue
1	168.43	126.85	198
2	171.29	128.53	201
3	171.03	126.45	199
4	169.52	125.37	197
5	167.99	125.66	194
6	171.46	127.4	200
7	170.34	126.14	199
8	169.47	125.18	195
9	169.3	127.85	197
10	172.04	129.86	201
11	170.06	128.33	200
12	170.42	127.02	201
13	167.82	124.85	193
14	172	128.58	200
15	172.45	128.13	201
16	173.05	128.9	201
17	168.14	124.97	195
18	170.11	126.63	199
19	170.02	127.33	199
20	169.2	126.02	195
21	168.67	126.64	196
22	168.72	126.34	196
23	169.09	126.43	196
24	168.92	126.28	197
25	170.26	125.41	196
26	173.37	127.98	203
27	172.14	127.71	202
28	170.54	128.67	200
29	158.2	125.87	196
30	170.93	128.4	200

Mean	169.83	126.99	##
Std. Dev	2.66	1.32	2.66

APPENDIX IV

CALIBRATION AND ERRORS DATA

Cokin
Cokin 003
Cokin 002
Cokin 001
Cokin 006
Cokin 024
Cokin 004
Cokin 005
Cokin 022
Cokin 020
Pastel Violet'
020, 022, 024

Red	Green	Blue
225.44	18.78	6.12
254	67.25	1
247.98	242.95	1.12
191.09	249.67	100.12
174.85	220.66	211.49
47.27	152.83	62.22
107.79	58.8	34.62
118.43	185.26	216.22
74.13	158.38	194.98
158.88	121.45	183.51
39.57	91.22	143.03

14th September 2004

Red	Green	Blue
220	20.65	7.34
254	67.48	1
246.52	245.43	1.27
204.22	251.45	104.26
178.04	227.8	225.37
48.45	159.06	63.69
108.79	58.84	35.6
119.02	188.7	221.47
74.2	163.09	200.62
160.71	121.37	191.55
38.95	95.73	150.34

24th September 2004

Red	Green	Blue
220.42	17.96	7.13
254	63.23	1
247.1	235.22	1
190.69	248.98	98.6
176.06	218.45	210.98
46.78	153.5	63.44
105.9	57.67	34.26
118.35	186.3	218.31
74.64	160.77	199.35
156.64	120.18	180.46
39.04	90.52	141.82

28th September 2004

Red	Green	Blue
218.1	18.43	7.57
254	65	1
247.92	240.73	1.3
194.88	249.06	102.16
175.74	219.3	212.35
46.21	150.55	64.21
104.62	56.89	34.62
116.63	179.93	209.96
73.74	158.5	196.26
154.92	117.97	176.14
38.19	89.33	139.52

6th October 2004

Cokin
Cokin 003
Cokin 002
Cokin 001
Cokin 006
Cokin 024
Cokin 004
Cokin 005
Cokin 022
Cokin 020
Pastel Violet'
020, 022, 024

Red	Green	Blue
215.05	18.29	6.46
254	62.9	1
247.61	240.96	1.05
192.19	249.72	101.72
175.47	218.12	210.97
46.36	151.17	62.52
104.38	57.97	34.28
117.23	185.07	215.85
73.02	156.98	193.91
155.65	118.8	178.64
39.86	93.66	147.31

7th October 2004

Red	Green	Blue
225.44	18.78	6.12
254	67.25	1
247.98	242.95	1.12
191.09	249.67	100.12
174.85	220.66	211.49
47.27	152.83	62.22
107.79	58.8	34.62
118.43	185.26	216.22
74.13	158.38	194.98
158.88	121.45	183.51
39.57	91.22	143.03

14th October 2004

Red	Green	Blue
224.01	18.66	5.49
254	69.72	1
245.96	246.66	1.47
199.65	249.58	103.54
177.58	223.12	217.06
48.32	153.05	64.43
108.4	58.77	35.08
118.11	184.2	214.31
74.66	158.97	195.49
158.26	120.15	180.51
40.12	93.47	145.18

21st October 2004

Red	Green	Blue
222.24	18.1	5.26
254	63.9	1
247.74	233.94	1
187.37	247.14	97.4
175.94	219.14	211.69
45.97	147.21	62.79
103.35	56.87	33.62
117.88	177.71	208.5
73.84	156.44	193.38
155.56	118.73	177.81
39.52	90.54	141.49

11th November 2004

Cokin
Cokin 003
Cokin 002
Cokin 001
Cokin 006
Cokin 024
Cokin 004
Cokin 005
Cokin 022
Cokin 020
Pastel Violet'
020, 022, 024

Red	Green	Blue
234.11	17.81	5.82
254	72.62	1
247.1	245.06	1.27
203.5	250.2	103.56
178.66	221.95	214.78
48.56	157.63	64.92
108.88	59.13	36.39
120.79	187.87	220.59
75.48	163.55	201
162.61	122.37	185.21
40.46	94.82	148.25

15th November 2004

Red	Green	Blue
221.05	18.27	6.13
254	67.78	1
248.01	241.65	1.07
196.1	248.36	100.88
180.48	220.07	211.92
48.53	153.68	62.68
109.14	58.25	35.12
122.48	185.19	215.31
76.21	159.57	195.11
158.56	119.03	178.03
38.33	92.01	142.54

18th November 2004

Red	Green	Blue
216.49	18.4	4.38
254	60.97	1
244.58	226.83	1
182.65	243.35	93.65
175.56	216.03	206.83
46.64	146.81	61.96
102.91	56.76	33.64
118.06	177.46	208.03
74.63	155.88	191.86
155.6	118.06	174.67
39.4	88.46	135.31

20th November 2004

Red	Green	Blue
214.47	18.34	6
254	64.34	1
248.12	234.03	1
189.09	247.93	101.07
176.09	218.96	210.58
48.61	151.4	63.92
106.89	57.63	35.37
119.49	185.6	217.23
75.49	158.96	198.74
158.09	120.13	179.13
38.05	87.58	132.5

24th November 2004

Cokin
Cokin 003
Cokin 002
Cokin 001
Cokin 006
Cokin 024
Cokin 004
Cokin 005
Cokin 022
Cokin 020
Pastel Violet'
020, 022, 024

Red	Green	Blue
226.06	18.13	5.87
254	67.87	1
246.75	244.37	1.2
193.02	248.52	99.09
179.84	222.96	216.82
49.37	157.38	64.95
109.97	58.81	37.27
120.54	185.35	216.82
76.4	162.47	200.03
161.95	121.18	182.11
40.73	95.24	148.5

25th November 2004

Red	Green	Blue
225.73	18.5	5.97
254	69.02	1
247.61	245.66	1.41
196.36	250.22	104.4
185.95	230.95	222.64
49.97	159.65	63.49
113.39	60.74	36.49
123.66	191.99	226.53
77.88	166.66	207.82
167.49	125.16	189.08
43.1	96.8	152.25

6th December 2004

Red	Green	Blue
230.7	17.81	6.25
254	69.92	1
245.42	247.16	1.51
201.59	249.67	104.55
178.01	221.69	217.58
48.11	151.06	63.29
111.05	59.29	38.63
122.86	187.37	221.88
76.31	162.36	201.23
164.11	123.12	187.49
42.12	91.64	142.48

8th February 2005

Red	Green	Blue
243.35	16.39	5.94
254	73.65	1
246.06	246.32	1.36
209.53	243.49	109.25
181.77	225.24	221.79
48.96	158.3	67.27
111.3	59.94	38.09
123.1	189.81	227.92
75.58	164.36	203.38
164.51	122.8	189.2
41.48	93.63	147.68

9th February 2005

Cokin
Cokin 003
Cokin 002
Cokin 001
Cokin 006
Cokin 024
Cokin 004
Cokin 005
Cokin 022
Cokin 020
Pastel Violet'
020, 022, 024

Red	Green	Blue
218.73	18.78	6.04
254	61.61	1
245.53	227.38	1
185.54	243.84	98.4
172.3	205.08	195.38
46.23	144.49	62.92
103.69	56.99	34.68
118.48	173.77	205.15
73.62	149.66	184.93
154.51	116.69	173.37
36.63	85.12	129.6

16th May 2005

Red	Green	Blue
222.94	18.98	5.71
254	67.48	1
248.38	235.59	1
191.62	247.95	101.44
177.94	216.8	210.83
47.77	147.87	63.54
104.9	56.84	32.71
120.54	182.21	214.55
76.1	156.53	194.68
157.68	118.54	177.04
39.49	88	135.53

17th May 2005

Red	Green	Blue
217.81	19.32	5.85
254	68.06	1
248.88	236.16	1
193.13	248.64	101.14
177.81	216.62	207.86
48.31	150.23	64.36
108.32	58.33	35.26
122.38	182.41	214.84
76.24	157.32	196.21
158.37	119.19	177.64
38.32	86.59	132.06

18th May 2005

Red	Green	Blue
205.79	19.44	6.96
254	59.63	1
244.66	227.06	1
182.69	240.53	95.27
171.52	204.39	192.53
45.51	141.74	61.39
97.81	54.64	33.45
117.93	169.61	198.79
74.35	146.46	180.18
149.59	112.85	162.58
35.64	77.86	112.06

19th May 2005

Cokin
Cokin 003
Cokin 002
Cokin 001
Cokin 006
Cokin 024
Cokin 004
Cokin 005
Cokin 022
Cokin 020
Pastel Violet'
020, 022, 024

Red	Green	Blue
196.82	20.18	7.57
254	53.38	1
239.04	221.91	1
179.88	234.47	92.28
170.1	203.85	193.03
44.83	136.99	59.59
95.72	54.18	33.26
114.14	166.65	194.78
73.97	149.65	185.24
150.52	114.08	167.82
38.4	87.1	134.43

17th August 2005

Red	Green	Blue
192.96	20.4	6.36
254	52.97	1
240.79	220.8	1
177.24	230.34	88.88
167.1	196.15	183.37
45.57	138.81	62.88
97.69	54.91	32.42
114.44	167.2	197.7
73.44	145.91	178.62
150.36	114.66	168.07
36.27	83.16	125.24

18th August 2005

Red	Green	Blue
210.27	18.53	6.83
254	62.21	1
249.05	234.1	1
191.68	247.24	94.13
178.25	211.71	200.38
48.52	150.4	61.84
104.41	56.56	33.45
121.34	180.7	210.33
75.6	151.86	186.61
155.51	117.58	171.31
38.42	86.02	130.15

22nd August 2005

Red	Green	Blue
221.05	18.32	6.58
254	69.46	1
248.01	241.93	1.03
196.1	248.74	102.14
180.48	222.39	218
48.53	153.65	64.64
109.14	59.34	37.02
122.48	185.27	219.88
76.21	163.8	201.98
158.56	122.71	185.96
38.33	92.51	144.72

18th October 2005

Cokin

Red	Green	Blue

Red	Green	Blue

Red	Green	Blue

Red	Green	Blue

Daily RGB determinations of Cokin Photographic Filters

Cokin 003	202.73	19.42	7.18	244.42	22.57	1	190.63	20.64	5.49	253.89	15.61	6.55
Cokin 002	254	58.08	1	254	60.33	1	254	53.57	1	254	91.3	1
Cokin 001	242.96	225.83	1	202.76	190	6.72	232.62	222.7	1	254	252.67	4.16
Cokin 006	181.09	236.86	96.92	182.09	237.04	95.78	177.16	213.82	82.18	227.36	244.82	93.45
Cokin 024	170.62	203.63	193.1	172.44	202.5	192.44	166.86	195.28	188.26	208.34	214.14	199.73
Cokin 004	46.25	143.31	62.82	46.94	144.8	63	47.93	135.89	59.9	60.1	153.99	64.61
Cokin 005	100.85	55.91	34.25	99.72	55.16	34.1	98.51	51.01	30.57	129.45	57.25	30.95
Cokin 022	118.48	172.8	203.61	118.1	170.41	200.68	115.99	161.85	180.24	147.2	182.04	202.51
Cokin 020	73.85	146.85	182.12	74.3	146.59	181.55	73.85	139.71	170.41	93.58	157.92	190.75
Pastel Violet'	150.94	114.43	167.78	152.82	114.87	169.54						
020, 022, 024	37.41	84.37	128.88	37.48	83.45	125.78	38	82	123.72	50.81	91.03	132.8
	14th November 2005			21st February 2006			22nd March 2006			New Bulb -25th March 2006		

Filter
Cokin 001
Cokin 002
Cokin 003
Cokin 004
Cokin 005
Cokin 006
Cokin 020
Cokin 022
Cokin 024
020, 022, 024

Red	Green	Blue
247.24	252.67	4.16
254	91.3	1
253.89	15.61	6.55
60.1	153.99	64.61
129.45	57.25	30.95
227.36	244.82	93.45
93.58	157.92	190.75
147.2	182.04	202.51
208.34	214.14	199.73
50.81	91.03	132.8

(first set of filters)

Red	Green	Blue
253	235	1.1
254	75.57	1
188.68	21.89	5.22
46.28	150.59	62.36
103.93	56.11	21.17
202.3	225.6	76.99
94.79	155.61	177.75
148.66	183.39	192.93
210.56	221.42	206.03
52	86.39	115.32

(second set of filters)

RGB determinations were made on the original set of Cokin photographic filters and the second set of filters purchased two years later. The determinations were made using the same equipment, on the same day, in quick succession of each other.

Veryhachium 1
Veryhachium 2
Veryhachium 3
Veryhachium 6
Veryhachium 7
Veryhachium 8
Veryhachium 9
Veryhachium 10
Veryhachium 11
Veryhachium 12
Veryhachium 13
Veryhachium 14
Veryhachium 15
Veryhachium 16
Veryhachium 17

Red	Green	Blue
224.2	229.69	192.9
222.65	229.43	182.91
223.62	230.2	196.88
222.71	226.49	177.71
226.01	230.26	205.31
223.06	224.4	157.22
228.36	233.09	190.6
222.4	228.77	199.68
221.25	207.12	112.85
223.31	228.27	165.47
218.7	226.49	201.27
219.22	228.55	195.35
221.27	229.24	193.94
223.07	228.52	188.41
222.95	196.82	101.59

15th November 2005
(Uncalibrated)

Red	Green	Blue
204.89	255.00	228.54
203.49	255.00	216.64
204.37	255.00	233.28
203.54	252.00	210.45
206.53	255.00	243.32
203.86	250.28	186.05
208.66	255.00	225.80
203.26	255.00	236.61
202.22	231.25	133.21
204.09	254.54	195.87
199.91	252.58	238.51
200.38	254.85	231.46
202.24	255.00	229.78
203.87	254.82	223.19
203.76	219.90	119.80

15th November 2005
(Calibrated)

Veryhachium 1
Veryhachium 2
Veryhachium 3
Veryhachium 6
Veryhachium 7
Veryhachium 8
Veryhachium 9
Veryhachium 10
Veryhachium 11
Veryhachium 12
Veryhachium 13
Veryhachium 14
Veryhachium 15
Veryhachium 16
Veryhachium 17

Red	Green	Blue
223.97	227.25	183.85
226.48	233.23	188.31
225.78	230.98	209.12
222.36	228.61	180.18
216.81	223.5	190.16
224.38	228.34	152.7
226.69	230.27	189.01
213.73	225.08	194.48
235.39	220.64	114.29
225.02	231.36	161.96
226.2	231.48	215.12
223.91	232.45	188.11
225.46	230.8	197.12
225.88	232.85	189.75
231.28	204.03	103.54

18th October 2004
(Uncalibrated)

Red	Green	Blue
215.91	235.38	194.45
218.32	241.55	199.15
217.65	239.23	221.09
214.37	236.78	190.58
209.05	231.52	201.10
216.31	236.51	161.60
218.52	238.50	199.89
206.09	233.15	205.66
226.86	228.57	121.10
216.92	239.62	171.37
218.05	239.74	227.42
215.86	240.74	198.94
217.34	239.04	208.44
217.74	241.16	200.67
222.92	211.45	109.77

18th October 2004
(Calibrated)

RGB data collected by the same user, on the same specimens of sample TL3 on two different days.

	Red	Green	Blue
Veryhachium 1	221.49	228.54	193.91
Veryhachium 2	224.09	231.27	185.89
Veryhachium 3	223.33	227.82	200.4
Veryhachium 4	228.22	232	165.12
Veryhachium 5	224.16	228.55	181.15
Veryhachium 6	224.39	229.38	179.48
Veryhachium 7	225.84	229.64	206.86
Veryhachium 8	223.39	226.08	154.6
Veryhachium 9	228.5	232.76	200.4
Veryhachium 10	226.14	229.09	207.92
Veryhachium 11	222.94	206.94	111.34
Veryhachium 12	224.15	231.77	175.6
Veryhachium 13	227.32	228.85	216.65
Veryhachium 14	226.06	231.27	182.32
Veryhachium 15	225.91	228.98	209.21
Veryhachium 16	226.31	230.31	190.14
Veryhachium 17	239.85	213.67	111.31

Dave Chew (DC) Uncalibrated

Red	Green	Blue
226.02	229.09	190.02
220.71	229.29	180.06
218.78	228.69	190.66
231.38	228.71	166.41
224.92	227.76	166.33
224.21	228.36	179.5
219.87	228	180.13
227.17	225.05	151.61
233.72	239.3	186.19
223.58	229.14	199.43
237.07	217.38	113.97
227.67	231.05	149.71
222.73	229.52	194.91
225.45	232.85	179.96
226.5	232.64	189.69
227.83	233.93	192.67
240.24	208.28	106.03

Aileen Bright (AB) Uncalibrated

	Red	Green	Blue
Veryhachium 1	226.67	230.54	201.67
Veryhachium 2	227.31	232.34	184.58
Veryhachium 3	224.71	232.26	193.11
Veryhachium 4	227	233.15	168
Veryhachium 5	226.15	228.09	167.7
Veryhachium 6	224.17	228.7	180.66
Veryhachium 7	225.61	229.47	208.56
Veryhachium 8	230.74	228.86	159.36
Veryhachium 9	237.83	230.85	199.73
Veryhachium 10	224.04	229.1	204.86
Veryhachium 11	234.11	212.48	108.09
Veryhachium 12	228.56	232.62	164.85
Veryhachium 13	228.53	230.91	223.53
Veryhachium 14	225.21	230.84	184.44
Veryhachium 15	226.14	228.9	215.16
Veryhachium 16	225.63	230.8	193.83
Veryhachium 17	230.71	202.18	102.51

Aoife Halloran (AH) Uncalibrated

Red	Green	Blue
224.2	229.69	192.9
222.65	229.43	182.91
223.62	230.2	196.88
224.81	227.66	164.19
226.79	228.58	175.24
222.71	226.49	177.71
226.01	230.26	205.31
223.06	224.4	157.22
228.36	233.09	190.6
222.4	228.77	199.68
221.25	207.12	112.85
223.31	228.27	165.47
218.7	226.49	201.27
219.22	228.55	195.35
221.27	229.24	193.94
223.07	228.52	188.41
222.95	196.82	101.59

Catherine Duggan (CD) Uncalibrated

RGB determinations made on the same specimens from sample TL3 by four different operators. The determinations were made on the same day and in quick succession of each other.

	Red	Green	Blue
Veryhachium 1	223.97	227.25	183.85
Veryhachium 2	226.48	233.23	188.31
Veryhachium 3	225.78	230.98	209.12
Veryhachium 4	222.36	228.61	180.18
Veryhachium 5	216.81	223.5	190.16
Veryhachium 6	224.38	228.34	152.7
Veryhachium 7	226.69	230.27	189.01
Veryhachium 8	213.73	225.08	194.48
Veryhachium 9	235.39	220.64	114.29
Veryhachium 10	225.02	231.36	161.96
Veryhachium 11	226.2	231.48	215.12
Veryhachium 12	223.91	232.45	188.11
Veryhachium 13	225.46	230.8	197.12
Veryhachium 14	225.88	232.85	189.75
Veryhachium 15	231.28	204.03	103.54

Leica/Qwin RGB determinations (Uncalibrated)

Red	Green	Blue
241	210	101
226	234	183
228	232	212
173	231	173
205	231	205
227	233	152
229	234	183
226	231	213
235	225	120
228	235	171
227	231	212
228	234	181
227	232	210
227	233	200
225	230	205

Photoshop ® RGB determinations (Uncalibrated)

RGB determinations made on the same *Veryhachium* specimens from samples TL3. Determinations were made using the Leica/Qwin image analysis system as well as the histogram tool in Adobe Photoshop ® CS.

	Red	Green	Blue
Veryhachium 1	223.97	227.25	183.85
Veryhachium 2	226.48	233.23	188.31
Veryhachium 3	225.78	230.98	209.12
Veryhachium 4	222.36	228.61	180.18
Veryhachium 5	216.81	223.5	190.16
Veryhachium 6	224.38	228.34	152.7
Veryhachium 7	226.69	230.27	189.01
Veryhachium 8	235.39	220.64	114.29
Veryhachium 9	225.02	231.36	161.96
Veryhachium 10	226.2	231.48	215.12
Veryhachium 11	223.91	232.45	188.11
Veryhachium 12	225.88	232.85	189.75
Veryhachium 13	231.28	204.03	103.54

Leica/Qwin system
(Uncalibrated)

Red	Green	Blue
215.91	235.38	194.45
218.32	241.55	199.15
217.65	239.23	221.09
214.37	236.78	190.58
209.05	231.52	201.10
216.31	236.51	161.60
218.52	238.50	199.89
226.86	228.57	121.10
216.92	239.62	171.37
218.05	239.74	227.42
215.86	240.74	198.94
217.74	241.16	200.67
222.92	211.45	109.77

Leica/Qwin system
(Calibrated)

	Red	Green	Blue
Veryhachium 1	211.09	239.94	188.19
Veryhachium 2	207.89	224.52	168.93
Veryhachium 3	211.56	242.33	193.49
Veryhachium 4	208.45	230.55	172.88
Veryhachium 5	211.62	242.89	192.47
Veryhachium 6	209.4	228.94	158.19
Veryhachium 7	211.81	239.46	183.57
Veryhachium 8	208.45	213.97	121.7
Veryhachium 9	209.48	227.88	158.93
Veryhachium 10	199.17	202.92	143.33
Veryhachium 11	211.04	233.87	163.39
Veryhachium 12	212.95	244.91	189.21
Veryhachium 13	202.96	203.9	111.82

Nikon/Lucia system
(Uncalibrated)

Red	Green	Blue
182.11	255.00	255.00
179.46	255.00	236.27
182.50	255.00	255.00
179.92	255.00	241.06
182.55	255.00	255.00
180.71	255.00	223.24
182.70	255.00	255.00
179.92	255.00	178.96
180.78	255.00	224.14
172.25	246.41	205.21
182.07	255.00	229.55
183.65	255.00	255.00
175.38	247.35	166.97

Nikon/Lucia system
(Calibrated)

RGB determinations were made on the same *Veryhachium* specimens using the Leica/Qwin system and the Nikon/Lucia system. The determinations were made by the same operator.

Cokin
Cokin 002
Cokin 001
Cokin 006
Cokin 024
Cokin 004
Cokin 005
Cokin 022
Cokin 020
020, 022, 024

Red	Green	Blue
207.01	213.2	39.37
206.55	52.17	0.1
46.95	75.34	26.55
83.94	14.19	1.25
193.29	217.63	124.47
79.14	103.46	107.73
133.25	148.04	138.59
181.57	193.96	166.5
25.06	22.86	31.82

RGB 'Standard' Determinations
Nikon/Lucia system

Red	Green	Blue
247.24	252.67	4.16
254	91.3	1
60.1	153.99	64.61
129.45	57.25	30.95
227.36	244.82	93.45
93.58	157.92	190.75
147.2	182.04	202.51
208.34	214.14	199.73
50.81	91.03	132.8

RGB 'Standard' Determinations
Leica/Qwin established values

APPENDIX V

VERYHACHIUM RGB DETERMINATIONS

Bolivia 3

RAW DATA

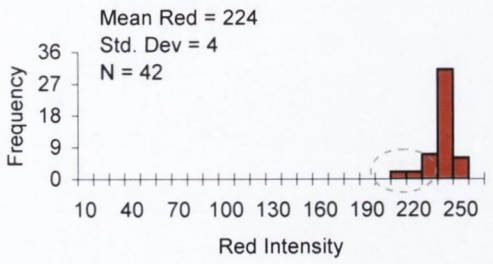

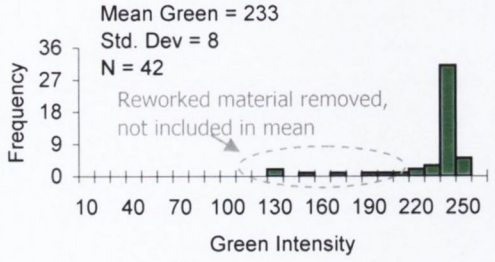

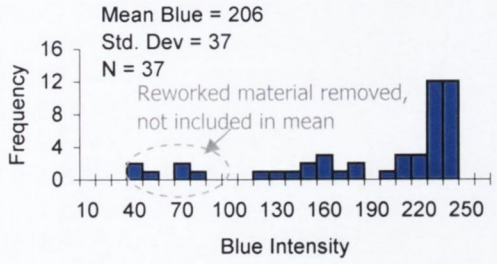

Number	Reference	Acritarch	Red	Green	Blue	Date	Colour
1	(2) N62/3	*Veryhachium*	239	242	237	14th Jan 04	
2	(2) U39/2	*Veryhachium*	229	240	237	14th Jan 04	
3	(2) P62/1	*Veryhachium*	241	242	236	14th Jan 04	
4	(2) P49/4	*Veryhachium*	239	243	234	14th Jan 04	
5	(2) S63/1	*Veryhachium*	238	240	234	14th Jan 04	
6	(2) R32/2	*Veryhachium*	237	239	234	14th Jan 04	
7	(2) U63/4	*Veryhachium*	235	237	233	14th Jan 04	
8	(2) N53/2	*Veryhachium*	235	236	233	14th Jan 04	
9	(2) M53/4	*Veryhachium*	235	237	233	14th Jan 04	
10	(2) S41	*Veryhachium*	234	235	233	14th Jan 04	
11	(2) O56	*Veryhachium*	233	235	231	14th Jan 04	
12	(2) Q59	*Veryhachium*	233	235	230	14th Jan 04	
13	(2) G39	*Veryhachium*	233	235	230	14th Jan 04	
14	(2) M57	*Veryhachium*	233	235	230	14th Jan 04	
15	(2) K60/2	*Veryhachium*	234	238	230	14th Jan 04	
16	(2) M51/2	*Veryhachium*	236	240	229	14th Jan 04	
17	(2) H39/4	*Veryhachium*	233	235	229	14th Jan 04	
18	(2) K41	*Veryhachium*	232	234	228	14th Jan 04	
19	(2) R40/2	*Veryhachium*	232	234	228	14th Jan 04	
20	(2) J65/1	*Veryhachium*	231	233	228	14th Jan 04	
21	(2) R41/1	*Veryhachium*	231	234	226	14th Jan 04	
22	(2) R40/4	*Veryhachium*	230	232	225	14th Jan 04	
23	(2) S62/1	*Veryhachium*	235	237	222	14th Jan 04	
24	(2) P63/2	*Veryhachium*	234	238	221	14th Jan 04	
25	(2) N38/3	*Veryhachium*	231	233	220	14th Jan 04	
26	(2) O43/4	*Veryhachium*	231	233	216	14th Jan 04	
27	(2) V42/2	*Veryhachium*	229	231	216	14th Jan 04	
28	(2) O34/1	*Veryhachium*	231	231	210	14th Jan 04	
29	(2) Q48/1	*Veryhachium*	226	228	209	14th Jan 04	
30	(2) S41	*Veryhachium*	228	231	204	14th Jan 04	
31	(2) W47/1	*Veryhachium*	231	231	194	14th Jan 04	
32	(2) U49/4	*Veryhachium*	241	234	179	14th Jan 04	
33	(2) S36/2	*Veryhachium*	229	232	171	14th Jan 04	
34	(2) L64/2	*Veryhachium*	234	232	168	14th Jan 04	
35	(2) Z44	*Veryhachium*	242	233	155	14th Jan 04	

Sample Bolivia 3 - Raw Data

Bolivia 3

RAW DATA

36	(2) Y62/4	*Veryhachium*	230	227	154	14th Jan 04	
37	(2) U66/4	*Veryhachium*	230	231	153	14th Jan 04	
38	(2) M41/2	*Veryhachium*	235	221	145	14th Jan 04	
39	(2) V53/4	*Veryhachium*	238	236	141	14th Jan 04	
40	(2) M52/1	*Veryhachium*	220	201	140	14th Jan 04	
41	(2) K59/1	*Veryhachium*	238	216	120	14th Jan 04	
42	(2) P50	*Veryhachium*	241	211	116	14th Jan 04	
43	(2) T42/2	*Veryhachium ®*	244	191	75	14th Jan 04	
44	(2) P64	*Veryhachium ®*	217	161	66	14th Jan 04	
45	(2) X40	*Veryhachium ®*	243	184	64	14th Jan 04	
46	(2) L66/4	*Veryhachium ®*	227	149	45	14th Jan 04	
47	(2) X40/2	*Veryhachium ®*	209	127	37	14th Jan 04	
48	(2) Q36/2	*Veryhachium ®*	203	127	37	14th Jan 04	

Can 9

Number	Reference	Acritarch	Red	Green	Blue	Date	Colour
1	(1) G40/3	*Veryhachium*	204	255	230	21st Feb 06	
2	(1) Q42/3	*Veryhachium*	207	255	255	21st Feb 06	
3	(1) Y58/1	*Veryhachium*	200	255	232	21st Feb 06	
4	(2) O37/3	*Veryhachium*	207	255	232	21st Feb 06	

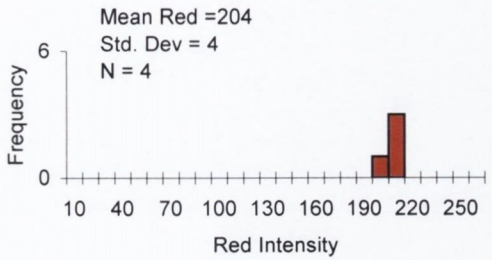

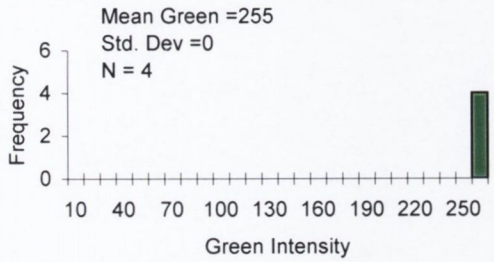

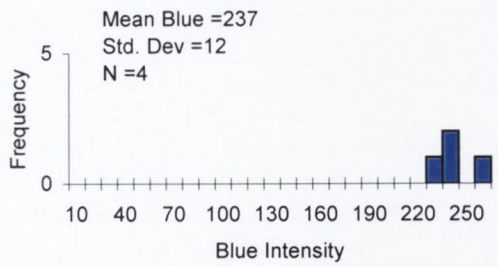

Sample Can 9 - Corrected Data

CC 3

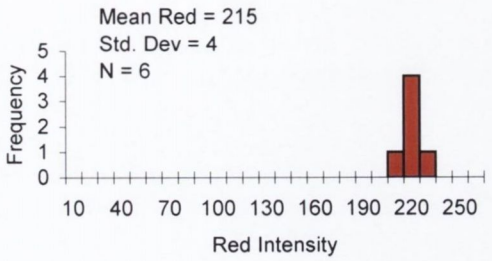

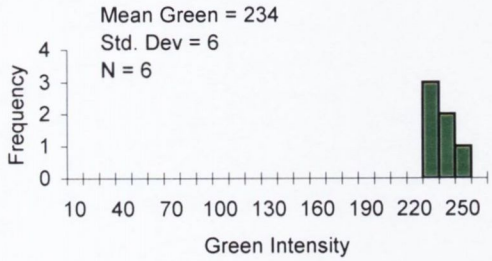

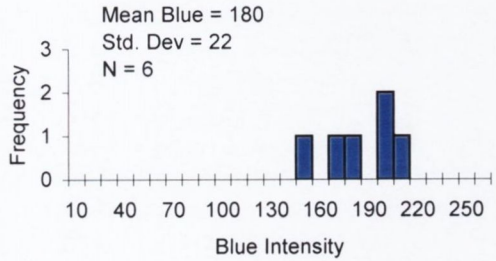

Number	Reference	Acritarch	Red	Green	Blue	Date	Colour
1	(1) V65	*Veryhachium*	210	230	209	14th Oct 04	
2	(2) T52/4	*Veryhachium*	211	230	192	14th Oct 04	
3	(4) P59/3	*Veryhachium*	218	244	192	14th Oct 04	
4	(4) Y38	*Veryhachium*	213	239	172	14th Oct 04	
5	(2) Q47/4	*Veryhachium*	221	228	167	14th Oct 04	
6	(4) V69/2	*Veryhachium*	217	232	149	14th Oct 04	

Sample CC3 - Corrected Data

JM 5

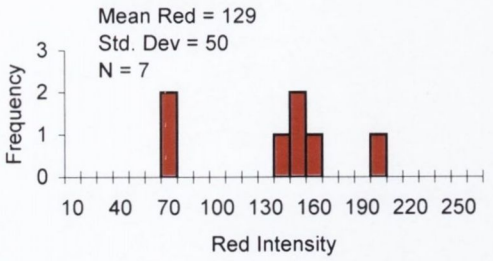

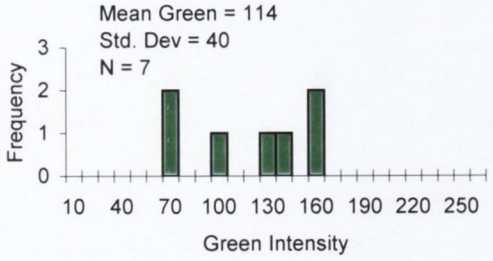

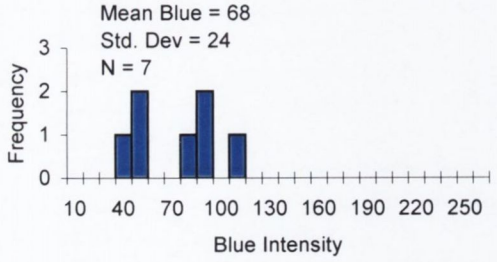

Number	Reference	Acritarch	Red	Green	Blue	Date	Colour
1	(1) P60	*Veryhachium*	61	64	47	22nd Aug 05	
2	(1) T66/2	*Veryhachium*	62	63	40	22nd Aug 05	
3	(2) X35	*Veryhachium*	137	98	45	18th Aug 05	
4	(2) G53/3	*Veryhachium*	145	122	74	18th Aug 05	
5	(2) Y35/1	*Veryhachium*	147	152	104	18th Aug 05	
6	(2) F41	*Veryhachium*	154	138	83	18th Aug 05	
7	(2) L35	*Veryhachium*	197	159	84	18th Aug 05	

Spread of RGB data in this sample was interpreted as variation between genera.

P 11

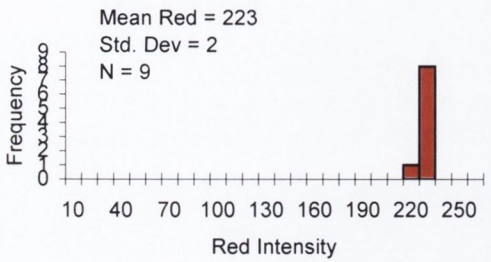

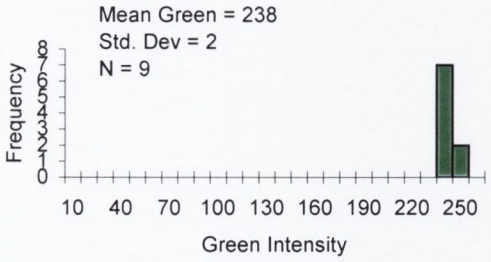

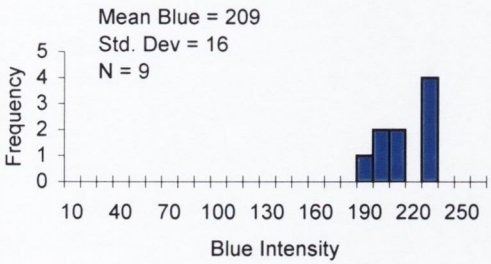

Number	Reference	Acritarch	Red	Green	Blue	Date	Colour
1	(1) O66/3	*Veryhachium*	225	240	186	15th Nov 04	
2	(1) B49/4	*Veryhachium*	223	241	194	15th Nov 04	
3	(1) C50/4	*Veryhachium*	219	235	195	15th Nov 04	
4	(1) X48	*Veryhachium*	222	237	201	15th Nov 04	
5	(1) L43	*Veryhachium*	222	237	209	15th Nov 04	
6	(1) F35/4	*Veryhachium*	223	236	223	15th Nov 04	
7	(1) W47	*Veryhachium*	226	239	225	15th Nov 04	
8	(1) L60/3	*Veryhachium*	221	237	227	15th Nov 04	
9	(1) X38/4	*Veryhachium*	225	241	230	15th Nov 04	

Sample P11 - Corrected Data

P 12

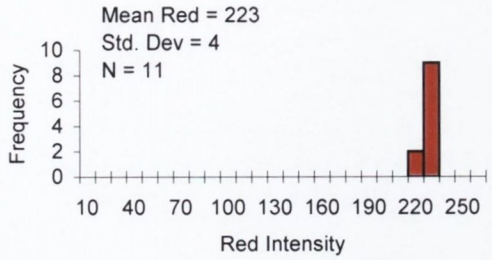

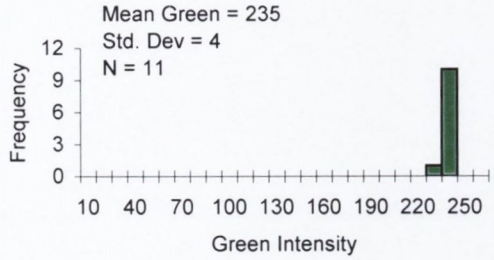

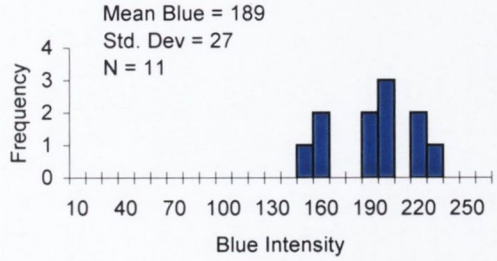

Number	Reference	Acritarch	Red	Green	Blue	Date	Colour
1	(1) S66/4	*Veryhachium*	229	232	145	15th Nov 04	
2	(1) M48/2	*Veryhachium*	228	230	153	15th Nov 04	
3	(1) P65/1	*Veryhachium*	227	227	157	15th Nov 04	
4	(1) R53/4	*Veryhachium*	223	237	182	15th Nov 04	
5	(1) V66	*Veryhachium*	222	236	189	15th Nov 04	
6	(1) D39/1	*Veryhachium*	223	238	197	15th Nov 04	
7	(1) T34/2	*Veryhachium*	219	236	197	15th Nov 04	
8	(1) M44	*Veryhachium*	217	236	200	15th Nov 04	
9	(1) T52/4	*Veryhachium*	222	236	211	15th Nov 04	
10	(1) G52	*Veryhachium*	223	238	219	15th Nov 04	
11	(1) N52/2	*Veryhachium*	223	238	227	15th Nov 04	

Sample P12 - Corrected Data

P13

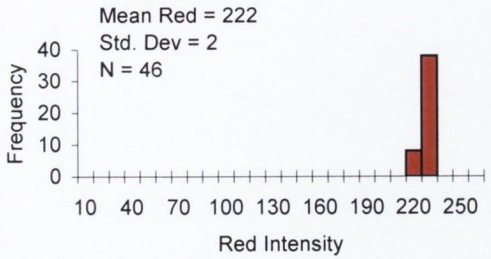

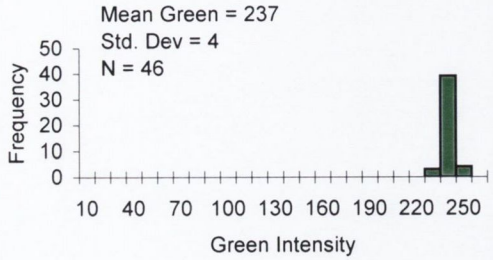

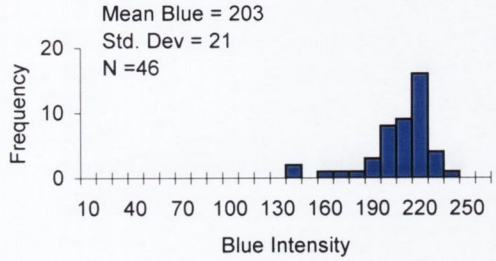

Number	Reference	Acritarch	Red	Green	Blue	Date	Colour
1	(1) W61/4	*Veryhachium*	222	236	231	15th Nov 04	
2	(1) F34/1	*Veryhachium*	220	234	229	15th Nov 04	
3	(1) N44	*Veryhachium*	223	236	225	15th Nov 04	
4	(1) O29/4	*Veryhachium*	222	237	225	15th Nov 04	
5	(1) G49	*Veryhachium*	224	237	224	15th Nov 04	
6	(1) J51/1	*Veryhachium*	223	236	220	15th Nov 04	
7	(1) E59	*Veryhachium*	223	238	219	15th Nov 04	
8	(1) R55/2	*Veryhachium*	223	237	219	15th Nov 04	
9	(1) J40/4	*Veryhachium*	223	237	218	15th Nov 04	
10	(1) W61/4	*Veryhachium*	222	238	218	15th Nov 04	
11	(1) M35	*Veryhachium*	221	236	218	15th Nov 04	
12	(1) O36/2	*Veryhachium*	221	236	218	15th Nov 04	
13	(1) M61	*Veryhachium*	225	240	217	15th Nov 04	
14	(1) W60/2	*Veryhachium*	222	237	217	15th Nov 04	
15	(1) J42	*Veryhachium*	216	239	216	15th Nov 04	
16	(1) R29	*Veryhachium*	220	236	215	15th Nov 04	
17	(1) H42/1	*Veryhachium*	222	238	214	15th Nov 04	
18	(1) N30/4	*Veryhachium*	223	242	214	15th Nov 04	
19	(1) W40/4	*Veryhachium*	222	238	211	15th Nov 04	
20	(1) F38/4	*Veryhachium*	223	236	211	15th Nov 04	
21	(1) J31/4	*Veryhachium*	223	238	210	15th Nov 04	
22	(1) F38/4	*Veryhachium*	220	240	210	15th Nov 04	
23	(1) N44	*Veryhachium*	222	239	209	15th Nov 04	
24	(1) S40	*Veryhachium*	222	238	209	15th Nov 04	
25	(1) Q31/2	*Veryhachium*	221	236	208	15th Nov 04	
26	(1) M63/1	*Veryhachium*	222	237	207	15th Nov 04	
27	(1) H38/4	*Veryhachium*	222	239	205	15th Nov 04	
28	(1) R44/3	*Veryhachium*	221	239	205	15th Nov 04	
29	(1) S40	*Veryhachium*	224	243	202	15th Nov 04	
30	(1) J35	*Veryhachium*	218	238	200	15th Nov 04	
31	(1) F34/1	*Veryhachium*	218	235	198	15th Nov 04	
32	(1) Q54	*Veryhachium*	220	238	196	15th Nov 04	
33	(1) U55	*Veryhachium*	222	239	196	15th Nov 04	
34	(1) S36/2	*Veryhachium*	219	237	195	15th Nov 04	
35	(1) O63/1	*Veryhachium*	223	238	193	15th Nov 04	

Sample P13 - Corrected Data

36	(1) U65/1	*Veryhachium*	225	241	192	15th Nov 04	
37	(1) P57/1	*Veryhachium*	221	239	192	15th Nov 04	
38	(1) M55/2	*Veryhachium*	222	238	191	15th Nov 04	
39	(1) M40/2	*Veryhachium*	224	237	184	15th Nov 04	
40	(1) U30/4	*Veryhachium*	223	239	184	15th Nov 04	
41	(1) W49	*Veryhachium*	223	240	183	15th Nov 04	
42	(1) S44/3	*Veryhachium*	224	239	177	15th Nov 04	
43	(1) G65/3	*Veryhachium*	223	235	168	15th Nov 04	
44	(1) H42/1	*Veryhachium*	225	229	156	15th Nov 04	
45	(1) M54	*Veryhachium*	219	221	137	15th Nov 04	
46	(1) Y38/2	*Veryhachium*	223	224	136	15th Nov 04	

P 14

Number	Reference	Acritarch	Red	Green	Blue	Date	Colour
1	(1) N28/4	*Veryhachium*	218	235	225	8th Feb 05	
2	(1) E31/1	*Veryhachium*	209	222	159	8th Feb 05	
3	(1) X36/4	*Veryhachium*	218	238	216	8th Feb 05	
4	(1) U40	*Veryhachium*	221	238	227	8th Feb 05	
5	(1) W42/2	*Veryhachium*	222	237	221	8th Feb 05	
6	(1) T59/3	*Veryhachium*	219	236	220	8th Feb 05	
7	(1) P61/4	*Veryhachium*	220	238	210	8th Feb 05	

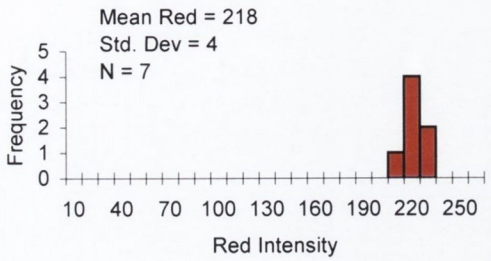

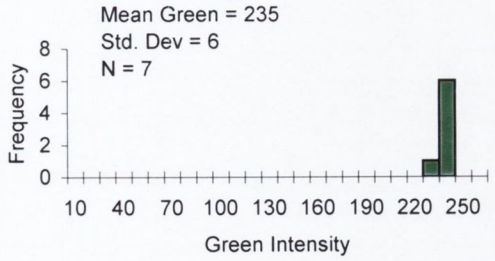

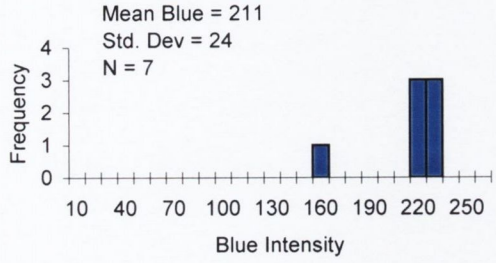

Sample P14 - Corrected Data

P 22

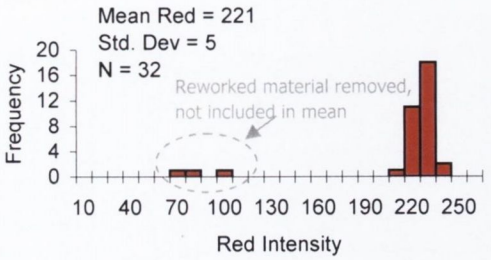

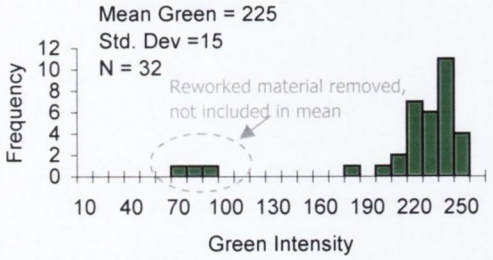

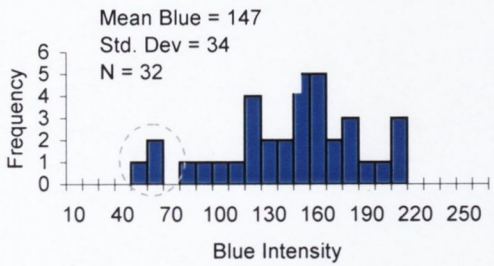

Number	Reference	Acritarch	Red	Green	Blue	Date	Colour
1	(1) X37/4	*Veryhachium*	219	241	209	18th Nov 04	
2	(1) G43	*Veryhachium*	220	242	202	18th Nov 04	
3	(1) R47/2	*Veryhachium*	216	238	201	18th Nov 04	
4	(1) J32/1	*Veryhachium*	220	244	200	18th Nov 04	
5	(1) G35	*Veryhachium*	219	238	186	18th Nov 04	
6	(1) P32/3	*Veryhachium*	221	240	174	18th Nov 04	
7	(1) Q45/2	*Veryhachium*	223	239	173	18th Nov 04	
8	(1) N39	*Veryhachium*	215	229	171	18th Nov 04	
9	(1) S33/4	*Veryhachium*	222	240	170	18th Nov 04	
10	(1) P48/1	*Veryhachium*	224	240	167	18th Nov 04	
11	(1) X41/2	*Veryhachium*	221	233	158	18th Nov 04	
12	(1) M39/2	*Veryhachium*	221	232	157	18th Nov 04	
13	(1) P35/3	*Veryhachium*	214	229	156	18th Nov 04	
14	(1) M41/3	*Veryhachium*	222	231	154	18th Nov 04	
15	(1) H34/1	*Veryhachium*	215	237	152	18th Nov 04	
16	(1) M43	*Veryhachium*	227	232	149	18th Nov 04	
17	(1) R43	*Veryhachium*	220	220	148	18th Nov 04	
18	(1) T32/1	*Veryhachium*	223	231	147	18th Nov 04	
19	(1) L31/2	*Veryhachium*	225	226	143	18th Nov 04	
20	(1) P31/2	*Veryhachium*	231	220	141	18th Nov 04	
21	(1) F37/3	*Veryhachium*	226	227	139	18th Nov 04	
22	(1) C34	*Veryhachium*	220	217	134	18th Nov 04	
23	(1) R39	*Veryhachium*	217	224	130	18th Nov 04	
24	(1) N44/4	*Veryhachium*	225	219	122	18th Nov 04	
25	(1) M39/2	*Veryhachium*	232	221	119	18th Nov 04	
26	(1) K41	*Veryhachium*	223	212	118	18th Nov 04	
27	(1) H35/4	*Veryhachium*	226	215	118	18th Nov 04	
28	(1) H41	*Veryhachium*	215	208	117	18th Nov 04	
29	(1) H45	*Veryhachium*	226	211	108	18th Nov 04	
30	(1) J33/4	*Veryhachium*	227	208	98	18th Nov 04	
31	(1) D32	*Veryhachium*	219	195	88	18th Nov 04	
32	(1) M39/2	*Veryhachium*	204	175	70	18th Nov 04	
33	(1) V35/1	*Veryhachium* ®	73	76	59	18th Nov 04	
34	(1) P36/4	*Veryhachium* ®	95	83	51	18th Nov 04	
35	(1) F43	*Veryhachium* ®	66	68	50	18th Nov 04	

Sample P22 - Corrected Data

P 23

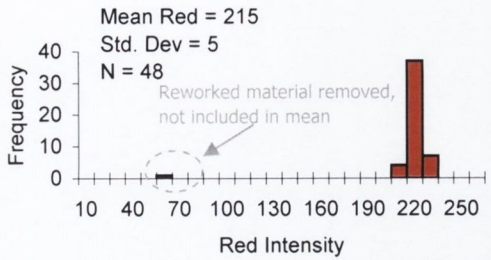

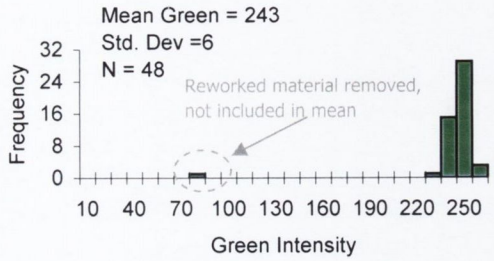

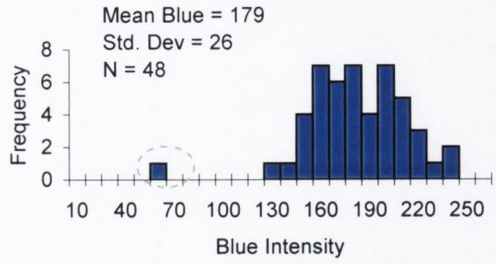

Number	Reference	Acritarch	Red	Green	Blue	Date	Colour
1	(1) Q46	*Veryhachium*	210	245	236	20th Nov 04	
2	(1) Q38	*Veryhachium*	212	249	231	20th Nov 04	
3	(1) U34	*Veryhachium*	212	250	227	20th Nov 04	
4	(1) P56/1	*Veryhachium*	220	239	215	21st Nov 04	
5	(1) J48	*Veryhachium*	212	250	211	20th Nov 04	
6	(1) J56/1	*Veryhachium*	219	238	211	21st Nov 04	
7	(1) K40/4	*Veryhachium*	212	250	210	20th Nov 04	
8	(1) P46/1	*Veryhachium*	210	248	208	20th Nov 04	
9	(1) T56	*Veryhachium*	220	239	208	21st Nov 04	
10	(1) H54	*Veryhachium*	221	237	203	21st Nov 04	
11	(1) Y54	*Veryhachium*	218	237	200	21st Nov 04	
12	(1) Q32/2	*Veryhachium*	212	251	196	20th Nov 04	
13	(1) M36	*Veryhachium*	210	247	192	20th Nov 04	
14	(1) C36/4	*Veryhachium*	209	245	192	20th Nov 04	
15	(1) K43/4	*Veryhachium*	212	249	192	20th Nov 04	
16	(1) L46/3	*Veryhachium*	217	253	191	20th Nov 04	
17	(1) S30/2	*Veryhachium*	210	247	191	20th Nov 04	
18	(1) J40/2	*Veryhachium*	212	249	190	20th Nov 04	
19	(1) S38	*Veryhachium*	211	249	189	20th Nov 04	
20	(1) H50/4	*Veryhachium*	219	239	188	21st Nov 04	
21	(1) D34	*Veryhachium*	213	249	185	20th Nov 04	
22	(1) X46/2	*Veryhachium*	212	245	181	20th Nov 04	
23	(1) P30/2	*Veryhachium*	215	248	180	20th Nov 04	
24	(1) N30/4	*Veryhachium*	210	243	175	20th Nov 04	
25	(1) R38/4	*Veryhachium*	213	245	174	20th Nov 04	
26	(1) R48/2	*Veryhachium*	213	245	174	20th Nov 04	
27	(1) O48	*Veryhachium*	215	248	171	20th Nov 04	
28	(1) R30	*Veryhachium*	211	243	171	20th Nov 04	
29	(1) O33/4	*Veryhachium*	213	245	170	20th Nov 04	
30	(1) H30	*Veryhachium*	214	243	169	20th Nov 04	
31	(1) C32/4	*Veryhachium*	213	246	168	20th Nov 04	
32	(1) N40/4	*Veryhachium*	212	242	168	20th Nov 04	
33	(1) F41/1	*Veryhachium*	214	246	168	20th Nov 04	
34	(1) M32	*Veryhachium*	216	245	166	20th Nov 04	
35	(1) S34/1	*Veryhachium*	213	246	166	20th Nov 04	

Sample P23 - Corrected Data

36	(1) V51/3	*Veryhachium*	224	237	159	21st Nov 04	
37	(1) O54	*Veryhachium*	224	239	159	21st Nov 04	
38	(1) O43/4	*Veryhachium*	215	243	157	20th Nov 04	
39	(1) E56	*Veryhachium*	226	237	155	21st Nov 04	
40	(1) M33/2	*Veryhachium*	213	239	151	20th Nov 04	
41	(1) P30/1	*Veryhachium*	216	238	151	20th Nov 04	
42	(1) E34	*Veryhachium*	221	242	150	20th Nov 04	
43	(1) V51/3	*Veryhachium*	225	233	150	21st Nov 04	
44	(1) H38/4	*Veryhachium*	215	241	149	20th Nov 04	
45	(1) S32/2	*Veryhachium*	218	238	143	20th Nov 04	
46	(1) P38	*Veryhachium*	216	233	141	20th Nov 04	
47	(1) M32	*Veryhachium*	217	234	136	20th Nov 04	
48	(1) V54/2	*Veryhachium*	225	226	130	21st Nov 04	
49	(1) C34/3	*Veryhachium* ®	55	71	60	20th Nov 04	

P 24

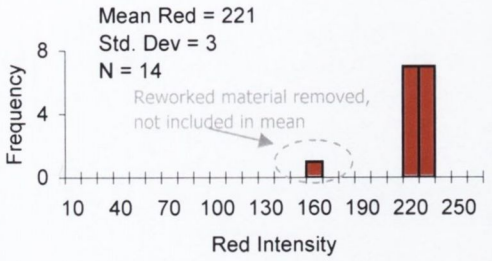

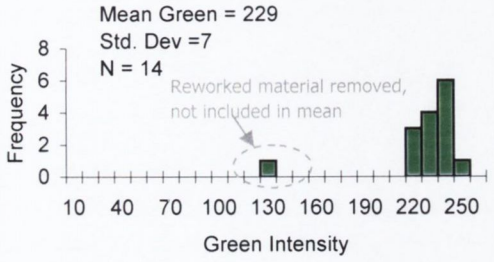

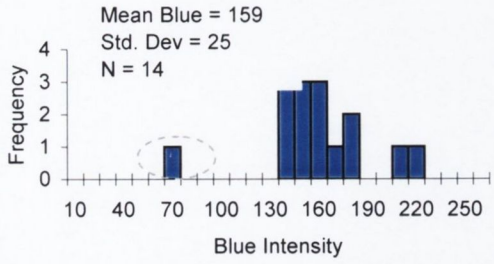

Number	Reference	Acritarch	Red	Green	Blue	Date	Colour
1	(1) U64/4	*Veryhachium*	219	236	211	21st Nov 04	
2	(1) G67	*Veryhachium*	219	237	208	21st Nov 04	
3	(1) T70/4	*Veryhachium*	219	232	174	21st Nov 04	
4	(1) P35	*Veryhachium*	220	234	172	21st Nov 04	
5	(1) Q58/2	*Veryhachium*	224	241	168	21st Nov 04	
6	(1) K69	*Veryhachium*	220	230	157	21st Nov 04	
7	(1) U64/4	*Veryhachium*	219	227	152	21st Nov 04	
8	(1) V66/1	*Veryhachium*	222	233	151	21st Nov 04	
9	(1) D39	*Veryhachium*	226	233	142	21st Nov 04	
10	(1) C65/4	*Veryhachium*	220	220	141	21st Nov 04	
11	(1) U63/2	*Veryhachium*	221	226	141	21st Nov 04	
12	(1) M53/3	*Veryhachium*	222	220	140	21st Nov 04	
13	(1) Q57/3	*Veryhachium*	224	221	135	21st Nov 04	
14	(1) E41/1	*Veryhachium*	226	219	133	21st Nov 04	
15	(1) H51/1	*Veryhachium* ®	151	123	64	21st Nov 04	

Sample P24 - Corrected Data

P 25

Number	Reference	Acritarch	Red	Green	Blue	Date	Colour
1	(1) D65/4	*Veryhachium*	104	111	74	21st Feb 06	
2	(1) M60/1	*Veryhachium*	96	100	61	21st Feb 06	
3	(1) O64/3	*Veryhachium*	62	70	52	21st Feb 06	
4	(1) F40/2	*Veryhachium*	49	64	49	21st Feb 06	

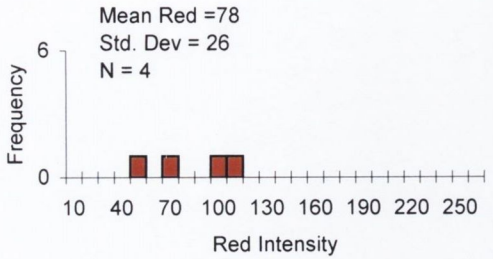

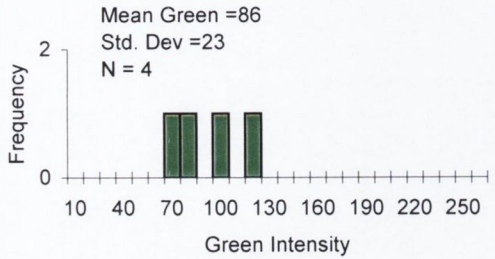

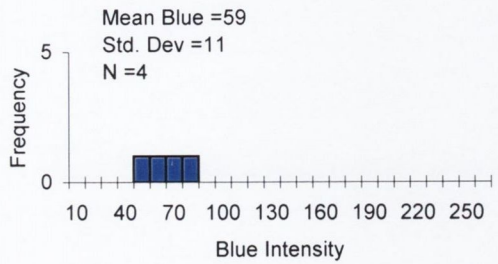

Spread in RGB data was interpreted as a result of variable degrees of thermal alteration between specimens.

Sample P25 - Corrected Data

Pet 3

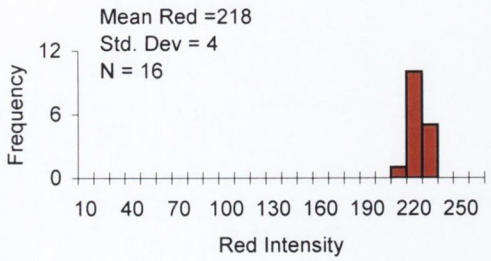

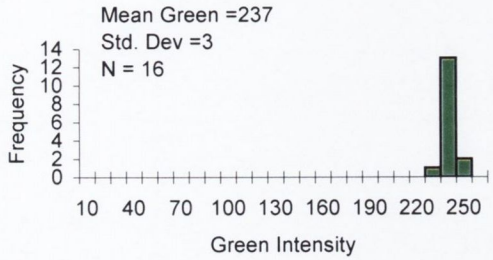

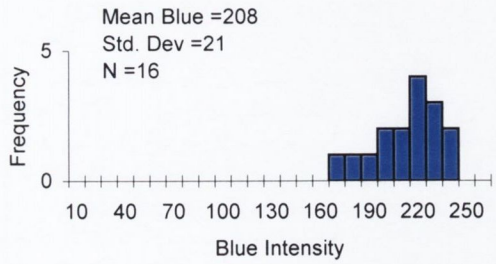

Number	Reference	Acritarch	Red	Green	Blue	Date	Colour
1	(1) N43/1	*Veryhachium*	222	239	236	24th Sept 04	
2	(1) U38/3	*Veryhachium*	222	236	234	24th Sept 04	
3	(1) M43/1	*Veryhachium*	226	240	227	24th Sept 04	
4	(1) W71/4	*Veryhachium*	218	239	225	24th Sept 04	
5	(1) F57/4	*Veryhachium*	216	239	224	24th Sept 04	
6	(1) S48/3	*Veryhachium*	223	238	219	24th Sept 04	
7	(1) T59/1	*Veryhachium*	219	235	218	24th Sept 04	
8	(1) R51/2	*Veryhachium*	217	234	215	24th Sept 04	
9	(1) M40	*Veryhachium*	217	242	210	24th Sept 04	
10	(1) U38/3	*Veryhachium*	213	236	206	24th Sept 04	
11	(1) H55/3	*Veryhachium*	220	238	201	24th Sept 04	
12	(1) J69/2	*Veryhachium*	221	239	199	24th Sept 04	
13	(1) H55/3	*Veryhachium*	218	239	194	24th Sept 04	
14	(1) Q39/1	*Veryhachium*	216	237	186	24th Sept 04	
15	(1) F60/3	*Veryhachium*	209	234	176	24th Sept 04	
16	(1) P38	*Veryhachium*	212	230	161	24th Sept 04	

Sample Pet 3 - Corrected Data

Rh19-P12

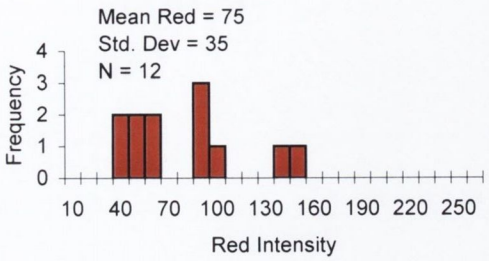

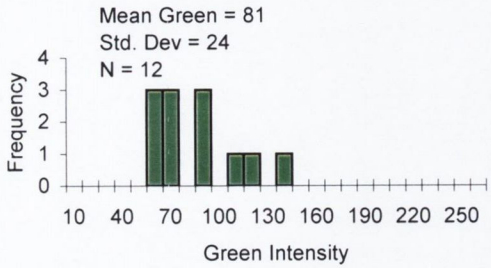

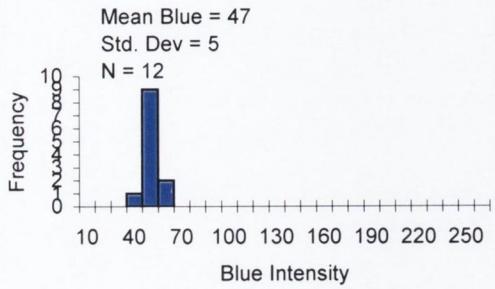

Number	Reference	Acritarch	Red	Green	Blue	Date	Colour
1	(2) N65/3	*Veryhachium*	144	132	50	18th August	
2	(1) V40/1	*Veryhachium*	132	115	45	18th August	
3	(1) S34/1	*Veryhachium*	95	106	59	18th August	
4	(2) P63/1	*Veryhachium*	84	82	41	18th August	
5	(1) W54/1	*Veryhachium*	84	86	44	18th August	
6	(2) Y61/1	*Veryhachium*	83	80	39	18th August	
7	(2) Z67/4	*Veryhachium*	60	67	47	18th August	
8	(2) L33/3	*Veryhachium*	57	65	49	18th August	
9	(1) S32/4	*Veryhachium*	49	68	54	18th August	
10	(2) V45/2	*Veryhachium*	43	60	47	18th August	
11	(1) X44/1	*Veryhachium*	39	59	47	18th August	
12	(1) S38	*Veryhachium*	35	57	45	18th August	

Spread in RGB intensities is believed to result from the degraded nature of these specimens

Sun 3

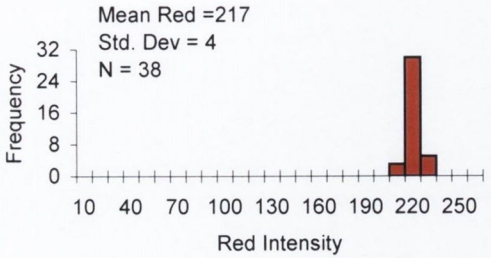

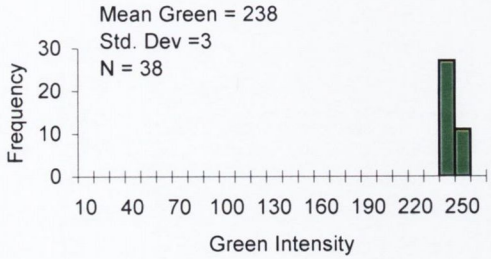

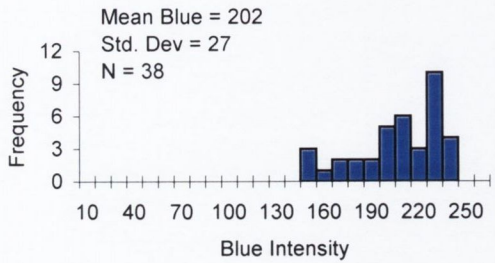

Number	Reference	Acritarch	Red	Green	Blue	Date	Colour
1	(1) P47	*Veryhachium*	214	238	236	14th Oct 04	
2	(6) K37/2	*Veryhachium*	219	241	235	14th Oct 04	
3	(6) J46/4	*Veryhachium*	213	238	233	14th Oct 04	
4	(5) J47	*Veryhachium*	219	241	233	14th Oct 04	
5	(5) T63/2	*Veryhachium*	215	239	229	14th Oct 04	
6	(6) O42	*Veryhachium*	213	237	227	14th Oct 04	
7	(5) N52	*Veryhachium*	218	240	227	14th Oct 04	
8	(5) Q48/2	*Veryhachium*	218	241	226	14th Oct 04	
9	(6) T54	*Veryhachium*	219	238	226	16th Oct 04	
10	(6) Z54	*Veryhachium*	217	241	225	14th Oct 04	
11	(5) R58	*Veryhachium*	217	238	223	14th Oct 04	
12	(3) P64/2	*Veryhachium*	215	239	221	14th Oct 04	
13	(6) K47/3	*Veryhachium*	214	239	221	14th Oct 04	
14	(6) S61/2	*Veryhachium*	219	241	221	16th Oct 04	
15	(7) H51	*Veryhachium*	215	234	219	16th Oct 04	
16	(7) N60/4	*Veryhachium*	221	239	216	16th Oct 04	
17	(5) H45/3	*Veryhachium*	218	244	213	14th Oct 04	
18	(5) L40	*Veryhachium*	217	241	208	14th Oct 04	
19	(7) S47	*Veryhachium*	217	239	207	16th Oct 04	
20	(3) V48/4	*Veryhachium*	205	232	207	14th Oct 04	
21	(6) M54	*Veryhachium*	220	239	203	16th Oct 04	
22	(6) H37	*Veryhachium*	216	242	201	14th Oct 04	
23	(6) T72/4	*Veryhachium*	212	240	200	14th Oct 04	
24	(7) S71/3	*Veryhachium*	209	234	199	16th Oct 04	
25	(6) M63/4	*Veryhachium*	219	239	197	16th Oct 04	
26	(5) O53	*Veryhachium*	216	244	196	14th Oct 04	
27	(7) J44/3	*Veryhachium*	221	241	193	16th Oct 04	
28	(6) T34	*Veryhachium*	216	241	190	14th Oct 04	
29	(6) K52/3	*Veryhachium*	217	239	186	14th Oct 04	
30	(5) Z59/4	*Veryhachium*	217	239	182	14th Oct 04	
31	(1) X71/2	*Veryhachium*	211	236	180	14th Oct 04	
32	(6) Q61	*Veryhachium*	218	235	178	16th Oct 04	
33	(5) K65/1	*Veryhachium*	206	232	169	14th Oct 04	
34	(6) P61/1	*Veryhachium*	218	236	166	16th Oct 04	
35	(6) P60	*Veryhachium*	221	238	157	16th Oct 04	

Sample Sun 3 - Corrected Data

36	(5) Z56/4	*Veryhachium*	226	235	148	14th Oct 04	
37	(5) E40/3	*Veryhachium*	219	235	142	14th Oct 04	
38	(5) Z35/4	*Veryhachium*	222	236	141	14th Oct 04	

Sun 7

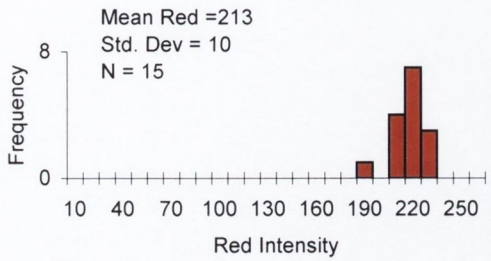

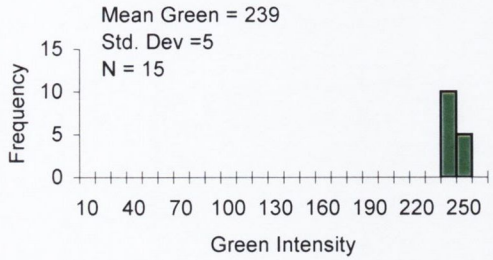

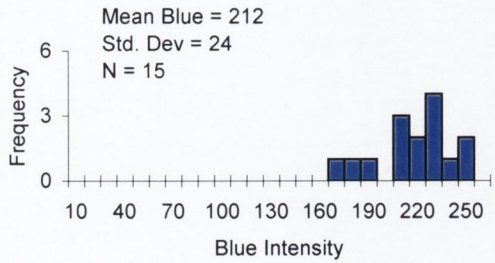

Number	Reference	Acritarch	Red	Green	Blue	Date	Colour
1	(6) Z67/1	*Veryhachium*	205	250	247	18th Aug 05	
2	(3) L48/1	*Veryhachium*	222	245	241	16th Oct 04	
3	(3) X54	*Veryhachium*	217	234	232	16th Oct 04	
4	(2) J64	*Veryhachium*	220	240	227	16th Oct 04	
5	(3) M71/2	*Veryhachium*	206	235	224	16th Oct 04	
6	(3) H71/2	*Veryhachium*	222	242	224	16th Oct 04	
7	(6) H69/3	*Veryhachium*	186	245	224	18th Aug 05	
8	(2) L59/4	*Veryhachium*	219	236	217	16th Oct 04	
9	(2) J52/4	*Veryhachium*	218	237	216	16th Oct 04	
10	(2) J49	*Veryhachium*	205	233	204	16th Oct 04	
11	(2) T45	*Veryhachium*	219	238	203	16th Oct 04	
12	(1) E60/4	*Veryhachium*	202	231	201	16th Oct 04	
13	(3) R75/1	*Veryhachium*	220	243	181	16th Oct 04	
14	(1) E56/2	*Veryhachium*	220	238	170	16th Oct 04	
15	(3) K69/2	*Veryhachium*	217	240	167	16th Oct 04	

Sample Sun 7 - Corrected Data

TL 1

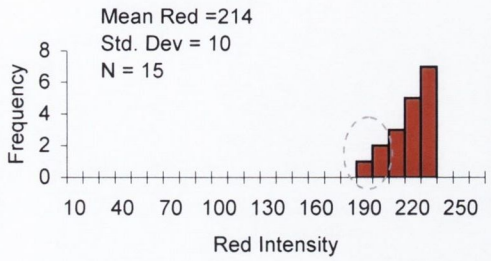

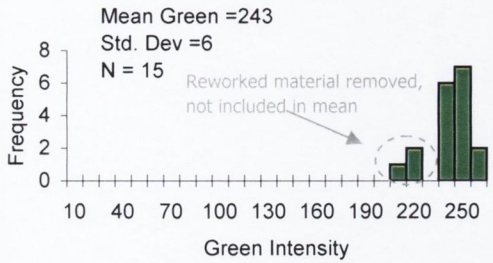

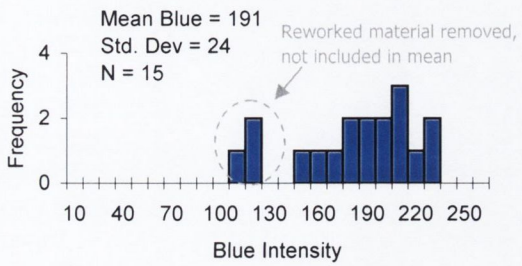

Number	Reference	Acritarch	Red	Green	Blue	Date	Colour
1	(1) J57	*Veryhachium*	210	245	226	22nd Aug 05	
2	(3) N41	*Veryhachium*	209	246	223	22nd Aug 05	
3	(2) Z55/2	*Veryhachium*	192	253	215	18th Aug 05	
4	(2) O41/4	*Veryhachium*	221	239	209	22nd Aug 05	
5	(B) H52/3	*Veryhachium*	222	241	204	22nd Aug 05	
6	(3) W70/2	*Veryhachium*	216	245	203	22nd Aug 05	
7	(2) M63	*Veryhachium*	197	256	199	18th Aug 05	
8	(3) N54/4	*Veryhachium*	204	238	194	22nd Aug 05	
9	(B) S59/3	*Veryhachium*	220	239	187	22nd Aug 05	
10	(B) Q55/2	*Veryhachium*	223	241	180	22nd Aug 05	
11	(B) Y69/1	*Veryhachium*	222	239	179	22nd Aug 05	
12	(2) F34/3	*Veryhachium*	222	239	177	22nd Aug 05	
13	(B) U55/2	*Veryhachium*	222	240	166	22nd Aug 05	
14	(2) K39/4	*Veryhachium*	209	249	155	18th Aug 05	
15	(B) U63/3	*Veryhachium*	224	235	148	22nd Aug 05	
16	(1) K50/4	*Veryhachium ®*	215	214	120	22nd Aug 05	
17	(1) T49	*Veryhachium ®*	214	214	119	22nd Aug 05	
18	(2) P41/3	*Veryhachium ®*	187	210	109	18th Aug 05	

Sample TL1 - Corrected Data

TL 2

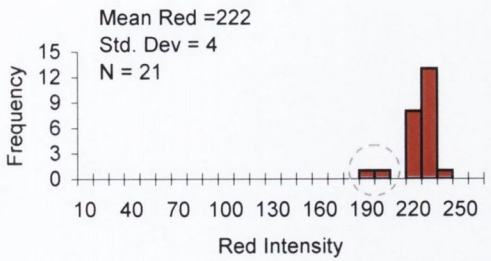

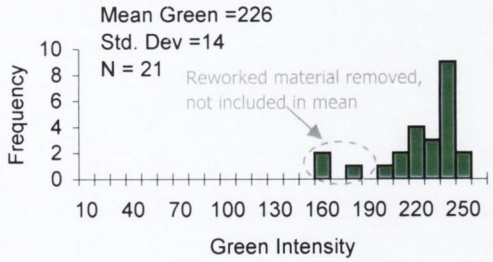

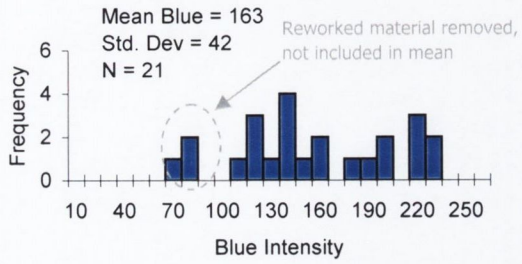

Number	Reference	Acritarch	Red	Green	Blue	Date	Colour
1	(B) G69/3	*Veryhachium*	219	236	230	8th Feb 05	
2	(2) J53/1	*Veryhachium*	221	243	223	8th Feb 05	
3	(5) W61/3	*Veryhachium*	218	237	219	8th Feb 05	
4	(3) X37/3	*Veryhachium*	220	237	218	8th Feb 05	
5	(1) V65/4	*Veryhachium*	217	235	211	8th Feb 05	
6	(3) H45/3	*Veryhachium*	222	237	200	8th Feb 05	
7	(B) M63	*Veryhachium*	224	243	190	8th Feb 05	
8	(1) O38/4	*Veryhachium*	219	237	182	8th Feb 05	
9	(3) U62/1	*Veryhachium*	221	233	178	8th Feb 05	
10	(4) N68/3	*Veryhachium*	226	231	158	8th Feb 05	
11	(B) F34/4	*Veryhachium*	226	237	151	8th Feb 05	
12	(1) TOM	*Veryhachium*	218	227	145	8th Feb 05	
13	(3) L45	*Veryhachium*	224	217	137	8th Feb 05	
14	(2) Y59/1	*Veryhachium*	227	221	134	8th Feb 05	
15	(3) K39/4	*Veryhachium*	223	213	132	8th Feb 05	
16	(3) N43/2	*Veryhachium*	225	215	132	8th Feb 05	
17	(3) P60/3	*Veryhachium*	222	210	123	8th Feb 05	
18	(B) W35/4	*Veryhachium*	219	205	120	8th Feb 05	
19	(4) N68/2	*Veryhachium*	236	222	119	8th Feb 05	
20	(B) U34/4	*Veryhachium*	220	208	115	8th Feb 05	
21	(2) U69/3	*Veryhachium*	222	197	101	8th Feb 05	
22	(4) K68/3	*Veryhachium* ®	217	178	76	8th Feb 05	
23	(3) K52/3	*Veryhachium* ®	190	152	70	8th Feb 05	
24	(5) Q48/1	*Veryhachium* ®	197	157	66	8th Feb 05	

Sample TL2 - Corrected Data

TL 3

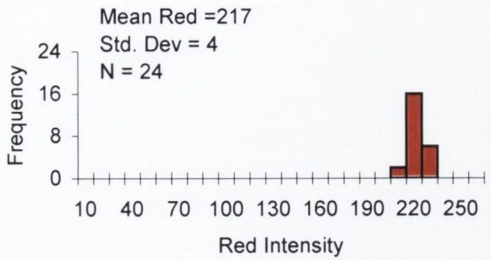

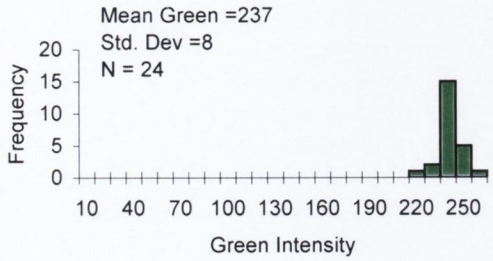

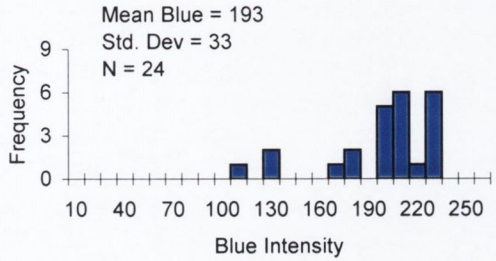

Number	Reference	Acritarch	Red	Green	Blue	Date	Colour
1	(1) O62/1	*Veryhachium*	218	240	227	18th Oct 04	
2	(2) H57/1	*Veryhachium*	219	239	226	18th Oct 04	
3	(2) O54	*Veryhachium*	223	252	222	18th Oct 04	
4	(1) G46/3	*Veryhachium*	216	236	222	18th Oct 04	
5	(2) X56/4	*Veryhachium*	221	243	222	18th Oct 04	
6	(1) S42/2	*Veryhachium*	218	239	221	18th Oct 04	
7	(1) T47/2	*Veryhachium*	218	240	210	18th Oct 04	
8	(1) T71	*Veryhachium*	217	239	208	18th Oct 04	
9	(2) P62/2	*Veryhachium*	217	240	207	18th Oct 04	
10	(1) P59/3	*Veryhachium*	206	233	206	18th Oct 04	
11	(2) M53/1	*Veryhachium*	222	247	203	18th Oct 04	
12	(1) N56/3	*Veryhachium*	209	232	201	18th Oct 04	
13	(1) O71/2	*Veryhachium*	218	241	201	18th Oct 04	
14	(2) T57	*Veryhachium*	219	238	200	18th Oct 04	
15	(1) E40/2	*Veryhachium*	218	242	199	18th Oct 04	
16	(1) R67/3	*Veryhachium*	216	241	199	18th Oct 04	
17	(1) W37/2	*Veryhachium*	216	235	194	18th Oct 04	
18	(1) Z51/4	*Veryhachium*	214	237	191	18th Oct 04	
19	(1) C46/4	*Veryhachium*	216	240	175	18th Oct 04	
20	(2) Q61/4	*Veryhachium*	217	240	171	18th Oct 04	
21	(1) R56/4	*Veryhachium*	216	237	162	18th Oct 04	
22	(2) N46/2	*Veryhachium*	225	228	123	18th Oct 04	
23	(2) U61/3	*Veryhachium*	227	229	121	18th Oct 04	
24	(1) Z74/5	*Veryhachium*	223	211	110	18th Oct 04	

There is a possibilty specimens 22,23, and 24 are reworked, but there is not sufficent variation in the RGB histograms to be certain, so they have not been removed from the data set.

Sample TL3 - Corrected Data

TL 7

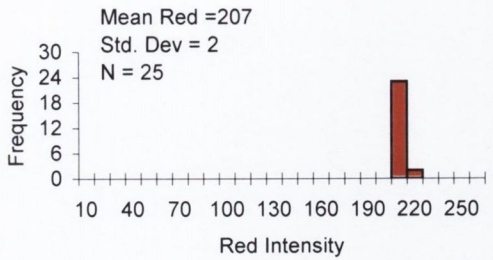

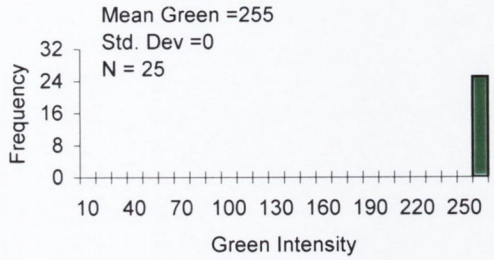

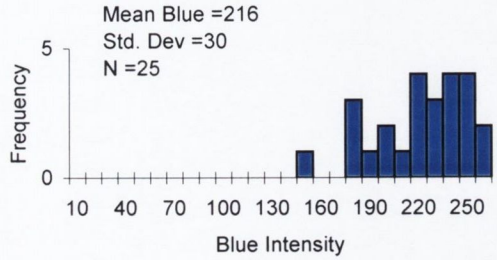

Number	Reference	Acritarch	Red	Green	Blue	Date	Colour
1	(1) U64/1	*Veryhachium*	206	255	255	21st Feb 06	
2	(2) R43	*Veryhachium*	207	255	255	21st Feb 06	
3	(2) N47	*Veryhachium*	206	255	249	21st Feb 06	
4	(3) M67/3	*Veryhachium*	205	255	247	21st Feb 06	
5	(3) Q54/2	*Veryhachium*	207	255	246	21st Feb 06	
6	(3) U41/4	*Veryhachium*	205	255	240	21st Feb 06	
7	(1) V49/3	*Veryhachium*	206	255	237	21st Feb 06	
8	(2) G43/1	*Veryhachium*	204	255	236	21st Feb 06	
9	(2) P47/3	*Veryhachium*	206	255	234	21st Feb 06	
10	(2) P49/3	*Veryhachium*	205	255	233	21st Feb 06	
11	(1) R43/2	*Veryhachium*	206	255	224	21st Feb 06	
12	(1) G44/1	*Veryhachium*	207	255	223	21st Feb 06	
13	(3) N54	*Veryhachium*	206	255	222	21st Feb 06	
14	(2) K39	*Veryhachium*	204	255	220	21st Feb 06	
15	(2) L39	*Veryhachium*	205	255	218	21st Feb 06	
16	(2) M45/1	*Veryhachium*	204	255	216	21st Feb 06	
17	(2) K54/1	*Veryhachium*	205	255	213	21st Feb 06	
18	(2) T64/4	*Veryhachium*	207	255	207	21st Feb 06	
19	(3) U53	*Veryhachium*	205	255	198	21st Feb 06	
20	(2) N62/4	*Veryhachium*	207	255	193	21st Feb 06	
21	(2) G45	*Veryhachium*	210	255	181	21st Feb 06	
22	(2) V44/4	*Veryhachium*	209	255	178	21st Feb 06	
23	(2) L51/4	*Veryhachium*	210	255	174	21st Feb 06	
24	(2) N52/1	*Veryhachium*	209	255	172	21st Feb 06	
25	(2) G35/4	*Veryhachium*	214	255	142	21st Feb 06	

Sample TL7 - Corrected Data

V 4

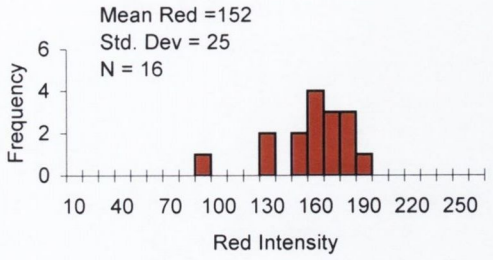

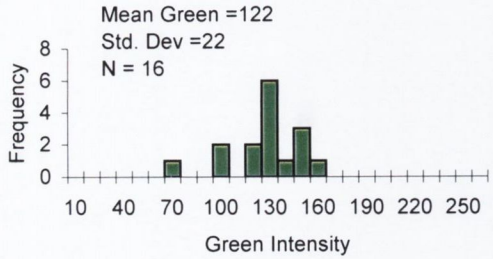

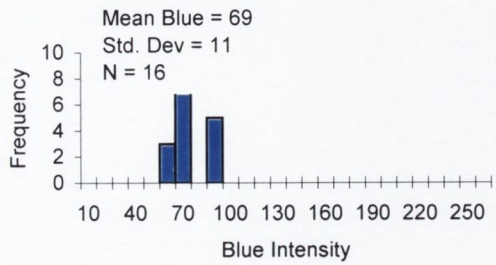

Number	Reference	Acritarch	Red	Green	Blue	Date	Colour
1	(1) Q56/2	*Veryhachium*	183	150	81	5th Dec 04	
2	(1) L69/4	*Veryhachium*	176	145	83	5th Dec 04	
3	(2) M34/3	*Veryhachium*	173	147	88	5th Dec 04	
4	(1) X72/2	*Veryhachium*	172	142	81	5th Dec 04	
5	(2) M43/3	*Veryhachium*	162	128	68	5th Dec 04	
6	(2) X47/1	*Veryhachium*	162	129	68	5th Dec 04	
7	(2) W53/2	*Veryhachium*	162	127	68	5th Dec 04	
8	(2) V45/1	*Veryhachium*	158	135	81	5th Dec 04	
9	(2) S55/4	*Veryhachium*	158	126	62	5th Dec 04	
10	(2) R53/4	*Veryhachium*	157	125	65	5th Dec 04	
11	(1) E54/1	*Veryhachium*	157	124	68	5th Dec 04	
12	(2) Q47/2	*Veryhachium*	143	114	67	5th Dec 04	
13	(2) K49/2	*Veryhachium*	142	113	66	5th Dec 04	
14	(2) O53/2	*Veryhachium*	127	93	50	5th Dec 04	
15	(2) U49/3	*Veryhachium*	121	94	57	5th Dec 04	
16	(1) W67/2	*Veryhachium*	81	67	52	5th Dec 04	

Spread of R and G intensities is interpreted as a result of thermal degradation which affects some, but not all of the specimens

V 5

Number	Reference	Acritarch	Red	Green	Blue	Date	Colour
1	(1) S36/3	*Veryhachium*	172	146	85	5th Dec 05	
2	(1) L36/3	*Veryhachium*	179	150	84	5th Dec 05	
3	(1) F34/4	*Veryhachium*	186	152	80	5th Dec 05	
4	(1) U54/3	*Veryhachium*	64	64	57	5th Dec 05	
5	(1) X36/3	*Veryhachium*	58	64	57	5th Dec 05	
6	(1) X36/4	*Veryhachium*	120	95	55	5th Dec 05	
7	(1) X34/4	*Veryhachium*	84	73	50	5th Dec 05	

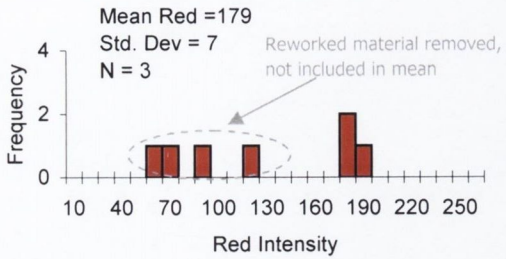

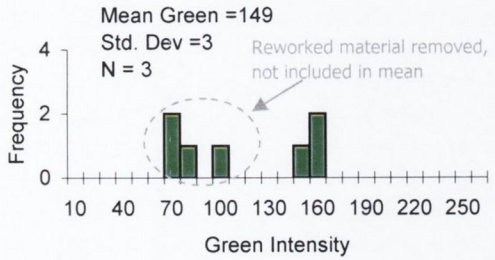

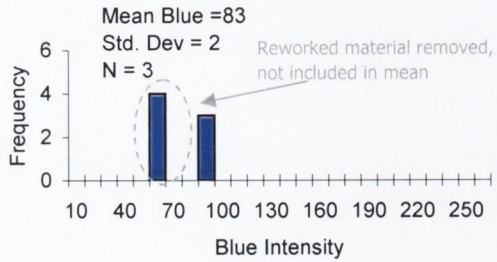

Sample V5 - Corrected Data

V 7

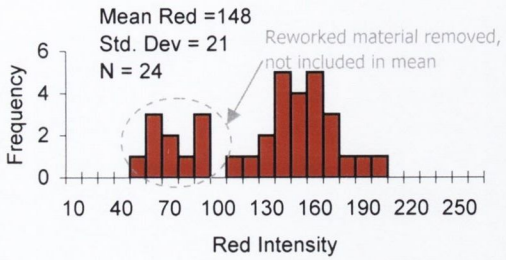

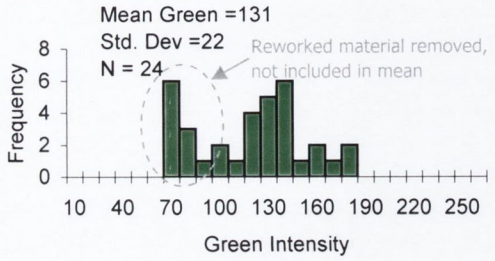

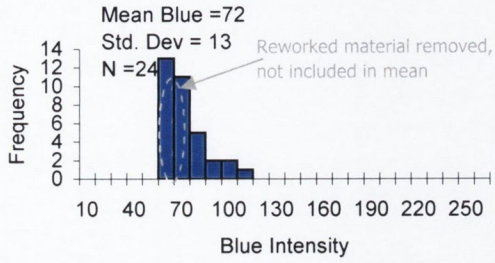

Number	Reference	Acritarch	Red	Green	Blue	Date	Colour
1	(1) O64/1	*Veryhachium*	198	179	99	24th Nov 05	
2	(1) N(Control)	*Veryhachium*	183	171	97	24th Nov 05	
3	(3) X55/4	*Veryhachium*	176	165	100	24th Nov 05	
4	(2) Y62/1	*Veryhachium*	166	154	87	24th Nov 05	
5	(3) J60/3	*Veryhachium*	166	153	84	24th Nov 05	
6	(1) O55	*Veryhachium*	160	143	76	24th Nov 05	
7	(3) J45/4	*Veryhachium*	159	138	74	24th Nov 05	
8	(3) V58	*Veryhachium*	156	132	67	24th Nov 05	
9	(1) Q57/2	*Veryhachium*	155	136	70	24th Nov 05	
10	(1) F37/1	*Veryhachium*	154	133	67	24th Nov 05	
11	(1) G57/3	*Veryhachium*	152	137	79	24th Nov 05	
12	(1) Q69/1	*Veryhachium*	147	127	68	24th Nov 05	
13	(1) V71/4	*Veryhachium*	146	124	61	24th Nov 05	
14	(3) N62/3	*Veryhachium*	146	126	66	24th Nov 05	
15	(1) U45/1	*Veryhachium*	143	131	75	24th Nov 05	
16	(3) F53/4	*Veryhachium*	139	122	65	24th Nov 05	
17	(1) L57/3	*Veryhachium*	138	117	62	24th Nov 05	
18	(3) O39/1	*Veryhachium*	137	123	76	24th Nov 05	
19	(3) Y40/4	*Veryhachium*	135	119	67	24th Nov 05	
20	(1) P67/2	*Veryhachium*	133	118	67	24th Nov 05	
21	(1) R65/4	*Veryhachium*	125	110	61	24th Nov 05	
22	(1) O70/1	*Veryhachium*	123	104	56	24th Nov 05	
23	(1) V38/2	*Veryhachium*	112	95	55	24th Nov 05	
24	(3) Z58/3	*Veryhachium*	106	92	53	24th Nov 05	
25	(1) R72/4	*Veryhachium ®*	89	78	50	24th Nov 05	
26	(3) R35/4	*Veryhachium ®*	88	83	59	24th Nov 05	
27	(3) H46/1	*Veryhachium ®*	88	77	51	24th Nov 05	
28	(3) G64/3	*Veryhachium ®*	80	75	54	24th Nov 05	
29	(1) U47/2	*Veryhachium ®*	68	68	54	24th Nov 05	
30	(1) X58/4	*Veryhachium ®*	64	67	53	24th Nov 05	
31	(3) W53/2	*Veryhachium ®*	54	67	57	24th Nov 05	
32	(1) U72/4	*Veryhachium ®*	54	67	56	24th Nov 05	
33	(1) H70/2	*Veryhachium ®*	53	65	56	24th Nov 05	
34	(3) P50	*Veryhachium ®*	47	65	54	24th Nov 05	

Sample V7 - Corrected Data

V 8

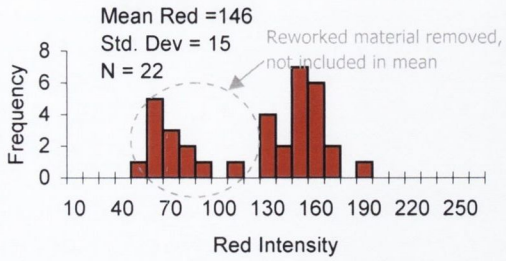

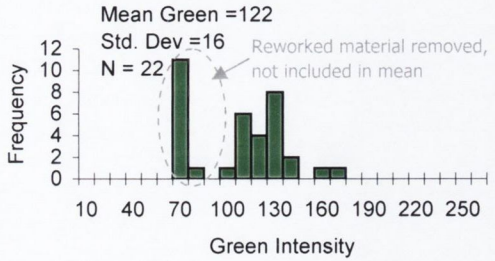

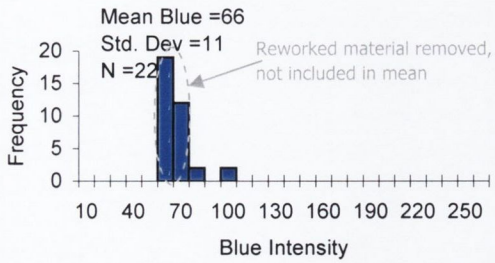

Number	Reference	Acritarch	Red	Green	Blue	Date	Colour
1	(1) J63/1	*Veryhachium*	184	166	96	25th Nov 04	
2	(1) Q43	*Veryhachium*	170	153	93	25th Nov 04	
3	(2) L37/4	*Veryhachium*	163	133	60	25th Nov 04	
4	(1) U56/4b	*Veryhachium*	157	132	71	25th Nov 04	
5	(2) R54/1	*Veryhachium*	157	129	69	25th Nov 04	
6	(2) D46/2	*Veryhachium*	154	127	66	25th Nov 04	
7	(1) P48/3	*Veryhachium*	152	126	64	25th Nov 04	
8	(2) Z66/2	*Veryhachium*	151	126	65	25th Nov 04	
9	(1) S67	*Veryhachium*	150	125	69	25th Nov 04	
10	(1) R38	*Veryhachium*	149	120	62	25th Nov 04	
11	(1) EF	*Veryhachium*	147	121	64	25th Nov 04	
12	(2) Q73/4	*Veryhachium*	145	115	58	25th Nov 04	
13	(2) Q62	*Veryhachium*	145	119	62	25th Nov 04	
14	(1) K40	*Veryhachium*	145	120	65	25th Nov 04	
15	(1) J48	*Veryhachium*	144	123	70	25th Nov 04	
16	(1) G53	*Veryhachium*	141	128	75	25th Nov 04	
17	(2) F43	*Veryhachium*	134	108	57	25th Nov 04	
18	(1) V73/4	*Veryhachium*	131	107	56	25th Nov 04	
19	(2) L67	*Veryhachium*	129	106	57	25th Nov 04	
20	(1) V38	*Veryhachium*	126	103	58	25th Nov 04	
21	(2) K49/4	*Veryhachium*	122	101	51	25th Nov 04	
22	(2) Z66/2	*Veryhachium*	120	104	63	25th Nov 04	
23	(1) R61/1	*Veryhachium* ®	108	90	57	25th Nov 04	
24	(2) G36	*Veryhachium* ®	87	77	55	25th Nov 04	
25	(2) O52/3	*Veryhachium* ®	73	67	51	25th Nov 04	
26	(2) V47/4	*Veryhachium* ®	72	67	52	25th Nov 04	
27	(2) P68	*Veryhachium* ®	70	69	54	25th Nov 04	
28	(2) U72/2	*Veryhachium* ®	66	70	61	25th Nov 04	
29	(1) M67/3	*Veryhachium* ®	65	67	57	25th Nov 04	
30	(1) E56	*Veryhachium* ®	54	64	58	25th Nov 04	
31	(1) U56/4a	*Veryhachium* ®	54	64	54	25th Nov 04	
32	(2) H43	*Veryhachium* ®	53	65	55	25th Nov 04	
33	(1) F61/1	*Veryhachium* ®	53	64	57	25th Nov 04	
34	(2) D37/4	*Veryhachium* ®	50	66	57	25th Nov 04	
35	(1) T64/2	*Veryhachium* ®	48	65	54	25th Nov 04	

Sample V8 - Corrected Data

Va115

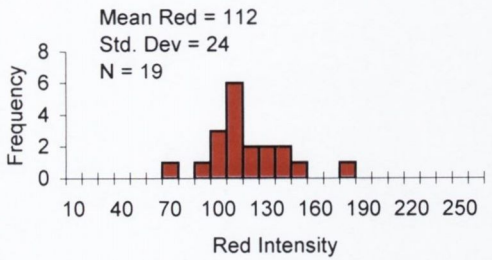

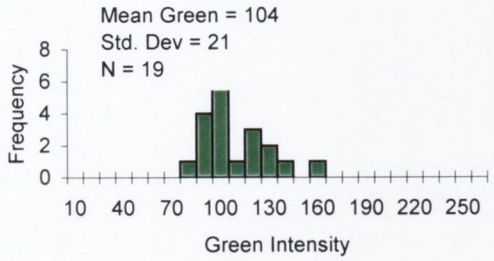

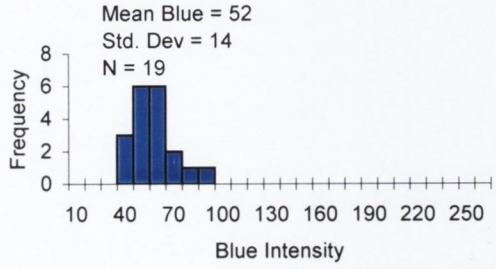

Number	Reference	Acritarch	Red	Green	Blue	Date	Colour
1	(1) N52	*Veryhachium*	170.33	158.59	89.58	22nd Aug 05	
2	(1) F65	*Veryhachium*	146.05	128.49	64.71	22nd Aug 05	
3	(1) O59/1	*Veryhachium*	138.57	132.15	71.18	22nd Aug 05	
4	(1) J43	*Veryhachium*	135.39	122.06	61.07	22nd Aug 05	
5	(1) K51/3	*Veryhachium*	128.03	115.16	52.82	22nd Aug 05	
6	(1) F58/2	*Veryhachium*	120.86	110.77	53.59	22nd Aug 05	
7	(1) M67/4	*Veryhachium*	118.85	109.29	54.89	22nd Aug 05	
8	(1) F62/4	*Veryhachium*	118.81	110.78	56.42	22nd Aug 05	
9	(1) O49/3	*Veryhachium*	109.29	97.73	49.03	22nd Aug 05	
10	(1) S60/2	*Veryhachium*	109.29	93.00	45.82	22nd Aug 05	
11	(1) L54/3	*Veryhachium*	102.04	92.78	53.39	22nd Aug 05	
12	(1) K34/1	*Veryhachium*	101.89	87.06	35.27	22nd Aug 05	
13	(1) M34/1	*Veryhachium*	101.12	90.48	44.06	22nd Aug 05	
14	(1) J49	*Veryhachium*	100.97	95.74	49.60	22nd Aug 05	
15	(1) L68/4	*Veryhachium*	98.40	91.18	40.10	22nd Aug 05	
16	(1) G65/3	*Veryhachium*	92.67	87.05	38.23	22nd Aug 05	
17	(1) V37/1	*Veryhachium*	90.26	83.85	32.77	22nd Aug 05	
18	(1) M38	*Veryhachium*	87.01	78.50	40.58	22nd Aug 05	
19	(1) R46/4	*Veryhachium*	64.06	86.25	52.16	22nd Aug 05	

Sample Va115 - Corrected Data

Va118

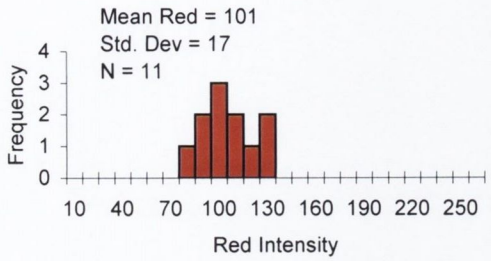

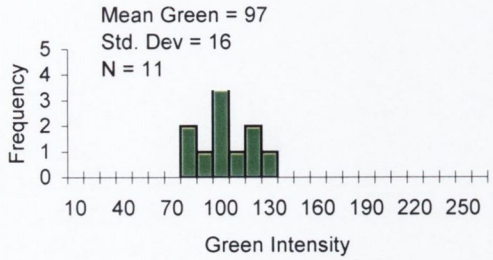

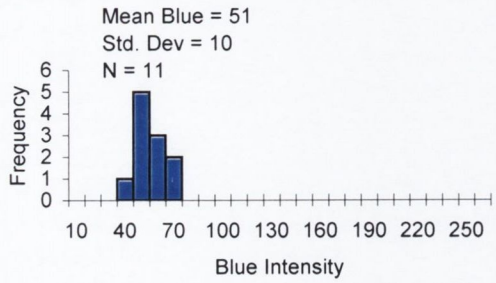

Number	Reference	Acritarch	Red	Green	Blue	Date	Colour
1	(1) O69/2	*Veryhachium*	130	120	69	22nd Aug 05	
2	(1) V36/4	*Veryhachium*	126	120	68	22nd Aug 05	
3	(1) D43/3	*Veryhachium*	116	112	59	22nd Aug 05	
4	(1) F32/2	*Veryhachium*	104	101	50	22nd Aug 05	
5	(1) G32/3	*Veryhachium*	101	95	41	22nd Aug 05	
6	(1) T45	*Veryhachium*	99	94	44	22nd Aug 05	
7	(1) K61/4	*Veryhachium*	96	96	49	22nd Aug 05	
8	(1) J53/3	*Veryhachium*	95	99	53	22nd Aug 05	
9	(1) K42/4	*Veryhachium*	85	81	39	22nd Aug 05	
10	(1) N67/4	*Veryhachium*	80	78	43	22nd Aug 05	
11	(1) J68/3	*Veryhachium*	77	75	43	22nd Aug 05	

Sample Va118 - Corrected Data

Va 47

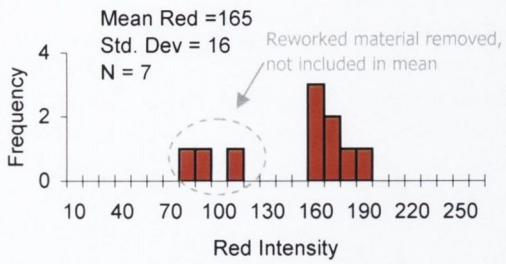

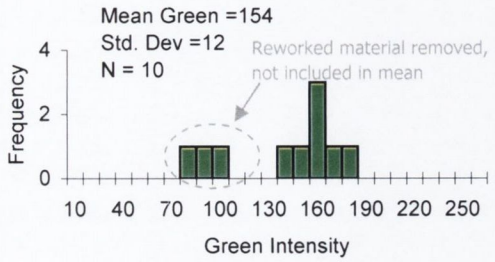

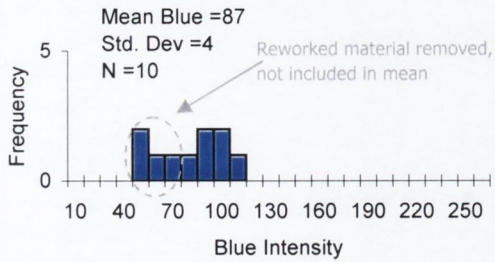

Number	Reference	Acritarch	Red	Green	Blue	Date	Colour
1	(2) P44/1	*Veryhachium*	182	173	101	22nd Aug 05	
2	(1) T46/1	*Veryhachium*	161	158	100	22nd Aug 05	
3	(2) G47/4	*Veryhachium*	165	157	92	22nd Aug 05	
4	(2) E58/4	*Veryhachium*	177	161	89	22nd Aug 05	
5	(1) V33/2	*Veryhachium*	160	151	89	22nd Aug 05	
6	(1) Q32	*Veryhachium*	155	139	70	22nd Aug 05	
7	(1) H31/1	*Veryhachium*	156	140	70	22nd Aug 05	
8	(2) X53	*Veryhachium* ®	89	80	50	22nd Aug 05	
9	(2) X46/1	*Veryhachium* ®	107	93	46	22nd Aug 05	
10	(2) W48/3	*Veryhachium* ®	74	70	43	22nd Aug 05	

Sample Va47 - Corrected Data

Wales 1

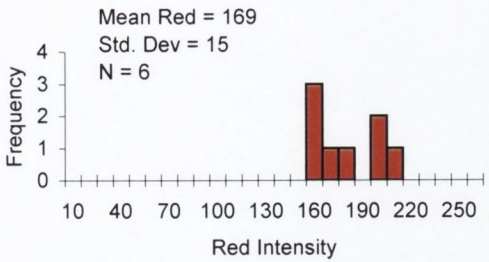

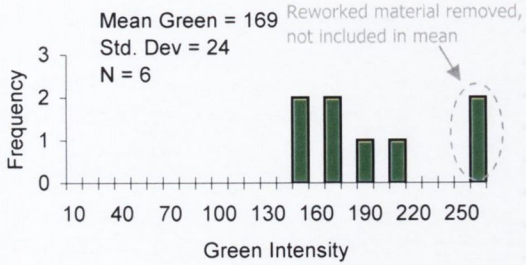

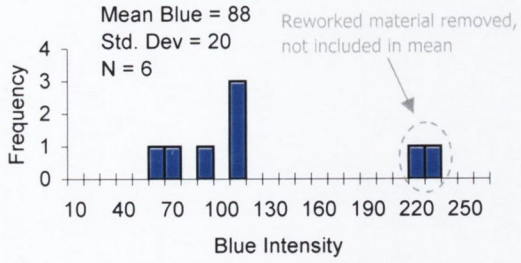

Number	Reference	Acritarch	Red	Green	Blue	Date	Colour
1	(1) K54/3	*Veryhachium*	160	143	59	14th Nov 05	
2	(6) S36/1	*Veryhachium*	166	149	69	14th Nov 05	
3	(3) Y65/3	*Veryhachium*	157	164	89	14th Nov 05	
4	(1) M47/1	*Veryhachium*	177	190	101	14th Nov 05	
5	(1) U60/3	*Veryhachium*	156	165	103	14th Nov 05	
6	(4) R62/3	*Veryhachium*	196	204	106	14th Nov 05	
7	(3) S32/3	*Veryhachium* ©	202	255	217	14th Nov 05	
8	(5) Q53/1	*Veryhachium* ©	199	254	228	14th Nov 05	

Sample Wales 1 - Corrected Data

WC 11

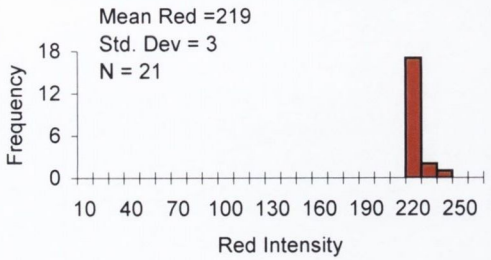

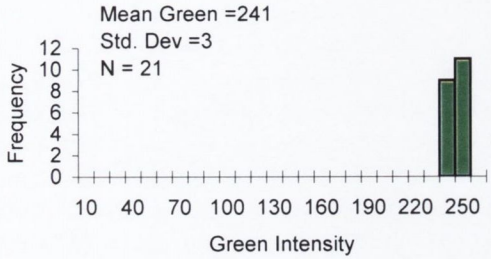

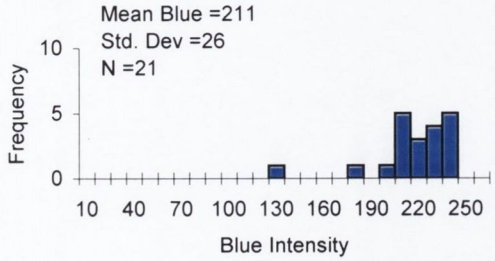

Number	Reference	Acritarch	Red	Green	Blue	Date	Colour
1	(1) O45	*Veryhachium*	220	239	235	21st Oct 04	
2	(1) O61/2	*Veryhachium*	222	242	235	21st Oct 04	
3	(1) Q44/4	*Veryhachium*	215	238	233	21st Oct 04	
4	(1) O45	*Veryhachium*	220	246	232	21st Oct 04	
5	(1) P62/1	*Veryhachium*	221	242	232	21st Oct 04	
6	(1) P62/3	*Veryhachium*	220	240	226	21st Oct 04	
7	(1) S44/1	*Veryhachium*	218	240	224	21st Oct 04	
8	(1) Q45/2	*Veryhachium*	220	241	222	21st Oct 04	
9	(1) V68/2	*Veryhachium*	216	239	221	21st Oct 04	
10	(1) R52/2	*Veryhachium*	220	249	219	21st Oct 04	
11	(1) P54/4	*Veryhachium*	220	242	213	21st Oct 04	
12	(1) K67/2	*Veryhachium*	219	240	212	21st Oct 04	
13	(1) O62/1	*Veryhachium*	217	242	209	21st Oct 04	
14	(1) N70/4	*Veryhachium*	212	237	206	21st Oct 04	
15	(1) M52/2	*Veryhachium*	220	241	203	21st Oct 04	
16	(1) O64/4	*Veryhachium*	218	240	202	21st Oct 04	
17	(1) D45/4	*Veryhachium*	219	241	201	21st Oct 04	
18	(1) W61/1	*Veryhachium*	218	239	194	21st Oct 04	
19	(1) H61/3	*Veryhachium*	220	241	177	21st Oct 04	
21	(1) Y54/3	*Veryhachium*	230	235	123	21st Oct 04	

It is probable that specimen 21 is reworked, however there is insufficent spread with the R and G data to be sure.

WC 15

Number	Reference	Acritarch	Red	Green	Blue	Date	Colour
1	(4) H43/4	*Veryhachium*	209	255	219	21st Feb 06	
2	(5) N53/3	*Veryhachium*	204	255	247	21st Feb 06	
3	(5) N53/4	*Veryhachium*	205	255	227	21st Feb 06	
4	(1) O49/1	*Veryhachium*	208	255	215	21st Feb 06	
5	(3) O59/4	*Veryhachium*	205	255	202	21st Feb 06	
6	(2) Y69/4	*Veryhachium*	211	255	174	21st Feb 06	

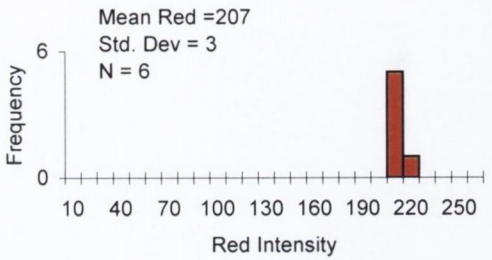

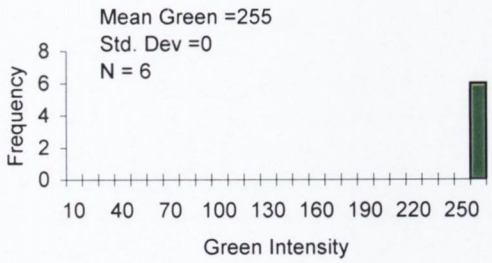

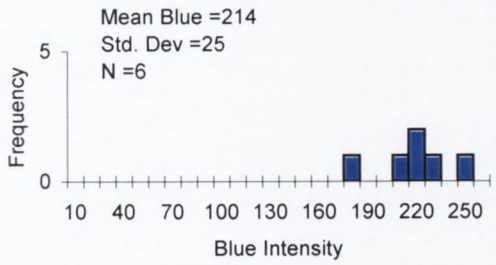

Sample WC15 - Corrected Data

WC 17

Number	Reference	Acritarch	Red	Green	Blue	Date	Colour
1	(1) H52/2	*Veryhachium*	204	255	222	21st Feb 06	
2	(2) S59	*Veryhachium*	206	255	210	21st Feb 06	
3	(2) U62/2	*Veryhachium*	207	255	161	21st Feb 06	

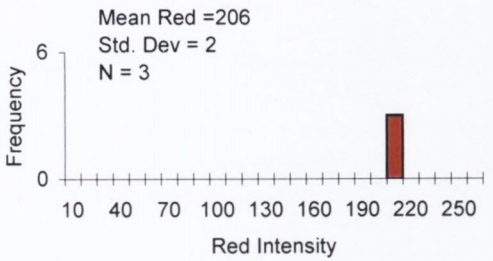

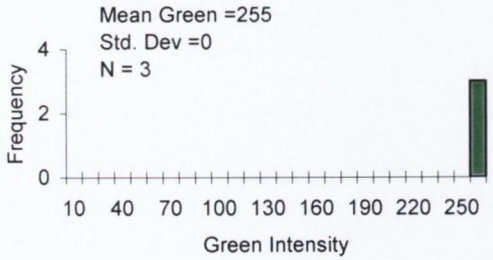

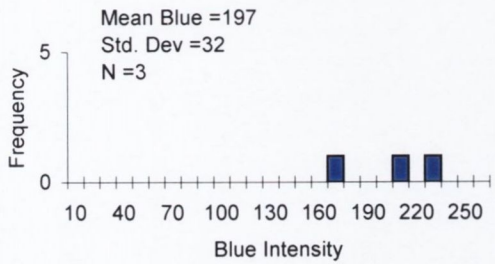

Sample WC17 - Corrected Data

APPENDIX VI

TASMANITES RGB DETERMINATIONS

Sample Name	Reference	Vesicle Red	Vesicle Green	Vesicle Blue	Vesicle	Fold	Fold - Red	Fold - Green	Fold - Blue	Diameter (μm)	Date	Rr(%)	Std. Dev.
P11	(1) V31/3	218.24	242.08	165.04			193.81	223.95	118.66	29.96	11th Nov 04	0.68	0.09
P11	(1) M34/4	224.59	226.06	116.50			184.27	190.19	71.84	32.52	11th Nov 04	0.68	0.09
P11	(1) O39/4	184.20	216.33	84.21			197.46	192.30	56.43	33.03	11th Nov 04	0.68	0.09
P11	(1) G31/2	228.07	211.34	82.82			210.39	185.75	62.45	34.31	11th Nov 04	0.68	0.09
P11	(1) D33	226.43	235.33	123.03			208.03	189.34	62.99	34.31	11th Nov 04	0.68	0.09
P11	(1) E49/4	219.59	225.91	118.15			208.43	196.47	71.30	34.82	11th Nov 04	0.68	0.09
P11	(1) N38/4	223.23	227.62	118.83			193.94	194.35	64.95	34.95	11th Nov 04	0.68	0.09
P11	(1) G38	220.08	234.89	140.97			216.81	197.47	65.14	35.07	11th Nov 04	0.68	0.09
P11	(1) M38	218.18	236.64	145.16			199.60	213.75	94.14	36.10	11th Nov 04	0.68	0.09
P11	(1) G34/2	223.79	224.69	134.64			204.71	217.64	123.92	36.86	11th Nov 04	0.68	0.09
P11	(1) T29/4	227.58	222.29	105.88			207.63	172.16	56.66	37.38	11th Nov 04	0.68	0.09
P11	(1) R33/1	220.99	215.44	92.92			204.63	198.70	83.19	38.40	11th Nov 04	0.68	0.09
P11	(1) V31/3	216.60	233.86	141.83			210.81	208.17	89.39	38.42	11th Nov 04	0.68	0.09
P11	(1) J33/4	220.32	218.29	104.62			222.68	200.94	62.02	38.72	11th Nov 04	0.68	0.09
P11	(1) O38/2	220.56	226.61	115.20			193.81	172.34	46.07	39.17	11th Nov 04	0.68	0.09
P11	(1) M43	220.07	237.44	132.73			207.96	203.95	80.11	39.33	11th Nov 04	0.68	0.09
P11	(1) T35/4	223.97	216.73	103.31			209.20	196.84	73.88	39.42	11th Nov 04	0.68	0.09
P11	(1) Q41/1	214.58	242.03	169.50			210.32	240.76	149.12	39.68	11th Nov 04	0.68	0.09
P11	(1) G29/3	217.75	232.41	151.23			226.36	227.66	102.91	39.68	11th Nov 04	0.68	0.09
P11	(1) K43	225.37	234.00	116.79			197.43	189.25	65.89	39.87	11th Nov 04	0.68	0.09
P11	(1) G29/3	222.68	218.00	109.02			198.05	180.94	69.41	39.94	11th Nov 04	0.68	0.09
P11	(1) N29	227.27	221.35	104.08			209.85	204.33	88.00	39.94	11th Nov 04	0.68	0.09
P11	(1) L34/4	223.17	238.54	141.02			188.72	198.95	80.98	40.19	11th Nov 04	0.68	0.09
P11	(1) Y38/4	223.79	233.00	128.14			200.15	191.70	73.62	40.45	11th Nov 04	0.68	0.09
P11	(1) V46/2	227.50	222.29	95.98			217.80	190.33	26.56	41.47	11th Nov 04	0.68	0.09
P11	(1) V38	223.42	235.26	130.94			185.86	174.81	50.32	42.24	11th Nov 04	0.68	0.09
P11	(1) U33/3	229.02	207.97	74.62			205.43	165.68	19.96	43.26	11th Nov 04	0.68	0.09
P11	(1) X40/4	224.24	220.61	96.85			178.40	163.12	48.08	44.31	11th Nov 04	0.68	0.09
P11	(1) W39	222.51	202.44	71.53			190.11	148.86	25.86	45.08	11th Nov 04	0.68	0.09
P11	(1) U39/1	227.16	210.05	79.60			219.97	185.47	37.84	45.73	11th Nov 04	0.68	0.09
P11	(1) L35/4	215.62	239.56	151.63			202.56	203.37	85.46	46.34	11th Nov 04	0.68	0.09
P11	(1) J51/1	219.40	239.55	144.46			201.39	196.41	73.31	46.81	11th Nov 04	0.68	0.09
P11	(1) T30/3	218.85	237.88	150.54			211.35	233.28	129.01	47.36	11th Nov 04	0.68	0.09

All RGB data is corrected

Sample Name	Reference	Vesicle Red	Vesicle Green	Vesicle Blue	Vesicle	Fold	Fold - Red	Fold - Green	Fold - Blue	Diameter (μm)	Date	Rr(%)	Std. Dev.
P11	(1) U33/1	227.99	214.38	87.83			208.60	190.74	49.40	51.46	11th Nov 04	0.68	0.09
P11	(1) D43/3	217.61	196.83	67.37			201.50	146.58	34.84	52.23	11th Nov 04	0.68	0.09
P11	(1) R31	225.91	219.70	97.69			201.85	170.25	36.83	52.38	11th Nov 04	0.68	0.09
P11	(1) W43/4	218.59	219.31	97.32			204.41	188.53	54.16	52.99	11th Nov 04	0.68	0.09
P11	(1) G41/1	225.65	213.15	84.29			208.92	166.20	26.56	53.76	11th Nov 04	0.68	0.09
P11	(1) R38/2	221.03	228.39	117.66			222.71	178.89	33.04	54.85	11th Nov 04	0.68	0.09
P11	(1) Q35/1	225.70	211.79	82.31			199.86	161.94	32.63	55.55	11th Nov 04	0.68	0.09
P11	(1) T38/1	224.49	225.92	105.53			220.60	184.94	41.00	57.35	11th Nov 04	0.68	0.09
P11	(1) S38/4	218.87	207.42	77.69			226.48	195.58	50.78	57.35	11th Nov 04	0.68	0.09
P11	(1) E35/2	223.95	216.02	95.15			196.87	144.81	22.77	60.67	11th Nov 04	0.68	0.09
P11	(1) U29/4	223.35	204.64	75.37			197.30	157.46	35.22	61.70	11th Nov 04	0.68	0.09
P11	(1) V30/3	219.62	194.01	60.73			191.80	148.57	14.15	68.36	11th Nov 04	0.68	0.09
P11	(1) N33/4	226.68	200.34	64.60			162.93	119.01	23.88	76.59	11th Nov 04	0.68	0.09
P11	(1) C41/3	224.33	208.48	76.92			205.26	171.23	28.34	76.81	11th Nov 04	0.68	0.09
P11	(1) D45/1	231.35	198.72	54.83			218.12	176.09	35.66	79.92	11th Nov 04	0.68	0.09
P11	(1) D38	202.67	140.17	16.03			138.62	83.47	19.19	83.71	11th Nov 04	0.68	0.09
P11	(1) F49	223.78	204.65	70.40			216.02	171.82	31.77	85.94	11th Nov 04	0.68	0.09
P11	(1) C34/4	227.71	219.29	95.23			202.87	167.37	31.65	86.02	11th Nov 04	0.68	0.09
P11	(1) G46	230.91	196.04	49.72			189.68	127.58	15.16	88.97	11th Nov 04	0.68	0.09
P11	(1) D39	214.18	155.29	21.03			192.51	130.24	15.69	89.09	11th Nov 04	0.68	0.09
P11	(1) T37/4	216.84	182.31	43.06			201.68	130.96	10.46	89.62	11th Nov 04	0.68	0.09
P11	(1) O47/3	224.32	218.62	89.64			215.91	191.88	46.31	91.06	11th Nov 04	0.68	0.09
P11	(1) W38	226.59	182.33	33.97			199.56	152.27	16.11	91.31	11th Nov 04	0.68	0.09
P11	(1) U30/2	214.47	199.45	73.02			200.41	157.25	28.09	91.91	11th Nov 04	0.68	0.09
P11	(1) T49	228.18	198.43	51.97			215.90	155.33	22.29	91.94	11th Nov 04	0.68	0.09
P11	(1) F33	210.73	175.43	39.25			206.05	147.00	12.88	94.21	11th Nov 04	0.68	0.09
P11	(1) Y47/1	214.44	159.46	21.08			179.59	129.71	22.25	97.54	11th Nov 04	0.68	0.09
P11	(1) S35/2	227.21	212.13	82.75			192.14	162.79	33.69	98.71	11th Nov 04	0.68	0.09
P11	(1) J39/3	224.25	181.69	33.08			189.96	132.03	12.11	99.33	11th Nov 04	0.68	0.09
P11	(1) R33/4	213.02	163.46	35.38			182.74	139.36	9.18	102.91	11th Nov 04	0.68	0.09
P11	(1) H38/1	219.41	164.89	20.71			182.16	117.90	10.42	104.13	11th Nov 04	0.68	0.09
P11	(1) N49	221.11	175.48	29.56			186.37	123.60	14.86	112.90	11th Nov 04	0.68	0.09
P11	(1) J40/1	195.40	122.97	8.61			160.11	83.88	8.44	115.62	11th Nov 04	0.68	0.09

All RGB data is corrected

Sample Name	Reference	Vesicle Red	Vesicle Green	Vesicle Blue	Vesicle	Fold	Fold - Red	Fold - Green	Fold - Blue	Diameter (μm)	Date	Rr(%)	Std. Dev.
Pet 3	(1) W52/2	216.59	243.78	175.08			212.90	239.92	138.19	33.79	7th Oct	0.68	0.08
Pet 3	(1) P70/4	220.90	241.43	145.43			205.09	217.52	78.17	36.85	7th Oct	0.68	0.08
Pet 3	(1) T68/2	215.23	235.91	150.95			224.37	228.32	107.34	37.08	7th Oct	0.68	0.08
Pet 3	(1) N44/2	219.25	228.84	122.31			188.93	185.53	60.38	38.66	7th Oct	0.68	0.08
Pet 3	(1) G55	213.93	241.40	205.72			207.49	227.74	150.43	38.66	7th Oct	0.68	0.08
Pet 3	(1) T75/4	210.99	229.79	134.95			218.82	212.80	90.49	39.94	7th Oct	0.68	0.08
Pet 3	(1) O39/1	217.72	240.16	153.35			209.02	226.94	112.77	40.45	7th Oct	0.68	0.08
Pet 3	(1) J71/3	217.79	231.57	135.40			215.06	206.19	89.13	40.70	7th Oct	0.68	0.08
Pet 3	(1) P39	217.47	244.54	187.69			213.29	241.48	159.74	40.96	7th Oct	0.68	0.08
Pet 3	(1) J59/3	216.71	242.56	183.20			200.71	236.36	152.51	41.63	7th Oct	0.68	0.08
Pet 3	(1) N67/3	196.89	223.21	176.50			210.55	216.93	90.55	42.04	7th Oct	0.68	0.08
Pet 3	(1) R72/2	218.98	234.52	140.05			218.29	223.19	106.66	42.39	7th Oct	0.68	0.08
Pet 3	(1) T66/2	214.42	239.45	154.68			211.31	222.32	108.86	43.10	7th Oct	0.68	0.08
Pet 3	(1) H63/2	213.83	237.33	166.87			214.89	210.95	84.33	43.99	7th Oct	0.68	0.08
Pet 3	(1) T52/2	225.51	232.40	113.21			207.82	204.83	74.66	44.29	7th Oct	0.68	0.08
Pet 3	(1) S44/3	214.70	243.68	186.27			198.51	218.71	115.72	45.31	7th Oct	0.68	0.08
Pet 3	(1) W42	217.51	238.43	143.70			204.40	218.95	110.11	45.47	7th Oct	0.68	0.08
Pet 3	(1) K59/3	214.83	244.54	149.33			205.85	198.24	59.14	45.76	7th Oct	0.68	0.08
Pet 3	(1) V71/4	223.21	233.69	128.90			209.96	193.66	50.21	45.83	7th Oct	0.68	0.08
Pet 3	(1) H55	219.25	238.51	144.02			215.65	229.03	109.56	46.59	7th Oct	0.68	0.08
Pet 3	(1) IC	223.33	235.27	136.33			202.19	201.06	70.79	47.05	7th Oct	0.68	0.08
Pet 3	(1) P50/2	222.46	240.37	120.91			236.50	213.26	63.66	47.36	7th Oct	0.68	0.08
Pet 3	(1) U72/3	223.33	231.09	120.08			205.79	198.01	74.79	50.43	7th Oct	0.68	0.08
Pet 3	(1) W37/4	219.12	236.31	141.66			210.58	218.32	91.68	51.20	7th Oct	0.68	0.08
Pet 3	(1) N52/2	219.11	242.29	153.21			198.96	202.25	68.60	51.97	7th Oct	0.68	0.08
Pet 3	(1) L71/1	229.05	228.37	103.24			215.58	174.87	25.47	52.50	7th Oct	0.68	0.08
Pet 3	(1) W63	217.91	240.05	154.07			219.51	234.81	123.26	54.84	7th Oct	0.68	0.08
Pet 3	(1) X63/2	206.99	215.21	134.62			219.34	207.38	72.98	56.15	7th Oct	0.68	0.08
Pet 3	(1) F67/2	220.25	172.82	37.88			216.24	169.52	29.75	60.68	7th Oct	0.68	0.08
Pet 3	(1) H67/3	231.02	215.46	74.93			210.57	182.16	42.58	64.09	7th Oct	0.68	0.08
Pet 3	(1) M72/4	227.97	209.10	61.63			190.75	173.43	23.93	65.54	7th Oct	0.68	0.08
Pet 3	(1) TR	223.39	225.80	103.26			211.52	216.81	77.08	66.82	7th Oct	0.68	0.08
Pet 3	(1) D65/4	227.20	224.07	89.65			217.28	165.93	14.27	69.48	7th Oct	0.68	0.08

All RGB data is corrected

Sample Name	Reference	Vesicle Red	Vesicle Green	Vesicle Blue	Vesicle	Fold	Fold - Red	Fold - Green	Fold - Blue	Diameter (μm)	Date	Rr(%)	Std. Dev.
Pet 3	(1) U52/4	227.33	208.70	68.22			216.03	183.76	40.23	70.66	7th Oct	0.68	0.08
Pet 3	(1) X42/3	225.73	230.70	109.13			209.75	198.67	51.68	71.17	7th Oct	0.68	0.08
Pet 3	(1) S44/3	232.80	208.74	45.46			199.06	157.93	23.92	76.29	7th Oct	0.68	0.08
Pet 3	(1) N55/1	218.97	242.10	149.31			226.01	219.99	80.21	77.16	7th Oct	0.68	0.08
Pet 3	(1) X70/4	223.92	177.04	24.63			201.85	152.08	19.71	79.37	7th Oct	0.68	0.08
Pet 3	(1) X37/4	227.83	229.90	110.55			210.23	190.57	66.79	83.20	7th Oct	0.68	0.08
Pet 3	(1) K55/1	231.86	201.40	42.90			228.89	195.63	40.72	93.18	7th Oct	0.68	0.08
Pet 3	(1) N72/2	237.31	210.15	77.76			202.13	160.85	30.86	93.44	7th Oct	0.68	0.08
Pet 3	(1) P66/4	221.24	239.46	144.57			220.22	234.00	75.11	115.09	7th Oct	0.68	0.08
Pet 3	(1) V59/1	230.65	233.87	108.34			211.66	190.40	39.48	120.38	7th Oct	0.68	0.08
Pet 3	(1) P42/3	235.19	194.10	36.80			215.81	157.65	13.05	121.09	7th Oct	0.68	0.08
Pet 3	(1) Y54/4	215.80	193.69	45.57			214.74	172.83	26.09	122.63	7th Oct	0.68	0.08
Pet 3	(1) H61/3	221.93	238.15	126.51			230.84	225.44	73.42	125.70	7th Oct	0.68	0.08
Pet 3	(1) G59/4	229.65	224.02	94.94			221.17	190.23	54.38	134.25	7th Oct	0.68	0.08
Pet 3	(1) F66 L	231.18	157.87	4.94			200.55	103.48	2.14	134.68	7th Oct	0.68	0.08
CC3	(3) R52/3	235.59	225.58	108.85			226.56	186.16	35.61	82.95	29th Sept 04	0.85	0.21
CC3	(3) T52/4	211.78	220.13	82.93			218.64	195.79	63.62	83.98	28th Sept 04	0.85	0.21
CC3	(3) Y54/3	224.00	230.16	120.19			201.44	209.40	97.98	85.51	28th Sept 04	0.85	0.21
CC3	(4) R36/2	216.56	234.87	152.78			222.60	222.88	105.05	88.08	28th Sept 04	0.85	0.21
CC3	(3) O37/4	226.00	224.36	89.01			182.50	135.41	32.03	91.14	28th Sept 04	0.85	0.21
CC3	(B) H47/3	214.48	228.72	173.69			227.87	237.65	140.70	92.16	29th Sept 04	0.85	0.21
CC3	(B) K49/4	226.46	234.39	135.74			238.11	242.96	131.25	93.44	29th Sept 04	0.85	0.21
CC3	(4) Q50/1	227.30	226.33	93.68			238.84	246.27	51.40	104.45	28th Sept 04	0.85	0.21
CC3	(B) X41	231.94	239.71	147.77			244.60	230.80	74.41	123.90	29th Sept 04	0.85	0.21
CC3	(B) V59/2	239.45	209.22	55.31			226.62	143.91	10.47	130.00	29th Sept 04	0.85	0.21
CC3	(3) J39/4	222.45	222.85	97.32			181.31	152.81	45.25	130.05	28th Sept 04	0.85	0.21
CC3	(1) R35/2	226.89	217.04	89.75			246.10	199.06	29.35	131.58	29th Sept 04	0.85	0.21
CC3	(B) 422/1014	220.43	182.33	42.41			153.62	104.63	14.20	134.89	28th Sept 04	0.85	0.21
CC3	(4) V64/4	225.29	213.63	86.98			210.43	168.20	37.57	136.70	28th Sept 04	0.85	0.21
CC3	(4) U43/1	225.38	234.21	123.52			227.83	196.50	67.69	139.78	28th Sept 04	0.85	0.21
CC3	(3) N47/4	233.97	192.37	24.85			221.08	150.67	3.13	145.92	28th Sept 04	0.85	0.21
CC3	(4) R49/1	224.22	188.83	33.50			200.13	139.16	5.20	152.35	28th Sept 04	0.85	0.21
CC3	(4) V60/1	196.92	197.27	101.34			223.79	172.80	13.07	153.09	28th Sept 04	0.85	0.21

All RGB data is corrected

Sample Name	Reference	Vesicle Red	Vesicle Green	Vesicle Blue	Vesicle	Fold	Fold - Red	Fold - Green	Fold - Blue	Diameter (μm)	Date	Rr(%)	Std. Dev.
CC3	(B) K71/1	240.47	175.11	26.95			138.22	66.97	21.88	156.93	29th Sept 04	0.85	0.21
CC3	(3) T59	229.11	177.18	13.98			188.27	128.26	17.87	164.34	28th Sept 04	0.85	0.21
WC11	(1) E54/4	218.65	241.44	175.38			209.68	227.00	137.43	38.91	6th Oct 04	0.91	0.40
WC11	(2) Q61/3	213.74	239.57	160.29			216.59	227.44	111.84	41.47	6th Oct 04	0.91	0.40
WC11	(1) F55	217.19	245.41	179.49			205.31	221.84	122.14	50.94	6th Oct 04	0.91	0.40
WC11	(1) W53	218.05	244.07	171.55			220.34	190.32	51.69	52.49	6th Oct 04	0.91	0.40
WC11	(2) G56	222.60	239.52	186.64			207.67	195.10	98.13	61.18	4th Oct 04	0.91	0.40
WC11	(1) H34/2	228.72	217.88	99.27			206.29	198.14	71.12	61.43	6th Oct 04	0.91	0.40
WC11	(2) N56/3	222.68	238.18	164.37			229.30	239.42	138.19	66.82	4th Oct 04	0.91	0.40
WC11	(2) K55/1	223.11	240.60	184.17			224.50	243.57	168.45	67.12	4th Oct 04	0.91	0.40
WC11	(2) S37/2	227.36	234.81	141.11			243.61	227.50	61.27	67.84	4th Oct 04	0.91	0.40
WC11	(2) X53/4	224.32	224.00	109.35			228.37	211.92	78.06	70.15	6th Oct 04	0.91	0.40
WC11	(1) T35	210.16	220.42	129.56			230.47	216.86	78.88	70.66	6th Oct 04	0.91	0.40
WC11	(1) T73	219.15	241.68	154.11			212.35	225.26	107.57	71.42	6th Oct 04	0.91	0.40
WC11	(2) Q40/3	224.74	235.42	142.01			227.86	235.60	120.01	72.19	4th Oct 04	0.91	0.40
WC11	(2) N44/2	221.91	236.45	165.24			240.78	230.28	106.67	72.7	4th Oct 04	0.91	0.40
WC11	(1) S36	229.81	233.52	111.98			228.78	206.46	77.87	73.73	6th Oct 04	0.91	0.40
WC11	(2) P50/2	226.16	233.28	130.65			237.20	229.00	83.28	74.75	4th Oct 04	0.91	0.40
WC11	(1) Q36	221.24	241.83	157.18			214.07	214.08	95.19	76.29	6th Oct 04	0.91	0.40
WC11	(1) J50/3	225.50	238.13	121.39			209.68	195.99	58.25	76.55	6th Oct 04	0.91	0.40
WC11	(2) J67/4	212.70	240.74	187.79			208.52	223.95	113.31	77.83	6th Oct 04	0.91	0.40
WC11	(2) G59/4	224.27	241.00	185.14			231.35	242.32	131.18	78.85	4th Oct 04	0.91	0.40
WC11	(2) X53/4	229.35	237.50	146.22			221.33	215.32	108.43	80.15	4th Oct 04	0.91	0.40
WC11	(1) W54	222.58	240.22	150.07			219.43	217.45	87.21	80.38	6th Oct 04	0.91	0.40
WC11	(2) Y39/4	228.56	234.54	139.60			232.24	206.91	82.04	82.69	4th Oct 04	0.91	0.40
WC11	(2) M51	233.16	223.91	91.23			228.23	184.91	45.70	82.95	4th Oct 04	0.91	0.40
WC11	(1) M70/1	222.80	241.06	138.78			223.91	219.51	75.96	85.5	6th Oct 04	0.91	0.40
WC11	(1) T52/2	232.57	236.39	105.74			227.03	214.04	67.52	87.3	6th Oct 04	0.91	0.40
WC11	(1) O46/3	219.53	241.79	165.55			210.18	225.50	108.75	91.39	6th Oct 04	0.91	0.40
WC11	(1) O58/2	224.15	214.44	95.80			216.89	199.74	44.61	91.65	6th Oct 04	0.91	0.40
WC11	(2) P66/2	215.24	240.15	168.79			225.10	237.74	126.08	93.7	6th Oct 04	0.91	0.40
WC11	(1) U62/2	219.60	244.19	160.18			213.47	237.52	132.82	94.21	6th Oct 04	0.91	0.40
WC11	(2) M37/2	222.52	210.18	86.93			215.86	172.87	41.72	95.75	4th Oct 04	0.91	0.40

All RGB data is corrected

Sample Name	Reference	Vesicle Red	Vesicle Green	Vesicle Blue	Vesicle	Fold	Fold - Red	Fold - Green	Fold - Blue	Diameter (μm)	Date	Rr(%)	Std. Dev.
WC11	(1) P43	218.76	237.31	142.64			221.82	198.73	58.23	98.05	6th Oct 04	0.91	0.40
WC11	(1) J66/2	228.52	204.79	71.27			212.19	200.57	82.61	101.12	6th Oct 04	0.91	0.40
WC11	(2) L48/2	224.45	240.29	184.50			221.89	234.85	152.37	109.31	4th Oct 04	0.91	0.40
WC11	(2) K49/2	219.99	232.46	184.05			231.67	228.42	132.95	110.13	4th Oct 04	0.91	0.40
WC11	(1) N67/4	219.36	242.06	172.66			221.45	237.94	123.96	114.43	6th Oct 04	0.91	0.40
WC11	(1) P33/3	231.55	212.87	82.04			190.31	170.67	62.98	122.36	6th Oct 04	0.91	0.40
WC11	(1) J70/1	223.09	216.84	89.38			219.52	192.41	72.33	127.49	6th Oct 04	0.91	0.40
WC11	(1) Q54	230.03	224.53	89.44			229.24	220.63	24.46	128.07	6th Oct 04	0.91	0.40
WC11	(2) L69/4	214.75	238.63	167.40			224.19	226.94	120.80	128.26	6th Oct 04	0.91	0.40
WC11	(2) T45	234.94	213.02	68.17			216.28	171.34	29.71	133.12	4th Oct 04	0.91	0.40
WC11	(1) L47/3	226.62	235.46	112.70			214.92	197.28	42.59	152.08	6th Oct 04	0.91	0.40
WC11	(2) K41/1	238.48	224.17	76.00			231.82	168.09	9.53	200	4th Oct 04	0.91	0.40
P22	(1) W29/2	207.14	160.07	69.66			124.77	85.18	26.27	37.38	5th Dec	0.92	0.15
P22	(1) Q49/4	197.21	135.69	51.93			91.35	65.80	39.14	37.63	5th Dec	0.92	0.15
P22	(1) W46/3	203.56	142.43	41.12			110.32	69.63	31.01	47.69	5th Dec	0.92	0.15
P22	(1) C30/4	236.00	207.56	87.55			162.46	124.43	37.68	51.46	5th Dec	0.92	0.15
Sun 3	(1) U62/4	220.96	237.22	157.56			224.65	240.91	9.26	35.33	4th Oct 04	1.08	0.32
Sun 3	(1) O71/4	235.26	200.88	52.68			218.55	178.69	45.88	40.45	4th Oct 04	1.08	0.32
Sun 3	(1) Q44/1	234.01	213.99	79.04			221.46	184.14	86.35	41.99	4th Oct 04	1.08	0.32
Sun 3	(1) G41/2	238.40	215.55	99.15			243.70	223.92	84.28	44.29	4th Oct 04	1.08	0.32
Sun 3	(1) L65/3	238.76	220.63	69.15			226.03	186.70	56.38	46.60	4th Oct 04	1.08	0.32
Sun 3	(1) H49	233.07	228.63	106.07			220.80	187.75	46.20	51.97	4th Oct 04	1.08	0.32
Sun 3	(1) L47/1	233.71	208.91	57.75			245.68	186.40	29.79	58.85	4th Oct 04	1.08	0.32
Sun 3	(1) P41	221.59	211.76	82.45			238.87	187.99	39.32	62.47	4th Oct 04	1.08	0.32
Sun 3	(1) P36/4	231.00	231.31	134.21			223.44	221.15	96.00	72.19	4th Oct 04	1.08	0.32
Sun 3	(1) K55/4	218.96	236.60	193.36			224.09	241.43	181.67	125.70	4th Oct 04	1.08	0.32
WC15	(2) K54/4	235.49	221.86	97.25			175.58	150.82	34.36	36.35	6th Oct	1.08	0.26
WC15	(5) Y48/3	225.26	237.88	146.70			217.57	242.42	146.58	36.88	6th Oct	1.08	0.26
WC15	(5) M54/1	217.93	242.66	223.93			221.32	248.30	163.88	37.63	6th Oct	1.08	0.26
WC15	(5) U44/3	226.98	228.23	119.28			224.60	242.98	140.11	39.94	6th Oct	1.08	0.26
WC15	(5) M37/2	214.35	240.53	185.54			216.08	239.92	141.88	45.82	6th Oct	1.08	0.26
WC15	(2) G59	219.09	246.73	191.63			219.98	246.19	148.34	50.18	6th Oct	1.08	0.26
WC15	(2) V44/2	209.23	237.21	210.15			213.17	241.11	157.64	52.27	6th Oct	1.08	0.26

All RGB data is corrected

Sample Name	Reference	Vesicle Red	Vesicle Green	Vesicle Blue	Vesicle	Fold	Fold - Red	Fold - Green	Fold - Blue	Diameter (μm)	Date	Rr(%)	Std. Dev.
WC15	(5) J84/1	218.72	242.98	162.93			224.20	226.07	107.42	56.58	6th Oct	1.08	0.26
WC15	(5) F38/2	215.15	243.78	176.08			212.65	219.76	114.61	58.37	6th Oct	1.08	0.26
WC15	(2) L53	219.72	241.25	148.62			216.31	229.93	104.38	64.25	6th Oct	1.08	0.26
WC15	(5) X66	221.24	245.81	168.85			233.91	226.90	103.65	66.82	6th Oct	1.08	0.26
WC15	(2) D44/3	216.10	236.52	159.13			189.93	198.78	115.81	67.81	6th Oct	1.08	0.26
WC15	(5) X40/2	223.89	220.01	88.84			209.43	167.73	34.61	78.85	6th Oct	1.08	0.26
WC15	(2) V48/2	221.19	246.73	204.28			234.48	227.99	96.16	79.25	6th Oct	1.08	0.26
WC15	(2) R56	221.20	242.72	152.86			221.03	217.02	86.08	80.89	6th Oct	1.08	0.26
WC15	(2) V38/4	210.71	228.89	141.45			223.05	214.98	88.31	81.67	6th Oct	1.08	0.26
WC15	(2) O64/2	234.98	227.47	80.64			209.57	145.27	21.29	82.25	6th Oct	1.08	0.26
WC15	(2) N46	222.84	243.20	158.30			226.67	221.94	87.52	83.2	6th Oct	1.08	0.26
WC15	(5) F50	228.38	232.99	117.21			232.30	220.88	72.82	84.79	6th Oct	1.08	0.26
WC15	(2) Y53/4	223.73	234.13	121.23			213.62	177.60	42.92	85.25	6th Oct	1.08	0.26
WC15	(5) M61/2	226.14	242.20	137.38			232.06	217.39	69.37	86.86	6th Oct	1.08	0.26
WC15	(2) M44/3	211.24	226.79	103.93			201.70	187.17	31.66	87.83	6th Oct	1.08	0.26
WC15	(2) P64/1	220.05	245.32	165.44			223.64	226.51	91.20	88.58	6th Oct	1.08	0.26
WC15	(5) Q71	230.78	227.78	102.78			228.77	199.85	25.99	89.89	6th Oct	1.08	0.26
WC15	(2) N53	214.28	238.08	170.32			202.47	222.80	138.20	90.63	6th Oct	1.08	0.26
WC15	(5) L60	223.38	237.86	145.47			225.23	232.10	130.91	91.09	6th Oct	1.08	0.26
WC15	(5) T47/2	222.44	247.16	174.23			228.42	222.09	93.25	94.98	6th Oct	1.08	0.26
WC15	(2) V43/4	228.41	218.94	6.87			211.84	166.13	35.63	100.87	6th Oct	1.08	0.26
WC15	(5) S46/2	220.29	242.56	175.56			227.97	233.70	129.52	122.01	6th Oct	1.08	0.26
WC15	(2) V42/1	233.65	208.17	54.95			209.63	159.36	30.55	128.07	6th Oct	1.08	0.26
WC15	(5) Y50/1	228.77	233.41	106.85			221.81	192.63	60.72	134.59	6th Oct	1.08	0.26
WC15	(2) J35/4	228.40	232.28	116.41			235.52	210.49	71.07	147.51	6th Oct	1.08	0.26
WC15	(2) F59/2	234.08	189.92	31.87			192.95	119.17	4.48	155.84	6th Oct	1.08	0.26
P25	(1) R48	209.56	177.33	81.96			114.63	89.89	24.88	34.58	5th Dec	1.09	0.15
P25	(1) F32	148.60	106.71	49.16			60.30	61.42	45.68	43.99	5th Dec	1.09	0.15
P25	(1) F60	159.71	102.44	32.21			74.94	53.66	36.84	47.17	5th Dec	1.09	0.15
P25	(1) S32/4	105.76	78.78	43.72			57.50	58.02	44.77	60.93	5th Dec	1.09	0.15
TL 3	(1) H49	227.28	236.80	136.73			203.46	201.79	88.42	47.10	4th Oct 04	1.28	0.32
TL 3	(2) T59/2	219.04	235.57	179.38			206.17	228.31	131.50	54.79	4th Oct 04	1.28	0.32
TL 3	(2) W50/1	224.71	238.25	167.92			231.91	213.88	90.63	72.19	4th Oct 04	1.28	0.32

All RGB data is corrected

Sample Name	Reference	Vesicle Red	Vesicle Green	Vesicle Blue	Vesicle	Fold	Fold - Red	Fold - Green	Fold - Blue	Diameter (μm)	Date	Rr(%)	Std. Dev.
TL 3	(2) T56	222.62	230.20	145.12			221.22	222.35	124.36	77.57	4th Oct 04	1.28	0.32
TL 3	(1) K52	232.12	226.47	116.61			212.95	195.98	64.56	78.08	4th Oct 04	1.28	0.32
TL 3	(1) K37/2	233.45	227.98	123.90			218.70	194.85	88.93	80.90	4th Oct 04	1.28	0.32
TL 3	(1) H45/3	224.77	238.58	156.25			209.74	214.44	98.68	84.22	4th Oct 04	1.28	0.32
TL 3	(2) U63/1	231.84	226.28	114.42			214.64	183.93	45.73	84.99	4th Oct 04	1.28	0.32
TL 3	(2) F47/1	227.50	225.24	125.11			211.17	165.12	34.76	86.26	4th Oct 04	1.28	0.32
TL 3	(1) R64	231.13	225.27	109.89			221.10	170.79	43.36	107.52	4th Oct 04	1.28	0.32
TL 3	(1) O61/2	224.63	223.98	124.30			223.62	187.34	47.64	135.94	4th Oct 04	1.28	0.32
TL 3	(2) O59/4	240.74	216.37	86.32			210.34	160.38	32.32	139.01	4th Oct 04	1.28	0.32
TL 3	(2) L56/3	230.36	216.08	92.96			228.68	197.26	60.18	144.39	4th Oct 04	1.28	0.32
TL 3	(1) Q36/2	235.46	192.68	43.99			206.17	132.17	19.25	168.19	4th Oct 04	1.28	0.32

All RGB data is corrected

APPENDIX VII

CORRELATION OF *VERYHACHIUM* RGB DATA AND VITRINITE REFLECTANCE DATA

Mean *Veryhachium* RGB determinations and vitrinite reflectance data (well preserved specimens)

Sample Name	Red	Std. Dev.	Green	Std. Dev.	Blue	Std. Dev	Colour	Rr(%)	Std. Dev.	N
CAN 9	204	4	255	0	237	12		0.5	0.09	12
P14	218	4	235	6	211	24		0.68	0.09	37
P11	233	2	238	2	209	16		0.68	0.09	22
WC11	219	3	241	3	211	26		0.79	0.24	100
CC3	215	4	234	6	180	22		0.85	0.21	90
P23	215	5	243	6	179	26		0.91	0.12	44
P22	221	5	225	15	147	34		0.92	0.15	28
WC17	206	2	255	0	197	32		0.94	0.32	94
TL7	207	2	255	0	216	30		1.03	0.27	40
WC15	207	3	255	0	214	25		1.08	0.26	32
SUN3	217	4	238	3	202	27		1.08	0.32	85
P12	223	4	235	4	189	27		1.17	0.25	6
SUN7	213	10	239	5	212	24		1.28	0.25	40
TL1	214	10	243	6	191	24		1.28	0.17	34
TL3	217	4	237	8	193	33		1.28	0.32	51
TL2	222	4	226	14	163	42		1.49	0.19	52
WALES 1	169	15	169	24	88	20		1.97	0.42	27
V5	179	7	149	3	83	2		2.13	0.21	13
V4	152	52	122	22	69	11		2.27	0.29	12
V7	148	21	131	22	72	13		2.31	0.3	11
V8	146	15	122	16	66	11		2.45	0.5	27
VA47	165	16	154	12	87	4		2.72	0.26	10

Mean *Veryhachium* RGB determinations and vitrinite reflectance data (degraded specimens)

Sample Name	Red	Std. Dev.	Green	Std. Dev.	Blue	Std. Dev	Colour	Rr(%)	Std. Dev.	N
P25	78	26	86	23	59	11		1.09	0.15	26
RH19 P-12	75	35	81	24	47	5		1.6	0.22	21
VA118	100	17	97	15	50	10		2.08	0.3	6
VA115	112	24	103	20	51	13		2.11	0.25	14
JM5	129	50	113	39	68	24		2.14		

Mean *Veryhachium* RGB determinations of reworked samples and samples without maturity data

All RGB determinations are corrected

Sample Name	Red	Std. Dev.	Green	Std. Dev.	Blue	Std. Dev	Colour
P24	221	3	229	7	159	5	
TL1 ®	205	15	213	2	116	5	
TL2 ®	201	14	162	13	71		
P24 ®	151		123		64		
P23 ®	55		71		60	2	
V8 ®	66	17	69	7	56	3	
V5 ®	82	27	74	15	55	3	
V7 ®	69	17	71	6	54	3	
VA47 ®	90	16	81	11	47		

All RGB determinations are corrected

APPENDIX VIII

CALCULATION OF CONFIDENCE INTERVALS

Confidence interval for an estimate of vitrinite reflectance given mean red intensity

Equations are taken from Davis (2002). Calculations were carried out with the assistance of Dr. James Killen.

Assume the data is normally distributed around the regression line. The residuals are distributed $N(0, \sigma^2_{yx})$.

$$\hat{\sigma}^2_{yx} = S^2_{yx} \frac{n}{(n-2)}$$

Since $n \leq 30$, t-tables (percentage points of the t distribution) are used with (n-2) degrees of freedom.

$$S^2_{yx} = \frac{\Sigma (Y_i - \hat{Y}_i)^2}{n}$$

where Y_i is the measured vitrinite reflectance of a sample and $\hat{Y}_i$ is the predicted vitrinite reflectance of a sample based on the mean red *Veryhachium* intensity of the sample.

For red intensity data: $S^2_{yx} = \frac{2.05}{22} = 0.093$

$$\hat{\sigma}^2_{yx} = 0.12 \times \frac{22}{20} = 0.1025$$

Width of 95% confidence interval:

$t_{n-2} = R_1 / \sqrt{\hat{\sigma}^2_{yx}}$

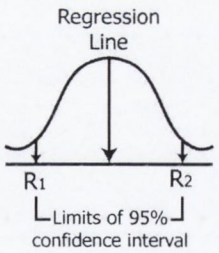

From T-tables, where $\alpha = 0.25$ and $\Phi = n-2 = 20$

$t_{n-2} = \pm 2.086$

so $R_1 = \sqrt{\hat{\sigma}^2_{yx}} \times 2.086$

$= \sqrt{0.1025} \times 2.086$

$= 0.67$

Similarly $R_2 = -0.67$

Thus there is a 95% probability that $\hat{Y}_i$, the predicted vitrinite reflectance value of a sample, based on mean red intensity, lies ± 0.67%R_r the true vitrinite reflectance value of the sample.

Width of 90% confidence interval:

$t_{n-2} = R_1 / \sqrt{\hat{\sigma}^2_{yx}}$

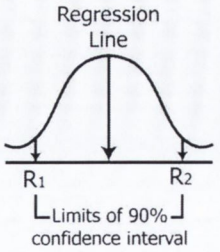

From T-tables, where $\alpha = 0.5$ and $\Phi = n-2 = 20$

$t_{n-2} = \pm 1.725$

so $R_1 = \sqrt{\hat{\sigma}^2_{yx}} \times 1.725$

$= \sqrt{0.1025} \times 1.725$

$= 0.55$

Similarly $R_2 = -0.55$

Thus there is a 90% probability that $\hat{Y}_i$, the predicted vitrinite reflectance value of a sample, based on mean red intensity, lies ± 0.55%R_r the true vitrinite reflectance value of the sample.

	Y_i	X_i	$\hat{Y}_i$	$Y_i - \hat{Y}_i$	$(Y_i - \hat{Y}_i)^2$
Sample Name	Reflectance	Red			
CAN 9	0.5	204	1.29	-0.79	0.62
P14	0.68	218	0.99	-0.31	0.10
P11	0.68	233	0.68	0.00	0.00
WC11	0.79	219	0.97	-0.18	0.03
CC3	0.85	215	1.06	-0.21	0.04
P23	0.91	215	1.06	-0.15	0.02
P22	0.97	221	0.93	0.04	0.00
WC17	0.94	206	1.25	-0.31	0.09
TL7	1.03	207	1.22	-0.19	0.04
WC15	1.08	207	1.22	-0.14	0.02
SUN3	1.08	217	1.01	0.07	0.00
P12	1.17	223	0.89	0.28	0.08
SUN7	1.28	213	1.10	0.18	0.03
TL1	1.28	214	1.08	0.20	0.04
TL3	1.28	217	1.01	0.27	0.07
TL2	1.49	222	0.91	0.58	0.34
WALES 1	1.97	169	2.03	-0.06	0.00
V5	2.13	179	1.81	0.32	0.10
V4	2.27	152	2.38	-0.11	0.01
V7	2.31	148	2.47	-0.16	0.03
V8	2.45	146	2.51	-0.06	0.00
VA47	2.72	165	2.11	0.61	0.37
					$\Sigma = 2.05$

Where $\hat{Y}_i$ is the predicted vitrinite reflectance of a sample based on the mean red *Veryhachium* intensity of the sample.

Vitrinite reflectance equivalent = -0.0211(mean red *Veryhachium* intensity) + 5.5917

Confidence interval for an estimate of vitrinite reflectance given mean green intensity

Assume the data is normally distributed around the regression line. The residuals are distributed $N(0, \sigma^2_{yx})$.

$$\hat{\sigma}^2_{yx} = S^2_{yx} \frac{n}{(n-2)}$$

Since $n \leq 30$, t-tables (percentage points of the t distribution) are used with (n-2) degrees of freedom.

$$S^2_{yx} = \frac{\Sigma (Y_i - \hat{Y}_i)^2}{n}$$

where Y_i is the measured vitrinite reflectance of a sample and $\hat{Y}_i$ is the predicted vitrinite reflectance of a sample based on the mean green *Veryhachium* intensity of the sample.

For green intensity data: $S^2_{yx} = \frac{1.43}{22} = 0.065$

$$\hat{\sigma}^2_{yx} = 0.065 \times \frac{22}{20} = 0.0715$$

Width of 95% confidence interval:

$t_{n-2} = R_1 / \sqrt{\hat{\sigma}^2_{yx}}$

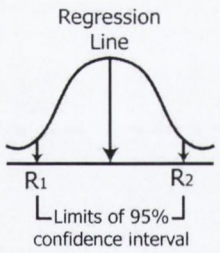

From T-tables, where $\alpha = 0.25$ and $\Phi = n-2 = 20$

$t_{n-2} = \pm 2.086$

so $R_1 = \sqrt{\hat{\sigma}^2_{yx}} \times 2.086$

$= \sqrt{0.0715} \times 2.086$

$= 0.56$

Similarly $R_2 = -0.56$

Thus there is a 95% probability that $\hat{Y}_i$, the predicted vitrinite reflectance value of a sample, based on mean green intensity, lies ± 0.56%R_r the true vitrinite reflectance value of the sample.

Width of 90% confidence interval:

$t_{n-2} = R_1 / \sqrt{\hat{\sigma}^2_{yx}}$

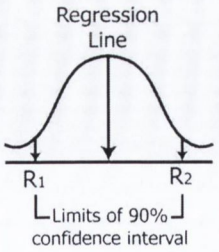

From T-tables, where $\alpha = 0.5$ and $\Phi = n-2 = 20$

$t_{n-2} = \pm 1.725$

so $R_1 = \sqrt{\hat{\sigma}^2_{yx}} \times 1.725$

$= \sqrt{0.0715} \times 1.725$

$= 0.46$

Similarly $R_2 = -0.46$

Thus there is a 90% probability that $\hat{Y}_i$, the predicted vitrinite reflectance value of a sample, based on mean green intensity, lies ± 0.46%R_r the true vitrinite reflectance value of the sample.

	Y_i	X_i	$\hat{Y}_i$	$Y_i - \hat{Y}_i$	$(Y_i - \hat{Y}_i)^2$
Sample Name	Reflectance	Green			
CAN 9	0.5	255	0.84	-0.34	0.12
P14	0.68	235	1.09	-0.41	0.17
P11	0.68	238	1.05	-0.37	0.14
WC11	0.79	241	1.02	-0.23	0.05
CC3	0.85	234	1.10	-0.25	0.06
P23	0.91	243	0.99	-0.08	0.01
P22	0.97	225	1.22	-0.25	0.06
WC17	0.94	255	0.84	0.10	0.01
TL7	1.03	255	0.84	0.19	0.04
WC15	1.08	255	0.84	0.24	0.06
SUN3	1.08	238	1.05	0.03	0.00
P12	1.17	235	1.09	0.08	0.01
SUN7	1.28	239	1.04	0.24	0.06
TL1	1.28	243	0.99	0.29	0.08
TL3	1.28	237	1.07	0.21	0.05
TL2	1.49	226	1.20	0.29	0.08
WALES 1	1.97	169	1.92	0.05	0.00
V5	2.13	149	2.17	-0.04	0.00
V4	2.27	122	2.52	-0.25	0.06
V7	2.31	131	2.40	-0.09	0.01
V8	2.45	122	2.52	-0.06	0.00
VA47	2.72	154	2.11	0.61	0.37
					$\Sigma = 1.43$

Where $\hat{Y}_i$ is the predicted vitrinite reflectance of a sample based on the mean green *Veryhachium* intensity of the sample.

Vitrinite reflectance equivalent = (mean green intensity – 303.41)/-66.22

Confidence interval for an estimate of vitrinite reflectance given mean blue intensity

Assume the data is normally distributed around the regression line. The residuals are distributed $N(0, \sigma^2_{yx})$.

$$\hat{\sigma}^2_{yx} = S^2_{yx} \frac{n}{(n-2)}$$

Since $n \leq 30$, t-tables (percentage points of the t distribution) are used with (n-2) degrees of freedom.

$$S^2_{yx} = \frac{\Sigma (Y_i - \hat{Y}_i)^2}{n}$$

where Y_i is the measured vitrinite reflectance of a sample and $\hat{Y}_i$ is the predicted vitrinite reflectance of a sample based on the mean blue *Veryhachium* intensity of the sample.

For blue intensity data: $S^2_{yx} = \underline{1.39} = 0.063$
22

$\hat{\sigma}^2_{yx} = 0.063 \times \underline{22} = 0.0695$
20

Width of 95% confidence interval:

$t_{n-2} = R_1 / \sqrt{\hat{\sigma}^2_{yx}}$

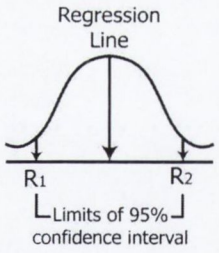

From T-tables, where $\alpha = 0.25$ and $\Phi = n-2 = 20$

$t_{n-2} = \pm 2.086$

so $R_1 = \sqrt{\hat{\sigma}^2_{yx}} \times 2.086$

$= \sqrt{0.0695} \times 2.086$

$= 0.54$

Similarly $R_2 = -0.54$

Thus there is a 95% probability that $\hat{Y}_i$, the predicted vitrinite reflectance value of a sample, based on mean blue intensity, lies ± 0.54%R_r the true vitrinite reflectance value of the sample.

Width of 90% confidence interval:

$t_{n-2} = R_1 / \sqrt{\hat{\sigma}^2_{yx}}$

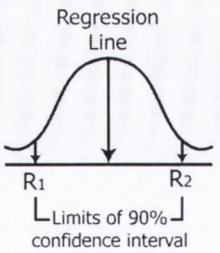

From T-tables, where $\alpha = 0.5$ and $\Phi = n-2 = 20$

$t_{n-2} = \pm 1.725$

so $R_1 = \sqrt{\hat{\sigma}^2_{yx}} \times 1.725$

$= \sqrt{0.0695} \times 1.725$

$= 0.45$

Similarly $R_2 = -0.45$

Thus there is a 90% probability that $\hat{Y}_i$, the predicted vitrinite reflectance value of a sample, based on mean blue intensity, lies ± 0.45%R_r the true vitrinite reflectance value of the sample.

	Y_i	X_i	$\hat{Y}_i$	$Y_i - \hat{Y}_i$	$(Y_i - \hat{Y}_i)^2$
Sample Name	Reflectance	Green			
CAN 9	0.5	255	0.61	-0.11	0.01
P14	0.68	235	0.87	-0.19	0.04
P11	0.68	238	0.90	-0.22	0.05
WC11	0.79	241	0.87	-0.08	0.01
CC3	0.85	234	1.19	-0.34	0.12
P23	0.91	243	1.20	-0.29	0.09
P22	0.97	225	1.53	-0.56	0.32
WC17	0.94	255	1.02	-0.08	0.01
TL7	1.03	255	0.82	0.21	0.04
WC15	1.08	255	0.84	0.24	0.06
SUN3	1.08	238	0.97	0.11	0.01
P12	1.17	235	1.10	0.07	0.00
SUN7	1.28	239	0.86	0.42	0.17
TL1	1.28	243	1.08	0.20	0.04
TL3	1.28	237	1.06	0.22	0.05
TL2	1.49	226	1.37	0.12	0.01
WALES 1	1.97	169	2.14	-0.17	0.03
V5	2.13	149	2.19	-0.06	0.00
V4	2.27	122	2.34	-0.07	0.00
V7	2.31	131	2.31	0.00	0.00
V8	2.45	122	2.37	0.08	0.01
VA47	2.72	154	2.15	0.57	0.32
					$\sum = 1.39$

Where $\hat{Y}_i$ is the predicted vitrinite reflectance of a sample based on the mean blue *Veryhachium* intensity of the sample.

Vitrinite reflectance equivalent = -0.0103(mean blue *Veryhachium* intensity) + 3.0482

APPENDIX IX

DIGITAL DATA

Images of most of the palynomorphs examined in this study are stored on the attached DVD. Unless otherwise stated, these are the images on which RGB determinations were made.

Images are named using the following system:

Sample name_Palynomorph_Slide number_England Finder Reference

E.g.: Sun3_very_4_e54_7 = Image of *Veryhachium* specimen from sample Sun 3, slide 4, England finder reference e54/7

The field of view for each image is 120µm.

Excel files for each day determinations were made are also included. These files contain the original RGB determinations made on specimens, the RGB determinations of the 'standards' for that day, and regression equation used to calibrate the data.

ASLIB THESIS DATA FORM

AUTHOR: Duggan, Catherine

TITLE: Acritarch and prasinophyte colours as thermal maturity indicators

DEGREE: Ph.D. Geology

YEAR: 2006

INSTITUTION: TRINITY COLLEGE DUBLIN

ACRITARCH AND PRASINOPHYTE COLOURS AS THERMAL MATURITY INDICATORS

By

CATHERINE DUGGAN

A thesis submitted in accordance with the requirements for the degree of Doctor of Philosophy

Department of Geology, University of Dublin, Trinity College.

June 2006

SUMMARY

Measurement of changes in the reflectivity of vitrinite (fossil woody material) in incident light is the standard technique for assessing the organic maturity of sedimentary rocks. However, vitrinite grains are rare or absent in pre Late Silurian sediments so thermal histories of these units cannot be investigated by this method. Also, marine hydrocarbon source rocks of Late Silurian and younger age often contain little or no vitrinite.

Acritarchs are enigmatic microfossils commonly found in Lower Palaeozoic sedimentary units and marine source rocks. Like miospores, the colour of acritarchs becomes darker with increasing thermal maturity. The colour of the long-ranging acritarch genus *Veryhachium* was calibrated as a thermal maturity indicator during this study. Rock samples were collected that contained vitrinite grains and *Veryhachium* specimens. The vitrinite reflectance of the sample was determined using standard techniques. Image analysis rather than traditional visual estimation was used to determine the colour of *Veryhachium*. Colour was described in terms of red, green and blue intensities (RGB). The RGB system is partially device dependent but 'standards' developed to correct for variations within and between systems were of only limited success. Mean blue and green *Veryhachium* intensities were found to be more sensitive to changes in thermal maturity than red intensity.

Prasinophytes are generally considered a class of green algae. An attempt was made to calibrate the colour of the prasinophyte *Tasmanites* with vitrinite reflectance. *Tasmanites* colour was found to be less useful than *Veryhachium* colour due to the more varied morphology of the former compared with the latter.

Two cases studies were completed. Mean *Veryhachium* RGB intensities were used to assess the thermal maturity of samples from well RH-3 in the Risha Gas Field, Jordan. Estimates of maturity using this technique were consistent with a previous thermal maturity study of the area using other methods. RGB determinations of *Veryhachium* from a Bolivian sample were used to successfully identify reworking.